Parallel control of hybrid propulsion aboard a fast naval combatant

Simulation based research for maximized acceleration

L. Mourik

System modeling
System control
Vessel response

TU Delft

Parallel control of hybrid propulsion aboard a fast naval combatant

Simulation based research for maximized acceleration

by

L. Mourik

to obtain the degree of Master of Science
at the Delft University of Technology,
to be defended publicly on wednesday august 18, 2021 at 14:00 PM.

Student number: 43235807
Project duration: June 8, 2020 – august 18, 2021
Thesis committee: Ir. G. J. Meijn, Damen Schelde Naval Shipbuilding, supervisor
Dr. Ir. L. Biert, TU Delft, supervisor TU Delft
Ir. K. Visser, TU Delft

This thesis is confidential and cannot be made public until august 18, 2026.

An electronic version of this thesis is available at `http://repository.tudelft.nl/`.

TU Delft

Summary

Environmental and operational challenges associated with an excessive fuel consumption have led to the need for future naval vessels to be less dependent on fossil fuels. This desire to be less dependent on fossil fuel has led to an increased interest into the implementation of hybrid diesel-electric propulsion into naval vessels. The chosen configuration is combined diesel-electric and diesel (CODLAD). However, there is a performance gap regarding the manoeuvrability between the previously implemented gas-turbine propulsion and the diesel-electric hybrid propulsion. In order to reduce this performance gap between a gas-turbine propulsion system and a diesel-eclectic propulsion system a new optimized control system needs to be developed. Therefore the main objective of this master thesis is improve the performance of the diesel-electric hybrid system.

To test the new control strategy a ship model is needed. This ship model consists out of the following sub models: A diesel engine, an electric drive, gearbox, propeller and a hull modeled by a resistance. Both the gearbox and hull will be fairly simple differential equations, integrating the total forces on the shaft and hull. The results of these integrations will give a rotational shaft speed and linear ship speed, respectively.

For the diesel engine a high power density combined with a relatively large maximum absolute power is needed. Although other engines would also qualify the MAN - V28/33D seams the best fit. The MAN -v28/23 is a high speed diesel engine equipped with a sequential turbocharger (STC) system delivering 10 MW of power. A mean value method used by Geertsma [10], implementing the Seiliger-process to predict engine torque is implemented. The Büchi balance with a variable effective area is used to model the sequential turbo charging system (STC). The fuel input of the diesel engine can be controlled to deliver the desired speed or desired torque.

For the electric drive an induction machine with 3 MW of power is selected. To model the response the electric drive has to the control input a fast but reasonably actuate model is needed. A circuit based model by Ong [20], which represents the induction machine in the 0QD axis is chosen. To control the torque the induction machine produces field-oriented control is used, when speed control is needed a cascaded controller will be implemented.

For overall control three suited control strategies, which produce a good acceleration are found during the literature research [14]. Namely, Adaptive Pitch Control (APC), Parallel Electric Speed Control (PESC) and diesel engine speed parallel with electric drive torque control. Based on these already existing control strategies new variations are tested. However all these control strategies use a fixed power split between the diesel engine and electric drive. This doesn't utilize the full potential of the electric drive to deliver almost instant full torque when the diesel engine is operated with speed control. Therefore this research presents the addition of a dynamic power split.

With conventional diesel engine speed control the induction machine only starts delivering additional torque at higher shaft speed. During the simulations the shaft speed at which the induction machine starts delivering additional torque was varied. No optimal for all intermittent accelerations as well as the slam start was found. It was however concluded that having the induction machine deliver its additional torque in the STC switching region maximized the margin between the static propeller load and the diesel engine limit. Lowering the shaft speed at which the induction machine starts delivering additional torque was beneficial for all accelerations.

Adaptive pitch control avoids the angle of attack peak, reducing the torque peak that can potentially overload the diesel engine. Adaptive pitch control is the only control strategy that operates at a low angle of attack, therefore it is the only control strategy which is less perceptible for cavitation. However this peak in angle of attack is responsible for the peak in thrust. Adaptive pitch control therefore needs large shaft speed fluctuations to be able to create a large thrust. Adaptive pitch control is therefore either slow or forces the diesel

engine to rapidly make large changes in its shaft speed. The rapid changes in shaft speed could increase the amount of wear inside the engine, reducing the time between maintenance.

During the simulations torque control for the diesel engine performs extremely well during acceleration. Using torque control for the diesel engine the static power distribution of the propeller load was varied. During these variations it was concluded that a large acceleration can be achieved with a heavy loading on the diesel engine in steady state, supported by a large torque production during acceleration by the induction machine. A heavy matching of the diesel engine was possible because the diesel engine only produced the power needed for the steady state propeller power as matched via the combinator. The induction machine is made responsible for keeping the speed and coping with disturbances. The induction machine is inherently more suited than the diesel engine, due to its fast response as well as it being able to produce full torque or maximum power without any negative adverse effects. However torque control is not available from manufacturers.

This research includes a novel implementation of a dynamic power split, which produced very promising results. The dynamic power split uses the diesel engine with speed control parallel with the electric drive in dynamic torque control. The dynamic torque control for the induction machine allow for optimal usage of the inherent characteristics of the electrical machine. Using dynamic torque control the induction machine is responsible for the high frequency load changes such as disturbances as well as the first part of the acceleration. The diesel engine governed by a slower integral dominated PI controller accounts for the low frequency load changes, including the higher load at a new steady sate. The diesel engine with speed control parallel with the electric drive in dynamic torque control produces excellent acceleration characteristics, making it a viable option to improve the acceleration characteristics of a diesel-electric hybrid system.

Since torque control is unavailable, either adaptive pith control or diesel engine speed control with a dynamic power split needs to be used to improve the acceleration characteristics of a diesel-electric hybrid system. When the cavitation behavior is deemed more important than the wear in the diesel engine, adaptive pitch can be tuned to be fast with as a consequence larger shaft speed fluctuations. When potential cavitation unimportant diesel engine speed control with a dynamic power split needs to be considered as an option.

Preface

This report is written in the framework of a world that is changing the way it looks towards fossil fuels. This report is build upon, and heavily influenced by the previous work of CDR. Dr. Ir. R Geertsma who produced an PhD thesis titled: "Autonomous control for adaptive ships with hybrid propulsion and power generation" [5].

I am grateful to have received the opportunity to perform my master thesis at Damen Schelde Naval Shipbuilding. Especially during the Corona crisis, as it could have added challenges for the communication and corporation between the university, Damen and myself. Looking back the challenges were minimal as Damen provided a workplace and face to face meetings which were in agreement to Covid standards.

First I would like to thank the head of my thesis committee SBN. (ret.) Ir. K. Visser for making it possible to do my thesis research into the specialization of marine engineering. I would also like to thank my supervisor from the University at Delft Dr. Ir. L. van Biert, for his time, feedback and support. Then I would like to use this opportunity to thank Gert-Jan from Damen Naval Ship Building for his weekly support and insight. During this period a recurring pain in my back and hip became at times quite severe, meaning a loss of sleep and performance during the day. The cause of this chronic pain eventually turned out to be "axiale spondyloartritis". I would like to thank Gert-Jan again for his very supporting and understanding attitude, even before a conclusion to the cause was reached.

Many thanks to my girlfriend, who supported me in various ways, including checking spelling and grammar of this report. I would also like to thank my aunt for forcing my dyslectic head into producing words and sentences that resembles the English language in a way the rest of the world can understand.

L. Mourik
Vlissingen, march 2021

Contents

1 Introduction

The availability of fuel in the future combined with the agreements regarding climate change have effect on the design of the propulsion plant of a naval vessel. The growing concerns about the environment and climate change from both the public and the government have led to more stringent regulations regarding pollution and emissions.

The European commission's joint research center [16] estimates that maritime industry related activities account for 3 to 5% of total CO_2 emissions. The European Union therefore states the goal of reducing atmospheric emissions from ships [16], as well as stating a target of 20% improvement in energy efficiency [3]. To limit the damage to the climate via greenhouse gas emissions produced by ships, the MARPOL convention has introduced mandatory measures to improve energy efficiency for ships [12]. Already existing technologies such as more efficient engines and propulsion systems are stated to be a large part of the solution to achieve the goal of producing less greenhouse gas emissions [12].

The mandatory measures mentioned above do not apply to naval vessels [13]. However, IMO does state that such vessels should adopt appropriate measures to be consistent with the present convention, as long as these measures are reasonable and do not impair the operations or operational capabilities of the vessel [13]. Although these lower CO_2 emission standards are not mandatory for naval vessels, government organizations like the the Ministry of Defence in the Netherlands have adopted ambitions regarding the emissions of naval vessels. Similar to the European Union, the Dutch Ministry of Defence has adopted the ambition to reduce fossil fuels usage in 2030 by at least 20% compared to 2010 [24].

Besides the reduction in emissions the reasons the Dutch Ministry of Defence has for reducing the usage of fossil fuel are mainly operational ones. Firstly, the freedom of action by operational commanders is reduced by the need to refuel. Secondly, it is also anticipated that the amount of fossil fuel available will diminish. Therefore a vessel with low fuel consumption would be easier to keep in service than one with a high fuel consumption. Thirdly, the logistical effort and costs involved in refueling as well as the risks during such operations are an important reason for reducing fossil fuel usage, this being of special importance when operating in remote areas [24].

Geertsma *et al*'s [10] work has shown that the above mentioned 20% reduction of fossil fuel dependency compared to current hybrid gas-turbine electric propulsion is feasible. The reduction can be accomplished almost completely by implementing hybrid diesel-electric propulsion and using power take-off mode. In Power take-off mode the electric auxiliary motor is used as a generator improving the efficiency of the overall propulsion system.

Defence organizations want a vessel that is operationally capable, meaning that during a threat the vessel should be highly manoeuvrable to position itself as fast as possible for optimal usage of radar and weapon systems. The operational capabilities of a naval vessel are severely impaired if the reduction in fuel usage leads to loss of manoeuvrable [10].

While it is proven feasible to reduce the fuel dependency the manoeuvrability quantified in acceleration is lower than for conventional systems. In Geertsma's work the transition from a gas-turbine to the chosen diesel-electric configuration will cause a reduction in top speed of 3 kts as well as a 20% reduction in acceleration performance. [10], meaning that at the state-of-the-art of hybrid control the modifications to the naval vessels which are necessary to reduce the fuel dependency bring adverse consequences to the acceleration performance.

Geertsma describes that the control strategy has a very significant contribution to the ships acceleration performance, and that with advanced control strategies the acceleration performance can nearly measure up to the gas-turbine propulsion [10]. IMO states that the measures for reducing emissions only need to be adopted as long as the operational capabilities are not impaired [13]. Therefore, there is the possibility for a control strategy to have a mode for operations where high manoeuvrability is required that does not take efficacy into account. Using an inherent efficient diesel electric propulsion plant in a different mode to meet operational standards.

A new control strategy needs to be engineered which uses the during transit efficient hybrid system with the purpose of producing maximum acceleration. During the acceleration the fuel usage is of low importance because of the vital function acceleration has for the operation of the naval vessel. Such a control strategy would make it possible to have a propulsion system that is fuel efficient during transit but still has a good performance during operations when it's necessary.

A drivetrain consisting of a diesel engine, e-motor and controllable pitch (CP) propeller uses less fuel compared to a gas-turbine, however it reduces the acceleration and manoeuvrability. The goal of this master thesis is to develop a control strategy that closes the gap between the excellent performance of the gas-turbine and the slower performance of a hybrid system.

1.1. Project goal and scope

Damen naval is producing high performing naval vessels with the emphasis on quality for over 140 years [2]. Therefore, to perform on the level that is expected from the naval sector, Damen naval wants the new vessels equipped with diesel-electric propulsion to deliver balanced efficiency and performance as well. This means that among other things these vessels need to possess good acceleration properties. In past designs gas-turbines were used as main engine, providing good acceleration. Recent developments surrounding fuel usage have led to the possibility of implementing diesel-electric propulsion. However, there is a gap between the acceleration performance of a gas-turbine and a diesel-electric propulsion. The acceleration characteristics of a diesel-electric population need to be improved to be compliant with operational needs. Therefore a new control strategy needs to be developed, providing the maximum achievable acceleration with a diesel-electric population system.

The propulsion system on board of the vessel described in Section 1.5 is depicted in Figure 1.1 and consists of a diesel engine, diesel generator, electric machine and CP propeller. Depending on the electric power demand of the propulsion system, an energy storage system might be added. With increasing components in the propulsion system, the degrees of freedom also increase. The degrees of freedom present in this propulsion system are the propeller pitch, diesel engine power and induction machine power. These degrees of freedom require choices to be made regarding the control strategy of the system. Different control strategies use the trade-offs inherent to the installed machines and systems to accomplish an optimum that is desired during the mode of operation.

The goal of this thesis is the understanding and development of a control system for hybrid propulsion that makes it possible to have a high-performance mode, reducing the gap between the performance of the gas-turbine and the performance of hybrid propulsion. In contrast to efficiency driven control the high-performance mode needs to maximize the manoeuvrability of the vessel. The manoeuvrability is measured in absolute acceleration, acceleration therefore has the highest priority in the new control system. MATLAB-Simulink® will be used in this study to model the diesel engine, electric drive and CP propeller. For this research the design of the vessel itself, including its power demand and main propulsion characteristic as presented in Table 1.1 are fixed. The model will be created to test the developed control systems. The control strategy focuses on achieving a maximum acceleration.

1.2. Research questions

The main question results from the literature research [14] and concerns the control strategy for the complete system. From literature it was found that with current control strategies the induction machine is only used as torque contributor, neglecting it potential of almost instant toque production. Current control strategies mainly focus on the static operating when designing a combinator, neglecting the dynamics in the transition between static operating points. Utilizing more degrees of freedom could result in a control strategy that uses the inherent qualities of the subsystems, resulting in a better performance. A working simulation model of the ship is needed to develop a control strategy. As described in section 1.5, the ship for which the control system will be optimized consists out of a diesel engine, electric machine and a CP propeller. The main research question for this master thesis is:

How can a hybrid diesel-electric propulsion system with a controllable pitch propeller be controlled for maximum acceleration?

The sub-questions are as follows:

1. *What combination of control methods at machine level provides the best acceleration performance?*
2. *How should the load be distributed between the electric drive and diesel engine during acceleration?*
3. *What is the optimal propeller load distribution over time to achieve the maximum overall acceleration?*

1.3. Research method

The overall aim of this research is to draw qualitative conclusions based on quantitative simulation results, therefore the ship model and subsystems will be kept the same between simulations. The level of (fine) tuning of individual control methods is also similar between control strategies. Firstly, the analysis phase is performed and documented in a literature research [14]. In this phase knowledge is gathered about the inherent qualities and modeling of the electrical machine, diesel engine and CP propeller. During the literature research various methods for machine level control were selected to be implemented in order to compare their performance.

Secondly, the modeling phase aims at developing a model capable of predicting dynamic behavior to a degree of accuracy that allows for the comparison between control strategies. Quantifying the difference in behavior of the equipment and the vessel. Important variables are the vessels' acceleration, the margin to the limits of the drivetrain, as well as the overall performance of the vessel and subsystems. Thirdly, the solution design phase will focus on the understanding of the characteristics of different control strategies for the subsystem. Using this understanding for the development and implementation of the control strategies which were selected in the literature research. These control strategies will be implemented into the MATLAB-Simulink® environment as well.

Finally, the different control solutions are tested on the vessel model and evaluated. Research will be conducted via first principal simulations, using standard control as a benchmark to which "new" control strategies will be compared. The simulations will generate quantitative results, which are then used to draw qualitative concussions from. The research questions will be answered based on the knowledge gathered during the literature research combined with the results from the simulation.

1.4. Thesis outline

This section will describe the content of each chapter, providing guidance on where to find the desired information. Chapter 1 describes the origin, scope, goal and setup of the research. Most importantly section 1.2 describes the research questions. Finally, the vessel specification onto which the simulations will be preformed is specified in section 1.5.

Chapter 2 describes the model used to simulate the naval vessel. Starting with an overview of the different subsystems and their inter-dependencies. Secondly a mathematical description of the diesel engine is given. Thirdly, both a description of the mathematics and implementation of the induction machine is given. Finally, the gearbox, propeller and hull are described, which is followed by a description of the matching procedure.

Chapter 3 describes the control options and limitations for the diesel engine, induction machine and CP propeller which are selected in the literature research. First the control methods and limitations of the diesel engine are discussed. Second the control and limitations of the induction machine are discussed. For the induction machine model that is used, field orientated control is derived and implemented. Finally the control options for the CP propeller are described.

Chapter 4 describes the control scenarios used for the vessel. The control scenarios are each different combinations of the possible subsystem control options. For each control scenario there are multiple simulations performed varying the settings for the diesel engine, induction machine or CP propeller. Finally, the results for all simulations are presented, discussed, and evaluated. Based on the evaluation improvements are made to following simulations.

Chapter 5 describes the conclusions that are drawn from the simulations. Most importantly section 5.2 describes the answers to the research questions. These conclusions are followed by opportunities for further research.

1.5. Vessel specifications

This section describes the naval combatant for which the parallel control will be implemented. The focus of this research lays on the overall performance of the vessel that is controlled with different control strategies, meaning that the equipment and ship stays the same between comparisons. The hull design and parameters are therefore out of scope for this research. The parameters are based on the case study of a fast frigate as proposed by Geertsma *et al.* (2017). These parameters are fixed and part of the research setup and are therefore discussed early in this report. Table 1.1 shows the vessels' specifications.

The ship is equipped with two drivetrains providing redundancy and the needed power to propel the vessel at the design speed of 27 kts. A layout for the two drivetrains is shown in Figure 1.1. The chosen configuration is combined diesel-electric and diesel (CODLAD). This Figure shows the two main diesel engines (1), gearboxes (2), the electric machines (MG), the CP propellers (3), the generator sets (G), as well as the AC network (4) with various users. The main engine is connected via a gearbox, which reduces the shaft speed and increases the torque to the CP propeller. The main engines can be operated alone or with the aid of the electrical drives. The main engine delivers efficient propulsion at high loads close to its envelope. Meaning, transit speeds, or at transit speed with the electric machine operating as generator (PTO). When the main engine is operated at part load it has a lower efficiency [7].

The electric machine is located after the gearbox and is coupled directly to the shaft driving the propeller. The electric machine is capable of driving the vessel at low speeds. This low speed operation of the electric drive gives the opportunity of keeping the gearbox stationary which reduces the noise signature. Only using the electrical propulsion also avoids running the main engine inefficiently at part load and it provides redundancy to the propulsion system. If the diesel engine is providing power but top speed is not needed, than the electric machine can be used as a generator (PTO). Part of the propulsion power from the main engine is than used to generate electrical energy. The electric drive operates at 690 volts which is considered low voltage. The advantage is the relatively limited safety risk when compared to high voltage. The disadvantage is a large amount of current needed to produce a large power output. Considering the size of the variable frequency

drive as well as the copper bars needed to transport the current the practical power limit for such low voltage is about 3 MW. At higher powers the currents would become excessive and a high voltage machine should be considered. As stated before when the mechanical drive engine is running, but top speed is not required, the electric machine can be used for generating electricity. This thesis focuses on the operational mode where both the main engine and the electric machine drive the propeller in parallel, emphasising 'performance' not on fuel economy .

It is assumed that the vessel is equipped with a generator set with in total 12 MW of power. The generator set itself is not part of the research and will not be modeled. In order to evaluate the power demand on the generator set the WÄRTSILÄ 31 product guide [31] is used. WÄRTSILÄ states that load ramp loads can increase from 0% till 60% in 20 seconds, after which the load ramp can increase from 60% to 100% in 60 seconds. WÄRTSILÄ does however state larger load increase for dynamic positioning like applications. In the WÄRTSILÄ 31 product guide [31] on p. 18 the following is stated: "In dynamic positioning applications loading ramps corresponding to 20-30 seconds from zero to full load are however normal". Welland is manufacturing diesel generators in the UK since 1950 [32] and states that for step loads with a frequency loss of less than 10% a step load acceptance of a turbocharged diesel generator lies between 50% to 80%.

Table 1.1: Frigate case study model parameters [7]

Hull				**Diesel engine**			
Ship mass	m	$5200 \cdot 10^3$	kg	Nominal power	P_{nom}	10.0	MW
Maximum ship speed	V_{max}	27	kts	Nominal engine speed	N_{nom}	1050	RPM
Resistance factor	C_1	5896	kg/m	Number of cilinders	i	20	
Number of propellers	k_p	2					
Thrust deduction factor	t	0.06		**Electric drive**			
				Nominal Power	P_{nom}	3.0	MW
CP Propeller				Nominal Voltage	V_{nom}	690	V
Diameter	D	4.8	m				
Design pitch diameter ratio	P/D_d	1.4		**Gearbox and shafting**			
Wake coefficient	w	0.02		Total moment of inertia	J_{tot}	12500	kgm^2

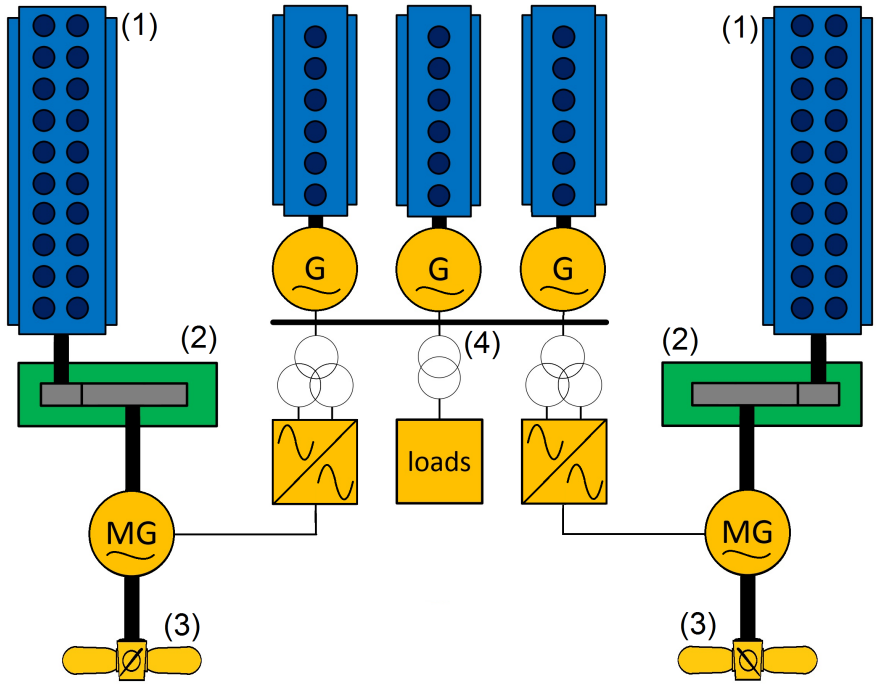

Figure 1.1: Hybrid propulsion scheme

2

Naval Vessel Model

This chapter describes the implemented complete ship model. This model is used to predict and compare the vessels' response to various control strategies. The aim for this chapter is to describe the physics that is included in the models as well as making it possible to recreate the model. Firstly, an overview of the complete model is given in section 2.1, describing the relationship between the submodels. Secondly the diesel engine model as used by Geertsma *et al.* 2017 is described in section 2.2. This model is implemented with minimal differences. Thirdly, the equations defining the induction machine are described in section 2.3. These equations are followed by a detailed description of the MATLAB-Simulink® implementation of this induction machine. Finally the gearbox, hull and propeller models are discussed in section 2.4. This section also includes the matching of the diesel diesel engine and induction machine to the propeller and hull.

2.1. Model overview

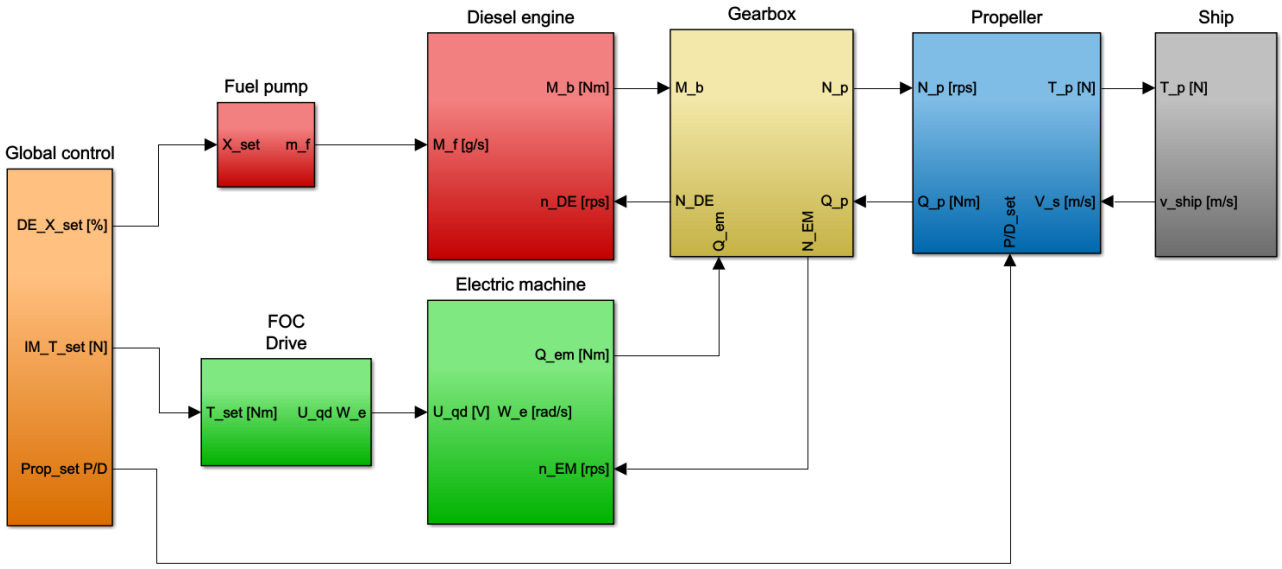

Figure 2.1: Naval vessel model overview

Figure 2.1 shows a overview of the complete ship model. The orange block named "Global control" contains the control for the different subsystems. As stated before the purpose of the model is to test different control scenarios. The different control modules that belong to each control scenario will be implemented in the global control block. The global control block dictates three setpoints from a lever position. Firstly, a fuel setpoint (X_{set}) for the fuel pump to obtain the desired behavior from the diesel engine. Secondly, The control sets a torque setpoint for the field orientated control drive of the induction machine. The demanded torque

can be generated directly via the lever setpoint or be the result of a speed controlled power demand. Finally the global control dictates the pitch or angle of attack for the propeller. Chapter 3 describes the different control strategies for the subsystems. These different subsystem control strategies are varied and combined to form scenarios which are discussed in Chapter 4.

The diesel engine receives fuel from the fuel (M_f) pump in accordance to the controls input. This fuel is converted into a torque (Q_{de}) which is delivery to the gearbox. The conversion from chemical energy to mechanical energy is performed with a four stroke combustion process. The diesel engine is equipped with sequential turbocharging. The rotational speed of the engine is dependent on the power balance as calculated in the gearbox. The diesel engine is discussed in more detail in section 2.2.

Electrical power is supplied to the induction machine via a variable frequency drive. The variable frequency drive is not modeled for the reasons discussed in section 2.3. The field orientated control block calculates the needed supply frequency (Ω_e) and voltage (U_{qd}) to drive the induction machine in such a way it produces the desired torque (Q_{im}).

Torque is provided to the "gearbox" subsystem by the diesel engine and the induction machine, while the propeller receives torque form this subsystem. It is important to note that only the diesel engine torque is transmitted through the gearbox, increasing the torque and reducing the shaft speed. This subsystem is the location where the torque balance is calculated. The torque balance results in a change in shaft speed which is the output from the gearbox subsystem to the diesel engine (N_{de}), induction machine and propeller ($N_{im} = N_p$).

The propeller subsection calculates the produced thrust (T_p) which is delivered to the ship, as well as the needed torque (Q_p) which is received from the gearbox subsystem. The subsection named "Ship" calculates the ship acceleration/deceleration that is the result of the ship resistance and the propeller thrust. The acceleration/deceleration results in ship speed (v_{SHIP}), which is an important variable for the propeller.

2.2. The Diesel engine

This section describes the diesel engine that is used during the MATLAB-Simulink® simulations. In subsection 2.2.1, the advantages and disadvantages of the chosen mean value model type are summarized. In subsection 2.2.3, the equations which are used to model the diesel engine are described. This section therefore determines the fundamental exclusion or inclusion of engine behavior. Validation of the model is performed by Geertsma *et al.* 2017.

2.2.1. Mean value modeling

A mean value model of a diesel engine is used to perform the simulations needed in this thesis. This section is a summary of the reasoning behind the choosing of a mean value model. A more detailed comparison between model types can be found in the literature research [14]. When the in-cylinder process is modeled with more detail, the difficulty adapting to different operating conditions, the complexity, computation time and amount of needed parameters increases [26]. Mean value models take simplicity and accuracy into consideration and have therefore been widely used in the modeling of large systems [26] [27]. Mean value methods can be used to predict the transient behaviour sufficiently accurate [1] [18], therefore they are used for evaluation of control models as well as the overall acceleration performance [10] [17]. Peak values in temperature and pressure, misfiring or other faults are not modeled, however their impact on the the overall behavior and acceleration of the ship which operates at a much larger time scale is assumed minimal. A mean value method is therefore considered the most suitable method for modeling the diesel engine as a subsystem to develop a control strategy. Due to its compromise between the needed engine data, accuracy and computational time, the model Geertsma uses for his analysis of the acceleration of a frigate [10] will be implemented using MATLAB-Simulink®.

2.2.2. Diesel engine parameters

In this section, the general parameters of the selected diesel engine as well as the more detailed parameters needed to model the engine are described. The diesel engine is selected with the goal of combining a high power density with a large maximum absolute power. Therefore the engine that is selected is a four-stroke engine that has a V-configuration, the largest amount of cylinders available, a high mean effective pressure, a high mean piston speed, a stroke/bore ratio close to one and is equipped with sequential turbocharging (STC). The Vee configuration leads to a tight packing of the energy delivering pistons. The high number of cylinders means a large total power. The high mean effective pressure implies a large power density per cylinder. The high mean piston speed means more torque producing expansion stokes will happen in a given time. The stroke/bore ratio close to one gives a relatively large area to the piston, meaning that the high pressure results in a large force. Finally, sequential turbocharging broadens the operating envelop resulting in more power availability at lower shaft speeds. The selected engine is presented in Figure 2.2 with its parameters summarized in Table 2.1.

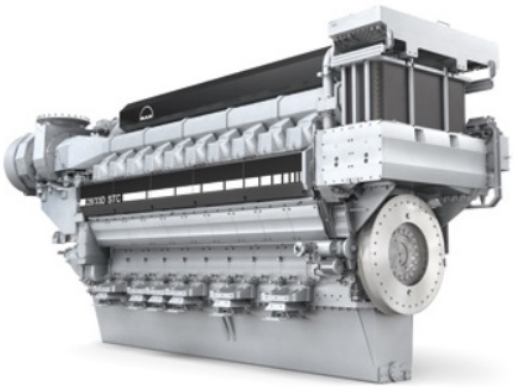

Figure 2.2: MAN V2833D

General parameters			
Nominal engine power	$P_{e_{nom}}$	9.1	MW
Maximum enige power	$P_{e_{max}}$	10.0	MW
Nominal engine speed	$n_{e_{nom}}$	16.7	rev/s
Number of cylinders	i_e	20	
Revolutions per cycle	k_e	2	
Nominal fuel consumption	$m_{SFC_{nom}}$	189	g/Wh
Maximum engine speed	N_{max}	1050	RPM
Minimum engine speed	N_{min}	300	RPM
Air swallow			
Stoichiometric air to fuel ratio	σ_f	14.5	
Nominal pressure at Seiliger 1	$P1_{nom}$	$4.52{\cdot}10^5$	Pa
Parasitic heat exchanger effectiveness	ϵ_{inl}	0.05	
Heat release			
Heat release efficiency	η_q	0.915	
Fuel injection time delay	τ_X	0.0151	s
Specific heat at const. pressure of air	$c_{p,a}$	1005	$J/kg \cdot K$
Specific heat at const. p of exhaust gas	c_{pg}	1100	$J/kg \cdot K$
Lower heating value of fuel	h_{HLV}	$42.7{\cdot}10^6$	J/kg
Constant volume portion gradient	$X_{cv_{grad}}$	-0.456	
Constant temperature portion	$X_{ct_{nom}}$	0.4	
Combustion efficiency	$\eta_{q_{comb}}$	1	
Mechanical conversion			
Nominal mechanical efficiency	$M_{loss_{nom}}$	0.9	
Mechanical efficiency gradient	$M_{loss_{grad}}$	0.5	

Cylinder parameters			
Bore diameter	D_b	0.28	m
Stroke length	L_s	0.33	m
Crank rod length	L_{CR}	0.64	m
Crank angle at inlet closure	α_{IC}	224	deg
Crank angle at exhaust open	α_{EO}	119	deg
Geometric compression ratio	ϵ_c	13.8	
Cylinder volume at Seiliger 1	V_1	0.0199	m^3
Seiliger cycle			
Maximum nominal cylinder pressure	$P_{3,4}$	$206{\cdot}10^5$	Pa
Temperature after the intercooler	T_c	323	K
Temperature of the inlet duct	T_{inl}	432	K
Gas constant of air	R_a	287	$J/kg \cdot K$
Polytropic exponent for expansion	n_{exp}	1.38	
Exhaust receiver and turbocharger			
Turbocharger time constant	τ_{TC}	5.0	s
Exhaust receiver time constant	τ_{pd}	0.01	s
Gas constant of exhaust gas air	R_g	287	$J/kg \cdot K$
Isentropic index of air	κ_a	1.4	
Isentropic index of the exhaust gas	κ_g	1.353	
Polytropic exponent for blowdown	n_{bld}	1.38	
Ambient pressure	P_{amb}	$1{\cdot}10^5$	Pa
Ambient temperature	T_{amb}	318	K
Pressure after turbocharger	P_{ex}	$1{\cdot}10^5$	Pa
STC lower switching threshold	$N_{STC_{high}}$	700	RPM
STC higher swiching threshold	$N_{STC_{low}}$	800	RPM

Table 2.1: MAN diesel engine data [10]

2.2.3. Diesel engine equations

The implemented model is proposed by Geertsma *et al.* 2017 in " Pitch control for ships with diesel mechanical and hybrid propulsion: Modelling, validation and performance quantification". The model is directly implemented except for two details: The first exception is the turbocharger efficiency, which is estimated using a lookup table directly based on FAT data. This replaces a quadratic function which is fit to the FAT data. The second change is the usage of sequential turbo charging (STC). STC is used to widen the operating envelope of the diesel engine.

Fuel

The behavior of the fuel pump is modeled with a first order differential equation 2.1. The time in equation 2.2 is estimated as the time required for half a stroke at nominal engine speed. The time delay is assumed constant due to its small value. The nominal fuel flow is calculated in equation 2.3. The nominal basic specific fuel consumption is given in g/kWh, therefore a factor $\frac{1}{3600 \cdot 1000}$ shows up to get a fuel flow in kg/s.

$$\frac{dm_f}{dt} = \frac{m_{f_{nom}} \cdot X_{set}(t) - m_f(t)}{\tau_X} \tag{2.1}$$

$$\tau_X = \frac{1}{4 \cdot n_{e_{nom}}} \tag{2.2}$$

$$m_{f_{nom}} = \frac{m_{bsfc_{nom}} \cdot P_{e_{nom}} \cdot k_e}{i_e \cdot n_{e_{nom}}} \cdot \frac{1}{3600 \cdot 1000} \tag{2.3}$$

Air swallow

The air swallow determines the amount of air available during combustion. The air excess ratio represents the ratio between the amount of air in the cylinder with respect to the amount of air needed for a chemically ideal combustion. In reality the air excess ratio needs to be larger than 1 due to the fact that the air fuel mixture is not homogeneous. The air excess ratio is also an important indicator for the thermal loading of the engine. This model decribes a 4-stroke engine with sufficient air slip, meaning all the combustion gasses of the previous cycle are no longer present. Therefore the pseudo air excess ratio can be used as presented in equation 2.4. The trapped air mass at the start of the combustion is determined using the ideal gas law as described in equation 2.5. The charge air pressure p_1 produced by the compressor of the turbocharger is discussed in subsection 2.2.3. The equation describing the temperature T_1 of the gas that fills the cylinder is described in section 2.2.3. The volume that is filled at the start of compression V_1 is determined by cylinder specific parameters as described in equation 2.6.

$$\lambda(t) = \frac{m_1(t)}{m_f(t) \cdot \sigma_f} \tag{2.4}$$

$$m_1(t) = \frac{p_1(t) \cdot V_1}{R_a \cdot T_1} \tag{2.5}$$

$$V_1 = \frac{\pi \cdot D_B^2 \cdot L_s \cdot r_c}{4(\epsilon_c - 1)} \tag{2.6}$$

The cylinder geometry is defined by the bore diameter D_B and stroke length L_S. ϵ_c represents the geometric compression ratio, which is directly determined from the cylinder dimensions. The geometric compression ratio is used to calculate the effective compression ratio r_c, for which the compression stroke effectiveness x_c is used. To calculate L_{BDC} is the distance between the top of the cylinder and the piston crown at bottom dead center (BDC). The distance between the top of the cylinder and the piston crown at the moment the inlet valve closes L_{IC} is dependent on the valve timing. To calculate L_{IC} the angle at which the inlet valve closes α_{IC} is needed as well as λ_{CR}. λ_{CR} is the ratio between the connecting rod (L_{CR}) and the crankshaft radius (R_{RC}) both in meters. The ratio of the volume inside the cylinder between the moment that the exhaust vale opens from the point when the exhaust valve is described in equation 2.14. The cylinder space length at the moment the exhaust valve opens (L_{EO}) is calculated using the angle when the exhaust valve opens (α_{EO}) as shown in equation 2.13.

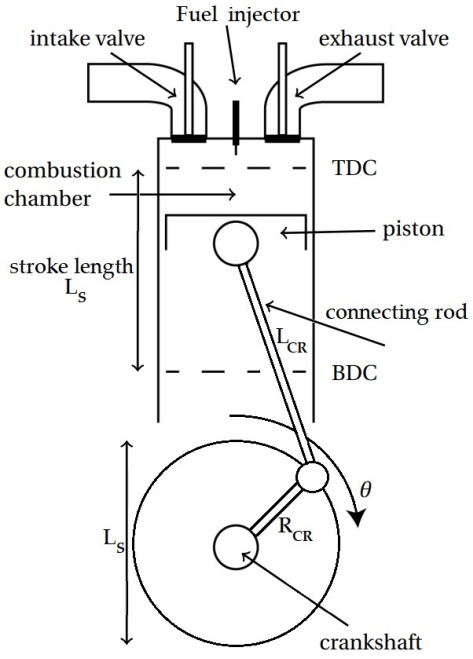

Figure 2.3: Schematic view of the geometry of cylinder, crank rod and crank shaft [4]

$$r_c = (\epsilon_c - 1) \cdot x_c + 1 \tag{2.7}$$

$$x_c = \frac{L_{IC}}{L_{BDC}} \tag{2.8}$$

$$L_{IC} = L_S\left(\frac{1}{\epsilon_c - 1} + \frac{1}{2}\left(1 - cos(\alpha_{IC}) + \frac{1 - r_{tg}}{\lambda_{CR}}\right)\right) \tag{2.9}$$

$$L_{BDC} = \frac{\epsilon \cdot L_S}{2L_{CS}} \tag{2.10}$$

$$r_{tg} = \sqrt{1 - \lambda_{CR}^2 \cdot sin^2(\alpha_{IC})} \tag{2.11}$$

$$\lambda_{CR} = \frac{L_S}{2L_{CS}} \tag{2.12}$$

$$L_{EO} = L_S \cdot \left(\frac{1}{\epsilon_c - 1} + \frac{1}{2}\left((1 - cos(\alpha_{EP})) + \frac{1 - r_{tg}}{\lambda_{CR}}\right)\right) \tag{2.13}$$

$$r_{eo} = \frac{L_{EO}}{L_{IC}} \tag{2.14}$$

Heat release

The model that Geertsma *et al.* describes uses the six stage Seiliger cycle. To model the heat release that takes place during an engine cycle the combustion process is divided into three stages. The heat released that is available for the production of work is split between these three stages. For the isochoric combustion equation 2.15 is used, in which the portion of heat that is released at this constant volume is represented by X_{cv}. For the isobaric combustion equation 2.16 is used. For the isothermal combustion equation 2.17 is used, in which the portion of the heat released at this constant temperature is represented by X_{ct}. The air excess ratio λ that is maintained within the engine operating limits this is high enough the assume the combustion efficiency to be unity $\eta_{comp} = 1$. The heat release efficiency η_q is considered inversely related to the engine speed as described in equation 2.18. The nominal value for the heat release efficiency $\eta_{q_{nom}}$ is estimated by Geertsma *et al.* using nominal engine parameters.

$$q_{23}(t) = X_{cv}(t) \cdot \frac{m_f(t) \cdot \eta_q(t) \cdot \eta_{comb} \cdot h^L}{m_1(t)} \tag{2.15}$$

$$q_{34}(t) = (1 - X_{cv}(t) - X_{ct}(t)) \cdot \frac{m_f(t) \cdot \eta_q(t) \cdot \eta_{comb} \cdot h^L}{m_1(t)} \tag{2.16}$$

$$q_{45}(t) = X_{ct}(t) \cdot \frac{m_f(t) \cdot \eta_q(t) \cdot \eta_{comb} \cdot h^L}{m_1(t)} \tag{2.17}$$

$$\eta_q(t) = 1 - (1 - \eta_{q_{nom}}) \cdot \frac{n_{e_{nom}}}{n_e(t)} \tag{2.18}$$

To calculate the part of the heat release at constant volume X_{cv} equation 2.19 is used. $X_{cv_{grad}}$ is a constant with a negative value. This means that the relative portion of heat released at the constant volume stage of the combustion becomes smaller as the engine speed increases. To calculate the part of heat released at constant temperature (X_{ct}) equation 2.21 is used. Observing this equation shows that the portion of the total heat released during the isothermal expansion increases when more fuel is added. While the temperature at the start of compression is assumed constant it is dependent on the steady state temperature after the intercooler and temperature of the inlet duct, in accordance to equation 2.22.

$$X_{cv}(t) = X_{cv_{nom}} + \left(\frac{n_e(t) - n_{e_{nom}}}{n_{e_{nom}}} - 1 \right) \cdot X_{cv_{grad}} \tag{2.19}$$

$$X_{cv_{nom}} = \frac{c_{v,a} \cdot T_1 \cdot r_c^{\kappa_a - 1} \cdot \left(\frac{p_{max_{nom}}}{p_{1_{nom}} \cdot r_c^{\kappa_a}} - 1 \right) \cdot m_{1_{nom}}}{\eta_q(t) \cdot m_{f_{nom}} h^L} \tag{2.20}$$

$$X_{ct}(t) = X_{ct_{nom}} \cdot \frac{m_f(t)}{m_{f_{nom}}} \tag{2.21}$$

$$T_1 = T_c + \epsilon_{inl} \cdot (T_{inl} - T_c) \tag{2.22}$$

Seiliger cycle

To calculate work that is needed/delivered in the cylinder during the the compression, combustion and expansion phases the six stage Seiliger cycle is used. To calculate the total work the six stage Seiliger cycle divides the closed cylinder process into a polytropic compression (1-2), isochoric combustion (2-3), isobaric combustion (3-4), isothermal combustion (4-5) and polytropic expansion (5-6). It is assumed that the gas behaves as an ideal gas and is of homogeneous composition. The work described in equation 2.42 is the specific work in watt per kilogram of mass flow through the cylinder.

Seiliger stage	Volume	Pressure	Temprature	Specific work	Heat
1-2 Compression	$\frac{V_1}{V_2} = r_c$	$\frac{p_2}{p_1} = r_c^{\kappa_a}$	$\frac{T_2}{T_1} = r_c^{\kappa_a - 1}$	$w_{12} = \frac{R_a \cdot (T_2 - T_1)}{\kappa_a - 1}$	-
2-3 Isochoric Combustion	$\frac{V_2}{V_3} = 1$	$\frac{p_3}{p_2} = a$	$\frac{T_3}{T_2} = a$	-	$q_{23} = c_{v,a} \cdot (T_3 - T_2)$
3-4 Isobaric Combustion	$\frac{V_3}{V_4} = b$	$\frac{p_4}{p_3} = 1$	$\frac{T_4}{T_3} = b$	$w_{34} = R_a \cdot (T_4 - T_3)$	$q_{34} = c_{p,a} \cdot (T_4 - T_3)$
4-5 Isothermal Combustion	$\frac{V_4}{V_5} = c$	$\frac{p_4}{p_5} = c$	$\frac{T_5}{T_4} = 1$	$w_{45} = R_a \cdot T_4 \cdot ln(c)$	$q_{45} = R_a \cdot T_4 \cdot ln(c)$
5-6 Expansion	$\frac{V_5}{V_6} = \frac{r_{eo} \cdot r_c}{b \cdot c}$	$\frac{p_5}{p_6} = \left(\frac{r_{eo} \cdot r_c}{b \cdot c} \right)^{n_{exp}}$	$\frac{T_5}{T_6} = \left(\frac{r_{eo} \cdot r_c}{b \cdot c} \right)^{n_{exp} - 1}$	$w_{56} = \frac{R_a \cdot (T_6 - T_5)}{n_{exp} - 1}$	-

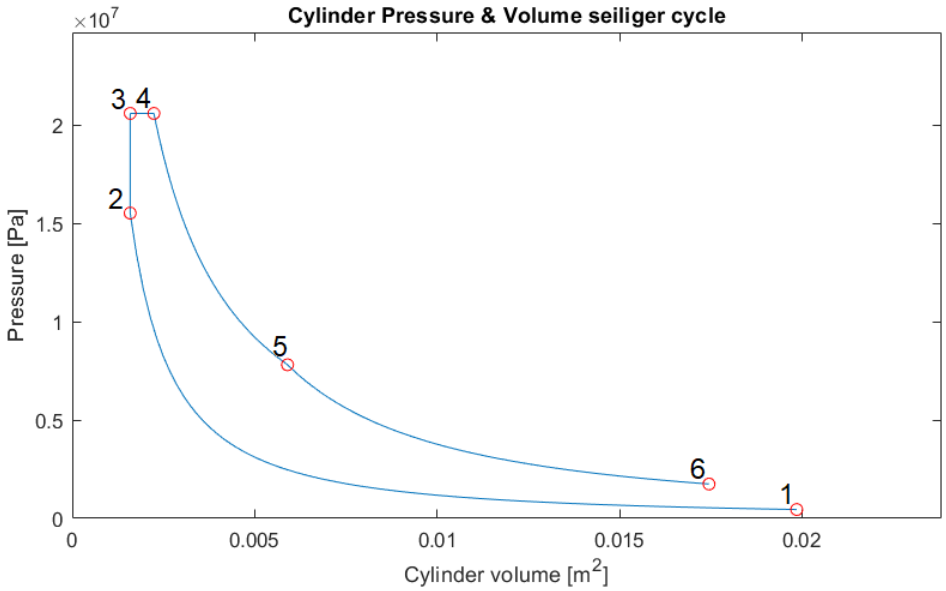

Figure 2.4: P-V diagram diesel engine

Exhaust receiver and turbocharger

The model described by Geerstma *et al.* uses *Zinner* blowdown to represent the process of blowdown after the exhaust valve opens, gas expelling during the exhaust stroke and scavenging after the inlet opens. The *Zinner* blowdown temperature (T_{bld}) as described in equation 2.23 uses a polytropic expansion coefficient which allows for heat loss to the cylinder, exhaust valve and exhaust duct. $p_{d,s}$ is the equilibrium pressure in the exhaust receiver. To calculate the exhaust receiver temperature ($T_d(t)$) equation 2.24 is used. The exhaust receiver temperature is the result of the combustion gasses expelled from the cylinder mixed with the scavenge flow that slips through the cylinder. For the temperature of the air that flows through the cylinder during scavenging temperature of at the start of combustion (T_1) is used.

$$T_{bld}(t) = \left(\frac{1}{n_{bld}} + \frac{n_{bld}-1}{n_{bld}} \cdot \frac{p_{d,s}(t)}{p_6(t)}\right) \cdot T_6(t) \tag{2.23}$$

$$T_d(t) = \frac{c_{p_g} \cdot T_{bld}(t) \cdot \big(m_1(t) + m_f(t)\big) + c_{p_a} \cdot T_{slip} \cdot s_{sl}(t) \cdot m_1(t)}{c_{p_g} \cdot \big(m_1(t) + m_f(t)\big) + c_{p_a} \cdot s_{sl}(t) \cdot m_1(t)} \tag{2.24}$$

The slip ratio (s_{sl}) is calculated using equation 2.25. The nominal slip ratio ($S_{sl_{nom}}$) is estimated using the normal air ($\dot{m}_{1_{nom}}$) and fuel ($\dot{m}_{f_{nom}}$) flow and depicted in equation 2.26. The non-dimensional scavenge flow which assumes isentropic flow trough a nozzle and choking above critical pressure is represented by equation 2.29.

$$s_{sl}(t) = s_{sl_{nom}} \cdot \frac{n_{e_{nom}}}{n_e(t)} \cdot \frac{m_{1_{nom}}}{m_1(t)} \cdot \frac{p_1(t)}{p_{1_{nom}}} \cdot \frac{\Psi_{sc}(t)}{\Psi_{sc_{nom}}} \tag{2.25}$$

$$S_{sl_{nom}} = \frac{\dot{m}_{t_{nom}} - (\dot{m}_{1_{nom}} - \dot{m}_{f_{nom}})}{\dot{m}_{1_{nom}}} \tag{2.26}$$

$$\dot{m}_{1_{nom}} = \frac{p_{1_{nom}} \cdot V_1 \cdot i_e \cdot n_e}{R_a \cdot T_1 \cdot k_e} \tag{2.27}$$

$$\dot{m}_{f_{nom}} = m_{bsfc_{nom}} \cdot p_{nom} \tag{2.28}$$

$$\Psi_{sc}(t) = \sqrt{\frac{2\kappa_g}{\kappa_g - 1}} \cdot \sqrt{\left(\frac{p_d(t)}{p_1(t)}\right)^{\frac{2}{\kappa_g}} - \left(\frac{p_d(t)}{p_1(t)}\right)^{\frac{\kappa_g+1}{\kappa_g}}} \tag{2.29}$$

To calculate the pressure before the turbine the pressure in the exhaust receiver (p_d) is calculated using a first order differential equation 2.30. The time delay (τ_{dp}) represents the time it takes for the considerable volume of the exhaust receiver to fill. The air swallow characteristics of the turbine determines the pressure before the turbine. The equilibrium pressure ($p_{d,s}$) is calculated using the elliptic law as shown in equation 2.31. The effective area of the turbine (A_{eff}) is fitted in the nominal operating point using the exhaust receiver pressure from the FAT data. As stated in the engine description [15] the MAN 28/33d STC incorporates two identical turbochargers. One turbocharger alone supplies sufficient charge air in low and medium speed running modes. The second turbocharger provides additional charged air at higher speeds. To simulate the usage of this sequential turbocharging system the effective area of the turbine is halved with respect to the nominal operating point for the lower rpm region.

$$\frac{\mathrm{d}p_d(t)}{\mathrm{d}t} = \frac{p_{d,s}(t) - p_d(t)}{\tau_{dp}} \tag{2.30}$$

$$p_{d,s}(t) = \sqrt{\frac{R_g \cdot T_d(t) \cdot \left(s_{sl}(t) \cdot \dot{m}_1(t) + \dot{m}_f(t)\right)^2}{\alpha_Z^2 \cdot A_{eff}^2} + p_{ex}^2} \tag{2.31}$$

$$\dot{m}_1(t) = m_1(t) \cdot i_e \cdot \frac{n_e(t)}{k_e} \tag{2.32}$$

$$\dot{m}_f(t) = m_f(t) \cdot i_e \cdot \frac{n_e(t)}{k_e} \tag{2.33}$$

To calculate the charge pressure (p_1) at stage one of the Seiliger cycle the first order differential equation 2.34 is used. The inertia related time delay (τ_{TC}) represents the time it takes for the turbocharger to reach equilibrium speed and pressure. The equilibrium turbocharger pressure ($p_{1,s}$) is calculated using equation 2.35. The equilibrium turbocharger pressure ratio (π_{com_s}) is estimated using the büchi power and flow balance, neglecting the losses in the inlet duct, filter and air cooler as shown in equation 2.36. The pressure ratio is calculated as described by Stapersma *et al.* [25] p.375 with a variable turbocharge efficiency based on a lookup table form FAT data, dependent on p_1. The lookup table for the turbocharge efficiency is determined by rewriting equations 2.35 till 2.39.

$$\frac{\mathrm{d}p_1(t)}{\mathrm{d}t} = \frac{p_{1,s}(t) - p_1(t)}{\tau_{TC}} \tag{2.34}$$

$$\pi_{com_s} = \frac{p_{1,s}(t)}{p_{amp}} \tag{2.35}$$

$$\pi_{com_s}(t) = \left(1 + \delta_f(t) \cdot \chi_g \cdot \eta_{TC}(t) \cdot r_{T_{TC}}(t) \cdot \left(1 - \frac{1}{\pi_{tur}^{\frac{\kappa_g - 1}{\kappa_g}}}\right)\right)^{\frac{\kappa_a}{\kappa_a - 1}} \tag{2.36}$$

$$\pi_{tur}(t) = \frac{p_d(t)}{p_{ex}} \tag{2.37}$$

$$r_{T_{TC}}(t) = \frac{T_d(t)}{T_{amb}} \tag{2.38}$$

$$\delta_f(t) = 1 + \frac{m_f(t)}{(1 + s_{sl}) \cdot m_1(t)} \tag{2.39}$$

Mechanical conversion
Equation 2.40 represents the torque delivered to the shaft. The specific work (w_i) derived in the Seiliger cycle is used. The specific work calculated in equation 2.42 is per unit of mass flow through a cylinder, per cylinder, per working stroke. Equation 2.41 is used to calculate the indicated moment that is produced by all the cylinders in the four-stroke engine combined. The losses are simplified by Geertsma to be dependent of engine speed only. Geertsma states that a model using both piston speed and mean effective pressure would directly relate engine losses to the load and speed of the engine. This approach would be more accurate, however this would also require more engine data which is unavailable. The losses are fitted to the nominal power at nominal speed.

$$M_e(t) = M_i(t) - M_{loss}(t) \tag{2.40}$$

$$M_i(t) = \frac{w_i(t) \cdot m_1(t) \cdot i_e}{k_e \cdot 2\pi} \tag{2.41}$$

$$w_i = w_{12} + w_{34} + w_{45} + w_{56} \tag{2.42}$$

$$M_{loss} = M_{loss_{nom}} \cdot \left((1 - M_{loss_{grad}}) + M_{loss_{grad}} \cdot \frac{n_e(t)}{n_{e_{nom}}} \right) \tag{2.43}$$

2.3. The Induction machine

To model the induction machine (IM) it has been determined in the literature research [14] that a circuit based model will be used. The model presented by Ong *et al.* 1998 is selected because of the possibility of predicting transient behavior and the fast calculation time. This circuit model for the induction machine does not explicitly include iron core losses, saturation or the possibility of fault modeling. Iron core losses are not the dominant losses at high loads. Iron core losses would be interesting in a study aiming at maximizing the efficiency, however this study does not focus on the efficiency of the control strategy. The equations are therefore not not rewritten to include the core losses. Within the operating envelope of the induction machine saturation does not occur. The control used will maintain the induced magnetic fields within the operating envelope, never operating with saturation. Therefore the exclusion of saturation is not a problem for this research. Fault modeling, such as burnt through isolation or flooding (short circuits) is not possible. This study is interested in the ships' dynamic response to different control strategies, therefore the lack of fault modeling is not a problem.

To supply the power to the induction machine a modern variable frequency drive is used, with a timescale in the order of milliseconds ($1 \cdot 10^{-3} s$). The timescale of the acceleration of the ship is in the tens of seconds ($1 \cdot 10^{1} s$), the timescale of the diesel dynamics is in seconds ($1 \cdot 10^{0} s$) and the timescale of the induction motor is in tenths of seconds ($1 \cdot 10^{-1} s$). The smaller time scale of the power supply compared to the mechanical parts of the ship imply that the dynamics of the power supply will have a negligible influence on the actual acceleration of the ship. Therefore the variable frequency drive is not modeled. Moreover, solving a system of with large time scale differences can result in numerical challenges. It is therefore assumed that the induction machine is fed with an ideal voltage source with balanced three phase power. This means that all three phases heave the same peak voltage (amplitude) and frequency, are sinusoidal distributed and have a phase shift of precisely 120 ° with respect to each other. The diesel generator side of the electrical power grit is outside the scope of this research and therefore not modelled. The resulting power demand from the induction machine during operations will be assessed against known generator specifications.

2.3.1. Induction machine parameters

Moto is used to calculate the parameters of the 3 MW induction motor. Moto is a parameter estimation tool that can be used to determine the equivalent circuit parameters of induction machines. The tool is intended for use in dynamic time-domain simulations such as stability and motor starting studies. Moto needs to be provided with the 'shape' of the power curve in terms of ratio between nominal, short-circuit and breakdown torque. Moto gives the equivalent circuit parameters that results in this behaviour. However using the parameters of Moto gives a the starting current, and thus the starting torque that is too high. Since this implementation of the induction motor does not use the starting torque this higher starting torque does not influence the accuracy of the model.

General parameters				**Equivalent circuit parameters**			
Nominal power	P_{IM}	3.0	MW	Stator resistance	R_s	$3.9 \cdot 10^{-3}$	ohm
Line to Line voltage Δ	U_{IM}	660	V	Rotor resistance	R_r	$3.5 \cdot 10^{-3}$	ohm
Synchronous speed	N_{syn}	100	RPM	Mutual inductance	L_m	$5.7 \cdot 10^{-3}$	H
Rated speed	N_{rat}	97.5	RPM	Stator self inductance	L_{ls}	$3.87 \cdot 10^{-4}$	H
Full load power factor	ϕ_{fl}	0.84	P/S	Rotor self inductance	L_{lr}	$1.82 \cdot 10^{-4}$	H
Full load efficiency	η_{fl}	0.939					
Breakdown torque ratio	T_{max}/T_{nom}	1.6					
Machine poles	p	16	#				

Table 2.2: Induction machine parameters

2.3.2. Clarke Park transformation

A model is chosen that represents the voltages and currents in their direct, quadrature and zero (QD0) components. Therefore to get from the three phase (abc) to the QD0 representation a Clarke Park transformation is needed. Since the power generation is not included, the final model does not perform this transformation, but rather directly provides the direct and quadrature voltages. To validate the model in a direct on line situation the transformation from three phases into the QD0 representation is modeled.

The division in quadrature and direct current is possible because the three phase voltages produce a single rotating magnetic field which can be represented by a vector with two independent parameters. The standard two parameters are: the angle representing the direction to which the magnetic field is orientated at that instant, and the length of the vector representing the field strength. This rotating magnetic field can also be represented in a reference frame which rotates at the synchronous speed of the rotor field, using a component in line with the rotor field and a component octagonal to the rotor field, the direct and quadrature components respectively.

Clarke transformation

$$\begin{bmatrix} U_\alpha \\ U_\beta \end{bmatrix} = \frac{2}{3} \begin{bmatrix} 1 & -\frac{1}{2} & \frac{1}{2} \\ 0 & \frac{\sqrt{3}}{2} & -\frac{\sqrt{3}}{2} \end{bmatrix} \begin{bmatrix} U_a \\ U_b \\ U_c \end{bmatrix} \tag{2.44}$$

Park transformation

$$\begin{bmatrix} U_q \\ U_d \end{bmatrix} = \begin{bmatrix} -sin(\theta) & cos(\theta) \\ cos(\theta) & sin(\theta) \end{bmatrix} \begin{bmatrix} U_\alpha \\ U_\beta \end{bmatrix} \tag{2.45}$$

2.3.3. Induction machine equations

The equations used to model the induction motor are basic circuit based correlations. The equivalent circuit of an induction motor represented in the qd reference frame is depicted in Figure 2.5. Although these equations can be written out to represent the currents and voltages in any reference frame, the choice is made to use the synchronous reference frame. This reference frame rotates with the induced field in the rotor. This equivalent circuit is described by equations 2.50 till 2.56. These voltage equations are a summation of three parts. The first part is the instantaneous voltage across the inductor, which is the voltage associated with the change of flux linkage over time. The basic form of the voltage across the inductor is shown in equation 2.49. The second part is the EMF which is due to the reference frame is made out of components. The basic form is shown in equation 2.47. The last part is the voltage-loss over the resistance of the conductor, in accordance to Ohm's law as shown in equation 2.48. The flux linkage shown equation 2.54 is the matrix representation of the basic equation 2.46. Equation 2.54 shows that a given flux linkage is produced by the magnetizing inductance of both the stator and the rotor as well as the leakage inductance of the stator or the rotor. Equations 2.55 and 2.56 describe the torque produced by the induction machine. Due to the usage of the voltages invariant Clarke-Park transformation a factor $\frac{3}{2}$ appears in these torque equations. As stated before a balanced supply is assumed therefore the zero sequence current can be neglected. The zero sequence equations are therefore omitted from the equations described by Ong *et al.* 1998. This results in the equivalent circuit depicted in Figure 2.5 and equations 2.50 till 2.56.

$$\lambda = L \cdot i \tag{2.46}$$

$$V_{EMF} = \omega \cdot \lambda \tag{2.47}$$

$$V_{ohm} = r \cdot i \tag{2.48}$$

$$V_{ind} = \frac{\mathrm{d}i}{\mathrm{d}t} \cdot L = \frac{\mathrm{d}\lambda}{\mathrm{d}t} \tag{2.49}$$

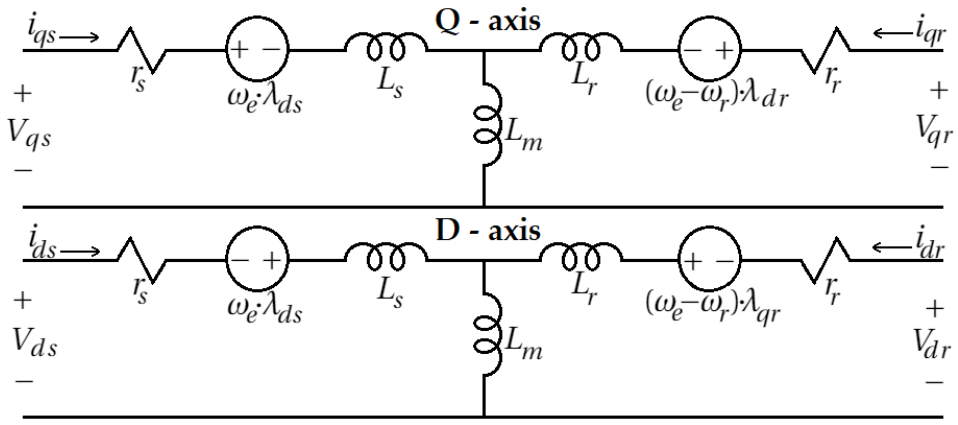

Figure 2.5: Induction machine equivalent circuit

Stator voltage equations

$$V_{qs} = \frac{\partial \lambda_{qs}}{\partial t} + \omega_e \cdot \lambda_{ds} + r_s \cdot i_{qs} \tag{2.50}$$

$$V_{ds} = \frac{\partial \lambda_{ds}}{\partial t} - \omega_e \cdot \lambda_{qs} + r_s \cdot i_{ds} \tag{2.51}$$

Rotor voltage equations

$$V_{qr} = \frac{\partial \lambda_{qr}}{\partial t} + (\omega_e - \omega_r) \cdot \lambda_{dr} + r_r \cdot i_{qr} \tag{2.52}$$

$$V_{dr} = \frac{\partial \lambda_{dr}}{\partial t} - (\omega_e - \omega_r) \cdot \lambda_{qr} + r_r \cdot i_{dr} \tag{2.53}$$

Flux linkage equation

$$\begin{bmatrix} \lambda_{qs} \\ \lambda_{ds} \\ \lambda_{qr} \\ \lambda_{dr} \end{bmatrix} = \begin{bmatrix} L_s + L_m & 0 & L_m & 0 \\ 0 & L_s + L_m & 0 & L_m \\ L_m & 0 & L_r + L_m & 0 \\ 0 & L_m & 0 & L_r + L_m \end{bmatrix} \begin{bmatrix} i_{qs} \\ i_{ds} \\ i_{qr} \\ i_{dr} \end{bmatrix} \tag{2.54}$$

Torque equations

$$T_{em} = \frac{3}{2}\frac{P}{2}\left(\lambda_{qr} \cdot i_{dr} - \lambda_{dr} \cdot i_{qr}\right) \tag{2.55}$$

$$T_{em} = \frac{3}{2}\frac{P}{2}\left(\lambda_{ds} \cdot i_{qs} - \lambda_{qs} \cdot i_{ds}\right) \tag{2.56}$$

2.3.4. Implementation

This section describes the MATLAB-Simulink® implementation for the equations provided in section 2.3.3 which describe the induction machine. Figure 2.6 shows the overview of the induction model. The output value of the model is the torque delivered to the shaft of the machine. The first input variable (1) is the power supply frequency in radians per seconds. The second input variable (2) is the supply voltage in the direct and quadrature reference frame in volts. The third input variable (3) is the mechanical rotational speed of the rotor in radians per seconds. The mechanical rotational speed (ω_{r_m}) of the rotor needs to be converted to the electrical rotational speed (ω_{r_e}) via equation 2.59. There are two input constants, namely the direct and quadrature rotor voltage as shown in equations 2.57 and 2.58. Both the quadrature and direct voltage are zero due to the usage of a squirrel cage rotor which is short circuited at its ends. The stator voltage and the rotor voltages are combined into a single vector. From the voltage vector the result of the cross coupling EMF and the voltage reduction due to Ohm's law is subtracted. This result is integrated to find the flux linkage λ. Equation 2.60 shows this implementation and is a rewritten form of equations 2.50 till 2.53.

$$V_{dr} = 0 \tag{2.57}$$

$$V_{qr} = 0 \tag{2.58}$$

$$\omega_{r_e} = \frac{P}{2} \cdot \omega_{r_m} \tag{2.59}$$

$$\begin{aligned} \lambda_{qs} &= \int \left(V_{qs} - \omega_e \cdot \lambda_{ds} - r_s \cdot i_{qs}\right) dt \\ \lambda_{ds} &= \int \left(V_{ds} + \omega_e \cdot \lambda_{qs} - r_s \cdot i_{ds}\right) dt \\ \lambda_{qr} &= \int \left(V_{qr} - (\omega_e - \omega_r) \cdot \lambda_{dr} - r_r \cdot i_{qr}\right) dt \\ \lambda_{dr} &= \int \left(V_{dr} + (\omega_e - \omega_r) \cdot \lambda_{qr} - r_r \cdot i_{dr}\right) dt \end{aligned} \tag{2.60}$$

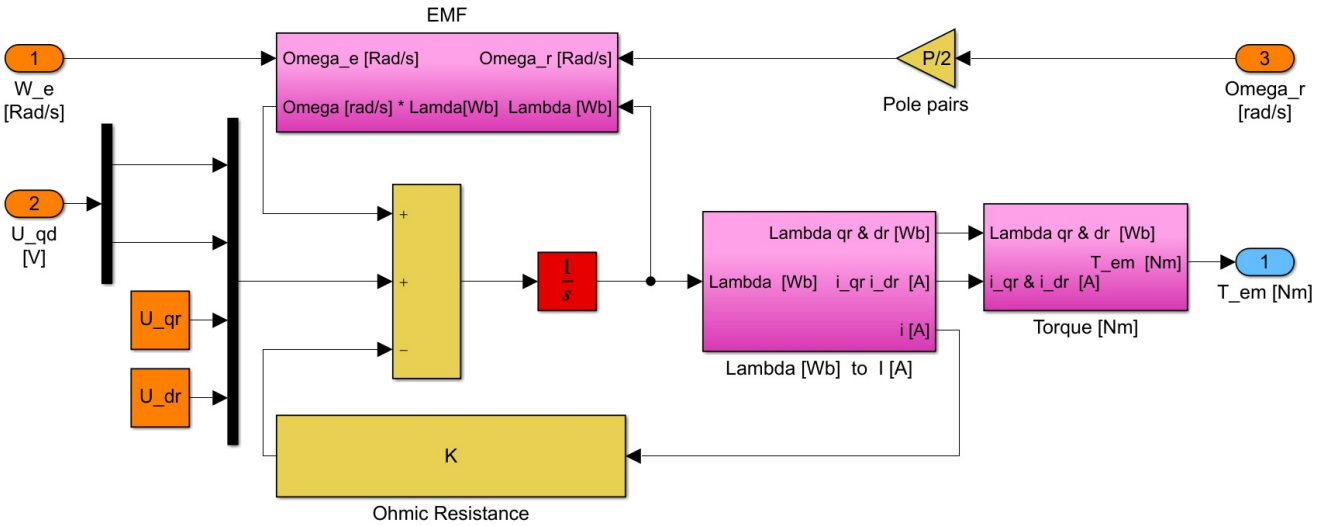

Figure 2.6: Overview Induction machine model

In the previous section both the voltage associated with the cross coupling EMF and the voltage drop due to ohmic resistances were used. Figure 2.7 shows the implementation of the calculations for voltage associated with the cross coupling EMF. This is the matrix equivalent of equation 2.47 and is rewritten as shown in equation 2.61. To calculate the voltage drop due to ohmic resistance depicted as (K) in Figure 2.6, equation 2.62 is solved.

$$\begin{bmatrix} -\omega_e \cdot \lambda_{ds} \\ \omega_e \cdot \lambda_{qs} \\ -(\omega_e - \omega_r) \cdot \lambda_{dr} \\ (\omega_e - \omega_r) \cdot \lambda_{qr} \end{bmatrix} = \begin{bmatrix} 0 & -\omega_e & 0 & 0 \\ \omega_e & 0 & 0 & 0 \\ 0 & 0 & 0 & -(\omega_e - \omega_r) \\ 0 & 0 & (\omega_e - \omega_r) & 0 \end{bmatrix} \begin{bmatrix} \lambda_{qs} \\ \lambda_{ds} \\ \lambda_{qr} \\ \lambda_{dr} \end{bmatrix} \tag{2.61}$$

$$\begin{bmatrix} r_s \cdot i_{qs} \\ r_s \cdot i_{ds} \\ r_r \cdot i_{qr} \\ r_r \cdot i_{dr} \end{bmatrix} = \begin{bmatrix} r_s & 0 & 0 & 0 \\ 0 & r_s & 0 & 0 \\ 0 & 0 & r_r & 0 \\ 0 & 0 & 0 & r_r \end{bmatrix} \begin{bmatrix} i_{qs} \\ i_{ds} \\ i_{qr} \\ i_{dr} \end{bmatrix} \tag{2.62}$$

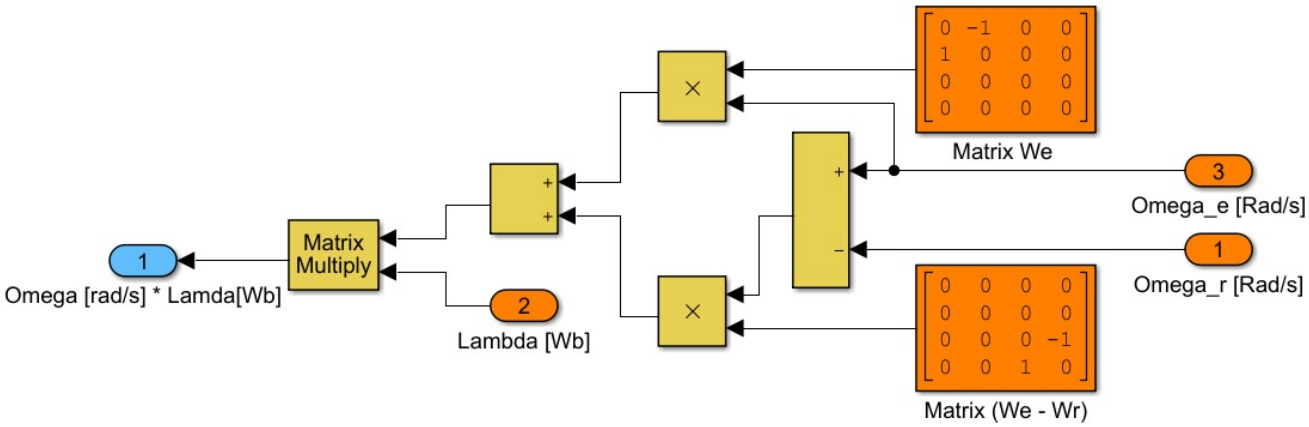

Figure 2.7: Cross coupling EMF

To calculate the current equation 2.63 is used. This a rewritten form of equation 2.54. The stator and rotor currents are used to calculate the voltage loss due to ohmic resistance as was shown in equation 2.62. To calculate the torque that is delivered by the induction machine, the rotor currents are used as is stated in equation 2.55 and is depicted in Figure 2.9. During the validation process the internal friction was known from the machine data, this friction is subtracted from the produced torque.

$$\begin{bmatrix} i_{qs} \\ i_{ds} \\ i_{qr} \\ i_{dr} \end{bmatrix} = \begin{bmatrix} L_s + L_m & 0 & L_m & 0 \\ 0 & L_s + L_m & 0 & L_m \\ L_m & 0 & L_r + L_m & 0 \\ 0 & L_m & 0 & L_r + L_m \end{bmatrix}^{-1} \begin{bmatrix} \lambda_{qs} \\ \lambda_{ds} \\ \lambda_{qr} \\ \lambda_{dr} \end{bmatrix} \tag{2.63}$$

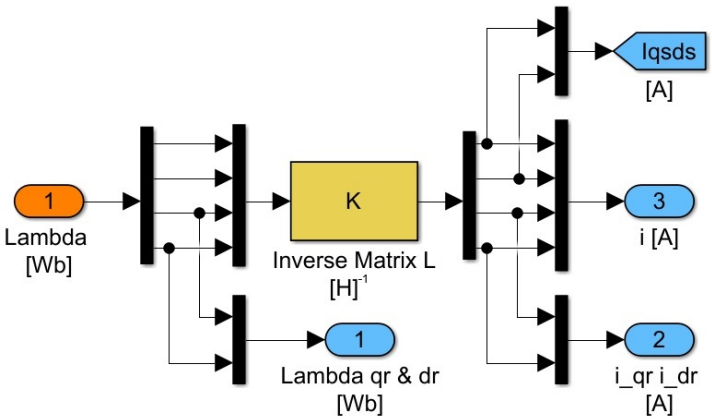

Figure 2.8: Lambda to current

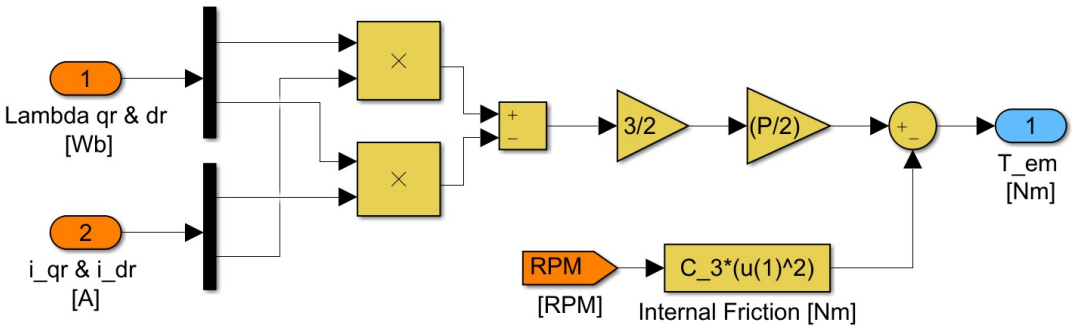

Figure 2.9: Torque production

2.3.5. Validation

To validate the model simulations were performed with an induction machine from which the operating current, voltage and power factor were known. This data is available from the manufacturer. The general characteristics of this induction machine are summarized in Table 2.3. The existing induction machine had a full test report containing the static operating results, the locked rotor and short circuit test. The stator resistance is directly measured while the other parameters were calculated based on the locked rotor and no load test. The estimated parameters are also shown in Table 2.3. Figure 2.10 shows the by the induction machine produced torque at a fixed supply frequency and variable slip, as well as the design load which uses the rated power at the rated speed.

General parameters				**Equivalent circuit parameters**			
Nominal power	P_{IM}	1.325	MW	Stator resistance	R_s	$8.25 \cdot 10^{-4}$	ohm
Line to Line voltage Δ_{RMS}	U_{IM}	450	V	Rotor resistance	R_r	$7.91 \cdot 10^{-4}$	ohm
Rated current	I_{rat}	1920.8	A	Mutual inductance	L_m	$1.86 \cdot 10^{-3}$	H
Synchronous speed	N_{syn}	1812.0	RPM	Stator self inductance	L_{ls}	$4.76 \cdot 10^{-5}$	H
Rated speed	N_{rat}	1801.3	RPM	Rotor self inductance	L_{lr}	$3.138 \cdot 10^{-5}$	H
Full load power factor	ϕ_{fl}	0.92	P/S				
Machine poles	p	4	#				

Table 2.3: Validation data induction machine

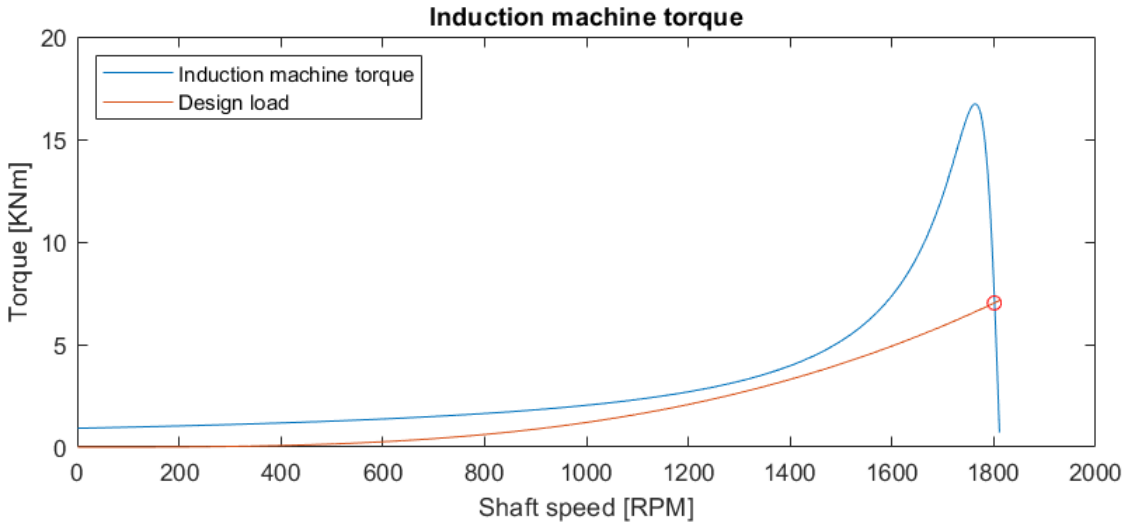

Figure 2.10: Induction machine Torque at variable slip

Tests on the above described induction machine are performed under two circumstances. The first simulation tests the model in static design condition at design torque and power, using field oriented control. Field oriented control is described in Chapter 3 section 3.2. The results of the steady state test in design conditions are displayed in Table 2.4. The second simulation uses the induction machine in direct on line conditions, directly connecting the induction machine to the net frequency of 60.4 hz at the voltage of 446.48 V which was needed to reach the design steady state. The first simulation which operates the induction at design speed and rated torque shows the needed supply frequency, voltage and power factor at the steady state. It can be observed that the needed voltage and the resulting current which are needed to produce the rated torque are slightly lower than the manufacturer documented. However an accuracy of 99% and 98% is accurate enough for the purpose of this research. The simplification of the equivalent circuit as shown in Figure 2.5 explains the small difference between the manufacturer data and the simulation results. Especially the elimination of the core losses, which would form a parallel path to the torque producing current is an explanation for the lowered stator current. The second simulations shows the start up in direct on line conditions. The simulation shows a very characteristic acceleration of the rotor and shaft. At first the stator field is very fast with respect to the rotor. The induced current and resulting magnetic field in the slowly rotating rotor is subjected to a very fast rotating stator field. The first 2 seconds the combination of the very slow rotor field and fast stator field produce a large torque that fluctuates in direction. This large torque makes the rotor vibrate while

it slowly speeds up. Near the rated speed and slip the rotor experiences the torque peak visible in Figure 2.10 before it snaps into the steady state rotor/slip position with respect to the stator field. This characteristic behavior of the induction machine implies that the model correctly represents both the steady state as dynamics of an induction motor.

Induction machine design load test				**Accracy**	
Produced mechanical power	P_{IM}	1.3250	MW	100.00	%
Supplied voltage Δ_{RMS}	U_{IM}	446.48	V	99.22	%
Delivered current	I_{IM}	1884.44	A	98.11	%
Synchronous speed @ supply frequency	N_{syn}	1812.01	RPM	100.00	%
Achieved speed	N_{rat}	1801.31	RPM	100.00	%
Power factor	ϕ_{fl}	0.9213	P/S	99.86	%

Table 2.4: Static test: Validation data induction machine

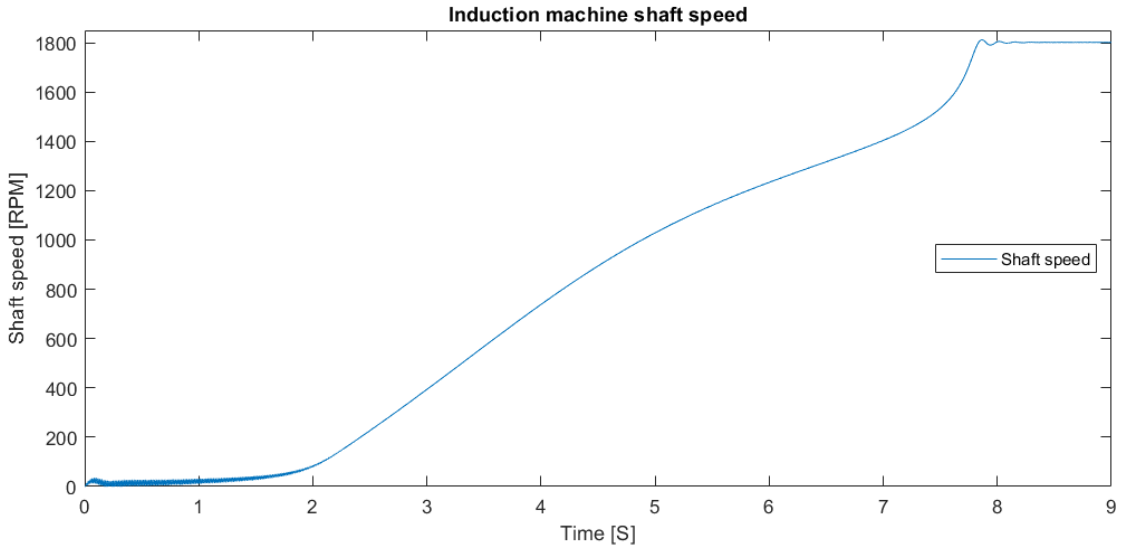

Figure 2.11: Dynamic test: Induction machine start up to design conditions

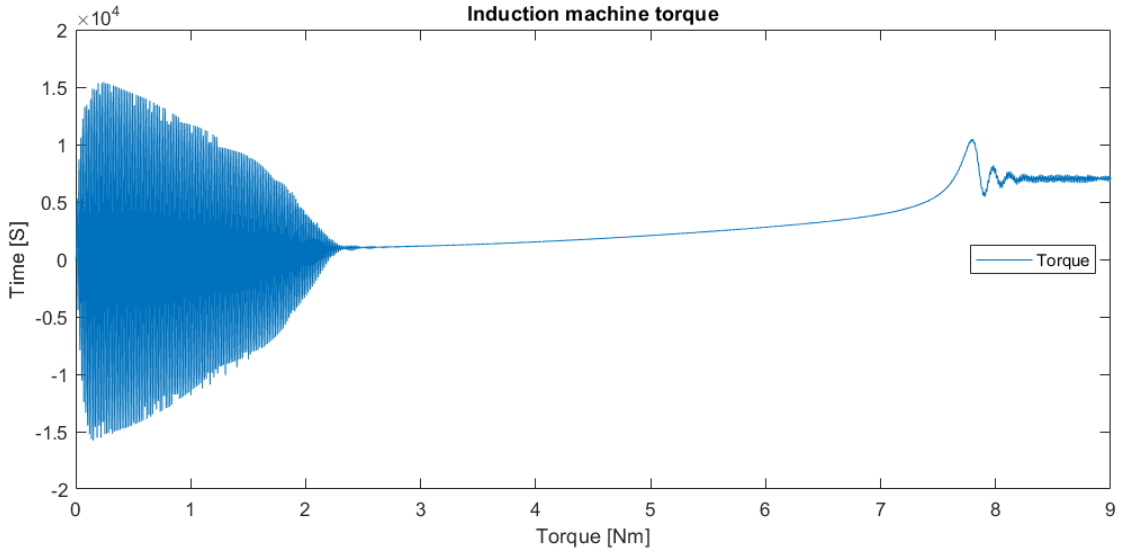

Figure 2.12: Dynamic test: Induction machine start up to design conditions

2.4. Gearbox, propeller and hull

To model the gearbox, propeller and the hull well known equations are used. Therefore these parts of the model are lumped together in short descriptions below. This section mostly uses Newton's second law of motion or rotation. Finally the combined power of the diesel engine and the electric motor is matched to the propeller in subsection 2.4.4.

2.4.1. Gearbox

The gearbox is modelled by implementing Newton's second law for rotation. The model uses a fixed efficiency for the transmission and shaft barrings. This a fixed efficiency and thus linearly increasing of the losses is a rough simplification of the real losses. A more accurate model can be achieved with a non linear correlation or the usage of heuristic estimates based on manufacturer data. It is assumed that a more accurate model would change the absolute outcome in the order of 1 - 3% but would not change the relative outcome between the different control strategies. The first order differential equation 2.64 shows the implementation of the shaft dynamics using a lumped inertia and therefore not modeling stiffness and vibration characteristics. The sum of the moment is taken at the propeller side, defined as stated in equation 2.65. The moment of the diesel engine Q_{DE} is reduced with the losses in the gearbox as well as the friction due to losses from the shaft barrings. The induction machine is located on the propeller shaft therefore there are now gearbox losses, there are however shaft baring losses which reduce the induction machine torque Q_{IM}.

$$\frac{\mathrm{d}n_{shaft}}{\mathrm{d}t} = \frac{\sum Q}{J_{tot}} \cdot \frac{1}{2\pi} \tag{2.64}$$

$$\sum Q = \left(Q_{DE} \cdot \eta_{gb} \cdot I_{gb} + Q_{IM}\right) \cdot \eta_{sh} - Q_P \tag{2.65}$$

2.4.2. Propeller

The goal of the propeller model is to calculate the thrust (T) as well as the torque (Q). The thrust determines the acceleration of the ship while the torque determines the engine load and the acceleration of the driving motors. To determine the thrust and torque the well established open water test data from the Wageningen c series produced by MARIN is used. The torque and thrust coefficients as traditionally determined for normal forward operation are defined as a function of the advance ratio (J). However the traditional open water diagram does not cover all operational modes possible with a CP propeller. The CP angle is capable of operating in four quadrants. The blade position in Figure 2.13 (b) can generate forward thrust at positive ship speed and forward thrust at negative ship speed. The blade position in Figure 2.13 (C) can generate reverse thrust at positive ship speed and reverse thrust at negative ship speed. The operation in all four quadrants means that the advance ratio is not suited to describe the complete operating area. Equation 2.74 shows the advance ratio (J) in which the rotational speed of the propeller (n_p) and the diameter of the propeller (D) are beneath the dividing line. When the rotational speed of the propeller is close to zero the advance ratio is close to infinite, resulting in unusable thrust and torque coefficients. MARIN uses thrust (C_T^*) and torque (C_Q^*) coefficients as a function of hydrodynamic pitch angle (β) that describe the entire four quadrant operation of the propeller. The thrust and torque coefficients are shown in equations 2.68 and 2.69 [34]. The thrust and torque coefficients are available in four quadrants and are variables of angle β. The characteristics of the Wagening C5-75 propeller are made available by DSNS. This is a Wageningen c propeller with five blades, a projected area of EA/AO = 0.75 and a design pitch of PD = 1.4

Propeller model

The propeller of a ship produces hydrodynamic thrust similar to the way an airplane wing produces lift. Due to the shape of the propeller blade and the angle of attack a pressure difference exists between the front- and backside of the propeller. The resulting force produced by the pressure differential across the blades are divided into the propeller's thrust and torque. Propeller thrust is the effective lift in the longitudinal direction of the ship. The torque is the drag and induced resistance that is associated with the rotation of an object through the water and the creation of lift respectively. Controlling the pitch angle varies the angle at which the resulting flow encounters the propeller blades. The angle at which the flow encounters the propeller is the main parameter that determines the amount of thrust and torque produced by the propeller. Figure 2.13 (a) shows the resulting flow velocity (V_R) on the propeller blade. V_R is a result of the vector summation of flow speed originating from the rotational speed (V_c) and advance speed (V_A). In the lifting line theory [21] the angle of attack (α) is used to calculate the lift produced by a wing. Changing the pitch is done by rotating the propeller blades. The actuation system of the propeller is simulated using a first order differential equation with a time constant of 1.7 seconds. This approach has only a limited accuracy, it was however found that

varying the settling time for the propeller did not result in large differences in acceleration. As mentioned above the thrust (T) and torque (Q) are calculated using well established four quadrant open water test results (Wageningen C) as defined in equations 2.68 and 2.69. Using the hydrodynamic pitch angle (β) to look up the corresponding lift and torque coefficients as defined in equation 2.66.

$$\beta = arctan\left(\frac{V_A}{0.7\pi \cdot n_p \cdot D}\right) \tag{2.66}$$

$$V_a = (1-w) \cdot V_s \tag{2.67}$$

$$T = C_T^* \cdot \frac{1}{2}\rho\left(V_A^2 + \left(0.7\pi \cdot n_p \cdot D\right)^2\right)\frac{\pi}{4} \cdot D^2 \tag{2.68}$$

$$Q = C_Q^* \cdot \frac{1}{2}\rho\left(V_A^2 + \left(0.7\pi \cdot n_p \cdot D\right)^2\right)\frac{\pi}{4} \cdot D^3 \tag{2.69}$$

(a) Flow velocities (b) Positive pitch angle [23] (c) Negative pitch angle [23]

Figure 2.13: Blade positions of a controllable pitch propeller

2.4.3. Hull

The ships acceleration ($\frac{dV_s}{dt}$) is calculated with Newton's second law of motion as depicted in equation 2.70. The resistance is dependent on the ship speed, a simple multiplication factor (Y) is used for the added resistance due to sea-state. Waves are not included in the model.

$$\frac{dV_s(t)}{dt} = \frac{K_p \cdot T_p - \frac{R(t)}{1-t}}{m_{ship}} \tag{2.70}$$

$$R(t) = Y \cdot C_1 \cdot V_S(t)^2 \tag{2.71}$$

2.4.4. Matching

Matching is done to deliver the combined power of the diesel engine and induction machine to the propeller at a shaft speed at which the propeller is able to transfer that power onto the water. When matching the propeller power demand and the available power of the engines an engine margin is used. This means the amount of continually available power from the engines is larger than the propeller needs in design conditions. Usually an engine margin that lies between 0.8 and 0.9 is used for fixed pitch propellers [34]. With fixed pitch propellers an engine margin is necessary to prevent the engines from overloading in off-design conditions. Off-design conditions include but are not limited to sea state, a change in displacement, sailing at restricted water depth and Hull fouling, which increases over time. Because the ship discussed in this report uses a CP propeller the overloading of the diesel engine can be avoided by reducing the pitch of the propeller. Reducing the pitch would however also mean a reduced maximum speed. It is desirable to be able to reach the design speed in a sea state above zero, or other resistance increasing factors. Therefore the design condition is defined with an increase in hull resistance of 9 % ($Y = 1.09$). Even though a CP propeller is used the matching is performed using the advance ratio (J) for normal forward operation as described by Woud *et al.* 2012. The propeller lift C_t^* and torque C_q^* constants which are defined in the four quadrant open water diagram are dependent on hydrodynamic inflow angle beta β and in order to use these constants, they need to be rewritten. The propeller constant needs to be rewritten into the thrust K_t and torque K_q coefficient dependent on J as is shown in equations 2.72 and 2.73. The hydrodynamic pitch angle can be converted into the advance ratio (J) using equation 2.75.

$$K_t = C_T^* \cdot \frac{\pi}{8}\left(J^2 + (0.7\pi)^2\right) \tag{2.72}$$

$$K_q = C_q^* \cdot \frac{\pi}{8}\left(J^2 + (0.7\pi)^2\right) \tag{2.73}$$

$$J = \frac{V_A}{n_p \cdot D} \tag{2.74}$$

$$J = 0.7\pi \cdot tan\left(\beta \cdot \frac{\pi}{180}\right) \tag{2.75}$$

$$K_{T,ship} = \frac{1}{\rho \cdot D^2} \cdot \frac{Y \cdot C_1}{k_p \cdot (1-t) \cdot (1-w)^2} \cdot J^2 \tag{2.76}$$

Solving equations 2.76 and 2.72 for the advance ratio (J) gives the shaft speed of the propeller at the design speed of the ship in accordance to equation 2.74, resulting in the following standard matching: the two propellers have a design pitch/diameter of 1.4 which propel the ship to 27.06 kn at a rotational speed of the diesel engines of 1050 rpm. At this rotational speed of the diesel engines the propellers and the induction machines have a rotational speed of 384.9 rpm meaning a gearbox with ratio i = 6.4155 is needed.

Gearbox, propeller and hull parameters

Drag coefficient	C_1	5896	$\frac{N}{m^2 \cdot s^2}$
Ship mass	m_{ship}	$5200 \cdot 10^3$	Kg
Thrust deduction	t	0.06	
Wake factor	w	0.02	
Relative rotative efficiency	η_r	1	
Propeller diameter	D_p	4.8	m
Propeller design pitch	P/D_{des}	1.4	
Zero thrust pitch	P/D_0	0.255	
Shock free entry angle	α_i	3.0	deg
Diesel engine speed	N_{De}	1050.0	RPM
Induction machine speed	N_{Im}	163.7	RPM
Propeller shaft speed	N_p	163.7	RPM
Gearbox ratio	i_{gb}	6.4155	
Gearbox efficiency	$\eta_g b$	0.98	
Shaft bearing losses	$\eta_s h$	0.99	
Design ship speed	V_s	27.06	kn

Table 2.5: gearbox, propeller and hull parameters

3

Subsystem control

The overall drivetrain used to propel the ship at the desired speed is build up by the diesel engine, induction motor and CP propeller. These subsystems need to be controlled on a machine level in order fulfill the setpoint given to them which can be a speed, pitch or torque level. This chapter discusses the different control methods used to control the diesel engine, induction motor and CP propeller. First in section 3.1 the control for the diesel engine is discussed. Secondly, the control for the electric drive is discussed in section 3.2. Finally the control for the CP propeller is discussed in section 3.3.

3.1. The Diesel engine

This section describes torque and speed control for the diesel engine. The input for control of the diesel engine is the fuel rack position. Section 3.1.1 describes the engine limits as set by the control, making sure the performance of the modeled engine does not exceed the performance of the actual engine. Theoretically both torque and speed control are viable options to control the diesel engine [14]. Torque control provides advantages regarding the overloading in sea-state, however it needs additional measures to prevent under- and overspeed. An additional advantage of torque control is the possibility of using speed control for faster reacting drivers, without creating an undefined static power balance. At the time this thesis is written torque control for the diesel engine is not available from the engine manufacturer. The difference in performance regarding the acceleration of the ship has been studied by Geertsma *et al.* 2016 and showed promising results. Therefore both torque and speed control are included in this thesis to be combined with new control mode variations and combinations. Both the speed and torque control use a PI-controller.

Speed control

Speed control is the convectional control for diesel engines. Speed control is used because it provides overspeed protection as well as giving the ship operator an intuitive and nearly linear relationship between lever settings and the resulting ship speed. As stated before PI-control is used for the speed control of the diesel. With speed control the setpoint is the desired engine speed (n_{set}) with the actual engine speed (n_{fb}) as feedback signal. The controller output is the unlimited fuel lever setpoint X_{set}. Anti wind-up is used to prevent large overshoots when the controllers fuel setpoint exceeds the limits as described in section 3.1.1. The fuel lever setpoint which is allowed to go to the fuel pump after the three limiters is denoted by W_{fb} and used as input for the anti wind-up. The mathematical description for the PI-controller is given in equation 3.1

$$X_{set} = K_P \cdot \frac{n_{set}(t) - n_{fb}(t)}{n_{nom}} + K_I \cdot \int_0^t \left(\frac{n_{set}(t) - n_{fb}(t)}{n_{nom}} \right) dt \tag{3.1}$$

Torque control

Using torque control for the diesel engine is discussed by multiple sources [29] [22] [6] . For the implementation discussed in this research the availability of a torque sensor is assumed. The torque sensor provides a feedback signal representing the torque that the diesel engine is delivering M_{fb}. The torque that the diesel engine is currently delivering is compared to the torque which is demanded by the control M_{set}. The controller output is the unlimited fuel lever setpoint X_{set}. Anti wind-up is used to prevent large overshoots when

the controllers fuel setpoint exceeds the limits. When the fuel demand exceeds the limits discussed in section 3.1.1 the error term that is integrated is reduced while the proportional error signal multiplied with K_p remains unchanged. In order to normalize the inputs for the PI-controller the error in torque is divided by the maximum torque M_{max} that can be delivered by the diesel engine. The mathematical description for the PI-controller is given in equation 3.2

$$X_{set} = K_P \cdot \frac{M_{set}(t) - M_{fb}(t)}{M_{max}} + K_I \cdot \int_0^t \left(\frac{M_{set}(t) - M_{fb}(t)}{M_{max}} \right) dt \tag{3.2}$$

3.1.1. Diesel engine limits

To make sure the performance of the modelled diesel engine does not exceed the performance of the actual engine three limiters are introduced. All limiters restrict the fuel flow toward the diesel engine. First, The engine envelope as shown in Figure 3.1 is implemented. For the implementation a lookup table is made for the maximum amount of fuel that is allowed to be injected into the cylinders. This lookup table defined for all engine speeds between 300 and 1050 rpm and compensated for the specific efficiency at that engine speed in such a way that precisely the maximum power is delivered. The control will prevent under- and overspeed, however minimal under and overspeed might still occur. Therefore the power envelope is extrapolated. For underspeed this means a strongly decreasing maximum power output. For overspeed this means a constant power output, resulting in a linearly decreasing allowed maximum fuel input. For application in high performance vessels such as the naval vessel discussed in this thesis range III is available resulting in 10 MW of power for a 20 cylinder configuration.

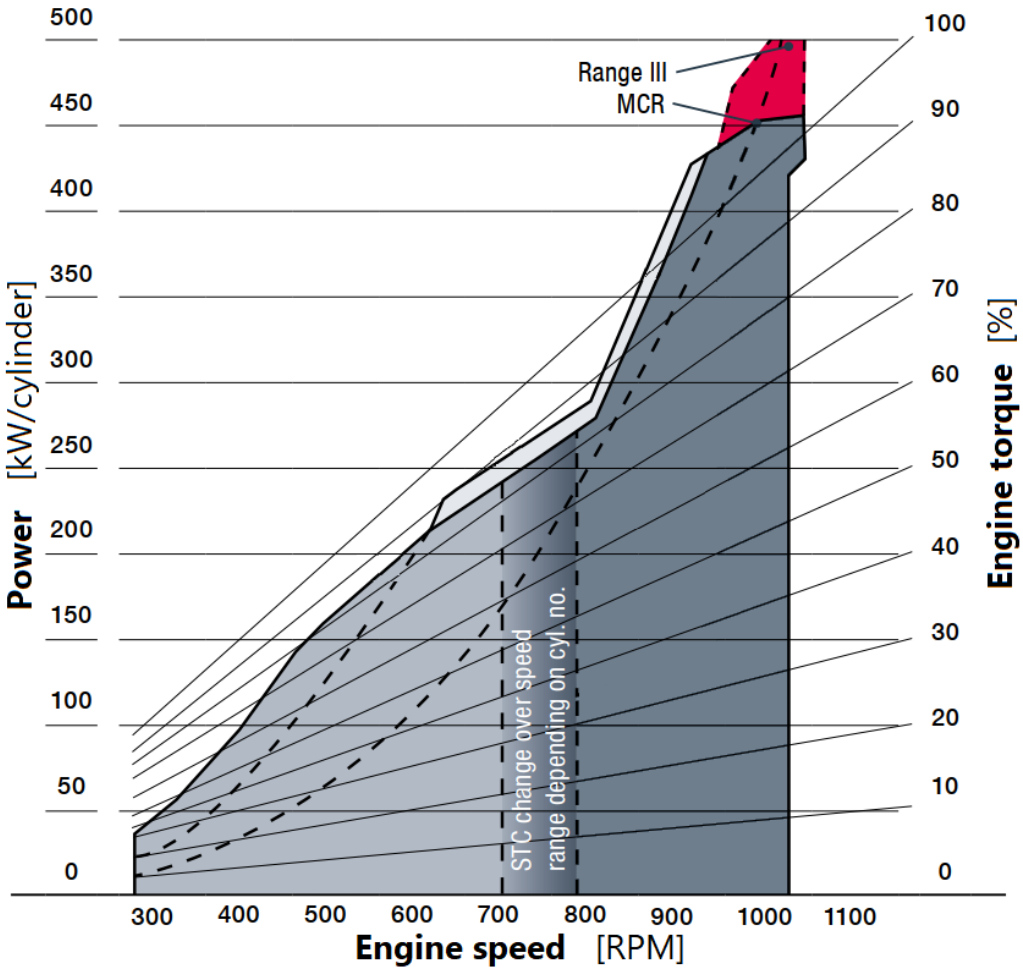

Figure 3.1: Engine envelope MAN V2833D STC

Low air excess ratio (λ) will result in incomplete combustion and thus soot forming. Nanda *et al.*2017 identifies a low air excess ratio as the cause of voluminous flame production, which in turn leads to high surface temperatures of engine components resulting in a high thermal loading and more maintenance. Nanda stated that adverse effects occur at air excess ratios as high as $\lambda = 1.2$. Therefore the minimal air excess ratio $\lambda = 1.3$ is used as fuel injection limit. Equations 2.4 till 2.6 are rewritten to calculate the maximum fuel input ($m_{f_{max,\lambda}}$) as depicted in equation 3.3. In the automotive industry an oxygen sensor is used, directly measuring the excess air, such a sensor is however sensitive for soot formation. During the starting phase of the diesel engine soot formation is almost inevitable, meaning that oxygen sensors are not used for marine applications. Therefore the charge pressure is used for the implementation of this fuel injection limiter, simulating the usage of a pressure sensor.

$$m_{f_{max,\lambda}}(t) = \frac{p_1(t) \cdot V_1}{R_a \cdot T_1 \cdot \sigma_f} \cdot \frac{1}{\lambda_{min}} \tag{3.3}$$

The final fuel injection limit is determent by the maximum power increase per unit of time allowed ($\frac{\mathrm{d}p}{\mathrm{d}t}$). As a guidance the manufacturer dictates a maximum power increase from 10% load to 100% load in 90 seconds. The implementation of this limit is simplified to a maximum increase in fuel injection. The maximum increase of fuel mass flow is 10% to 100% in 90 seconds. It is chosen to work with the maximum power increase allowed because we are interested in maximum acceleration in combat situation, therefore the increased maintenance from such a manoeuvre is acceptable.

3.2. The Induction machine

To control the induction machine field orientated control (FOC) is used. The choice for FOC is explained in the literature research [14]. This section of the report first describes the FOC in detail, after which the PI-controller for the current is discussed in section 3.2.3. The limitations are discussed in section 3.2.3. Finally it is explained how torque and speed control are achieved in sections 3.2.4 and 3.2.5.

3.2.1. Field orientated control

This section shows the derivation for the implementation of FOC. First the working principle behind FOC is briefly discussed. After which each element used with FOC is derived, each element of the derivation ends with the equation that is implemented.

Working principle

FOC uses a two axis reference frame which represents the three phase sinusoidal voltages and currents in a quadrature and direct components. The quadrature current is the current which produces a magnetic field that is orthogonal to the magnetic field of the rotor. The direct component of the current is producing a magnetic field which is in line with the magnetic field of the rotor.

The magnetic fields of the rotor and stator are at the lowest energy state when these magnetic fields are aligned. When the stator and rotor fields are misaligned there will be a resultant magnetic force which is directed to align the rotor field with the stator field. The resultant magnetic force is at its maximum when the rotor and stator fields are orthogonal with respect to each other.

The quadrature current of the stator produces a magnetic field that is per definition at 90 degrees to the magnetic field of the rotor, meaning that the quadrature current is the torque producing current. The direct current is per definition in line with the rotor field, therefore this is a non torque producing current. Since this research uses an induction machine the direct current is used to induce a current through the rotor, resulting in the rotor field. FOC keeps the d-axis of the rotor as close to 90 degrees to the q-axis of the stator as possible, generating the maximum amount of torque for a given current.

Deriving torque equation

The rotor of the induction machine is a squirrel cage, meaning that there are no slip rings and therefore no direct ways to measure or set the rotor currents. The stator current is directly measurable, and therefore suited for control with feedback. For efficient operation and maximum torque the direct current of the stator (i_{ds}) is controlled to be precisely the amount to induce a fully developed rotor field (λ_{dr}) onto the d-axis, while the field on the q-axis of the rotor remains zero ($\lambda_{qr} = 0$). The quadrature component of the stator current (i_{qs}) is set to produce the desired torque.

The torque equations 2.55 and 2.56 given by Ong *et al.* [20] describe the produced torque with either both the stator current and flux or both the rotor current and flux. As described above when using FOC the stator current and the rotor flux have known values, therefore equation 2.56 will be rewritten to include the rotor flux.

$$T_{em} = \frac{3}{2}\frac{P}{2}\left(\lambda_{ds} \cdot i_{qs} - \lambda_{qs} \cdot i_{ds}\right) \tag{3.4}$$

The stator flux linkages of both the q- and d- axis are substituted by their respective flux linkages and currents in accordance to equation 2.54, this results in the following equation:

$$T = \frac{3}{2} \cdot \frac{P}{2} \cdot (L_s \cdot i_{ds} \cdot i_{qs} + L_m \cdot i_{dr} \cdot i_{qs} - L_s \cdot i_{qs} \cdot i_{ds} - L_m \cdot i_{qr} \cdot i_{ds}) \tag{3.5}$$

Simplifying by eliminating terms that are equal but with opposite signs gives:

$$T = \frac{3}{2} \cdot \frac{P}{2} \cdot (L_m \cdot i_{dr} \cdot i_{qs} - L_m \cdot i_{qr} \cdot i_{ds}) \tag{3.6}$$

Adding and subtracting the following term $\frac{L_m^2}{L_r} \cdot i_{qs} \cdot i_{ds}$ will eventually lead to the desired terms in the final equation. This gives the following equation:

$$T = \frac{3}{2} \cdot \frac{P}{2} \cdot (\frac{L_m^2}{L_r} \cdot i_{qs} \cdot i_{ds} - \frac{L_m^2}{L_r} \cdot i_{qs} \cdot i_{ds} + L_m \cdot i_{dr} \cdot i_{qs} - L_m \cdot i_{qr} \cdot i_{ds}) \tag{3.7}$$

Extracting the term $\frac{L_m}{L_r}$ to be outside the brackets and rewriting results in:

$$T = \frac{3}{2} \cdot \frac{P}{2} \cdot \frac{L_m}{L_r} \cdot ((L_m \cdot i_{qs} \cdot i_{ds} + L_r \cdot i_{dr} \cdot i_{qs}) - (L_m \cdot i_{qs} \cdot i_{ds} + L_r \cdot i_{qr} \cdot i_{ds})) \tag{3.8}$$

Substituting λ_{dr} and λ_{qr} results in equation 3.9. This equation possesses all the needed terms for FOC and matches the equation given by Trzynadlowski *et al.* [28] p.121.

$$T = \frac{3}{2} \cdot \frac{P}{2} \cdot \frac{L_m}{L_r} \cdot (\lambda_{dr} \cdot i_{qs} - \lambda_{qr} \cdot i_{ds}) \tag{3.9}$$

Deriving q-axis stator current setpoint

For the power supply of the stator the electrical frequency ω_e as well as the stator voltages V_{ds} and V_{qs} need to be set. Although FOC is a known control method which is already used in industry, the frequency and voltages as can be used specifically for Ong's model [20] for an induction machine are derived below.

To calculate the amount of current needed for the induction machine to produce the desired torque (T_{IM}) equation 3.9 is rewritten. With FOC the full rotor field is induced on the d-axis, therefore the flux on the q-axis is zero $\lambda_{qr} = 0$. This is done so the produced torque is dependent on the quadrature stator current without the negative torque produced by the product of the direct stator current and quadrature rotor flux ($i_{ds} \cdot \lambda_{qr} = 0$). This gives the following equation for the stator current:

$$i_{qs} = \frac{T_{IM}}{\lambda_{dr}} \cdot \frac{2}{3} \cdot \frac{2}{P} \cdot \frac{L_r}{L_m} \tag{3.10}$$

Deriving d-axis stator current setpoint

Below the rated speed the rotor flux is kept constant at its nominal value, ensuring the torque (T_{IM}) is only dependent on the quadrature stator current (i_{qs}). Above the rated speed the back emf of the rotor becomes too large to overcome at rated voltage, meaning that to maintain the rated flux above rated speed would need a stator voltage above the rated value, which could damage the insulation of the stator windings. Therefore, above rated speed the rated voltage limits the torque produced by the induction motor. Above the rated speed the constant voltage and consequently the constant power region starts. In this operating region the rotor flux (λ_{dr}) is reduced to increase the rotor speed in accordace to Trzynadlowski *et al.* [28] p.162 as depicted in equation 3.11.

$$\lambda_{dr} = \begin{cases} \lambda_{dr_{rated}} & for \quad \omega_r(t) \leq \omega_{r_{rated}} \\ \lambda_{dr_{rated}} \cdot \frac{\omega_{r_{rated}}}{\omega_r(t)} & for \quad \omega_r(t) > \omega_{r_{rated}} \end{cases} \tag{3.11}$$

To derive the stator current setpoint which will lead to the desired rotor flux (λ_{dr}) the equation 2.54 is rewritten as follows.

$$\lambda_{dr} = L_m \cdot i_{ds} + (L_r + L_m) \cdot i_{dr} \tag{3.12}$$

$$i_{ds} = \frac{\lambda_{dr}}{L_m} - \frac{(L_r + L_m)}{L_m} \cdot i_{dr} \tag{3.13}$$

Equation 3.13 gives the stator current. This is however still a function of the rotor current, which due to the rotor being a squirrel cage rotor is not directly measurable. Therefore the equation 2.53 describing the d-axis rotor voltage with two simplifications is substituted. First the d-axis rotor voltage is zero ($V_{dr} = 0$) due to the rotor being short circuited at both ends. The second simplification is that FOC controls the q-axis rotor flux to be zero ($\lambda_{qr} = 0$). Implementing these simplifications gives equation 3.14 which is rewritten into equation 3.15. Substituting this equation into equation 3.13 gives the final equation for the d-axis stator current setpoint as depicted in equation 3.16.

$$0 = \frac{\partial \lambda_{dr}}{\partial t} + r_r \cdot i_{dr} \tag{3.14}$$

$$i_{dr} = -\frac{\partial \lambda_{dr}}{\partial t} \cdot \frac{1}{r_r} \tag{3.15}$$

$$i_{ds} = \frac{\lambda_{dr}}{L_m} + \frac{(L_r + L_m)}{L_m \cdot r_r} \cdot \frac{\partial \lambda_{dr}}{\partial t} \tag{3.16}$$

Deriving frequency setpoint

To derive the stator frequency ω_e equation 2.52 describing the q-axis current of the rotor is rewritten with two simplifications. First the q-axis rotor voltage is zero due to it being short circuited at the rotor ends. Second since the q-axis rotor flux is kept zero with FOC the derivative is also zero. Implementing the simplifications gives equation 3.17. Rewriting this equation gives an expression for the supply frequency ω_e.

$$0 = (\omega_e - \omega_r) \cdot \lambda_{dr} + r_r \cdot i_{qr} \tag{3.17}$$

$$\omega_e = -\frac{r_r}{\lambda_{dr}} \cdot i_{qr} + \omega_r \tag{3.18}$$

Equation 3.18 shows an expression for the supply frequency of the stator. It is important to note that the stated rotor speed ω_r is its electrical speed in radians per second (rad/s). To calculate the supply frequency using this formula the q-axis current of the rotor needs to be known. As stated previously there is no direct way of measuring of controlling the rotor current. Therefore equation 2.54 describing the q-axis rotor flux is used. Implementing the knowledge that the q-axis flux of the rotor is equal to zero ($\lambda_q r = 0$) gives equation 3.19, from which the q-axis rotor current can be extracted and substitute into equation 3.18, giving the final equation for the supply voltage frequency ω_e shown in equation 3.21

$$0 = L_m \cdot i_{qs} + (L_r + L_m) \cdot i_{qr} \tag{3.19}$$

$$i_{qr} = -\frac{L_m}{(L_r + L_m)} \cdot i_{qs} \tag{3.20}$$

$$\omega_e = \frac{r_r}{\lambda_{dr}} \cdot \frac{L_m}{(L_r + L_m)} \cdot i_{qs} + \omega_r \tag{3.21}$$

Axis decoupling

As discussed previously FOC calculates setpoints for the stator and rotor current, which is regulated using a stator current feedback signal and a PI-controller to set the stator voltages. It can be observed that in the equations for the q- and d-axis voltage the flux of the other axis is also present, meaning that at the moment a new torque setpoint is given the q-axis voltage (V_{qs}) is changed resulting in a new q-axis current (i_{qs}). This change would then affect the d-axis via the q-axis flux. Both voltage equations are repeated below for convenience. This "leakage" from one axis to the other leads to undesirable voltage, flux and torque fluctuations. Since this relationship is known and dependent on motor characteristics it can be eliminated with feed forward control. Hence this section describes the derivation and the compensation term used for the feed forward elimination of the cross-coupling between the axis.

$$V_{qs} = \frac{\partial \lambda_{qs}}{\partial t} + \omega_e \cdot \lambda_{ds} + r_s \cdot i_{qs}$$

$$V_{ds} = \frac{\partial \lambda_{ds}}{\partial t} - \omega_e \cdot \lambda_{qs} + r_s \cdot i_{ds}$$

Q-axis decoupling

The cross-coupling term for the q-axis stator voltage (V_{qs}) can be seen as the middle part of equation 2.50. This cross-coupling term is given in equation 3.22.

$$U_{qs_{cross}} = \omega_e \cdot \lambda_{ds} \tag{3.22}$$

Substituting the q-axis stator flux into equation 3.22 gives equation 3.23.

$$\omega_e \cdot \lambda_{ds} = \omega_e \cdot ((L_s + L_m) \cdot i_{ds} + L_m \cdot i_{dr}) \tag{3.23}$$

Equation 3.23 is dependent on the rotor current, which is not directly measurable. Therefore the d-axsis rotor current is rewritten to be dependent on the d-axis stator current. Using the d-axis rotor flux equation 2.54.

The derivation of the d-axis rotor current from the d-axis rotor flux equation can be seen below.

$$\lambda_{dr} = L_m \cdot i_{ds} + (L_r + L_m) \cdot i_{dr} \tag{3.24}$$

$$i_{dr} = \frac{\lambda_{dr}}{L_r + L_m} - \frac{L_m}{L_r + L_m} \cdot i_{ds} \tag{3.25}$$

The expression for the d-axis rotor current of equation 3.25 is substituted into equation 3.23 and rewritten. This gives the final expression for the feed-forward decoupling voltage ($U_{qs_{comp}}$). This decoupling voltage needs to be added to the voltage setpoint for the q-axis of the stator. The expression for the decoupling voltage is described in equation 3.26.

$$U_{qs_{cross}} = \omega_e \cdot \left(i_{qs} \cdot \left(L_s + L_m - \frac{L_m^2}{L_r + L_m} \right) + \frac{L_m \cdot \lambda_{dr}}{L_r + L_m} \right) \tag{3.26}$$

D-axis decoupling
The cross-coupling term for the d-axis stator voltage (V_{ds}) can be seen as the middle part of equation 2.51. This cross-coupling term is given in equation 3.27.

$$U_{ds_{cross}} = \omega_e \cdot \lambda_{qs} \tag{3.27}$$

Implementing the q-axis stator flux into equation 3.27 gives:

$$\omega_e \cdot \lambda_{qs} = \omega_e \cdot ((L_s + L_m) \cdot i_{qs} + L_m \cdot i_{qr}) \tag{3.28}$$

Equation 3.28 is dependent on the rotor current, which is not directly measurable. Therefore the q-axsis rotor current is rewritten to be deppendent on the q-axis stator current. Using the q-axis rotor flux equation 2.54 with the simplification that the q-axis rotor flux is equal to zero ($\lambda_{qr} = 0$). The derivation of the q-axis rotor current from the q-axis rotor flux equation can be seen below.

$$0 = L_m \cdot i_{ds} + (L_m + L_s) \cdot i_{dr} \tag{3.29}$$

$$i_{qr} = -\frac{L_m}{L_r + L_m} \cdot i_{qr} \tag{3.30}$$

The expression for the q-axis rotor current of equation 3.30 is substituted into equation 3.28 and rewritten. This gives the final expression for the feed-forward decoupling voltage ($U_{ds_{comp}}$). This de-coupling voltage needs to be subtracted from the voltage setpoint for the d-axis of the stator. The expression for the de-coupling voltage is described in equation 3.31.

$$U_{ds_{comp}} = -\omega_e \cdot i_{qs} \cdot \left(L_s + L_m - \frac{L_m^2}{L_r + L_m} \right) \tag{3.31}$$

3.2.2. Equations field orientated control

Below the equations used to implement FOC are repeated. The quadrature axis current setpoint is determined using equation 3.32. The direct axis current setpoint is determined using equation 3.33. The supply frequency of the variable frequency drive is set in accordance to equation 3.34. The voltages that will be demanded from the variable frequency drive are controlled using PI-controllers that are described in section 3.2.3. This voltage will be compensated to reduce the cross-coupling between the axis with equations 3.35 and 3.36.

$$i_{qs} = \frac{T_{IM}}{\lambda_{dr}} \cdot \frac{2}{3} \cdot \frac{2}{P} \cdot \frac{L_r}{L_m} \tag{3.32}$$

$$i_{ds} = \frac{\lambda_{dr}}{L_m} + \frac{(L_r + L_m)}{L_m \cdot r_r} \cdot \frac{\partial \lambda_{dr}}{\partial t} \tag{3.33}$$

$$\omega_e = \frac{r_r}{\lambda_{dr}} \cdot \frac{L_m}{(L_r + L_m)} \cdot i_{qs} + \omega_r \tag{3.34}$$

$$U_{qs_{cross}} = \omega_e \cdot \left(i_{qs} \cdot \left(L_s + L_m - \frac{L_m^2}{L_r + L_m} \right) + \frac{L_m \cdot \lambda_{dr}}{L_r + L_m} \right) \tag{3.35}$$

$$U_{ds_{comp}} = -\omega_e \cdot i_{qs} \cdot \left(L_s + L_m - \frac{L_m^2}{L_r + L_m} \right) \tag{3.36}$$

3.2.3. Current control in FOC

To control the current that flows through the induction machine a series PI-controller is used. The proportional gain and the integral gain are based on the inductance and resistance of the induction machine to achieve an good controller. The choosing of the control parameters is done using the inductance and resistance parameters of the motor in accordance with Texas instruments [33]. The mathematical description of the PI-controller that is used to set the stator voltage on the q- and d-axis is given in equation 3.37 and 3.38.

$$U_{qs,set} = (L_{ls} + L_m) \cdot \left(\left(I_{qs,set} - I_{qs,fb} \right) + \frac{R_s}{L_{ls} + L_m} \int \left(I_{qs,set} - I_{qs,fb} \right) dt \right) \tag{3.37}$$

$$U_{ds,set} = (L_{ls} + L_m) \cdot \left(\left(I_{ds,set} - I_{ds,fb} \right) + \frac{R_s}{L_{ls} + L_m} \int \left(I_{ds,set} - I_{ds,fb} \right) dt \right) \tag{3.38}$$

Current limiter

The current setpoints that are generated by the FOC equations 3.32 and 3.33 still need to be bound to limitations. When too much torque is demanded for the induction machine the current demand from the FOC becomes too high. When the total current demand is too high the current setpoint for the d-axis is maintained while the current setpoint for the q-axis is limited in accordance to equation 3.39. Preserving the current through the d-axis maintains the magnetic field on the rotor.

$$I_{qs,max} = \sqrt{I_{max}^2 - I_{ds,set}^2} \tag{3.39}$$

Voltage Limiters

The PI-controller setpoint for the voltage is combined with the compensating voltage to decouple the q- and d- axis. To make sure the resulting voltage demand does not exceed the limitation of the induction machine a voltage limitation is implemented. This voltage limitation limits the voltage magnitude while preserving the phase of both the q- and d-axis.

3.2.4. Torque control

Torque control for the induction machine is achieved with setting the requested torque from the global control as input for a PI-controller. This PI-controller with anti wind-up and a limitation for the maximum torque sets a torque setpoint directly to the previously discussed FOC drive.

3.2.5. Speed control

Speed control for the induction machine using FOC can be achieved by cascaded PI-control. Providing an increased or decreased torque setpoint to the FOC diver depending on the difference between shaft speed setpoint and the actual shaft speed feedback. In general it can be stated that speed control for the induction machine should not be combined with speed control for the diesel engine. Operating both systems in speed control could lead to fluctuating loads between the diesel engine and induction machine. This fluctuating load would be the result of an improperly defined system. In such a system both the diesel engine and the induction machine could account for an increasing load, decreasing load, or the reduction in power provided by the other motor. When the induction machine is operated with speed control the diesel engine will need to deliver a torque close to the actual propeller load. The diesel engine (10 MW) delivers this power to ensure the lower power (3 MW) of the induction machine is capable of adding enough torque to reach the required shaft speed. The mathematical description of PI-controller to control the shaft speed is given in equation 3.40

$$T_{set} = K_P \cdot \frac{n_{set}(t) - n_{fb}(t)}{n_{nom}} + K_I \cdot \int_0^t \left(\frac{n_{set}(t) - n_{fb}(t)}{n_{nom}} \right) dt \tag{3.40}$$

3.2.6. Dynamic torque control

As stated above speed control could lead to an ill defined mathematical problem in which both the diesel engine and the induction machine will try to maintain the desired shaft speed. During testing it became apparent that the inherent quality of fast torque production of the induction machine generates better results with speed control. The diesel engine on the other hand suffers from overloading when the load increases too quickly. Therefore when operating the diesel engine in speed control, which is available from manufacturers, it would be beneficial to use the fast torque generating capabilities of the induction machine. The fast torque generating capabilities of the induction machine could be used to aid in producing the peak torque during acceleration. Therefore even when speed control for the diesel engine is used a speed loop which aids during the acceleration of the ship is beneficial. The induction machine possesses both a torque control loop and a speed loop. To avoid creating an ill defined mathematical problem the speed loop for the induction machine is created to only possess a proportional (K_P) control. The speed loop for the diesel engine contains both a proportional (K_P) and integral (K_I) gain, in which the integral gain will be dominant. Such a controller uses the inherent fast torque producing capabilities of the induction machine to produce torque in accordance to a proportional gain for the high frequency load fluctuations. After which the diesel engine controlled which is mainly integrating control will account for the low frequency load changes and eliminates the steady state error in the shaft speed. When the shaft speed is reached the induction machine will only produce the amount of torque set for the steady state balance controlled by the torque control loop. The speed loop for the induction machine will simply add an additional torque setpoint via cascaded control to the steady state torque distribution set during matching. The mathematical description of this P- speed PI- torque controller is given in equation 3.41 and 3.42 .

$$T_{set,dyn} = K_P \left(N_{set} - N_{fb} \right) \tag{3.41}$$

$$IM_{T,set} = K_P \left(T_{set} + T_{set,dyn} - T_{fb} \right) + K_I \int \left(T_{set} + T_{set,dyn} - T_{fb} \right) dt \tag{3.42}$$

3.3. Propeller

During the research phase, three control modes for the propeller are used. Firstly, a combinator curve is used. In total two combinator curves are tested. The second control mode is adaptive pitch control (APC). APC uses the possibility of controlling the pitch to maintain the desired angle of attack. To assess the limitation for the acceleration when fixed pitch propeller is used a third operation mode of the CP propeller is tested. In this third operation mode the pitch of the CP propeller is fixed at its design pitch of P/D =1,4, mimicking a fixed pitch propeller.

3.3.1. Combinator control

During acceleration manoeuvres the propeller has a higher load due to the higher angle of attack. The load the propeller puts on the engine can't be allowed to exceed the engine envelope. To prevent the propeller load from exceeding the engine envelope precautionary measures are implemented. The first measure is ensuring enough engine margin in the form of clearance between the steady state propeller load and the engine envelope. The second measure is limiting the rate of change in lever setpoint the ship. By lowering the pitch a CP propeller can widen the gap between the engine envelope and the propeller curve, allowing for faster engine acceleration and therefore faster power availability. Two combinators are used during the simulation.

The usage of a CP propeller makes the thrust that the propeller generates dependent on two parameters, the shaft speed and the pitch angle. Vrijdag *et al.* 2010 described that the ship speed behaves almost linearly with the virtual shaft speed. Virtual shaft speed as expressed in equation 3.43 is a function that links the pitch settings and the actual shaft speed. In this equation the nominal pitch is denoted by θ_{nom} , the current pitch is denoted by θ and the pitch at which the propeller produces zero thrust is denoted by θ_0.

$$n_{virt} = \frac{\theta - \theta_0}{\theta_{nom} - \theta_0} \cdot n \tag{3.43}$$

The first combinator is set on the design pitch and can be seen in simulation number 1 of chapter 4. To accommodate low speed setpoints the pitch increases from the zero thrust pitch till design pitch (P/D = 1,4) at the minimum shaft speed, above the minimum shaft speed the pitch is kept constant at design pitch (P/D_{des}). This combinator is expected to be fuel efficient but leaves less margin for an increased propeller load during acceleration.

The second combinator implements a higher minimum rpm and a lower pitch setting and can be seen in simulation number 2 of chapter 4. To accommodate the speed setpoint the pitch increases from the zero thrust pitch (P/D_0) till a pitch of P/D = 1,2 at the minimum operational shaft speed of 400 RPM. Above this shaft speed the pitch increases linearly to full design pitch (P/D_{des} = 1,4) at full rpm (1050). This combinator is expected to be less fuel efficient but also cause a larger margin for acceleration.

3.3.2. Adaptive pitch control

Adaptive pitch control controls the propeller blade angle for optimal inflow of the water. Adaptive pitch control was first proposed by Vrijdag *et al.* 2010 to improve cavitation behavior and implemented with adaptations by Geertsma *et al.* 2018 to give better fuel efficiency and acceleration. The maintained angle of attack of the water onto the propeller blade ensures good cavitation characteristics, efficient power transfer and lowers the load from the propeller during acceleration. Adaptive pitch control is implemented without significant changes form Geertsma [9]. A short description of the control follows. Rewriting the virtual shaft speed from equation 3.43 gives the shaft speed setpoint presented in equation 3.44, which will be used for the diesel or electric motor speed control. Equation 3.44 has exchanged the pitch angle for the P/D setting. This modification is allowed since it is a relative scale between a fully pitched propeller and the zero thrust pitched propeller.

$$n_{set}(t) = \frac{P/D_{nom} - P/D_0}{P/D(t) - P/D_0} \cdot n_{virt,set} \tag{3.44}$$

Figure 3.2: Inflow angle on propeller

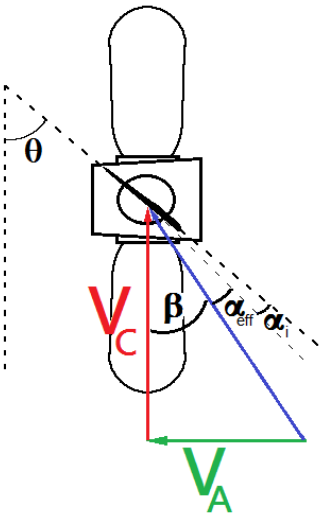

To get the desired angle of attack (α_{eff}) the propeller pitch angle (θ_p) set using the equations as defined by Vrijdag [30] as described below. Calculating the effective angle of attack of the water onto the propeller blades is done using equation 3.45. With β defined as the inflow angle of the water into the propeller plane. The Vrijdag coefficient in this research denoted with cv_1 is used to calibrate the effective angle of attack with the center point of the cavitation bucket. For this thesis the cavitation characteristics are out of scope. Therefore $cv_1 = 1$ is used both for determining the nominal effective angle of attack in design conditions and for controlling the effective angle of attack, meaning the effect of cv_1 cancels out. For the shock free inflow $\alpha_i = 3$ is used both for determining the nominal effective angle of attack in design conditions and for controlling the effective angle of attack. Figure 3.2 shows the inflow angles on a propeller blade. Both cv_1 and α_i are in correspondence with Geertsma *et al.* 2018 p.163. The propeller parameters are summarized in Table 2.5. The angle of the propeller (θ_p) is calculated at 70% of the radius using the pitch setting as described in equation 3.46.

$$\alpha_{eff}(t) = \Theta_p - \beta - \alpha_i \tag{3.45}$$

$$\Theta_p = arctan\left(\frac{P/D(t)}{0.7 \cdot \pi}\right) \tag{3.46}$$

$$\beta = arctan\left(\frac{cv_1 \cdot v_a(t)}{0.7 \cdot \pi \cdot n_p(t) \cdot D_p}\right) \tag{3.47}$$

PI-control with anti wind-up is used to control the propeller pitch. The mathematical description of the PI-controller is given in equation 3.48. The relative pitch setpoint ($P/D_{r,set}$) can be converted to the actual pitch setpoint as is described in equation 3.49, meaning that $P/D_{r,set} = 0$ corresponds to the zero thrust pitch and $P/D_{r,set} = 1$ corresponds to the design pitch. Equation 3.50 is used as the setpoint for the pitch angle. The feedback of the actual pitch is used to calculate the current pitch angle in accordance to equation 3.46.

$$P/D_{r,set} = K_p \frac{\Theta_{p,set}(t) - \Theta_{p,fb}(t)}{\Theta_{p,nom}} + K_I \int_0^t \left(\frac{\Theta_{p,set}(t) - \Theta_{p,fb}(t)}{\Theta_{p,nom}}\right) dt \tag{3.48}$$

$$P/D(t) = P/D_{r,set} \cdot (P/D_{des} - P/D_0) + P/D_0 \tag{3.49}$$

$$\Theta_{p,set}(t) = \alpha_{eff,set}(t) + \beta(t) + \alpha_i \tag{3.50}$$

$$\Theta_{p,fb} = arctan\left(\frac{P/D_{fb}(t)}{0.7 \cdot \pi}\right) \tag{3.51}$$

Control limitations

The minimum shaft speed combined with the design pitch results in a low ship speed. This ship speed is the minimum ship speed that is achievable with a design pitch. With conventional control in this region the shaft speed is the constant and changing the speed is achieved by varying the pitch angle. With adaptive pitch control the design angle of attack can not be maintaind at low speeds. At low speeds less thrust is required due to the low resistance. Maintaining the design angle of attack at the minimum rpm results in too much thrust, resulting i a larger ship speed that wanted. At low speeds the angle of attack is therefore reduced. To set the pitch that gives the wanted speed below the design angle of attack equation 3.52 is used. Furthermore the diesel or induction motor, depending on which of them is governed by speed control, protects the overall system from over- and underspeed, by controlling the fuel or voltage setpoints.

$$P/D_{r,max} = \frac{n_{virt,set}}{n_{shaft,min}} \tag{3.52}$$

4

Control scenarios

The primary focus of this chapter is to discuss the results obtained from the different control scenarios. Section 4.1 describes an overview of all simulations. This overview includes a short description of each control mode. These individual subsystem control modes were discussed in Chapter 3. Section 4.2 till section 4.13 describe each simulation scenario. For each scenario the results are discussed after which the control strategy is evaluated. In the scenario evaluation improvements for the next simulation are discussed, eventually resulting in a total of twelve scenarios.

4.1. Scenarios overview

Conventional diesel engine speed control with induction machine torque support			
Sim. no.	**Diesel engine control**	**Induction amchine control**	**Propeller control**
1	Speed control	Torque control	Transit pitch setpoints
2	Speed control	Torque control	Acceleration pitch setpoints
3	Speed control	Sweep of torque starting rpm	Transit pitch setpoints

Electrical speed control with diesel engine torque support			
Sim. no.	**Diesel engine control**	**Induction machine control**	**Propeller control**
4	Torque control	Speed control	Transit pitch setpoints
5	Sweep torque distribution	Speed control	Transit pitch setpoints

Adaptive pitch control			
Sim. no.	**Diesel engine control**	**Induction machine control**	**Propeller control**
6	Speed control slow	Torque control	Angle of attack control
7	Speed control fast	Torque control	Angle of attack control

Dynamic power split control			
Sim. no.	**Diesel engine control**	**Induction machine control**	**Propeller control**
8	Dynamic torque control	Speed control	Transit pitch setpoints
9	Speed control	Dynamic torque control	Transit pitch setpoints
10	Speed control	Dynamic torque control	Acceleration pitch setpoints

Fixed pitch propeller with improved control			
Sim. no.	**Diesel engine control**	**Induction machine control**	**Propeller control**
11	Speed control	Fixed "optimal" torque control	Fixed pitch
12	Speed control	Dynamic torque control	Fixed pitch

Table 4.1: Control scenarios overview

Conventional diesel engine speed control with induction machine torque support
The first set of simulations shown in Table 4.1, numbering from 1 till 3 uses conventional control. Conventional control uses the diesel engine in speed control and the induction machine in torque control. The CP propellers' pitch is set via a combinator curve. For simulation numbers 1 and 2 the induction machine only contributes additional torque at higher rpm's. Simulation number 2 uses a lowered pitch setting for the CP propeller, providing a larger margin between the static power demand of the propeller and the diesel engine envelope. Simulation number 3 varies the rpm at which the induction motor starts delivering additional torque.

Electrical speed control with diesel engine torque support
The second set of simulations shown in Table 4.1 include simulation numbers 4 and 5. These simulations use electrical speed control with diesel engine torque support, meaning the induction machine delivers the increased load demand during acceleration, enabling the torque setpoints of the diesel engine to be set close to its operating limits. Simulation number 5 investigates the ideal division of torque between the diesel engine and the induction machine. During simulation number 5 the static torque setpoints of the diesel engine were varied, resulting in a different power distribution between the diesel engine and the induction machine.

Adaptive pitch control
The third set of simulations shown in Table 4.1 include simulation numbers 6 and 7. These simulations use adaptive pitch control to maintain a predetermined angle of attack onto the propeller. This specific control mode is described in section 3.3.2. Simulation number 6 is an implementation of slow adaptive pitch control, in which the rate of change in engine speed is moderate. Simulation number 7 is an implementation of fast adaptive pitch control, in which large changes in engine speed are accepted to benefit the acceleration behavior.

Dynamic power split control
The fourth set of simulations shown in Table 4.1 includes simulation numbers 8, 9 and 10. The simulations implement a dynamic power split between the diesel engine and the induction machine. When the shaft speed does not match the shafts speed setpoint (during acceleration) the engine that operates under torque control is given a higher torque setpoint. This effectively shares the dynamic load between the induction motor and the diesel engine. Simulation number 8 is an implementation of a dynamic power split with the diesel engine operating under torque control with the electric machine operating under speed control. Both simulation number 9 and 10 are an implementation of dynamic power split control with the diesel engine in speed control with additional torque from the induction machine.

Fixed pitch propeller with improved control
The fifth set of simulations shown in Table 4.1 is aimed at improving the acceleration performance of a fixed pitch propeller. Simulation numbers 11 and 12 implement well performing control strategies from previous scenarios in a vessel with the propeller fixed at a P/D of 1,4. Simulation number 11 uses conventional diesel engine speed control with induction machine torque support. From simulation 3 the optimal compromise is implemented. This compromise defines at which rpm the induction machine starts delivering torque support. Simulation number 12 implements the dynamic power split as tested in simulation number 9 onto the fixed pitch propeller.

4.1.1. Dynamic load limitation

At a given propeller pitch and shaft speed the propeller load will be larger during acceleration than in the steady state speed. This higher load is due to the combination of the newly increased propeller shaft speed while the ship speed, and therefore the advance velocity (V_A) lags behind. This newly increased propeller speed will eventually results in a steady state at a higher ship speed. However during acceleration the advance velocity is relatively low compared to the rotational speed, this results in a larger angle of attack during acceleration. The larger angle of attack during the acceleration creates a higher thrust and results in a higher engine load than at the steady state ship speed. This higher engine load during an acceleration can exceed the engine envelope which would overload the engine. Therefore, an input demand limitation is used to account for the above described dynamics. The rate at which the lever setpoint can be increased is limited to control the amount the acceleration deviates from the steady state conditions. This effectively controls the

amount of additional load needed during an acceleration. For all scenarios that need such a lever setpoint change rate limitation this limitation is minimized in such a way that during the slam start the propeller load does not exceed the diesel engine envelope. An example in which the diesel engine is governed by speed control is shown in Figure 4.1. The power in Figure 4.1 is the power at the propeller. It can be observed that the propeller load has increased, resulting in a higher diesel load.

The diesel engine envelope is divided into three ranges. These ranges are indicated by the orange arrows in Figure **??**. The first rate limiter is used in range 1, range 1 is the constant shaft speed region. In this region only the propeller pitch is increased, for speed control to increase the fuel input to the diesel engine an error between the actual shaft speed and the shaft speed setpoint is needed. In region 1 the allowed change rate in lever setpoint is tuned in such a way that the shaft speed only deviates 20 rpm from the minimum set shaft speed. The second rate limiter is used in range 2, range 2 is defined as the rpm range between the minimum set rpm and the end of the STC switching region at 800 rpm. The change rate in lever setpoint is tuned in such a way that the power produced by the diesel engine does not exceed the envelope. During the simulations it became clear that the corner point in the diesel envelope at 800 rpm was limiting. The third rate limiter is used in range 3, range 3 is defined between the end of the STC switching region at 800 rpm and the maximum shaft speed at 1050 rpm. In region 3 the lever change rate limiter is tuned in such a way that the diesel engine power demand does not encounter the engine envelope until the maximum power cap which starts at around 1000 rpm.

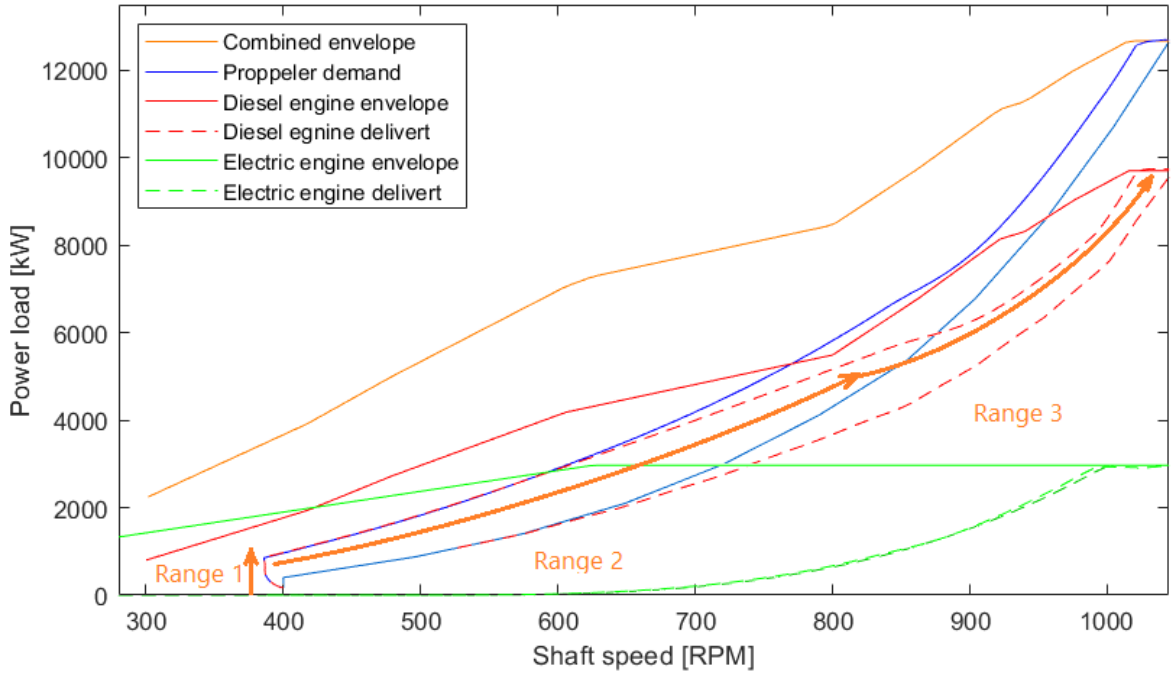

Figure 4.1: Dynamic load limitation ranges

4.1.2. Scenarios comparison layout

For ease of use and comparison between pages and control scenarios all results follow a similar layout. Each scenario is build up as follows: description, tuning and limitations, simulation results of the slam start and the staircase sprint with at the end a control evaluation. In the description the general arrangement of the control scenario is discussed, describing the control mode for the diesel engine, induction machine and propeller. The thoughts behind the control strategy are explained in the description as well. Tuning and limitations describes the choices made during the tuning process that influence the performance of the vessel. The simulation results firstly discusses the slam start and secondly discusses the staircase sprint. For most scenarios preventing the engine from overloading during the slam start was the limiting factor for maximum acceleration. Each simulation ends with an evaluation, discussing the possible improvements for a next simulation.

4.2. Scenario 1: Benchmark with conventional diesel speed control

Control mode	
Diesel engine	Speed control
Induction machine	Torque Control
CP propeller	Standard combinator

4.2.1. Description

This scenario represents the conventional control and serves as a benchmark for the other scenarios to be compared against. This control mode uses speed control for the diesel engine, torque control for the induction machine and setpoints following a combinator for the pitch of the propeller. The electric support is only available at higher shaft speeds. The propeller pitch increases from zero thrust to design pitch in the constant shaft speed region. From the combinator displayed in Figure 4.118 it is clear that full torque is not available at high rpm's. This is due to the electric machine operating at its maximum power in the constant power region where flux weakening is used. This combinator gives the static matching as depicted in Figure 4.3.

Figure 4.2: Combinator curves

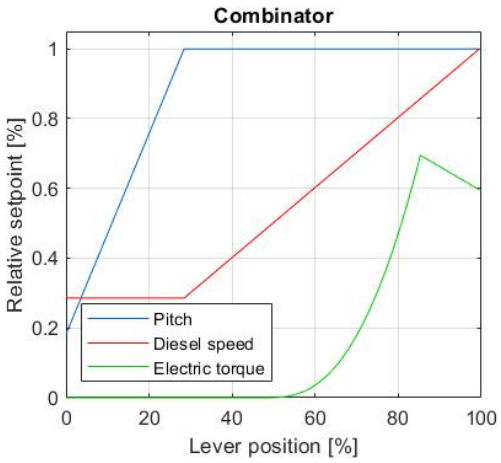

Tuning and limits

As described in section 2.4.4 at given shaft speed the propeller load is higher during acceleration than at constant speed. This simulation uses the diesel engine in speed control. The induction machine operates under torque control, only contributing a fixed amount of torque at a given shaft speed. This implies that during acceleration the larger propeller load at a given rpm is delivered by the diesel engine. When the controller is unlimited the governor will increase the fuel input when the shaft rpm is lower than the rpm setpoint, possibly resulting in overloading the diesel engine. To prevent overloading of the diesel engine the allowed change rpm setpoint, translated in lever setpoint is regulated with a rate limiter as described in section 2.4.4.

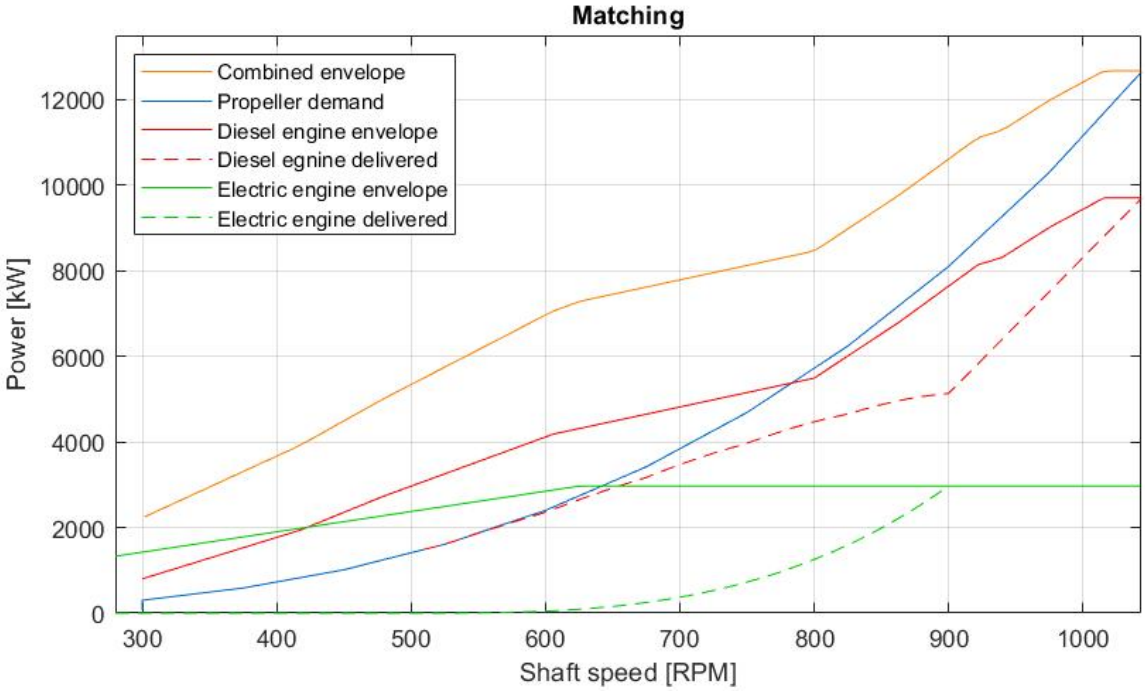

Figure 4.3: Matching of the diesel engine and the induction machine to the propeller

4.2.2. Slam start: simulation results

Figure 4.4 shows the dynamic power demand of the propeller on both the diesel engine and the induction motor. In the static matching there is an adequate margin between the diesel engine load and the envelope. During the slam start the increased dynamic power demand shows that there is a "bottleneck" limiting the overall acceleration. At 800 rpm which is just after the STC switching region the margin between the power demand and the diesel engine envelope is minimal. This clearance is the limiting factor during the acceleration. The induction machine delivers its full power contribution at 900 rpm. It seems that full power of the induction machine at a lower rpm would use the power reserve resulting in a larger margin between for the diesel engine envelope and load line. Figure 4.5 shows the the ship speed setpoint as a result of the lever setpoint, the actual ship speed and the acceleration. Figure 4.5 shows the acceleration during a slam start, four sharp chines in the line are visible at around 50 190, 235 and 300 seconds. The kink in acceleration at 50 seconds is caused by the transition from the constant shaft region to region 2. The kink in acceleration at 190 seconds is caused by the transition from region 2 to region 3 at the STC switching region as described in Figure 4.1. The kink in acceleration at 235 seconds is caused by the induction machine reaching its power limit as shown n Figure 4.6. The kink in acceleration at 300 seconds is caused by diesel engine reaching its power limit.

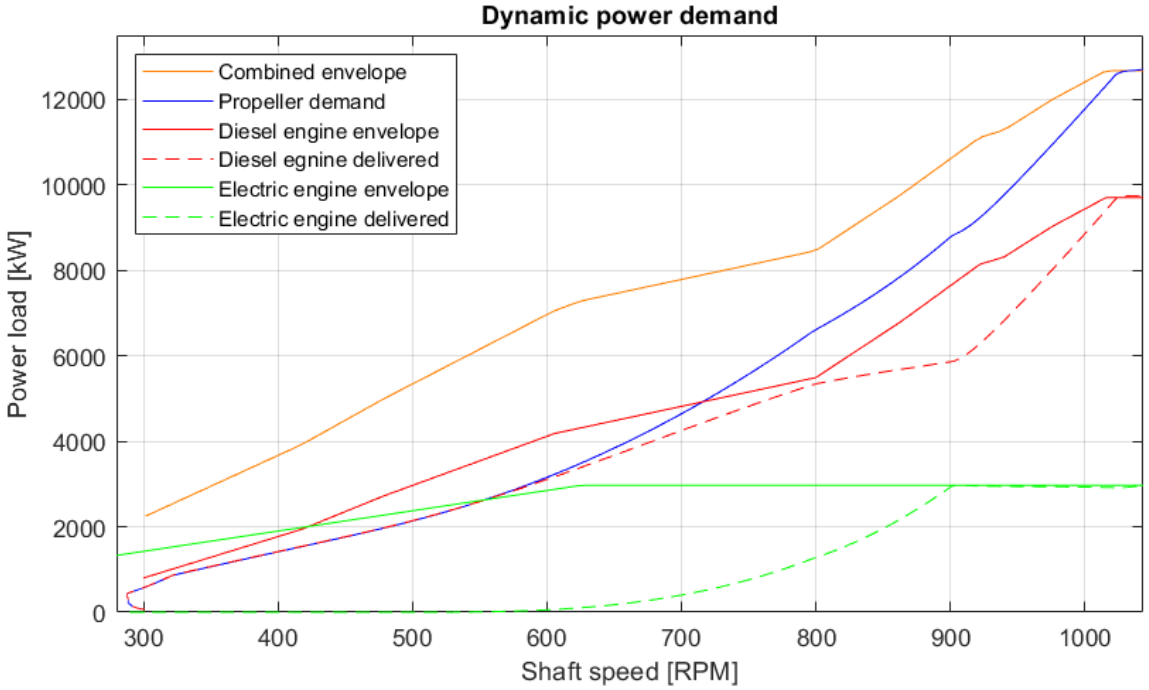

Figure 4.4: Dynamic propeller load on diesel engine and induction machine

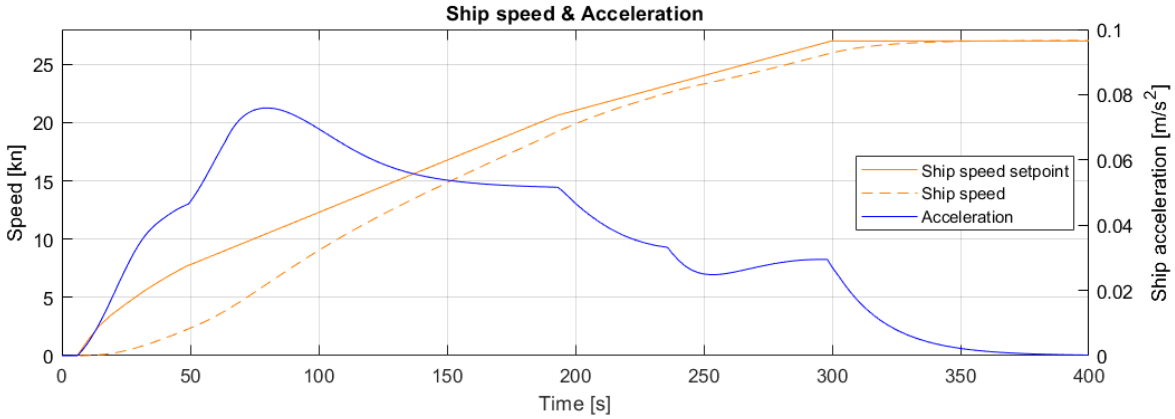

Figure 4.5: Ship speed and acceleration

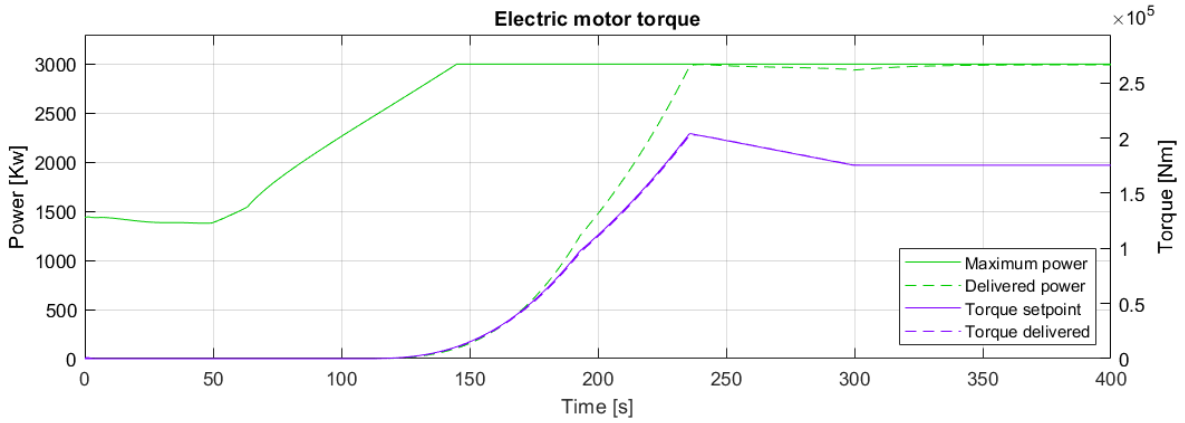

Figure 4.6: Induction machine torque control

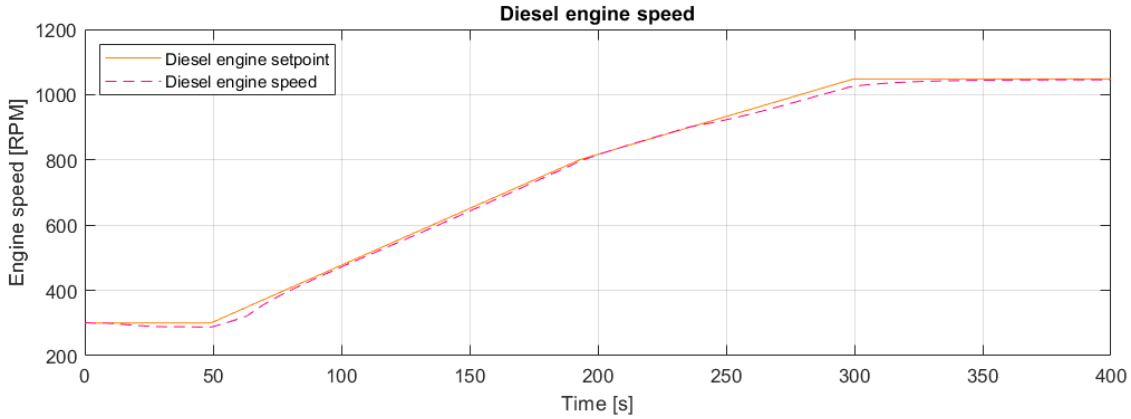

Figure 4.7: Diesel engine speed control

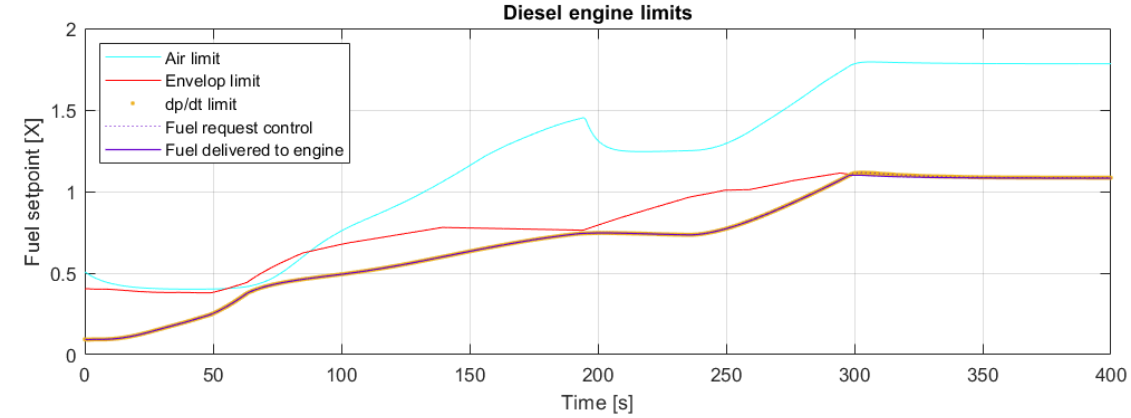

Figure 4.8: Diesel engine limits

Figure 4.8 depicts the diesel engine limits. The maximum fuel increase rate $\frac{d \cdot X}{d \cdot t}$ is due to it being dependent on the current fuel flow a zone surrounding the current fuel flow. The cyan color depicts the amount of fuel which may be injected into the engine while maintaining the minimum air excess ratio of 1.3. It can be observed that at 70 seconds the fuel is almost limited due to the turbo leg. At 190 seconds the dip in air pressure associated with the switching to two turbos can be observed. The red line depicts the maximum fuel injection due to the engine envelope. At 300 seconds the maximum power is reached and thus the engine envelope line corresponds with the fuel input line.

4.2.3. Staircase sprint: simulation results

Figure 4.9 shows the dynamic load demand by the propeller as well as the delivered load from both the diesel engine and induction machine. It can be observed that all the increased propeller load needed during acceleration is delivered by the diesel engine. Each acceleration of 5 kn creates a hump in the propeller load and engine speed. This increase in propeller load is due to the advance velocity lagging behind the shaft rpm, which results in a higher angle of attack and an increased torque demand compared to the steady state. When the ship speed setpoint is reached the angle of attack onto the propeller blades reduced to its steady state value, resulting the propeller load decreasing to its steady state load. The small overshoot in engine speed is caused by this decreasing propeller load, since the PI controller that governs the diesel engine speed only reduces the fuel setpoint when the measured shaft speed becomes larger than the setpoint. At 900 second the induction machine reaches its power limit, causing the dip in acceleration shown in Figure 4.10.

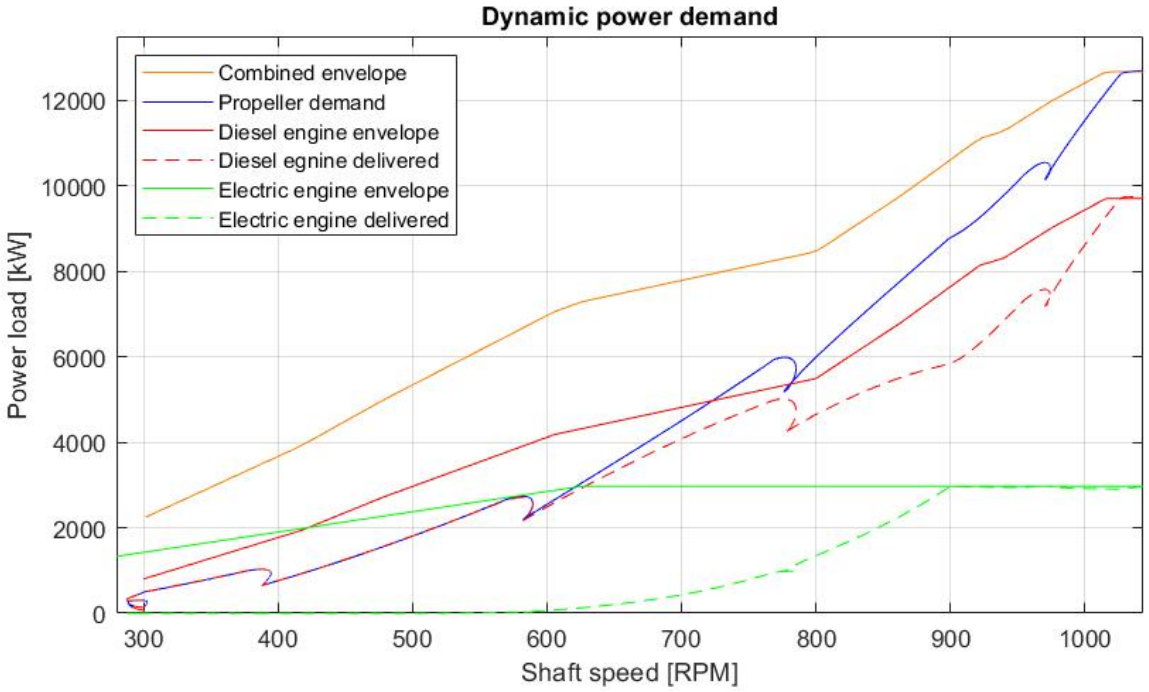

Figure 4.9: Dynamic load on diesel engine and induction machine

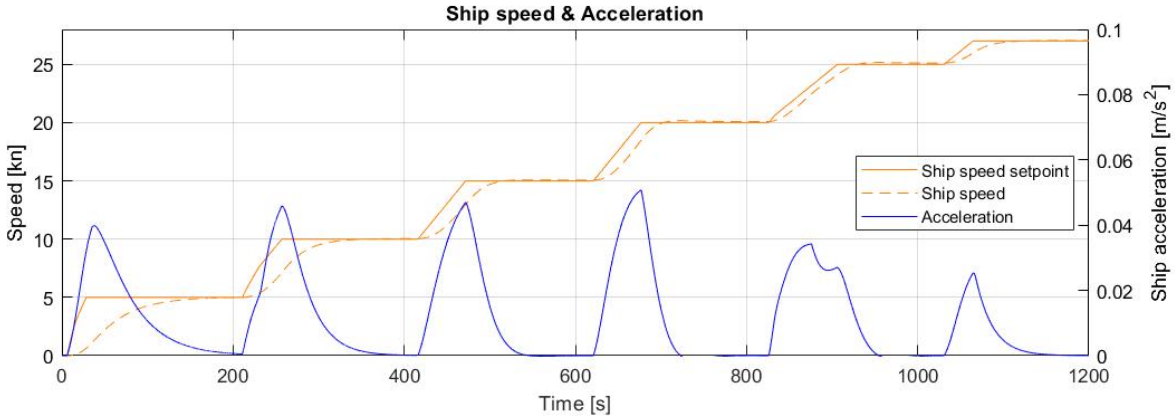

Figure 4.10: Ship speed and acceleration

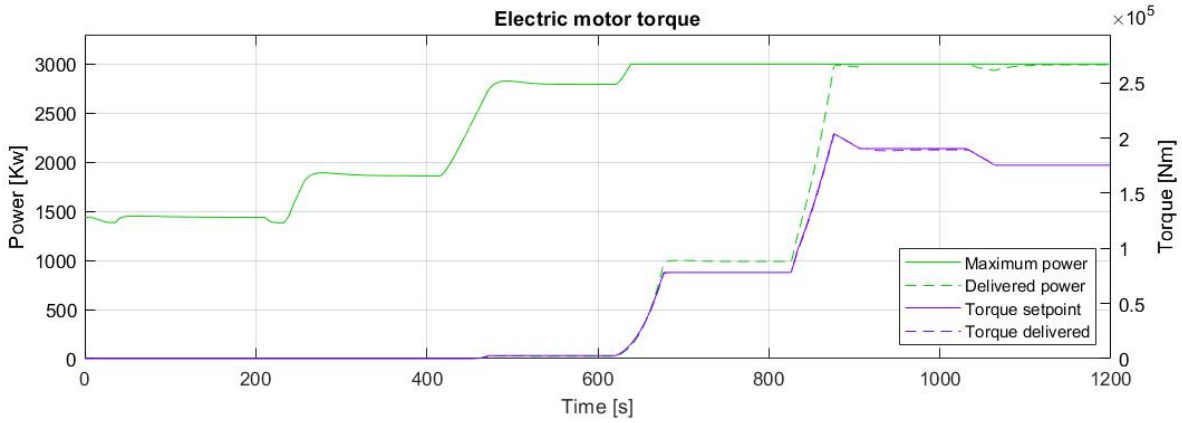

Figure 4.11: Induction machine torque control

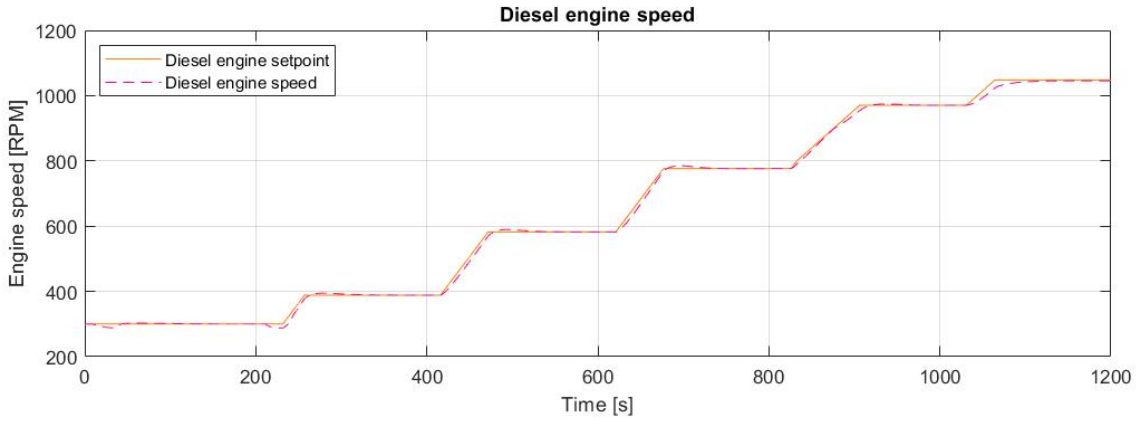

Figure 4.12: Diesel engine speed control

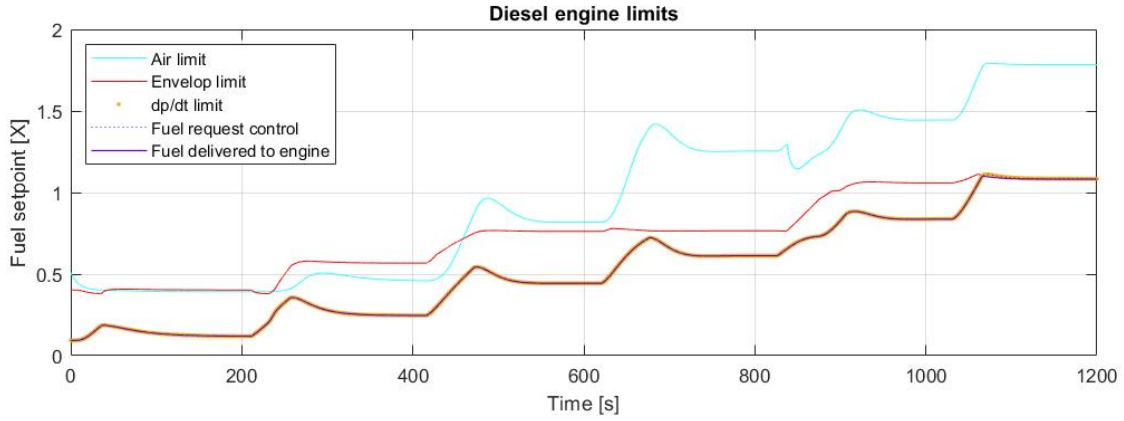

Figure 4.13: Diesel engine limits

4.2.4. Control evaluation

Figure 4.10 shows the accelerations for the staircase sprint. Table **??** shows the absolute acceleration time it takes for the vessel to reach 90% of the ship speed setpoint. 90% is to emphasize the rise time of the acceleration. This captures the characteristics of the start and the middle of the acceleration, excluding the settling time. The accelerations from 0 till 5 kn is relatively slow, taking 130 seconds. This is remarkable since it is a low increase in absolute power. At zero speed the propeller, which rotates but doesn't produce thrust, needs 65 kW. During the acceleration from 0 to 5 kn the peak propeller power is 303 kW after which it reduces to a steady state load of 135 kW. The diesel engine is capable of producing 800 kW at this minimal shaft speed. The reason this acceleration takes relatively long is because a large underspeed is not acceptable. The PI controller which governs the diesel engine speed needs an error in the shaft speed to increase the fuel setpoint. Since the error is limited to be small to prevent underspeed the fuel increase rate is small. This has as a consequence that the pitch of the propeller can only be increased slowly resulting in a slow acceleration. In this region the induction machine does not contribute any torque. The relatively slow acceleration from 0 to 5 kn is common for all following control strategies. The acceleration from 25 to 27 kn is limited by the total available power, which is the same for all simulations. It is therefore concluded that the accelerations from 5 till 25 kn are the most interesting for evaluation and comparisons. The acceleration from 5 till 10 kn takes in total 88.8 seconds with a peak acceleration of 0.046 m/s^2. This peak acceleration happens at 46 seconds after the acceleration starts. The other accelerations have a similar profile, with acceleration peaks around 0.045 m/s^2 and this peak occurring at about half the total acceleration time. Resulting in acceleration peaks that are low and quite spread out.

Speed [kn]	**0-5**	**5-10**	**10-15**	**15-20**	**20-25**	**0-27**
Total time [s]	130.3	88.8	72.9	61.4	73.3	288.0
Maximum acceleration [m/s^2]	0.040	0.046	0.047	0.050	0.025	0.076
Time at maximum acceleration[s]	31	46	55	56	48	73

Table 4.2: Simulation number 1: Acceleration times

It can be concluded that the amount of power the diesel is allowed to generate just after the STC switching zone at 800 rpm is limiting for the overall acceleration. Figure 4.3 shows at 800 rpm that the engine envelope allows for the maximum usage of 5.59 MW engine power. The static power demand at 800 rpm is 4.53 MW, meaning 82.5% of the engine power is used. However during acceleration it becomes clear that the higher propeller load does become a problem. Using the lever rate limiters as defined at the start of this chapter the diesel engine delivers 97% of the total amount of power it can deliver at 800 rpm. From Figure 4.9 it becomes clear that with the current control of the induction machine the diesel engine is required to deliver the full dynamic load during acceleration. Clearly this does not use the full potential or the induction motor. Following control scenarios will focus on a better usage of the induction machine as well as minimizing the restrain on the lever setpoint. This restrain on the lever setpoint directly influences the maximum acceleration.

4.3. Scenario 2: Diesel speed control with reduced pitch

Control mode	
Diesel engine	Speed control
Induction machine	Torque Control
CP propeller	Lowered pitch combinator

Figure 4.14: Combinator curves

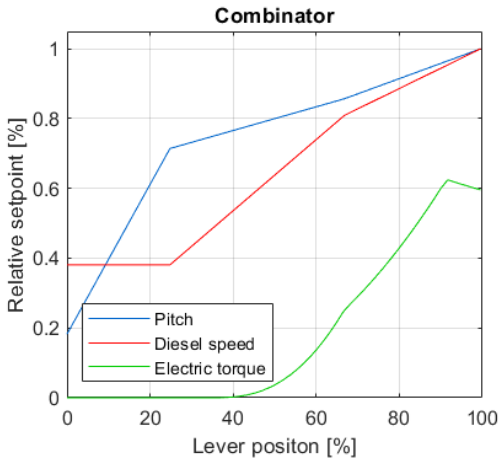

4.3.1. Description

This scenario represents conventional control used for acceleration, using speed control for the diesel engine with torque support at higher rpm's from the induction machine, as is currently the standard. Full torque is not available but full power is. This is due to the electric machine operating in the constant power region where flux weakening is used. A combinator is used to control the pitch of the propeller. The propeller pitch setpoints are lowered compared to simulation number 1. Lowering the pitch setpoints creates more clearance in the static matching of the diesel engine, allowing for a faster acceleration. In addition to the lowered pitch compared to the previous scenario 1 described in section 4.2, the minimum shaft speed is also increased to 400 rpm. In the constant shaft speed region the pitch is increased from the zero thrust pitch to a P/D of 1.0. From 20% to 65% of the lever setting the P/D increases to 1.2 and at 100% of the lever setting the pitch is the full design P/D of 1.4. This combinator gives the static matching as depicted in Figure 4.15. At the engine speed of 800 rpm which was the previously identified bottleneck at scenario 1 the diesel engine now produces 66% of the 5.49 MW available power. The contribution of the induction machine remains at the same virtual shaft speed as with simulation 1. Due to the lower pitch at a given shaft speed this results in the induction machine delivering full power at a higher absolute shaft speed.

Tuning and limits

A lever setpoint rate limiter is used as discussed in section 2.4.4. This rate limiter is tuned in such a way that the dynamic demand on the diesel engine during a slam start is the limiting factor.

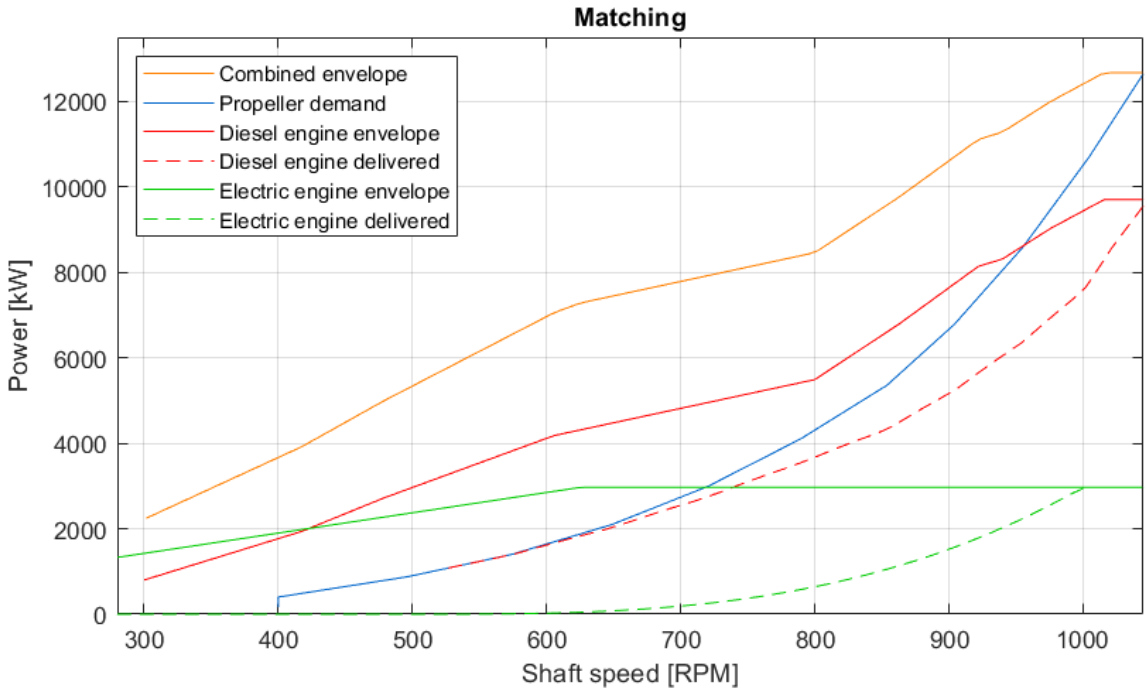

Figure 4.15: Matching of the diesel engine and the induction machine to the propeller load

4.3.2. Slam start: simulation results

During the slam start simulation it is found that increasing the load acceptance by lowering the pitch of the propeller makes a big difference to the overall acceleration. However, with the reduced pitch settings the "bottleneck" at 800 rpm which is just after the STC switching region still exists. Figure 4.16 shows the dynamic power demand of the propeller on both the diesel engine and the induction motor. This figure shows that during acceleration the engine load at the low spot in the engine envelope at an engine speed of 800 rpm is 5.17 MW which is about 94% of the available power at this shaft speed. Again this engine load is the result of the allowed rate of change in the lever setpoint, which is higher than with the benchmark. Figure 4.17 shows that with this reduced pitch setpoint the new peak acceleration has increased and the total acceleration time is shortened by about a 100 seconds. In Figure 4.17 which depicts the acceleration four sharp chines in the line are visible at around 40 120, 170 and 190 seconds. The kink in acceleration at 40 seconds is caused by the transition from the constant shaft region to region 2. The kink in acceleration at 120 seconds is caused by the transition from region 2 to region 3 at the STC switching region as described in Figure 4.1. The kink in acceleration at 170 seconds is caused by the induction machine reaching its power limit as shown in Figure 4.18. The kink in acceleration at 190 seconds is caused by diesel engine delivering the maximum power.

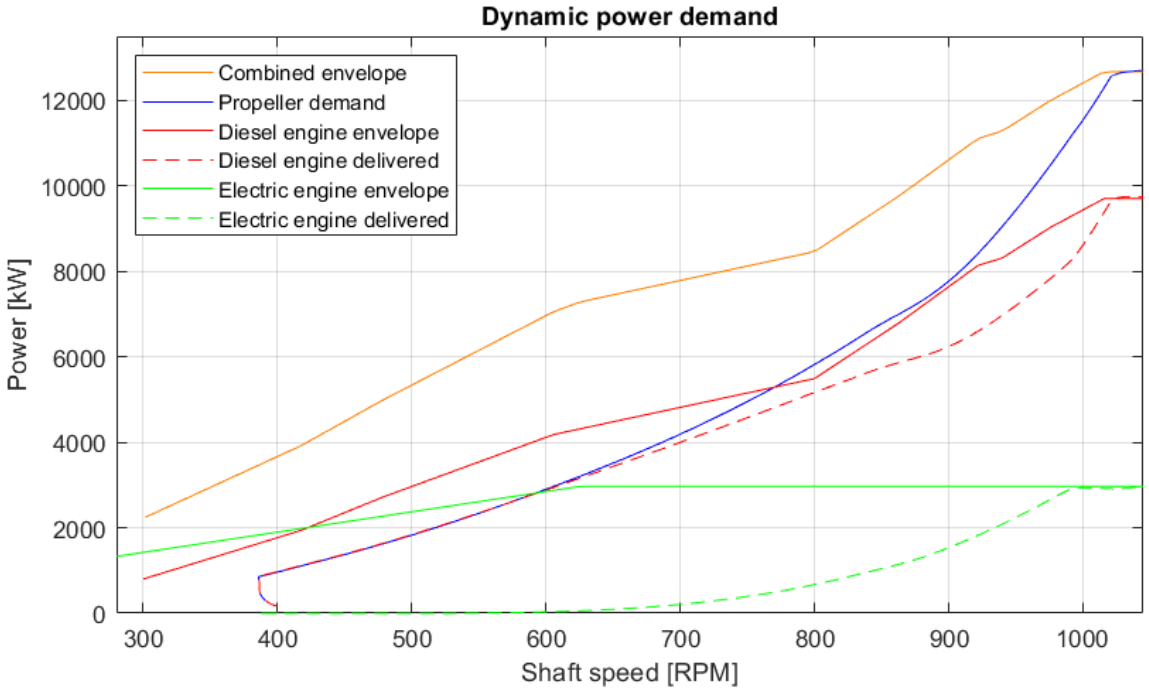

Figure 4.16: Dynamic power demand

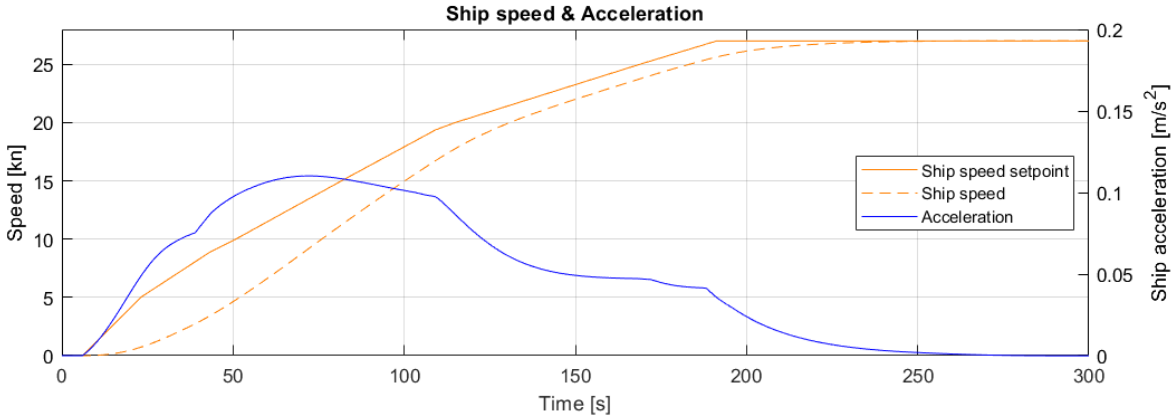

Figure 4.17: Ship speed and acceleration

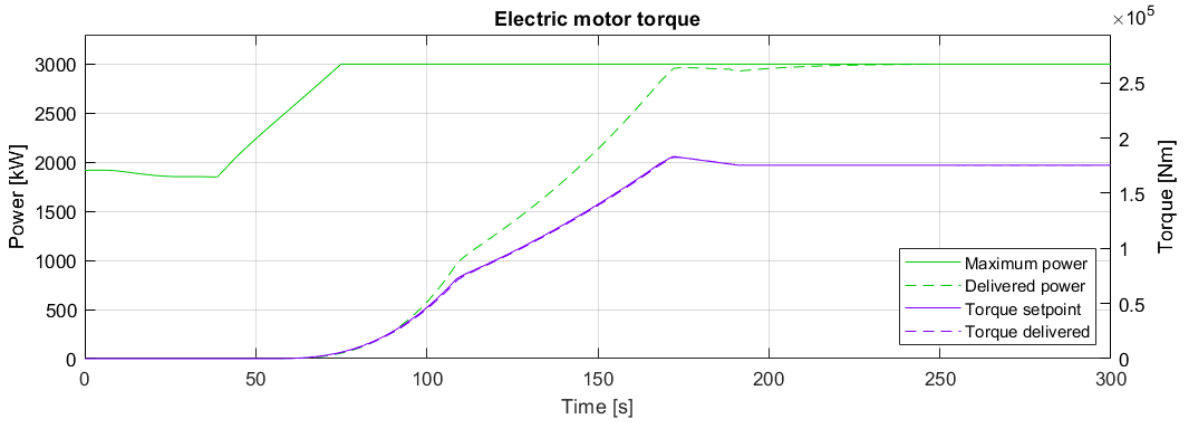

Figure 4.18: Electric machine torque and power

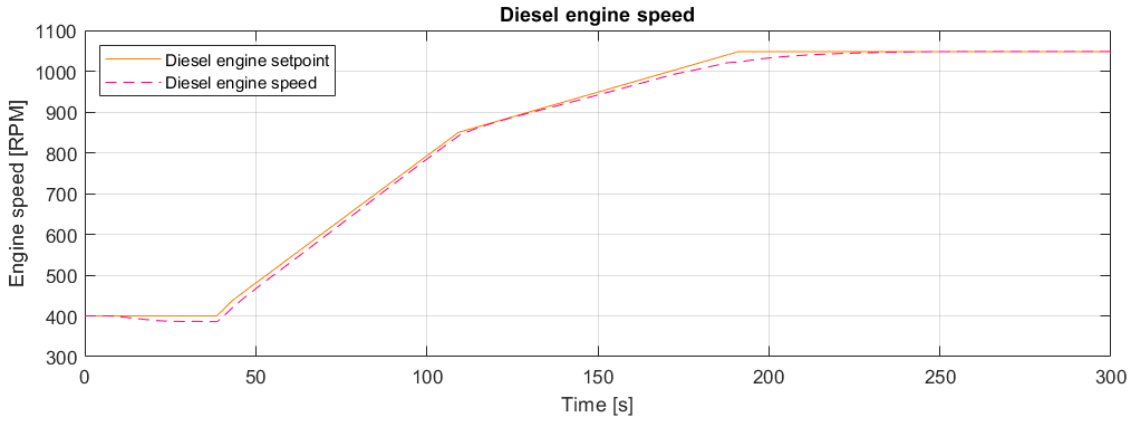

Figure 4.19: Diesel engine speed

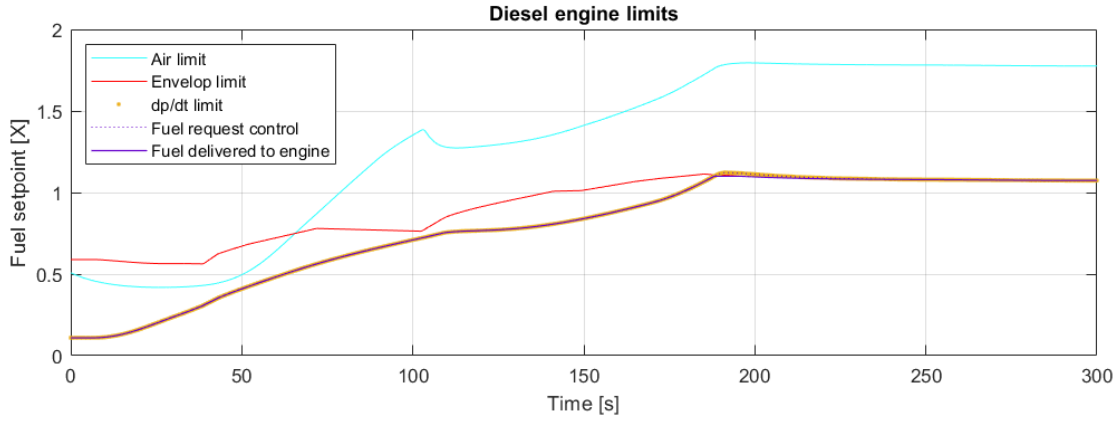

Figure 4.20: Diesel engine limits

4.3.3. Staircase sprint: simulation results

Figure 4.21 shows the dynamic load of the propeller during the staircase sprint. By comparing the dynamic load of the propeller with simulation number 1 as given in Figure 4.10 it is concluded that the margin of the diesel engine with its envelope has increased. This observation is confirmed when comparing Figure 4.13 of simulation 1 to Figure 4.25, meaning that lowering the pitch is an effective means for increasing the diesel engine margin. From the staircase sprint it is concluded that increasing the load acceptance by lowering the pitch of the propeller makes a big difference to the acceleration time. Figure 4.22 shows more condensed acceleration times with a higher peak value compared to the benchmark scenario 1 depicted in Figure 4.10. Table **??** as shown in the control evaluation shows a quantitative overview of the results.

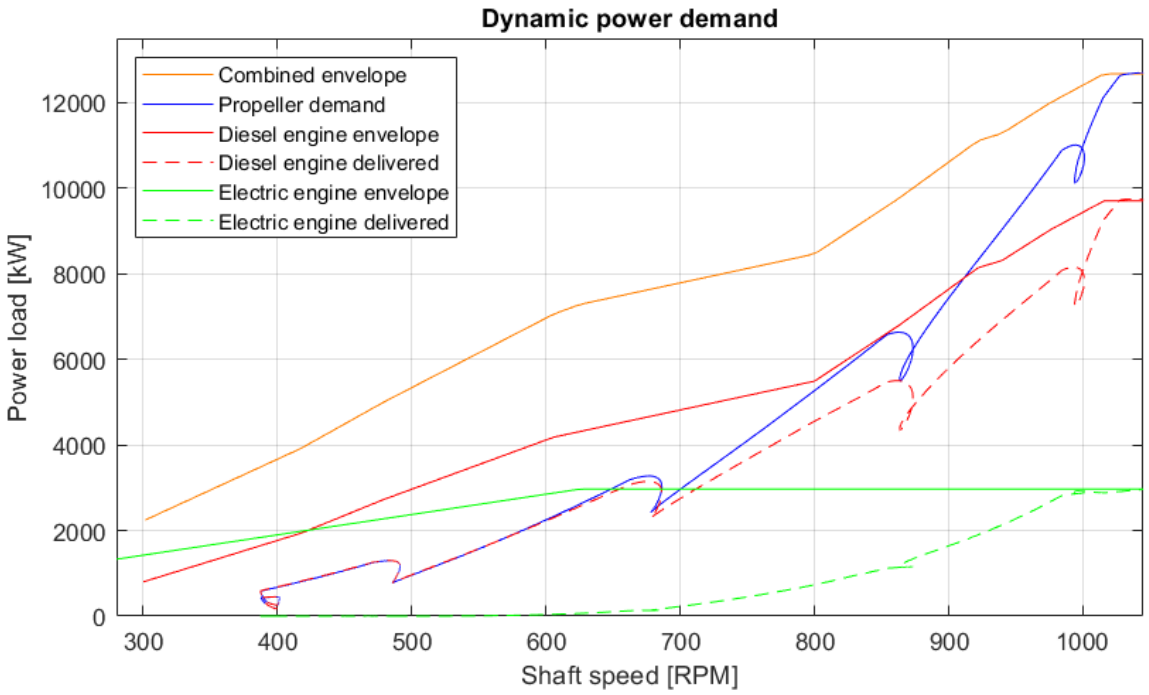

Figure 4.21: Dynamic power demand

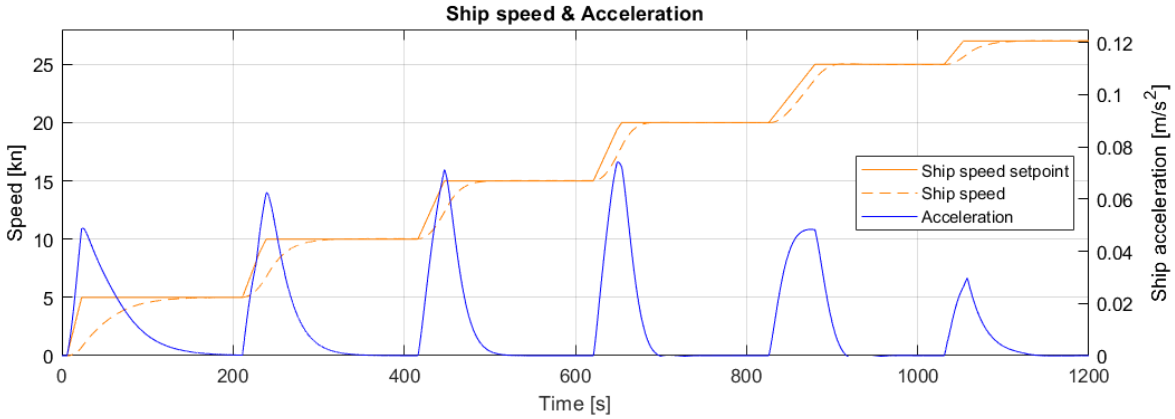

Figure 4.22: Ship speed and acceleration

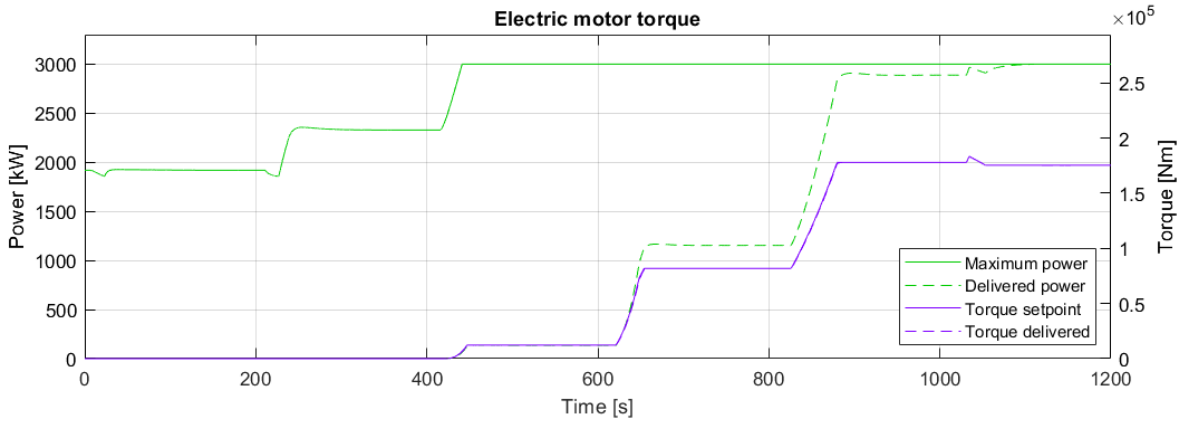

Figure 4.23: Electric machine torque and power

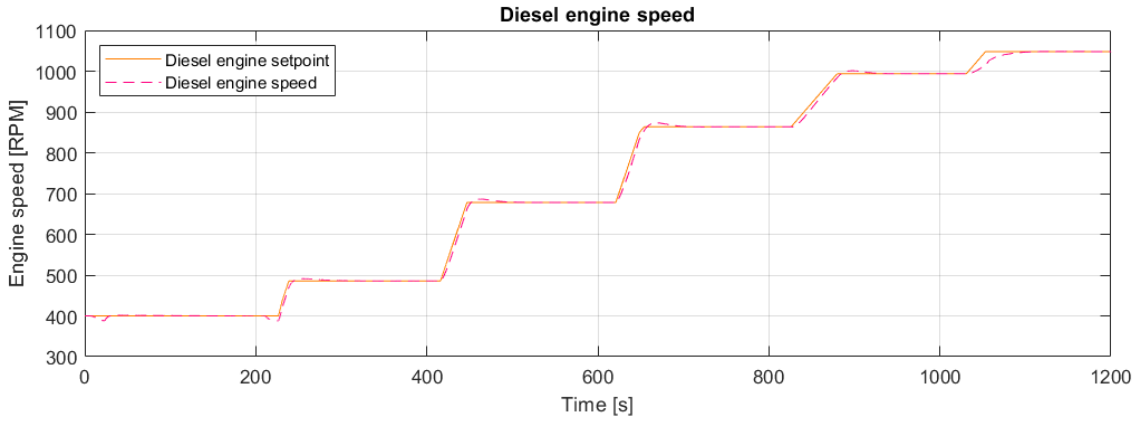

Figure 4.24: Diesel engine speed

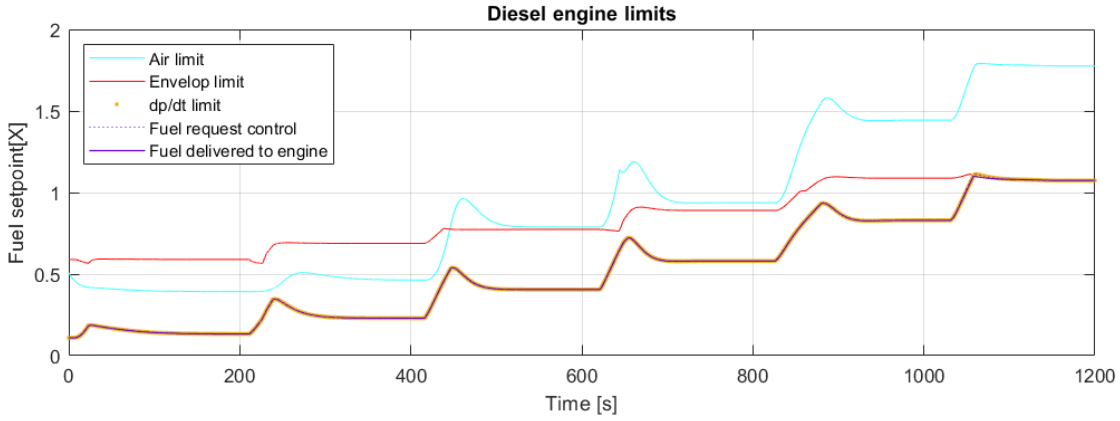

Figure 4.25: Diesel engine limits

4.3.4. Control evaluation

Comparing the acceleration times from simulation number 1 and 2 it is observed that the needed time to reach 90% of the ship speed setpoint is reduced. The acceleration time for the accelerations from 5 to 10 and 20 to 25 are reduced by 26%. The acceleration time for the accelerations from 10 to 15 and 15 to 20 are reduced by 32%. The acceleration time needed for the slam start is reduced by 36%. It is concluded that the accelerations peak values have increased significantly, up to 48% for the acceleration from 15 to 20 kn. The shape of the acceleration graph as shown in Figure 4.22 is compared to Figure 4.10. The acceleration times are shorter and the peaks are higher, resulting in a more condensed acceleration. The general shape of the peaks although sharper remains similar, with the peak in acceleration around or past the middle of the acceleration manoeuvre. As an example the peak acceleration for the manoeuvre from 15 to 20 kn is at 29 seconds while the total acceleration takes 41.9 seconds, meaning the peak occurs at $\frac{2}{3}$ of the total acceleration.

Speed [kn]	**0-5**	**5-10**	**10-15**	**15-20**	**20-25**	**0-27**
Total time [s]	109.9	65.51	49.6	41.9	54.3	185.5
Maximum acceleration [m/s^2]	0.049	0.062	0.071	0.074	0.048	0.11
Time at maximum acceleration[s]	17	28	31	29	48	65

Table 4.3: Simulation number 2: Acceleration times

During this simulation the pitch setpoints were reduced to create a larger static margin between the engine limit and the propeller load. Lowering of the pitch setpoint successfully increased the load acceptance of the diesel engine which allows for higher acceleration. This lowered pitch setting prescribed by the combinator curve does mean that even when the newly set speed is reacted the propeller still operates at this lowered pitch setting, reducing the propellers' efficiency. In addition to the lowered efficiency this control scenario still doesn't use the electric motor effectively, as can be seen in Figure 4.23. For the accelerations up to 15 kn the induction machine isn't used at all, and for the accelerations from 15 to 27 kn the induction machine does not contribute to the increased propeller load during acceleration. While the induction machine is inherently suited for almost instant full torque production. It should be noted that while the diesel engine envelope is the limiting factor there is still a large margin between the propeller load and the total combined envelope of the diesel engine and induction machine. Lowering the pitch setting does mitigate the limiting factor during acceleration. However it does not fundamentally improve the control strategy and keeps running into the diesel engines limitations without using the inherent benefits of the induction engine.

4.4. Scenario 3: Induction machine torque control sweep

Control mode	
Diesel engine	Speed control
Induction machine	Torque control sweep
CP propeller	Standard combinator

Figure 4.26: Combinator curves

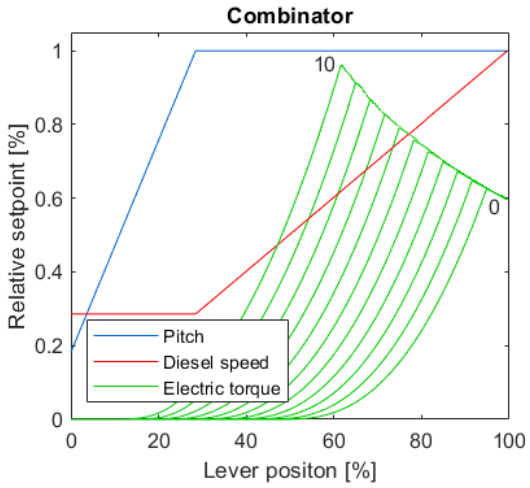

4.4.1. Description

From simulation numbers 1 and 2 it was concluded that the engine margin of the diesel engine was the limiting factor when the diesel engine operates in speed control. Lowering the propeller load by reducing the pitch improved the acceleration in simulation number 2. However during acceleration the increased dynamic load from the propeller which is delivered by the diesel engine needs to be controlled to prevent the diesel engine from exceeding its envelope. With previous simulations the diesel engine envelope remained the limiting factor for the acceleration, before the total combined envelope was completely used. During this simulation the shaft speed at which the induction machine start contributing torque to the propeller shaft is varied. The static propeller load demand is partly taken over by the induction machine when it starts to deliver torque, resulting in a reduction of the static load for the diesel engine and eventually a larger margin between the propeller load and the diesel engine envelope. The zero in the combinator curve as shown in Figure 4.26 represents a very late start for the induction machine to start contributing torque. With such a late start there is almost no margin between the static power load and the diesel envelope. Number ten represents the earliest start of the electric machine for it to start contributing torque. With such an early start the induction machine almost provides the entire propeller load at lower shaft speeds. In total eleven variations were simulated, varying the rpm at which the induction motor starts delivering torque.

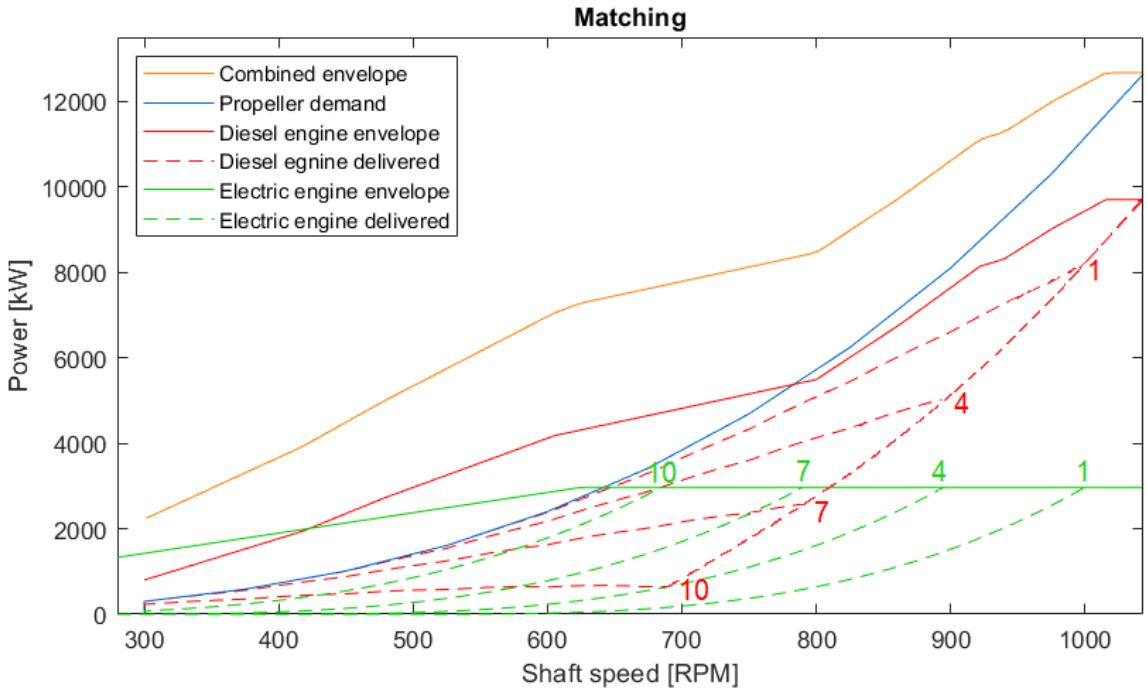

Figure 4.27: Matching of propeller load with the diesel engine and induction machine, torque contribution sweep

Tuning and limits
All eleven variations were tuned, lever setpoint rate limiters were used to keep the propeller load on the diesel engine from exceeding the engine envelope. Figure 4.27 shows the static power demand on both the diesel engine as the induction machine. Only four of the eleven matching graphs are drawn to keep the graph readable. It is important to realize that variation zero is shown by the lowest load on the induction motor and as a consequence this results in the heaviest static load on the diesel engine. Figure 4.27 shows the matching for variations one, four, seven and ten.

4.4.2. Slam start: simulation results

For the slam start varying the point at which the induction machine begins to provide torque to the propeller shaft gives the acceleration time as can be observed in Figure 4.28. It can be observed that the lower the shaft speed at which the electric motor starts producing torque the faster the acceleration. An early contribution from the induction machine results in a larger static power reserve for the diesel engine. With the diesel engine in speed control this increased power reserve is available for a large dynamic power demand from the propeller. With an early contribution from the induction machine, combined with a high power production by the diesel engine the total power transferred into the water is very large, resulting in a good acceleration. However it can be observed that although the acceleration continues to improve with an earlier electrical contribution this positive correlation becomes less pronounced.

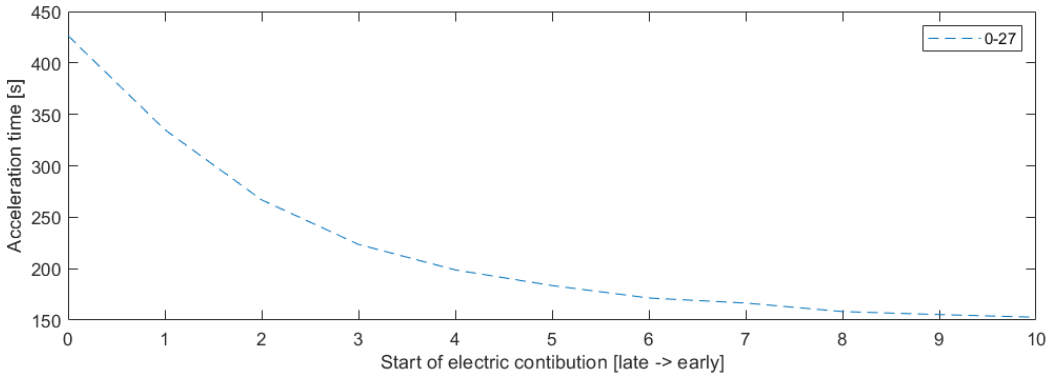

Figure 4.28: Induction machine torque control sweep: Slam start acceleration time

4.4.3. Staircase sprint: simulation results

Figure 4.29 which depicts the results for the staircase sprint shows a more interesting result than the slam start. With conventional control the electric motor only contributes torque at high shaft speeds. Conventional control would correspond with variation 0 or 1 in this sweep. However based on Figure 4.29 it can be stated that such a static matching gives the worst acceleration performance. It is therefore concluded that an electrical torque contribution starting at a lower shaft speed is preferred for all sprint regions.

Both the acceleration times of the sprints from 0 to 5 kn and 25 to 27 do not change much between simulations. As stated in simulation number 1 the sprint from 0 to 5 kn is limited by the need for the PI speed governor to detect an error in shaft speed and the necessity to prevent underspeed for the diesel engine. The acceleration from 25 to 27 kn is limited by the total amount of available power. Therefore both acceleration times do not improve with a shift in static distribution of the induction machine.

The acceleration from 5 to 10 kn shows a slight preference for induction machine to start delivering torque at low shaft speeds. The acceleration time of the sprint from 10 to 15 kn also shows a reduced acceleration time for an earlier start of the induction machine. However this positive correlation is strongest for variation numbers 0 till 4 and after variation number 6 the acceleration time doesn't improve much. The acceleration time of the sprint from 15 to 20 kn appears optimal with at variation 6, corresponding with a full electric torque contribution at 790 rpm. This means that the acceleration time of the sprint from 15 to 20 kn is lowest when the induction machine effectively widens the diesel envelope around the switching region of the STC. The acceleration time of the sprint from 20 to 25 kn appears optimal at variation 5. From Figure 4.29 it can therefore be concluded that there is no single static matching that is optimal for all accelerations. It should be

noted that for accelerations at lower shaft speed it is preferred to have the electric torque contribution start at low shaft speed, and that for accelerations at higher shaft speeds it is preferred to have the electric torque contribution at high shaft speeds. The explanation why a positive effect on all accelerations occurs when the induction machine starts delivering torque from a low shaft speed, can be found in the diesel engine having a larger power reserve in the static matching. This power reserve is then available for delivering a larger dynamic load to the propeller. When the shaft speed at which the induction machine starts delivering additional torque coincides with the shaft speed range of a particular acceleration this is especially beneficial for that acceleration. The additional load from the propeller which is associated with the acceleration is than partially produced by the static contribution from the induction machine.

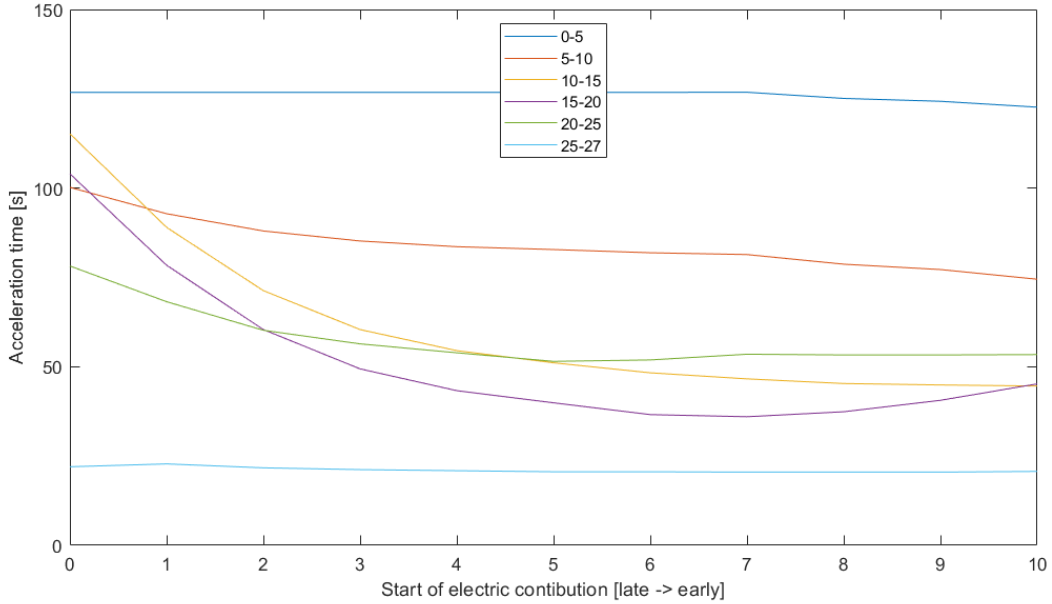

Figure 4.29: Induction machine torque control sweep: Staircase sprint acceleration times

4.4.4. Simulation evaluation

From the simulations it is concluded that for a slam start full electrical torque from the start gives the best acceleration. From the staircase sprint it is concluded that an improved acceleration occurs when the additional torque produced by the induction machine is produced early, creating a larger margin between the diesel engine static load and its envelope. In addition it was concluded that an optimum acceleration occurs when the additional torque produced by the induction machine is produced precisely in the shaft speed range of that particular sprint. This means that when the diesel motor is governed by speed control and the electric machine is governed by torque control there is no fixed optimum that can be used for all accelerations. When a fixed matching an thus power split is used a choice needs to be made which acceleration range is prioritized. It can be concluded that for acceleration purposes a very late start for contributing electrical torque is not preferred, however such a division is the case with conventional control. Such a late torque contribution is however preferred for efficiency reasons, because a heavy loaded diesel engine is more efficient. A fixed matching is therefore always a compromise between low, middle or high speed accelerations as well as the efficiency of the propulsion system. In order to remedy this, the next set of control strategies investigate a more dynamic distribution. In these control strategies the focus is on creating a high load on the diesel engine during steady state, while using the induction machine during accelerations.

4.5. Scenario 4: Electrical speed control with diesel engine torque support

Control mode	
Diesel engine	Torque control
Induction machine	Speed control
CP propeller	Standard combinator

4.5.1. Description

This scenario uses torque control for the diesel engine, speed control for the induction machine and pitch via combinator for the propeller. The relative low power of the induction machine compared to the propeller power demand means that during the steady state sailing the diesel engine needs to produce a large part of the required propeller power. The diesel engine torque setpoints are based on the steady state load of the propeller, producing 90% of the propeller load. With the diesel engine only producing torque based on steady state torque setpoint all dynamic torque required for an acceleration needs to be produced by the induction machine. This configuration incorporates the findings of simulation number 3, which state that it is preferred to have a high diesel engine load in the steady state and a large load on the induction machine during accelerations. Figure 4.30 shows the combinator and Figure 4.31 shows the associated matching.

Figure 4.30: Combinator curves

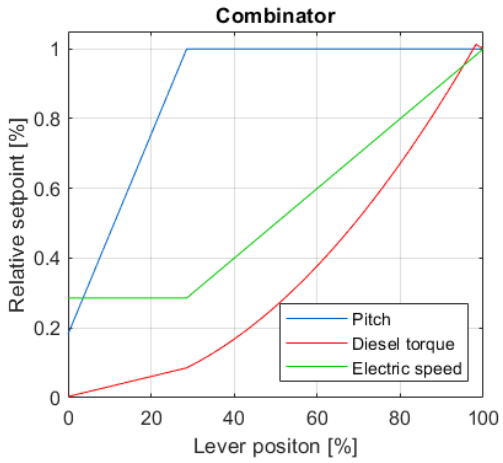

Tuning and limits

During the constant shaft speed region 1, as defined in the section about the dynamic load limitations, a rate limiter for the lever setpoint is needed. The lever setpoint rate limiter prevents the actuation system of the propeller pitch to change from the zero pitch setpoint to the design pitch setpoint in a matter of seconds, which would result in a large shaft speed drop. During testing it became clear that there is no need for a lever setpoint rate limit from fuel rack positions above the minimum shaft speed region. The key difference being the large additional power input from the induction machine. This additional power increases the shaft speed fast enough such that the diesel engine power output, limited by the maximum allowed fuel increase rate, remains bellow the diesel engine envelop.

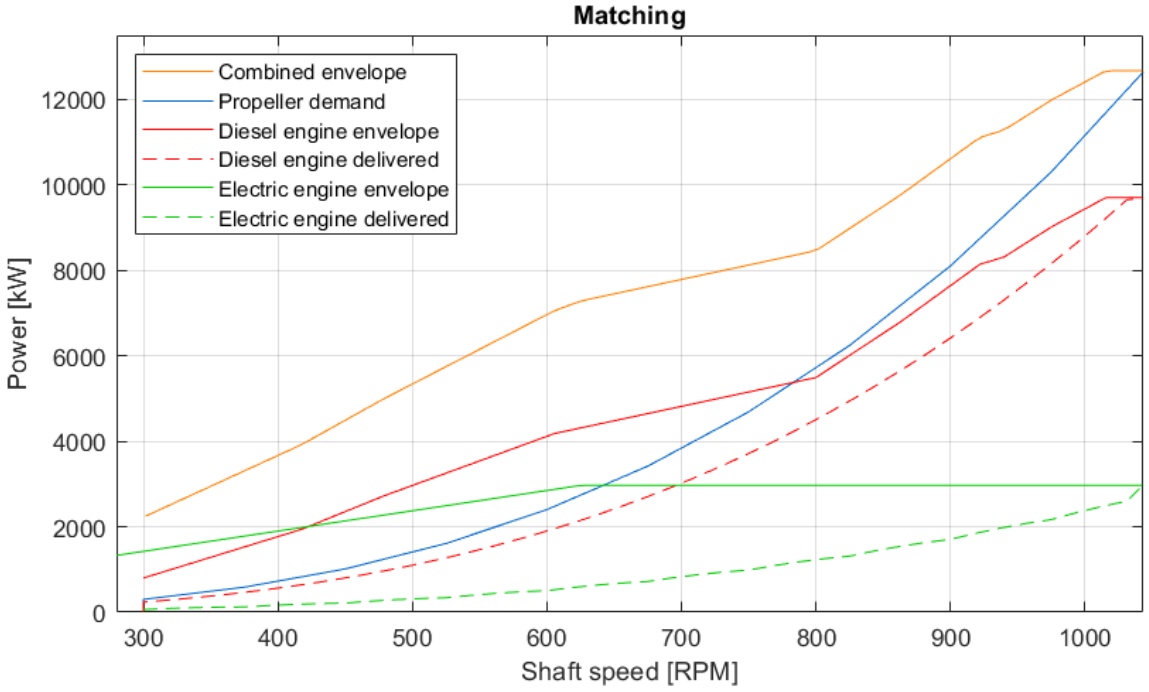

Figure 4.31: Matching of the propeller load with the diesel engine and induction machine

4.5.2. Slam start: simulation results

Figure 4.32 and Figure 4.34 show that during the slam start the induction machine delivers full available power for the entire acceleration time. The diesel engine does not exceed its envelope but is loaded very close to its envelope as can be seen in Figure 4.32. The propeller load is close to the total envelope of the combined electric motor and diesel engine. This means that a large amount of power is directed onto the propeller, resulting in a very high acceleration of 0.18 m/s^2 as can be seen in Figure 4.33. The acceleration in Figure 4.33 shows four sharp transitions. The first transition happens at 20 second, this is when the propeller reaches design pitch. This transition is followed by a large increase in acceleration, which is due to the electrical propulsion increasing its torque output very rapidly. At 23 seconds the acceleration continues to increase but at a slower pace, this is due to the induction machine reaching its maximum torque, producing the maximum power at that shaft speed. At 50 seconds the acceleration starts to reduce. This is the moment the induction machine transitions into the constant power region meaning that the only increase in power to the propeller is coming from the diesel engine. At 100 seconds the last transition in acceleration is visible, which is explained by the diesel engine reaching its torque limit. Compared to the slam start of simulation numbers 1 and 2 as can be seen in Figure 4.5 and Figure 4.17 the acceleration increases faster, is larger and experiences less restrictions that originate in system limitations.

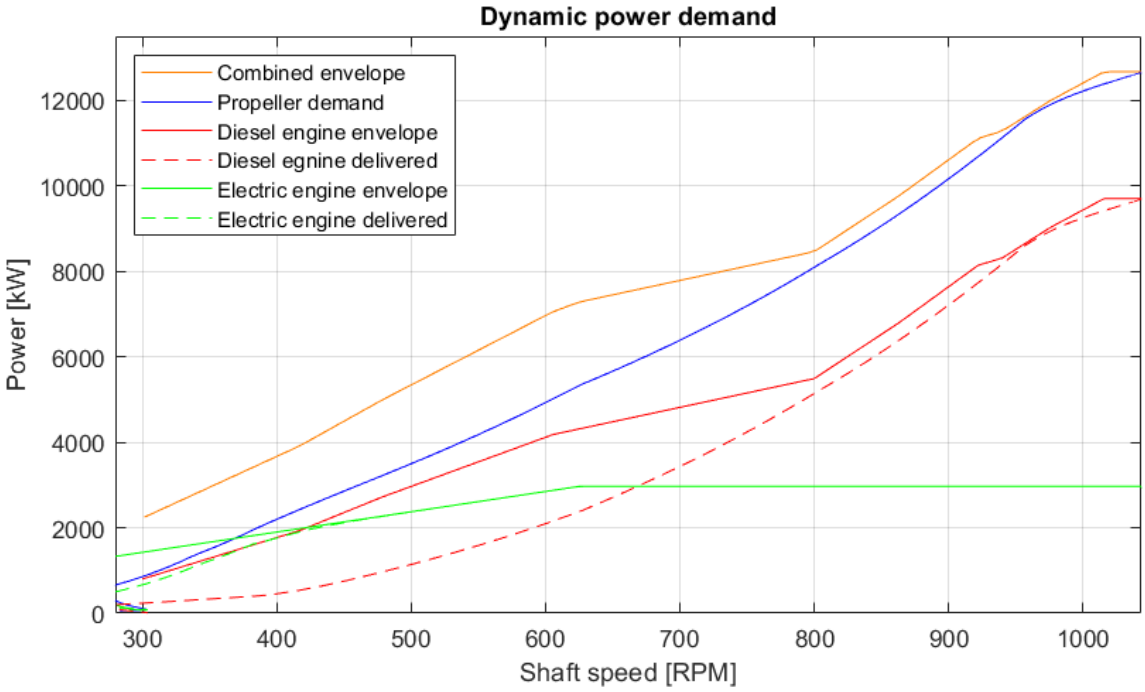

Figure 4.32: Dynamic power demand

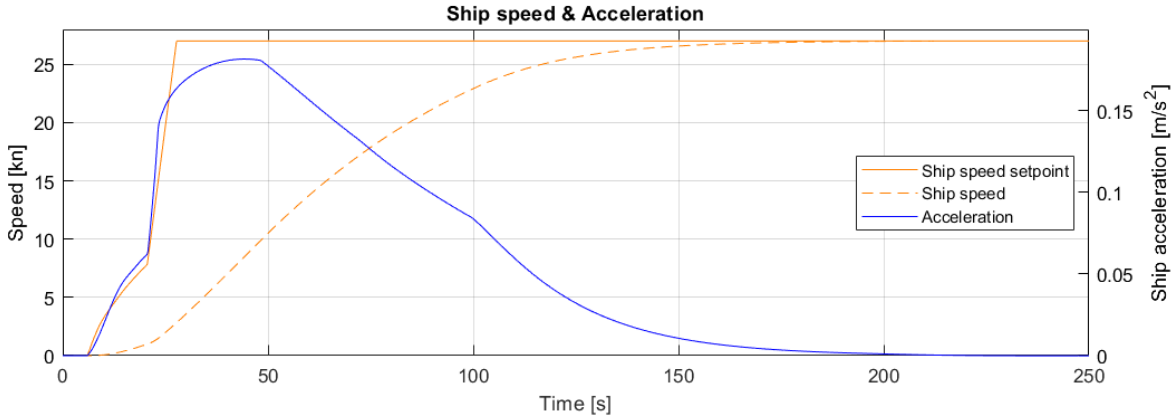

Figure 4.33: Ship speed and acceleration

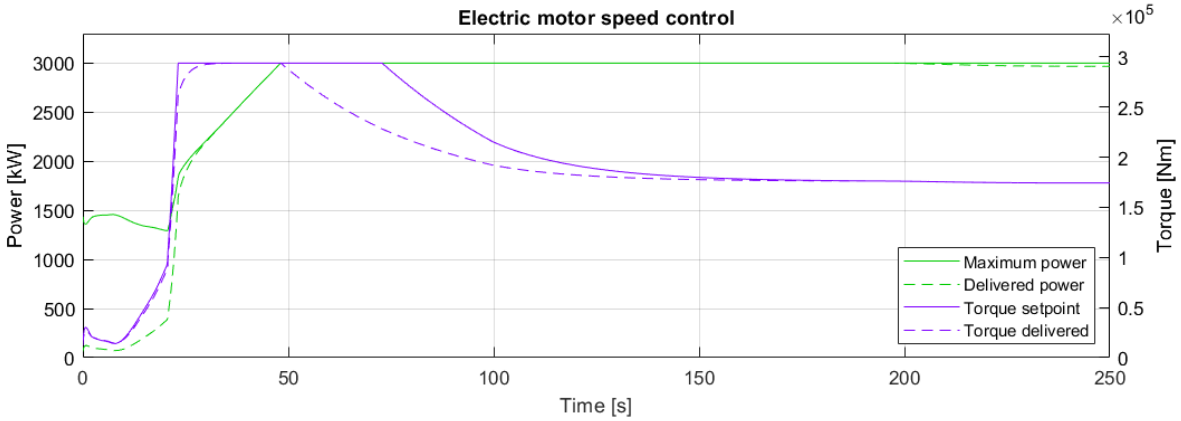

Figure 4.34: Induction machine torque and power

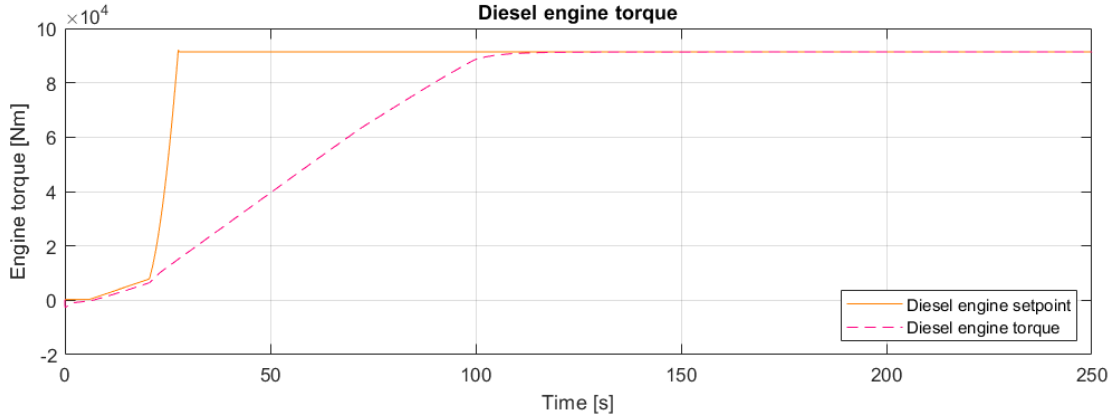

Figure 4.35: Diesel engine torque

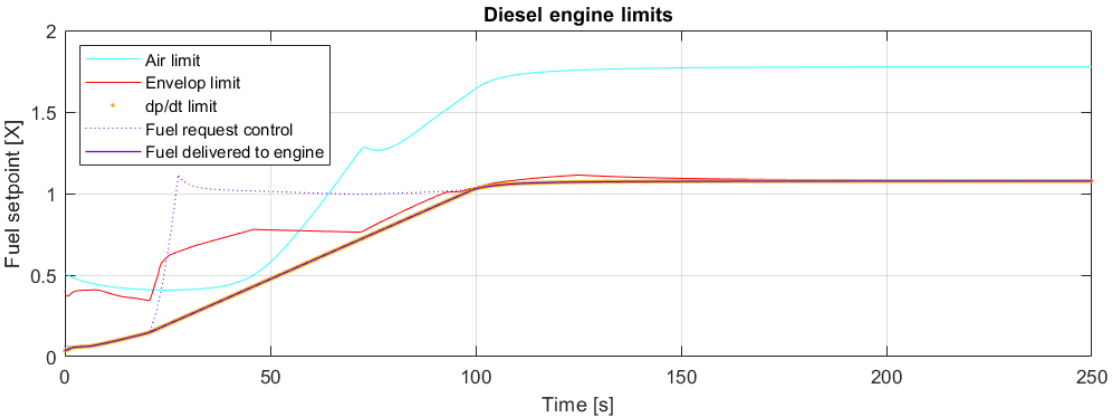

Figure 4.36: Diesel engine limits

Figure 4.35 shows that the torque setpoint that is given to the diesel engine increases fast, the torque produced by the diesel increases at a constant but much slower rate. Figure 4.36 explains the slower torque production of the diesel engine. The fuel input requested by the control is very large, the actual fuel input to the diesel engine follow the maximum fuel increase rate $\frac{d \cdot X}{d \cdot t}$. Figure 4.34 shows that after the propeller is set to design pitch at 20 seconds the electrical propulsion delivers its maximum power. This control mode uses the maximum power from the induction machine and increases the power output of the diesel engine at the maximum allowed rate. The combined knowledge of the propeller operating at design pitch, the electrical propulsion operating at maximum power and the diesel engine increasing its power output by the maximum increase rate allowed explains the very large acceleration observed in Figure 4.33.

4.5.3. Staircase sprint: simulation results

The dynamic load during the staircase sprint is shown in Figure 4.37. It can be observed that the diesel engine operates with sufficient clearance to the envelope. When the ship reaches its new speed setpoint, acceleration stops and the propeller power reduces to its steady state. Even though the pitch setpoints are equal due to the larger acceleration the propeller load is larger than with scenario 1. This is due to the larger acceleration and a larger deviation from the steady state operating points. Figure 4.37 shows that the diesel engine, operating under torque control is much less influenced by the changing propeller load. The small fluctuations after each acceleration are due to a small overshoot in shaft speed. This overshoot in shaft speed is due to the propeller load reducing when the steady state ship speed is reached. The electric propulsion machine delivers the increased torque during acceleration. Figure 4.38 shows the peak in acceleration is very close to the start of the acceleration. The lack of an distinct peak in acceleration 20 to 25 is cased by the induction machine reaching its power limit. In the sprint from 15 to 20 kn the peak of the acceleration occurs 11 seconds after the start of the acceleration which takes 26.9 seconds. In simulation number 2 the acceleration peak was reached at $\frac{2}{3}$ of the total acceleration time, using electrical speed control this peak has moved forward to $\frac{11}{27}$ of the total acceleration time. The faster development of the acceleration, increased peak value of the acceleration and the overall reduced acceleration time results in a very high, sharp and condensed acceleration profile that occurs directly after the start of a manoeuvre. A quantitative overview of the acceleration times is given in Table 4.4.

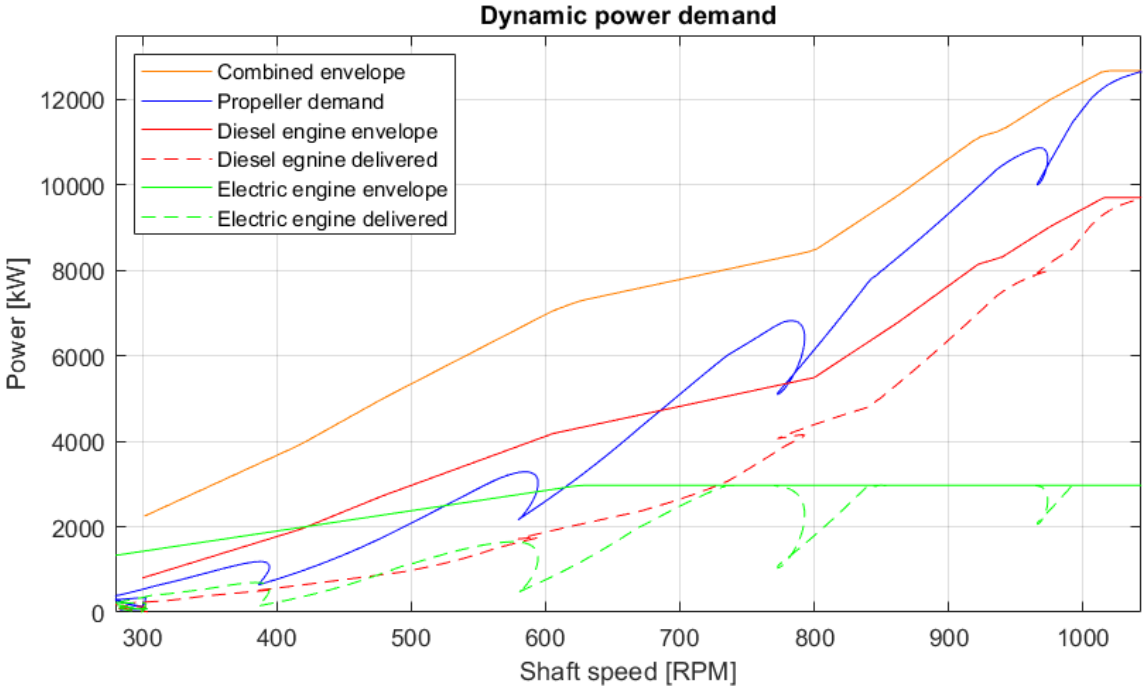

Figure 4.37: Dynamic power demand

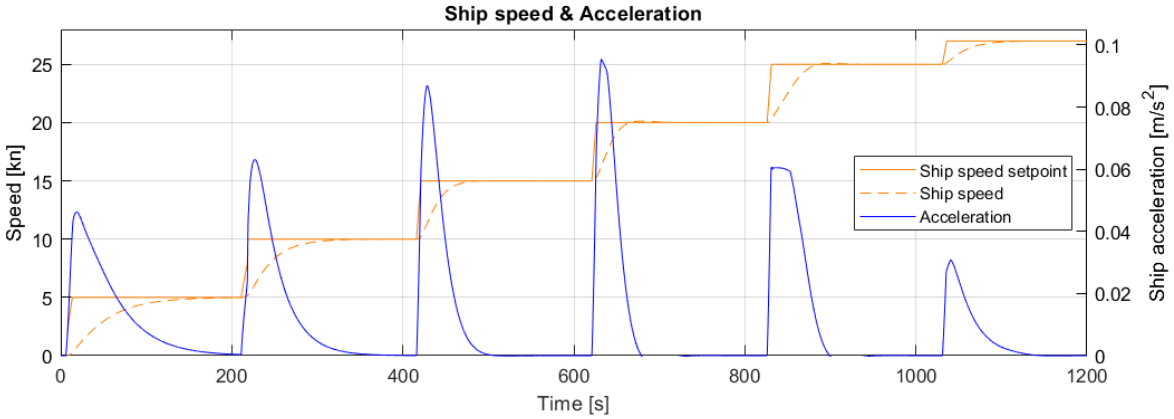

Figure 4.38: Ship speed acceleration

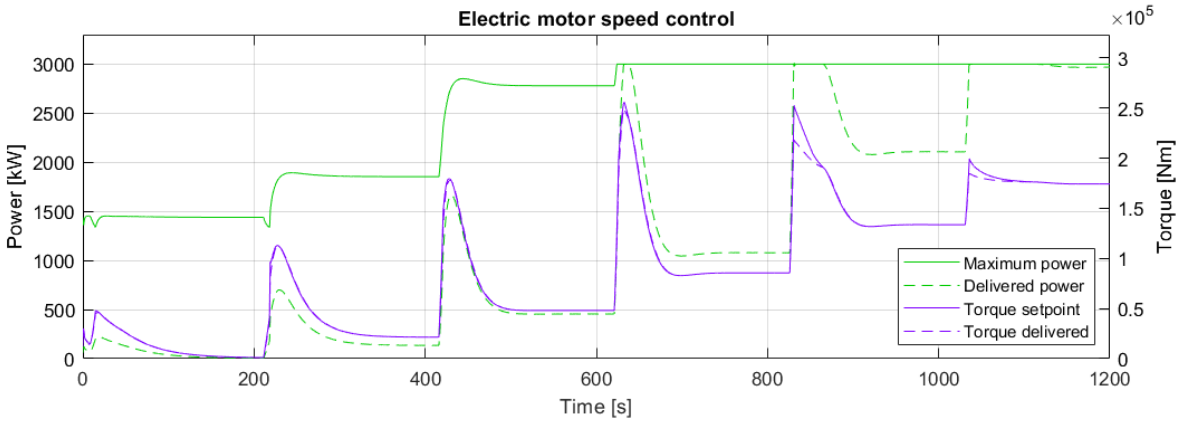

Figure 4.39: Induction machine torque

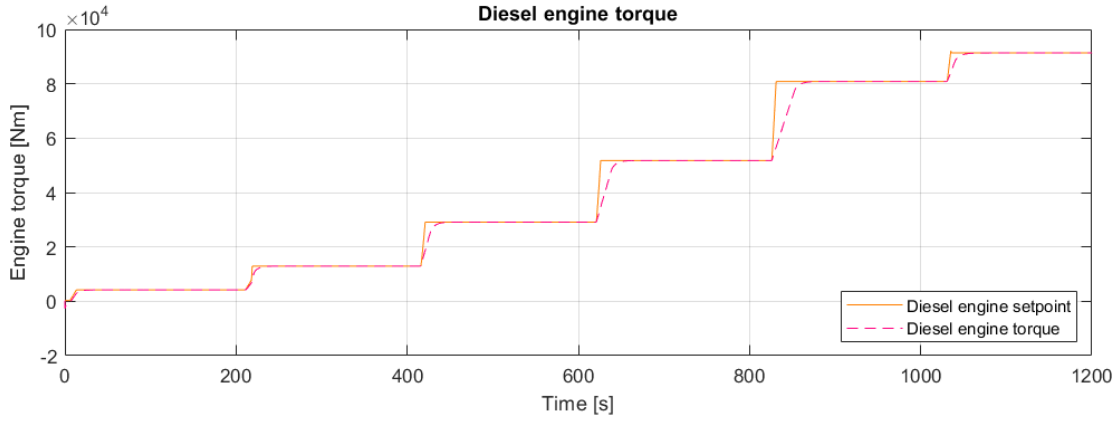

Figure 4.40: Diesel engine torque

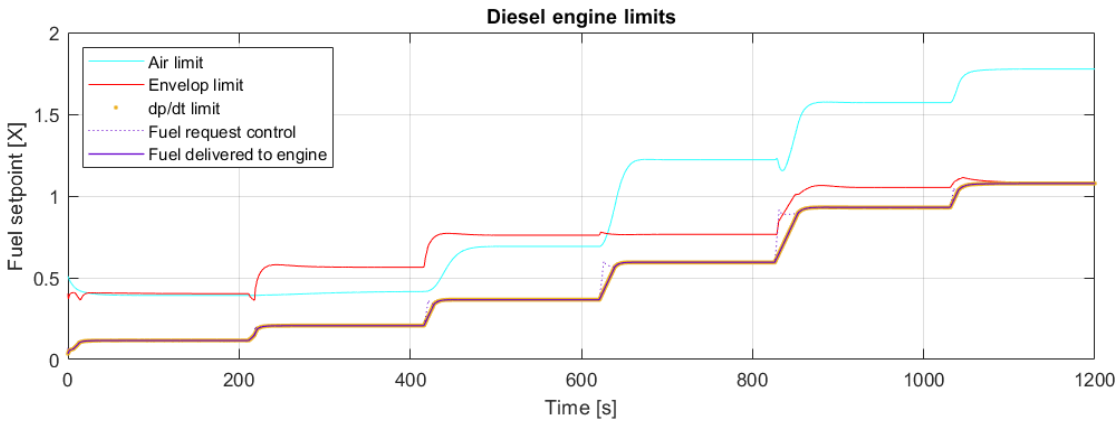

Figure 4.41: Diesel engine limits

Figure 4.39 shows that the potential of the induction machine to produce torque almost instantly is used effectively. Figure 4.40 and Figure 4.41 show that the torque of the diesel engine increases linearly against the maximum allowed increase fuel increase rate. Figure 4.41 further shows that when operating the diesel engine under torque control the limits increase simultaneously with the diesel engine load. When using conventional control the diesel engine load increased before the limits increased.

4.5.4. Control evaluation

Table 4.4 and Figure 4.38 show that electrical speed control is significantly faster than the simulation numbers 1 and 2. The total acceleration from 10 to 15 kn takes 25 % less time, from 15 to 20 kn takes 36 % less time and from 20 to 25 kn takes 35 % less time than conventional control with a reduced pitch as shown in simulation number 2.

Speed [kn]	**0-5**	**5-10**	**10-15**	**15-20**	**20-25**	**0-27**
Total time [s]	121.5	70.2	37	26.9	35.4	119.4
Maximum acceleration [m/s^2]	0.046	0.063	0.087	0.095	0.06	0.18
Time at maximum acceleration[s]	11	25	13	11	5	38

Table 4.4: Simulation number 4: Acceleration times

Overall the performance of electrical speed control is very good. In steady state the diesel engine is loaded close to but not exceeding the diesel engine envelope, ensuring efficient operation. During acceleration the induction machine delivers the full dynamic power. The torque peak needed for the acceleration is produced very fast by the induction machine. It is therefore concluded that both the induction machine and the diesel engine are used effectively. A large total power output can be realised with torque control for the diesel engine, combined with speed control for the induction machine. Firstly, this large power increase is possible due to the induction machine almost instantly delivering a large amount of power during acceleration. Therefore using the induction machine to its full potential. Secondly, this large power increase is possible due to the possibility of matching the power output of the diesel engine in for the static propeller power demand close to the engine envelope. Operating the diesel engine close to its envelope is possible because using torque control makes the diesel engine insensitive to variations in propeller power demand. During the simulation, apart from the constant shaft speed region, no rate limiters were needed on the lever setpoint. The diesel engine power is increased with the maximum amount of power allowed by the manufacturer. Because the diesel engine and the induction machine are capable of providing the propeller load, an alternative combinator with a reduced pitch is deemed unnecessary. The total combined power delivery to the propeller results in a large thrust peak and an associated large peak in acceleration. The power increase of the diesel engine during a slam start and staircase sprint follows the maximum power increase as prescribed by the manufacturer. Combined with the knowledge that the induction machine speed control also delivers a large power, it can be stated that the power availability and delivery to the propeller is close to optimal during the acceleration of the shaft. However this maximum power increase stops when the static torque setpoint is reached, while during acceleration a larger amount of torque could be produced without overloading the diesel engine. Following this simulation two points of interest will be researched in following simulations. Firstly the next simulation will need to confirm if there is an optimal static matching between the diesel engine and the induction machine while using electric speed control. Secondly it will be explored if the remaining margin for the diesel engine can be used with additional control inputs. Reintroducing part of the dynamic load into the control loop of the diesel engine might enable the utilization of the remaining power reserve that exists with this electrical speed control.

4.6. Scenario 5: Diesel engine torque control sweep

Control mode	
Diesel engine	Torque control sweep
Induction machine	Speed control
CP propeller	Combinator

4.6.1. Description

This simulation uses torque control for the diesel engine, speed control for the induction machine and a pitch setpoint following a combinator for the propeller. From scenario 4 it was concluded that torque control for the diesel engine with speed control for the induction machine provided fast acceleration. This simulation group will vary the amount of torque the diesel delivers. The combinator depicted in Figure 4.42 shows all 6 variations. This combinator results in the static matching as is depicted in Figure 4.43. Variation 0 represents a heavy torque setpoint for the diesel engine and thus consequently a light static load for the induction machine. Variation 5 represents a light torque setpoint for the diesel engine and thus consequently a heavy static load for the induction machine. As with scenario 4 it was found no lever rate limiter was needed for the speed setpoint above the minimum shaft speed region.

Figure 4.42: Combinator curves

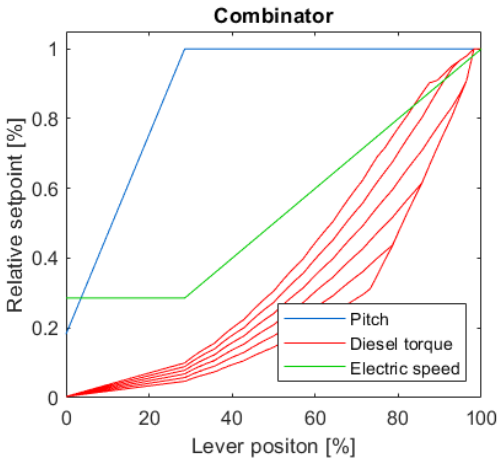

Tuning and limits

The torque setpoint for the diesel engine is varied between two boundaries. For the static power distribution the maximum amount of torque the diesel engine is allowed to produce is 95% of maximum diesel torque according to its envelope. The minimum amount of torque the diesel engine needs to deliver is set such that the induction machine delivers a maximum of 95% of its total available power. This ensures that the last 5% of the induction machines' power is available to maintain and control the desired shaft speed. The static torque setpoint of the diesel engine is varied from 95% of the static propeller torque and reduces in steps of 10%. Variation 0 therefore produces 95% of the propeller torque while variation 5 produces 45% of the static propeller torque.

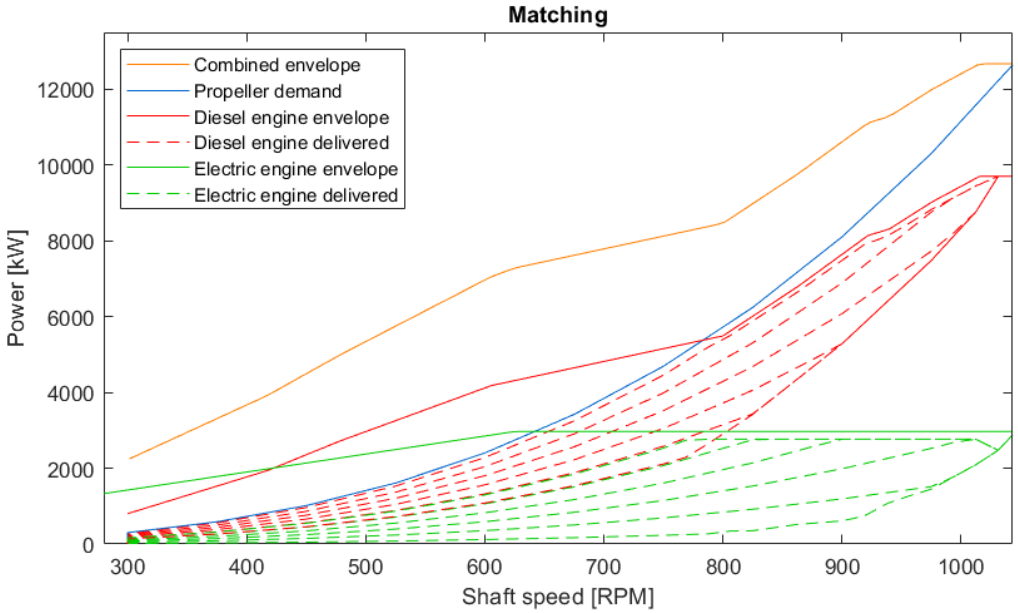

Figure 4.43: Matching variations

4.6.2. Slam start: simulation results

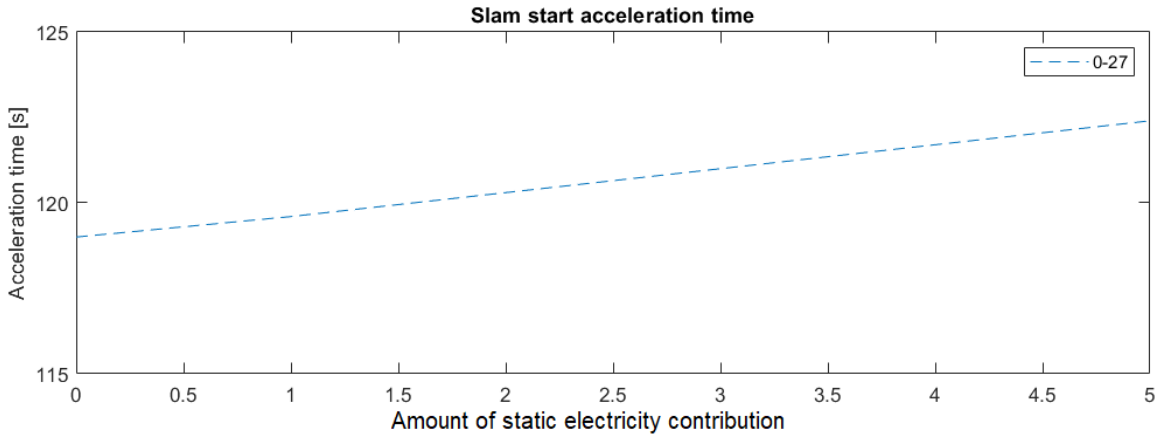

Figure 4.44: Slam start acceleration times

4.6.3. Staircase sprint: simulation results

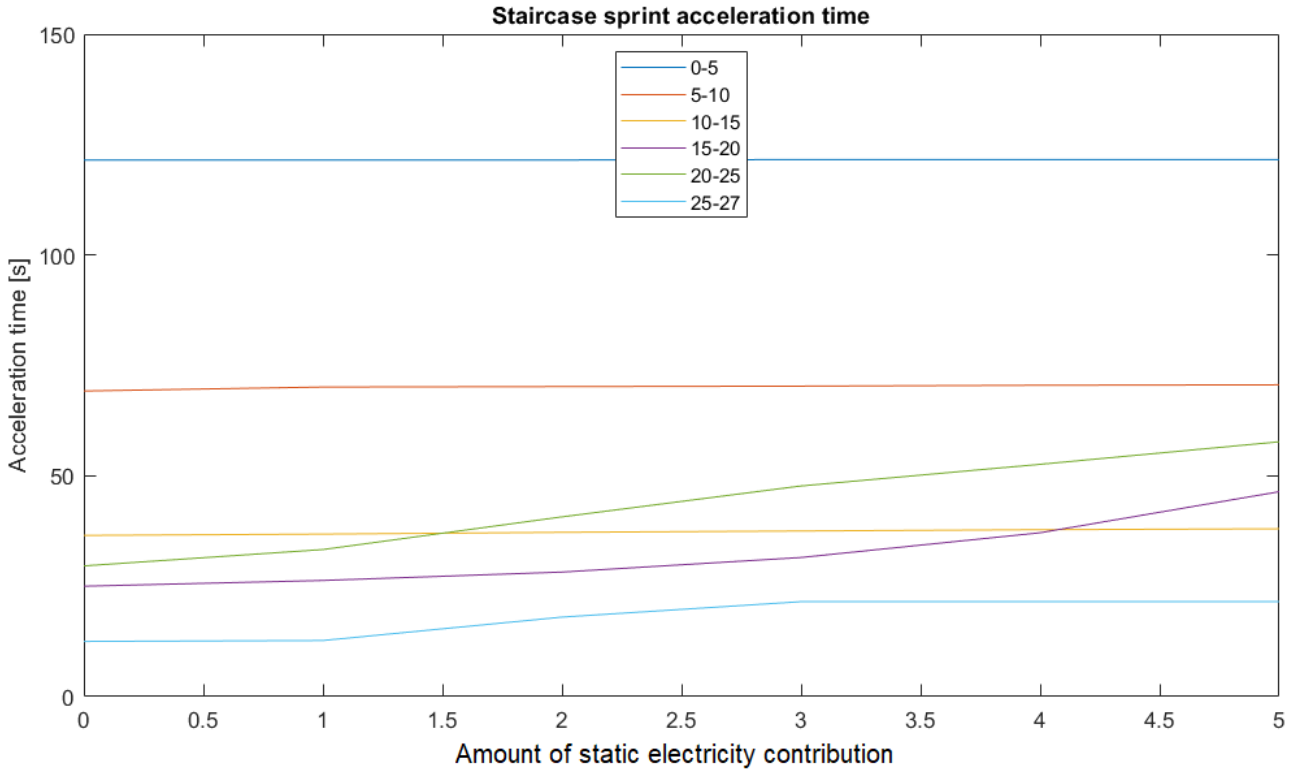

Figure 4.45: staircase sprint acceleration time

4.6.4. Control evaluation

From Figure 4.44 and Figure 4.45 it can be seen that for both the slam start and the staircase sprint the fastest acceleration is achieved at variation 0. This variation sets the torque setpoint for the diesel engine to be 95% of the propeller load. This matching therefore uses a large amount of power from the diesel engine in steady state. As a consequence the induction machine contributes only a small portion of the propulsion power when the ships sails at a steady state ship speed. This maximizes the power reserve in the induction machine. Due to the induction machine operating in speed control this large power reserve is used during the accelerations. variation 0 with a heavy static loading for the diesel engine results in both the diesel engine and the induction machine producing a high amount of power for the entirety of the acceleration manoeuvre. The high power output of both the diesel engine and the induction machine explains why variation 0 gives the best acceleration performance. It should however be stated that at the time of writing of this report torque control is not available from manufacturers. Based on this simulation it can however be stated that heavy loading on the diesel engine in steady state, combined with a large power availability from the induction machine which is used during acceleration gives a fast acceleration performance.

4.7. Scenario 6: Adaptive pitch control

Control mode	
Diesel engine	Slow speed control
Induction machine	Torque control
CP propeller	Angle of attack control

4.7.1. Description

This control strategy uses the CP propeller to control the angle of attack of the inflowing water on the propeller blades. The induction machine is used in torque control mode. The diesel engine is used in speed control mode. Slow engine speed integrating control is used to prevent large shaft speed fluctuations. The angle of attack is controlled to be the angle of attack in the design condition, which is 4 degrees. Previous control strategies aimed at providing enough torque to power through the torque peak associated with the higher angle of attack during acceleration. This control strategy uses the CP propellers to control the angle of attack to be 4 degrees. By keeping the angle of attack at 4 degrees the torque peak is avoided, with two goals. The original goal as defined by Vrijdag [30] was preventing cavitation during acceleration. The second goal is preventing the power needed for the propeller to exceed the operating envelope of the propulsion system.

Tuning and limits

From the tuning process it became apparent that for accelerations starting in the lower ship speed range the shaft speed setpoint will change quite severe. For example at a speed increase from 0 to 5 kn the shaft speed setpoint would increase from 300 rpm to 1050 rpm to eventually be reduced back to 300 at the final ship speed of 5 kn. The source of such a large fluctuation during one acceleration can be found in the combination of the pitch and virtual shaft speed setpoint as described in equation 3.44. The pitch is used to set the angle of attack which is in turn dependent on the rotational speed and ship speed. This means that the pitch is linked to the ship speed, meaning that at low speed the allowed pitch is very low. When represented with a change in virtual shaft speed setpoint at low ship speeds, the relatively low pitch and the new higher virtual shaft speed setpoint lead to a large real shaft speed setpoint. These large changes in engine speed setpoint for relatively low changes in speed at low speeds are unwanted and eliminated by a variable engine speed limitation. Therefore in addition to the shaft speed being limited between 300 rpm and 1050 rpm a limit is introduced that takes into account the final shaft speed at the new ship speed setpoint. The implementation is shown in equation 4.1, in which a scalable constant (C_{apc}) can be used to set the maximum amount of times the dynamic shaft speed can exceed the steady state shaft speed. For this simulation ($C_{apc} = 2$) is used, meaning that in the previous example of an acceleration from 0 to 5 kn, with a steady state shaft speed at 5 kn of 300 rpm, the maximum shaft speed during acceleration will be 600 rpm.

$$n_{shaft,max} = C_{apc} \cdot n_{shaft,final} \tag{4.1}$$

During the tuning process it became apparent that fast/aggressive tuning of the diesel motor also results in large and fast shaft speed oscillations. This tendency towards unstable behavior is explained by the method of calculating the pitch and shaft speed setpoint. Pitch and shaft speed are linked meaning that at a given ship speed, engine and pitch can fluctuate together. To counter this inherent tendency for instability both the diesel engine and the pitch actuation are tuned give a slower response. For APC no rate limiters were needed for the change in lever setpoint.

4.7.2. Slam start: simulation results

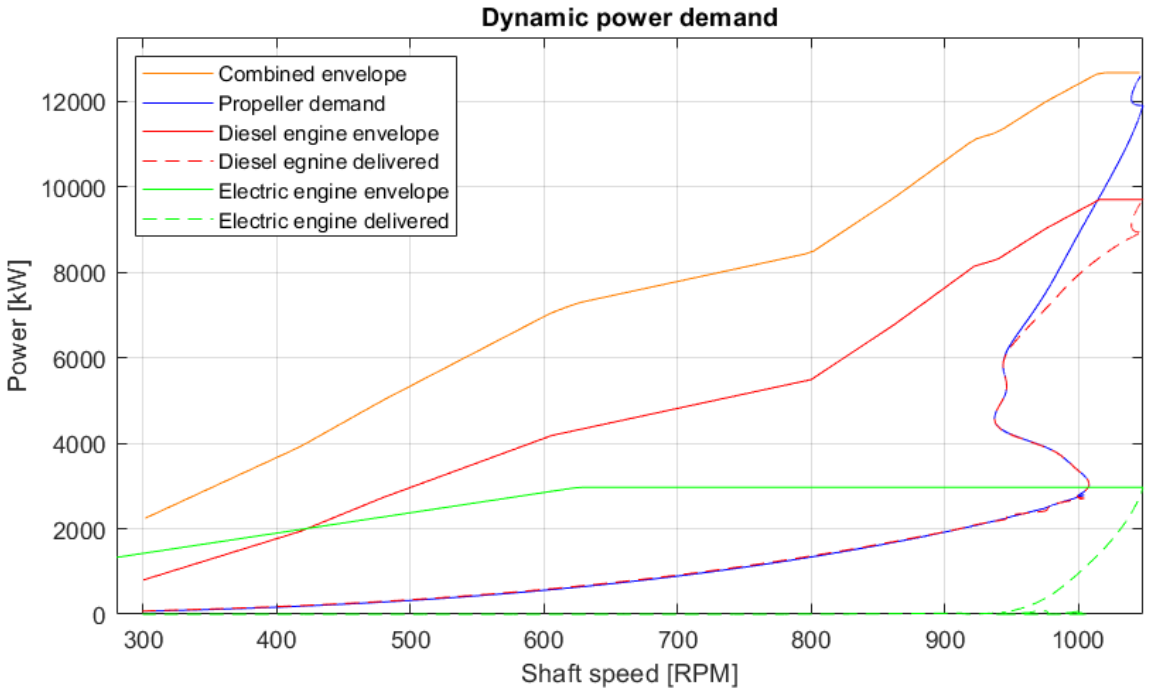

Figure 4.46: APC slow: Slam start dynamic load on diesel engine and induction machine

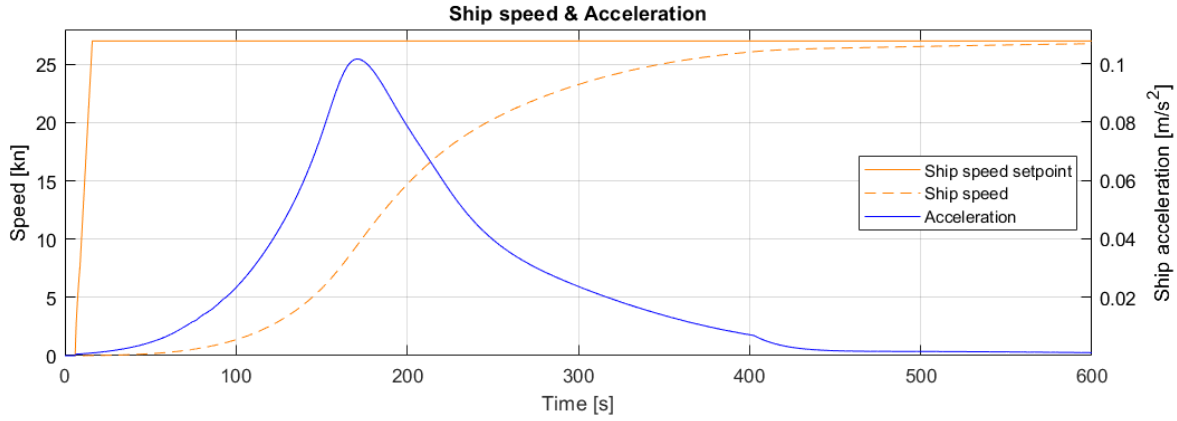

Figure 4.47: APC slow: Slam start ship speed and acceleration

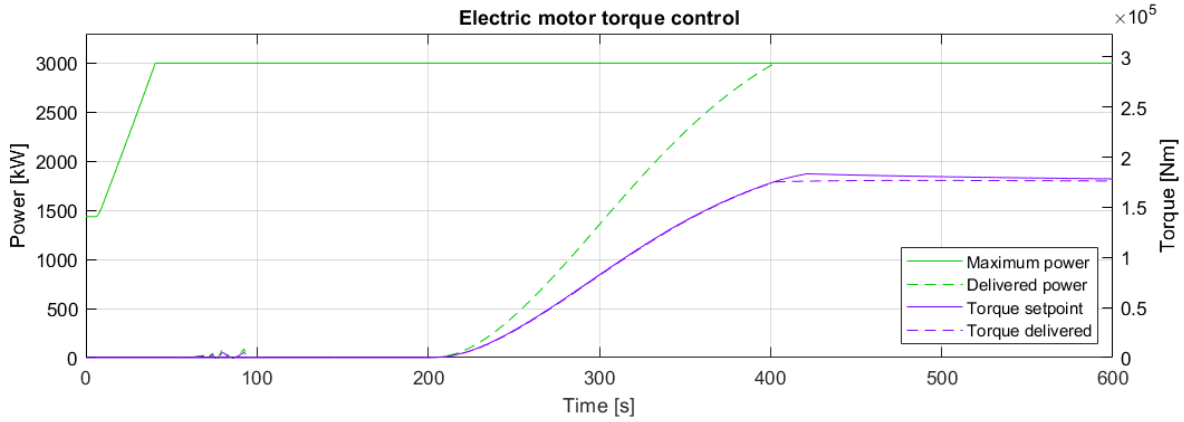

Figure 4.48: APC slow: Slam start induction machine torque production

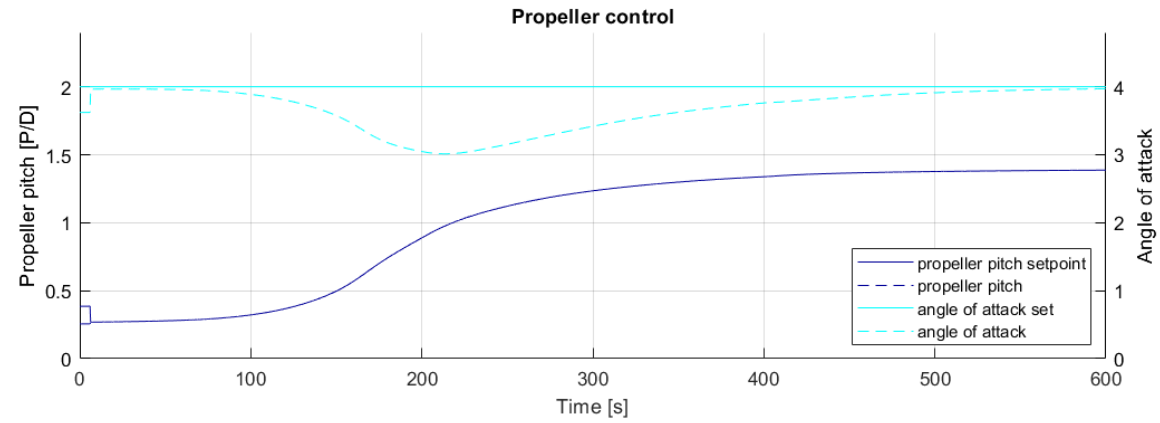

Figure 4.49: APC slow: Slam start propeller pitch and angle of attack

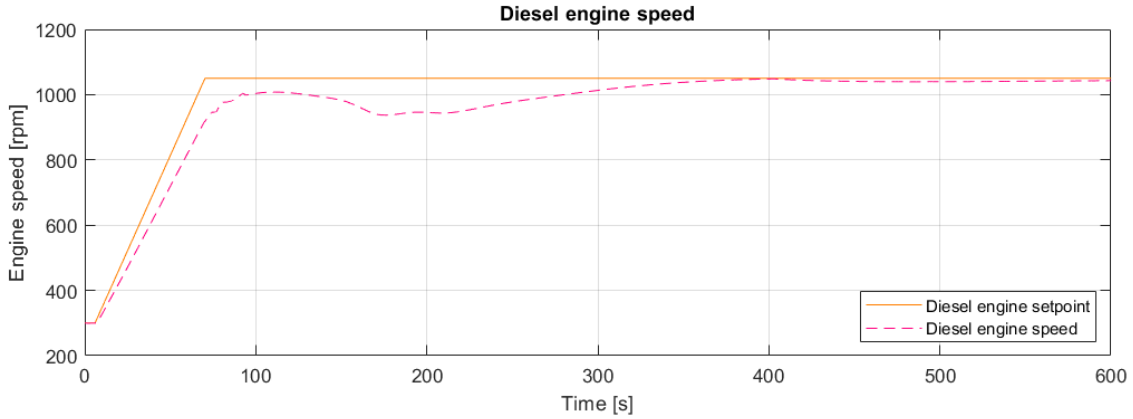

Figure 4.50: APC slow: Slam start diesel engine speed and setpoint

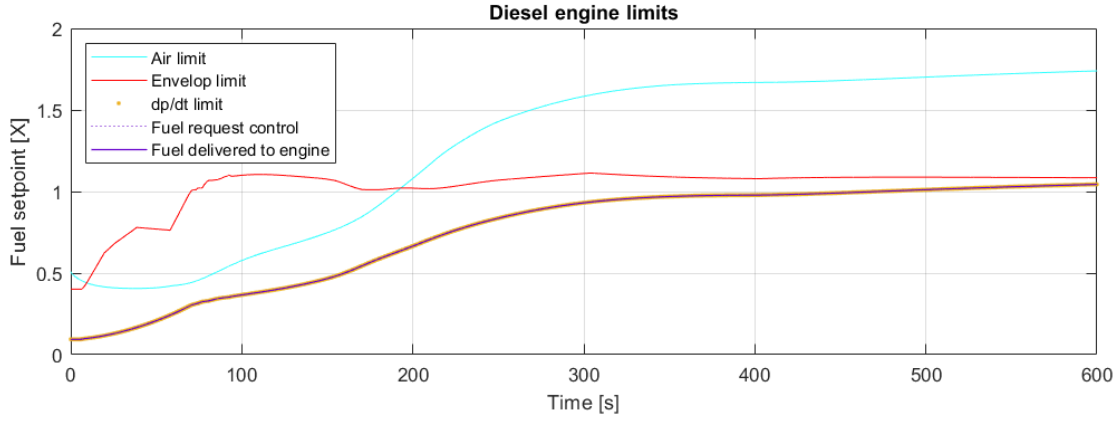

Figure 4.51: APC slow: Slam start diesel engine limits

Figure 4.46 shows that during a slam start the torque peak associated with a larger angle of attack is effectively avoided. During the slam start the diesel engine increases shaft speed with, at the start, a low pitch setting ensuring the correct angle of attack of 4 degrees. During the slam start the pitch increases as the ship speed increases, as can be observed in Figure 4.61 and Figure 4.47. Looking at Figure 4.61 and Figure 4.50 it becomes apparent that when the pitch is increased the slow integrating speed control governing the diesel engine can't increase the fuel setpoint fast enough to keep the shaft speed at the desired level. This explains the reduction in shaft speed that can also be seen in Figure 4.46. Figure 4.46 and Figure 4.51 show that during the

acceleration manoeuvre the diesel engine has sufficient clearance from its limits. It is observed that the load on the diesel engine follows a very different path through the engine envelope than in previous simulations. It can be seen that first the shaft speed increases, which is than followed by a larger engine load. Figure 4.47 shows that the acceleration manoeuvre takes a very long time, in total 369.5 seconds are needed to reach 90% of the final ship speed setpoint. The acceleration profile looks very different than the previous scenarios. However the acceleration peak of 0.1 m/s^2 is about 50% smaller that with electrical speed control as seen in simulation number 4. Furthermore this peak takes a long time to develop and is located at 163 seconds after the start of the acceleration. The acceleration profile does not show any sharp increases or decreases in acceleration, which in previous simulations was associated with the limits of the propulsion system. Instead gradually increasing and then decreasing acceleration is measured. This can be explained by the constant angle of attack with a pitch that follows the ship speed, gradually increasing the power transferred to the water. This means that the torque peak associated with the larger angle of attack during accelerations is effectively avoided, but at the expense of the larger thrust the propeller provides at this larger angle of attack.

4.7.3. Staircase sprint: simulation results

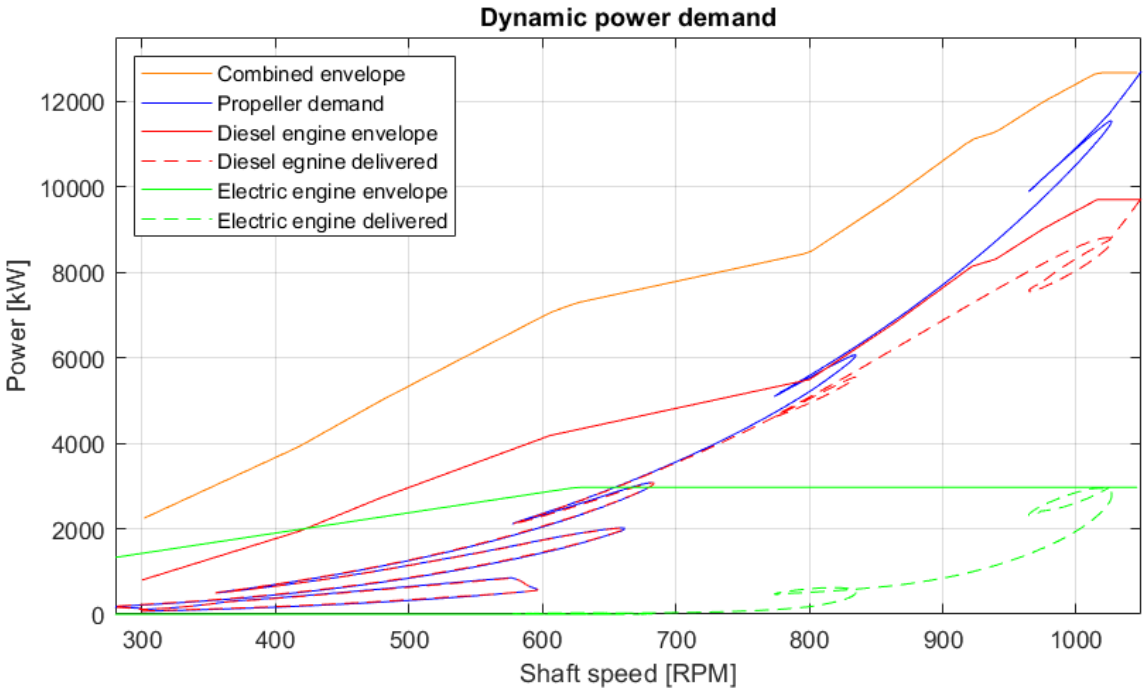

Figure 4.52: APC slow: Staircase sprint dynamic load on diesel engine and induction machine

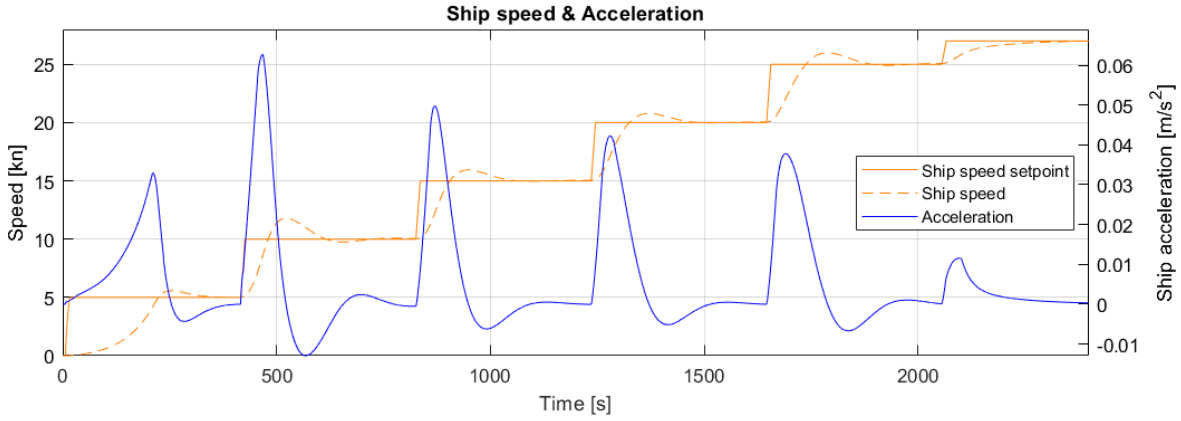

Figure 4.53: APC slow: Staircase sprint ship speed and acceleration

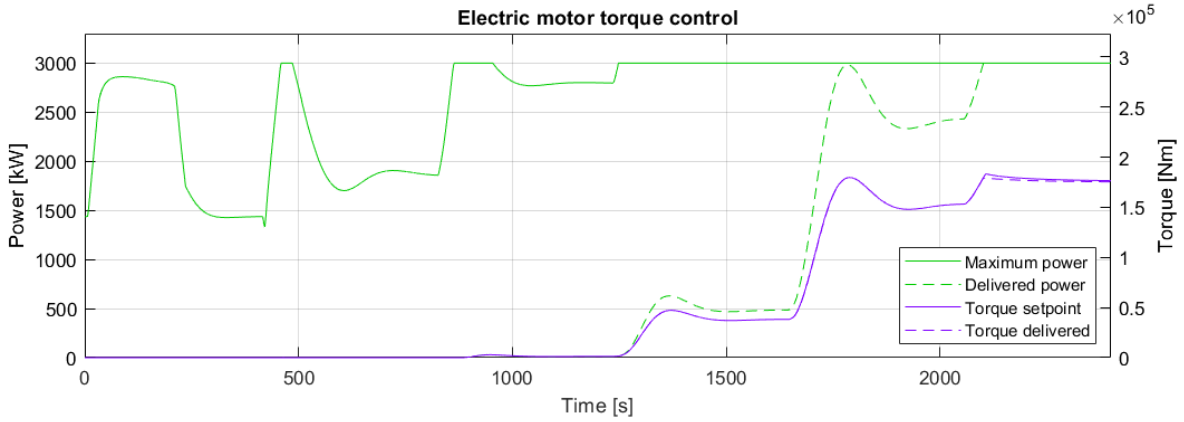

Figure 4.54: APC slow: Staircase sprint induction machine torque production

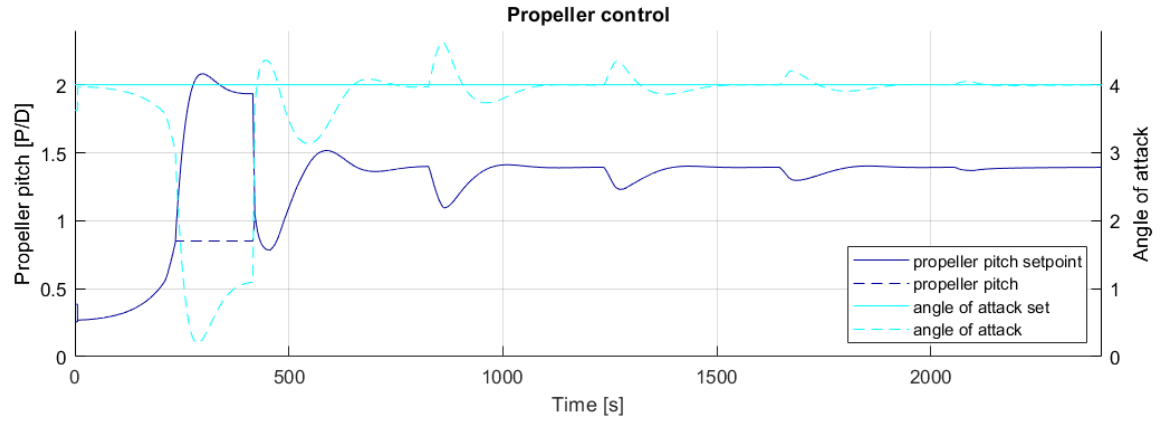

Figure 4.55: APC slow: Staircase sprint propeller pitch and angle of attack

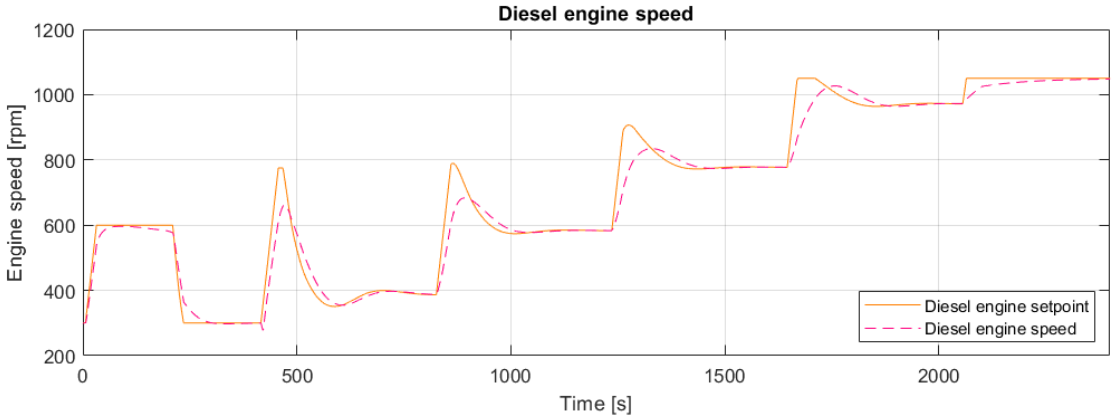

Figure 4.56: APC slow: Staircase sprint diesel engine speed

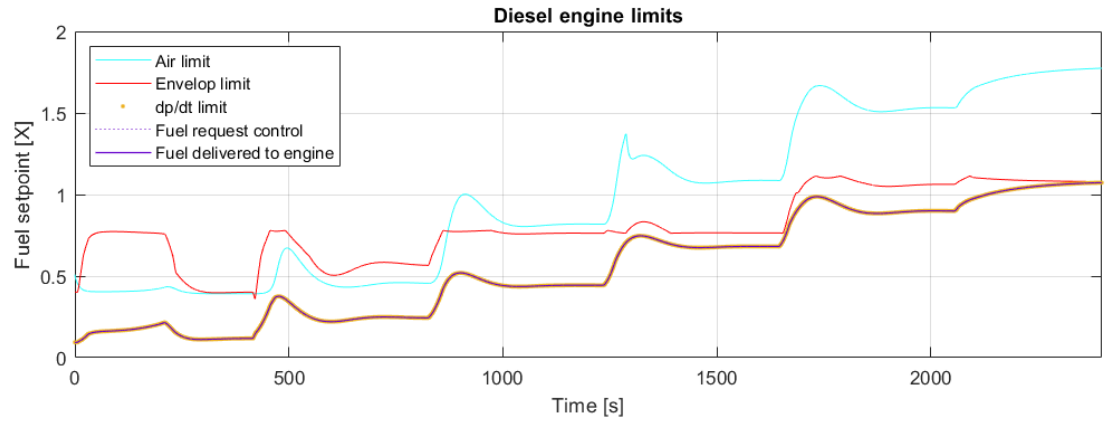

Figure 4.57: APC slow: Staircase sprint diesel engine limits

Figure 4.52 shows the behavior of the APC at intermittent accelerations with a 5 kn interval. For each acceleration an increase in shaft speed is observed. This initial increase in shaft requires a small amount of power due to the low pitch as can be seen in Figure 4.55. When the ship speed picks up the propeller pitch increases to maintain the desired angle of attack. As a consequence in order to maintain the desired virtual shaft speed the absolute shaft speed reduces back to its steady state operating point. This increase and decrease in shaft speed can be seen in Figure 4.56. Figure 4.55 and Figure 4.56 show that the diesel engine accelerates with the propeller at a lowered pitch and as a consequence needing less power. Figure 4.55 shows that during the intermittent acceleration from 0 to 5 kn the angle of attack can't be maintained, this is due to the limitation that set a maximum pitch at the lower speed. Figure 4.53 shows the acceleration and ship seed. It is visible

that APC has some inherent instability in the ship speed, this originates in the interaction between the pitch and shaft speed which together results in the desired virtual shaft speed giving the desired ship speed. The settling into the steady state of both the shaft speed and the pitch, which are dependent on each other cause the oscillation in the ship speed.

4.7.4. Control evaluation

Figure 4.53 shows that the acceleration of APC has a distinctly different profile when compared to previous scenarios. The gradual increase in acceleration caused by the maintaining of a set angle of attack results in lower peak accelerations than the peak acceleration found with electrical speed control. For the intermittent acceleration from 15 to 20 kn the total acceleration time is 69.1 seconds with a peak acceleration of 0.042. This peak acceleration occurs after 45 seconds, meaning this acceleration develops slow. This version of APC using slow integrating speed control for the diesel engine is at the intermittent acceleration from 15 to 20 kn 61% slower than the electrical speed control used in scenario 4. Table 4.5 shows the absolute acceleration data for all accelerations.

Speed [kn]	**0-5**	**5-10**	**10-15**	**15-20**	**20-25**	**0-27**
Time [s]	213.3	59.6	67.0	69.1	68.4	369.5
Maximum acceleration [m/s^2]	0.032	0.062	0.050	0.042	0.038	0.10
Time at maximum acceleration[s]	211	49	45	41	45	163

Table 4.5: Simulation number 6: Acceleration times

This version of APC, which uses slow integrating speed control for the diesel engine eliminates the torque peak associated with the larger angle of attack during accelerations. This avoiding of the torque peak during acceleration is however at the expense of the larger thrust the propeller provides at this larger angle of attack. The lack of a larger angle of attack and the associated large thrust peak at the start of an acceleration makes APC with slow integrating speed for the diesel engine slower than other control candidates. It can be observed in Figure 4.55 that during sailing at a constant slow speed the effective design angle of attack can not be maintained. Maintaining the design angle of attack at the minimum shaft speed would result in a higher ship speed, therefore the angle of attack is limited. Although the propeller operates quite efficient at the constant angle of attack, the reduced peak in torque does lead to a reduced peak in thrust, therefore directly limiting the acceleration. To improve the acceleration in simulation number 7 the equation 2.68 describing the thrust produced by a propeller is evaluated, for convenience it is repeated below.

$$T = C_T^* \cdot \frac{1}{2}\rho\left(V_A^2 + \left(0.7\pi \cdot n_p \cdot D\right)^2\right)\frac{\pi}{4} \cdot D^2 \tag{4.2}$$

The total produced thrust is dependent on the propeller shaft speed n_p squared. Simulation number 7 will investigate the effect of increasing the propeller shaft speed propeller. Increasing the propeller shaft speed at the same ship speed and thus the same advance velocity V_A will reduce the hydrodynamic pitch angle (β). To maintain the fixed angle of attack with the reduced (β) the pitch will also need to be reduced. The thrust coefficient C_T^* is both depending on the hydrodynamic inflow angle as well as the pitch of the propeller. It will therefore be interesting to test if an increased shaft speed will result in an increased acceleration. Simulation number 7 will investigate what can be achieved with APC when the governor of the diesel engine is tuned more aggressively. A more aggressive tuning of the diesel engine shaft speed governor will potentially result in a faster increasing and decreasing shaft speed, possibly allowing the fixed angle of attack to create a larger amount of thrust. This could potently enhance the acceleration performance of APC.

4.8. Scenario 7: Fast adaptive pitch control

Control mode	
Diesel engine	Fast speed control
Induction machine	Torque control
CP propeller	Angle of attack control

4.8.1. Description

The fast APC discussed in this section is an adaptation following the slow APC discussed is simulation 6. The only difference it that this version uses a larger proportional gain for the PI controller of the diesel engine. This section only discusses the differences in results between simulation numbers 6 and 7, a more in dept evaluation can be found in simulation 6. In the control evaluation of scenario 6 it was speculated that a more aggressive governor could result in a sharper shaft speed increase and possibly a larger and faster thrust increase during acceleration. It should however be stated that this version operates with large engine speed fluctuations.

Tuning & trade offs APC fast

As stated above the governor controlling the speed of the diesel engine is tuned with a larger proportional gain. Furthermore in scenario 6 the maximum shaft speed during an acceleration was limited. This limitation was defined to be no more than two times the steady state shaft speed associated with the new ship speed setpoint. This limitation on the shaft speed during acceleration is removed, making it possible for the shaft speed to fluctuate between the absolute maximum and minimum shaft speed for every acceleration.

4.8.2. Slam start: simulation results APC fast

Figure 4.58 shows the slam start using APC. In simulation number 6 the governor could not increase the fuel setpoint fast enough to account for the increase in pitch during the acceleration. This resulted in a drop is shaft speed during acceleration. With the more aggressively tuned governor the drop is shaft speed is still present but much less pronounced as can be seen in Figure 4.62. Compared to simulation number 6 the different subsystems and the acceleration show the same characteristics and the graphs follows a very similar shape. The only difference is that this simulation with a more aggressively tuned diesel engine is faster. The acceleration as shown in Figure 4.59 now takes 280 seconds which is a 24 % improvement compared to simulation number 6. The peak acceleration of the slam start is now 0.13 m/s^2 which is 30% larger than the acceleration found in simulation number 6.

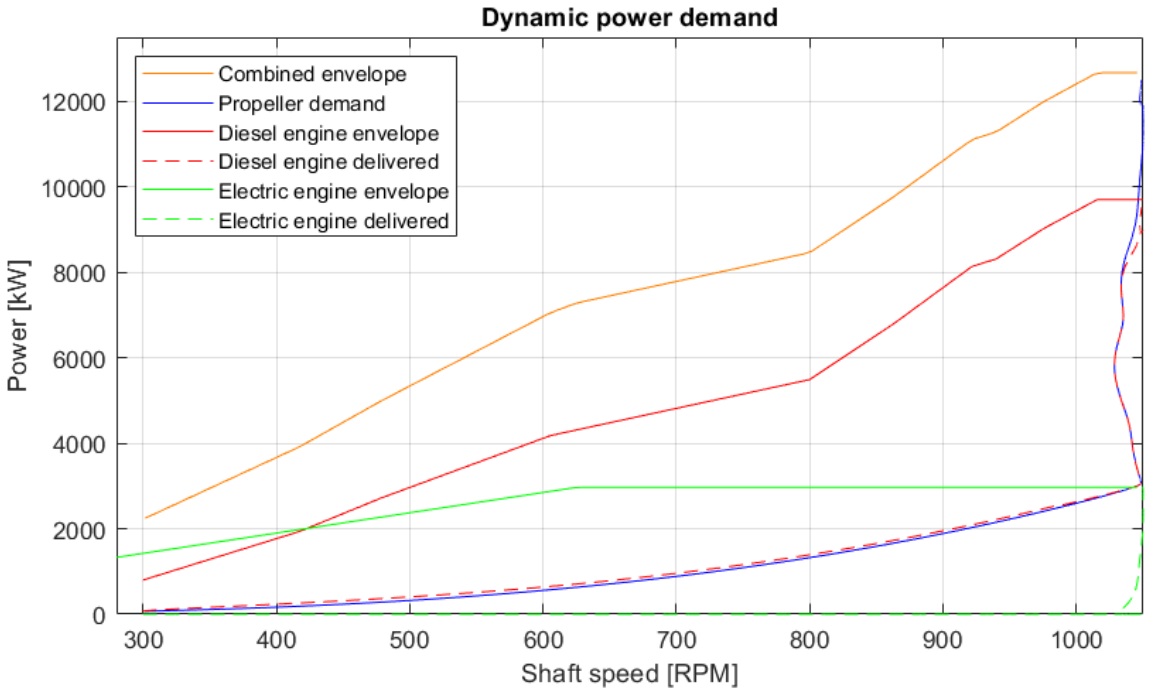

Figure 4.58: APC fast: slam start dynamic load

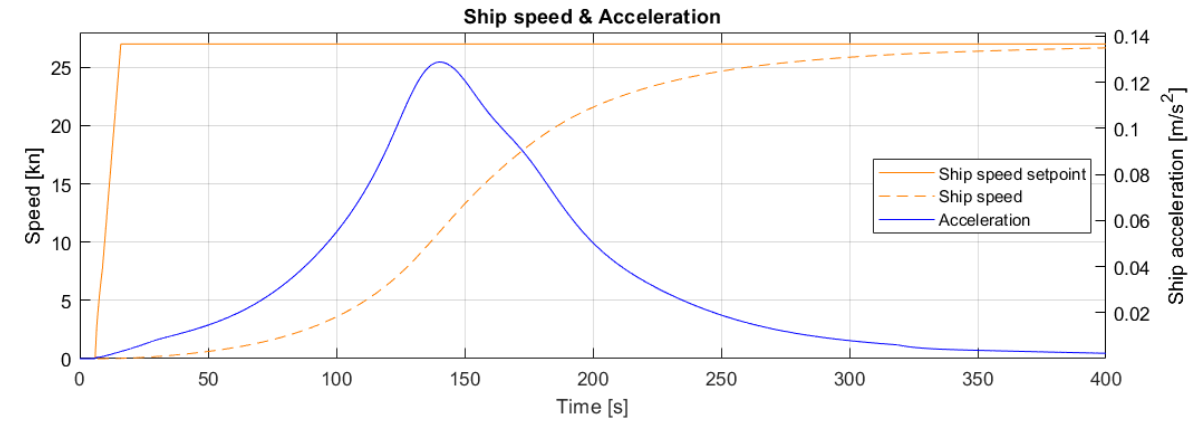

Figure 4.59: APC fast: ship speed and acceleration time

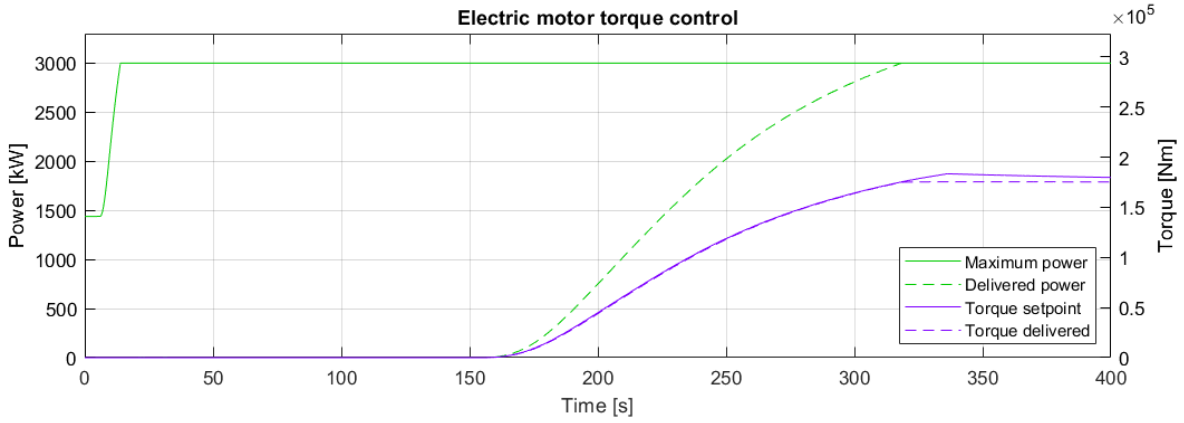

Figure 4.60: APC fast: induction machine torque and power

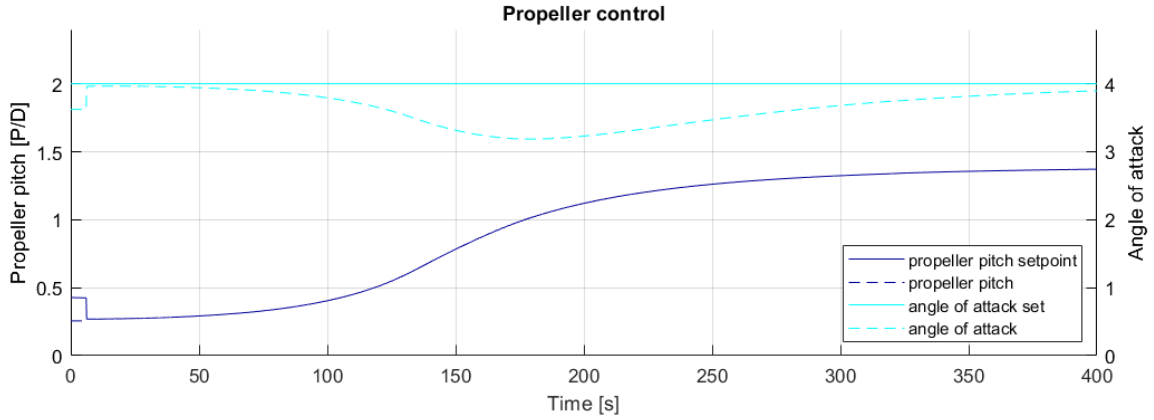

Figure 4.61: APC fast: propeller pitch and angle of attack

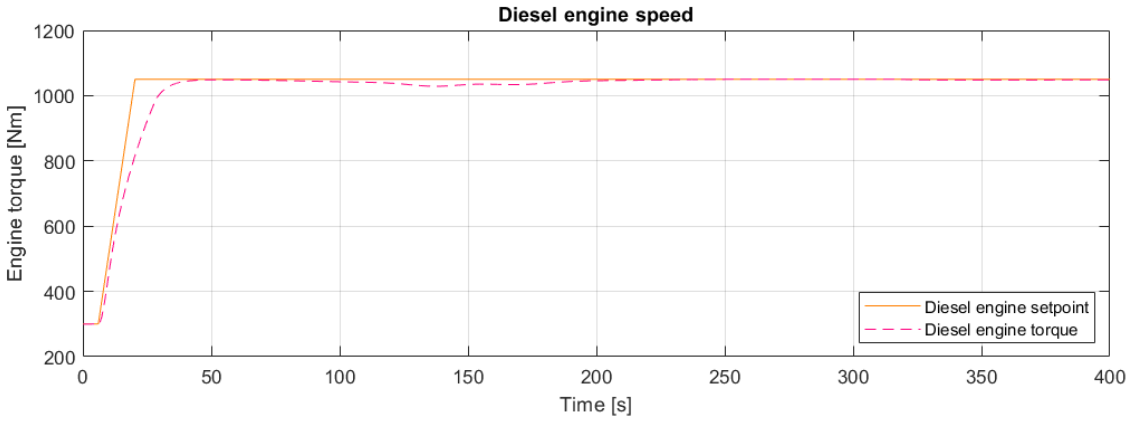

Figure 4.62: APC fast: diesel engine speed

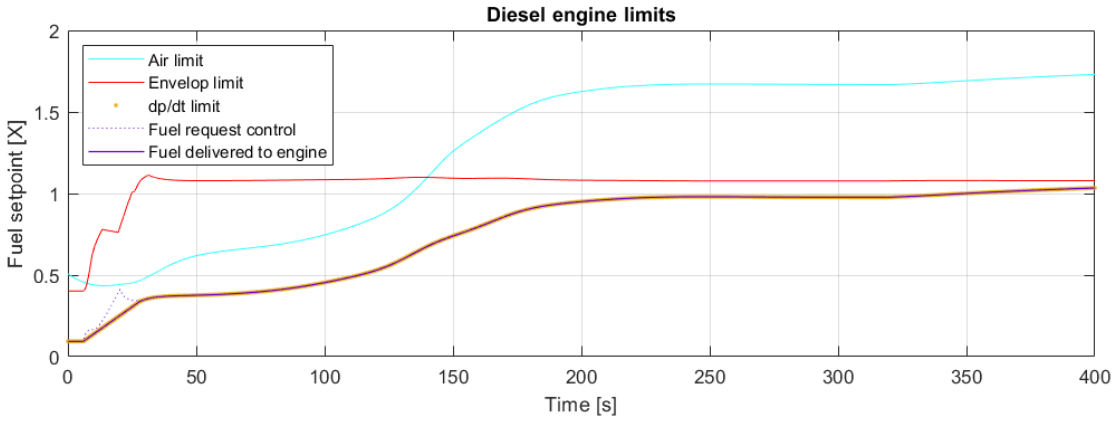

Figure 4.63: APC fast: diesel engine limits

4.8.3. Staircase sprint: simulation results APC fast

Figure 4.64 and Figure 4.68 show that for each acceleration the engine speed is increased greatly. For instance the intermittent acceleration from 0 to 5 kn has the largest fluctuation in shaft speed and starts at a shaft speed of 300 rpm and increases to a shaft speed of 1045 rpm. This large and fast increase in shaft speed reduces the acceleration time to 104 seconds which is slightly less than half of what was needed for the same change in speed setpoint in simulation number 6. For the other intermittent accelerations the sharper increase in shaft speed is less pronounced but still observable when comparing Figure 4.68 to Figure 4.56. The acceleration time is reduced by about 40% compared to simulation number 6. The shape and overall behavior of the acceleration is the same as simulation 6 as can be seen when comparing Figure 4.65 to Figure 4.53. It should however be noted that the inherent instability in the settling of the shaft speed and propeller pitch becomes more pronounced.

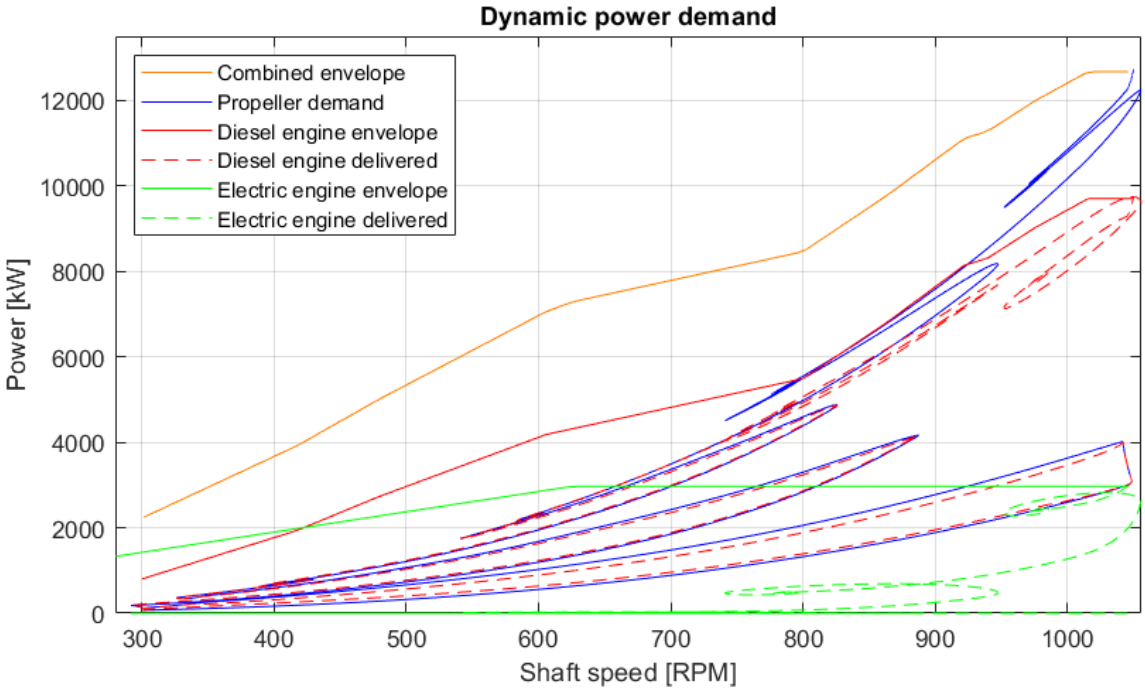

Figure 4.64: APC fast: dynamic load demand

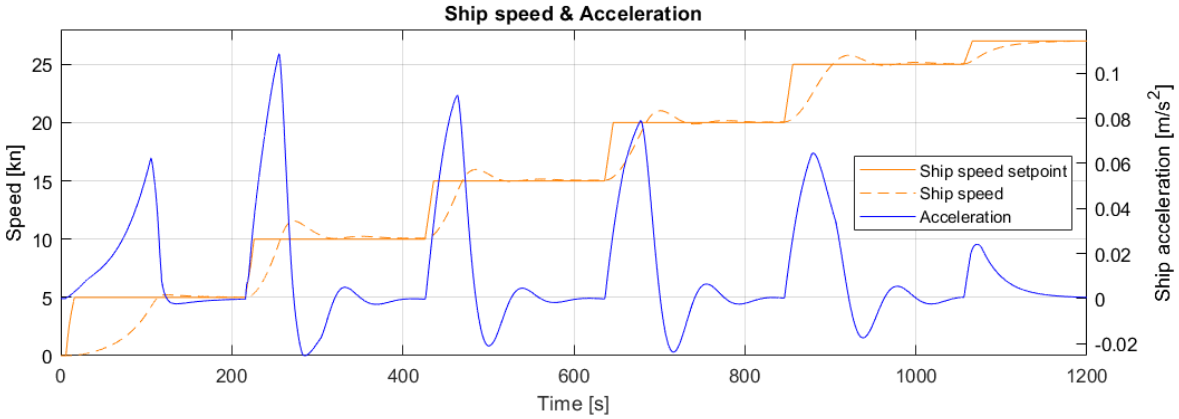

Figure 4.65: APC fast: Ship speed and acceleration

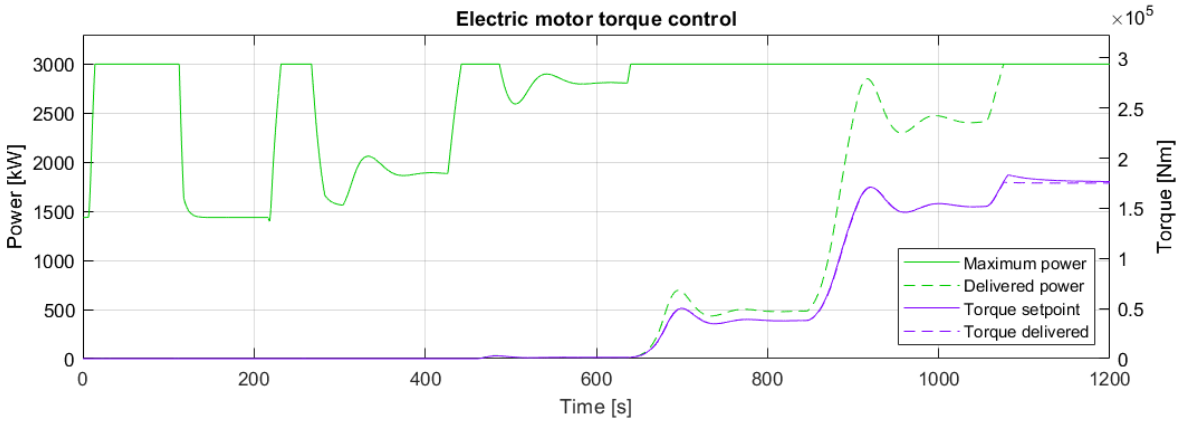

Figure 4.66: APC fast: induction machine torque and power

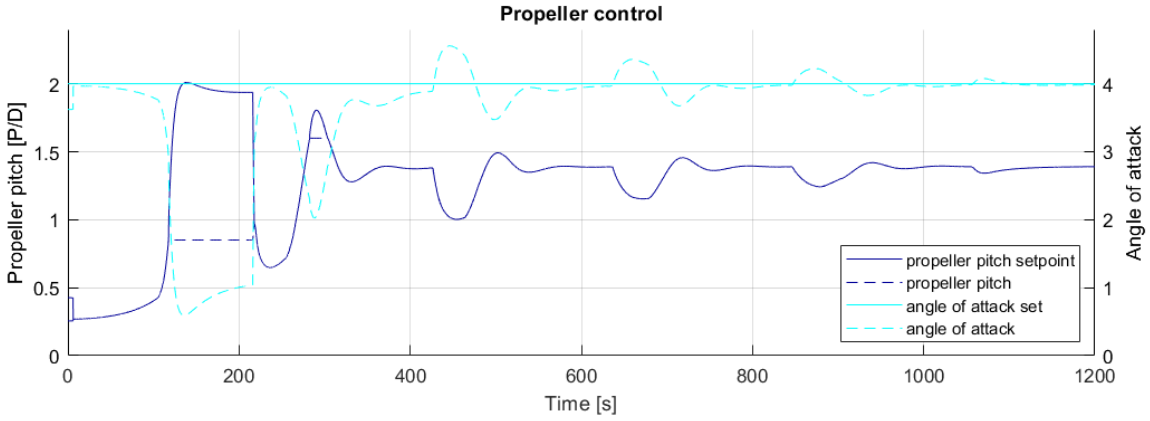

Figure 4.67: APC fast: propeller pitch and angle of attack

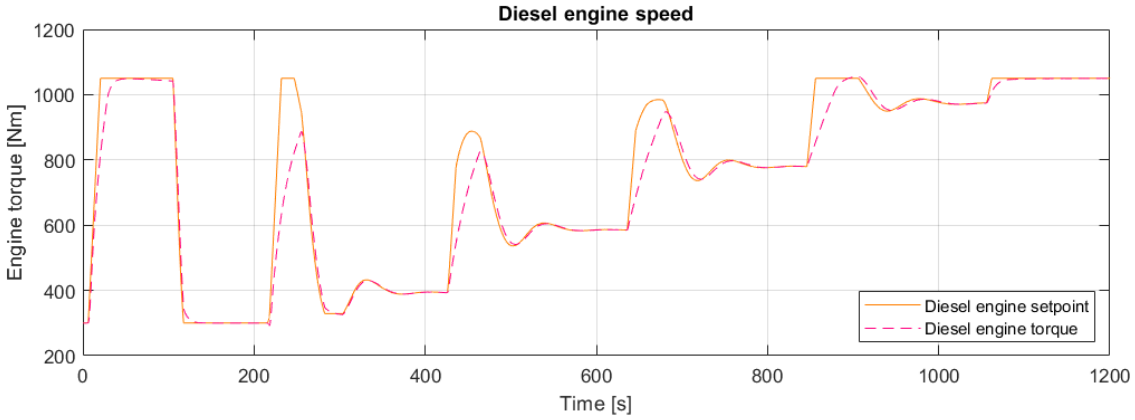

Figure 4.68: APC fast: staircase acceleration diesel engine speed

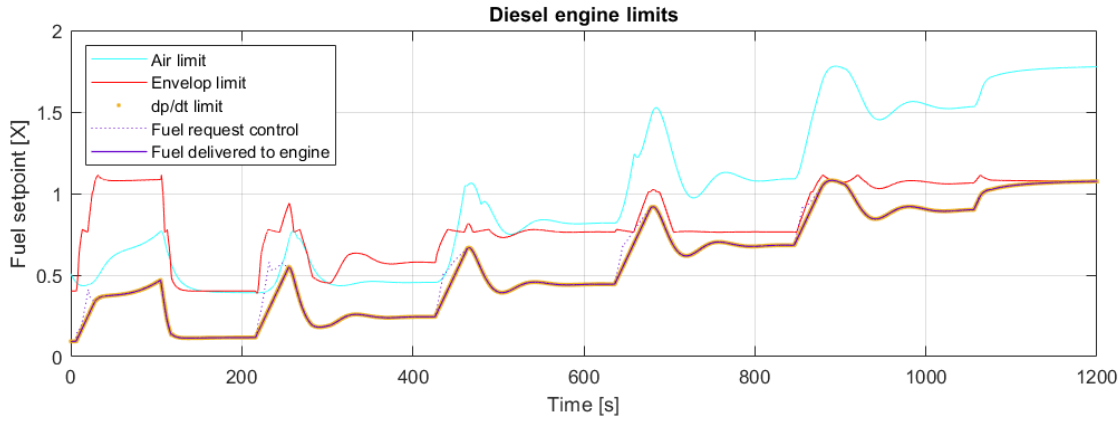

Figure 4.69: Diesel engine limits

4.8.4. Control evaluation APC fast

This simulation shows a significant improvement in acceleration time compared to simulation number 6 which used slow integrating speed control for the diesel engine. Table 4.6 gives a quantitative overview of the different accelerations. During the intermittent accelerations from 5 to 10 kn and 15 to 20 kn the maximum acceleration occurs after 90% of the ship speed is reached. Compared to simulation number 6 the time needed for the intermittent accelerations has reduced by about 40 %. Although simulation 7 shows that APC can be very fast electrical speed control as shown in simulation number 4 is slightly faster. For instance the intermittent acceleration from 15 to 20 kn takes 15 % less time when using electrical speed control.

Speed [kn]	**0-5**	**5-10**	**10-15**	**15-20**	**20-25**	**0-27**
Total time [s]	104.5	38.1	39.0	41.6	43.3	280.9
Maximum acceleration $[m/s^2]$	0.062	0.11	0.089	0.079	0.064	0.13
Time at maximum acceleration$[s]$	99	40	38	42	33	133

Table 4.6: Simulation number 7: Acceleration times

From this scenario it can be observed that APC can result in good acceleration behavior. The large increase in shaft speed results in a much larger thrust increase than can be achieved with the diesel engine governed by slow integrating control as in simulation number 6. However to achieve these good accelerations the diesel engine has to cope with large engine speed fluctuations, especially for small accelerations. Also it would still be a question if the governor can remain stable with disturbances like waves or other external disturbances and off design conditions. For real implementation such aggressive behavior would be unacceptable as the fast fluctuations in engine speed and engine load would result in engine wear and therefore additional maintenance. Therefore in the following comparison with other control strategies the slower APC implementation will be used.

In addition to this variation of APC which uses fast diesel engine speed control a preliminary test was performed with the induction machine delivering a larger additional torque contribution during acceleration. When the induction machine produces a large additional torque during the acceleration, the instability in shaft speed and pitch intensifies resulting in fast shaft speed fluctuations. It is concluded that when using APC power availability is not the limiting factor for achieving a larger acceleration. This preliminary attempt to use the induction machine more effectively in combination with APC was therefore not successful.

Simulation 6 using APC does show that the acceleration performance is limited when the angle of attack is maintained. To investigate the gain in performance scenarios 8, 9 and 10 will power through the torque peak. Using the findings from simulation number 5 the aim will be a high static load on the diesel engine while using the fast torque developing capabilities of the induction machine during acceleration.

4.9. Scenario 8: Diesel engine torque control with dynamic power split

Control mode	
Diesel engine	Dynamic torque
Induction machine	Speed control
CP propeller	Combinator

4.9.1. Description

This scenario uses a dynamic power split with the diesel in torque control. From scenario 4 it was concluded that when the diesel engine operates in torque control the margins during acceleration were sufficiently large. This simulation will use this margin from the diesel engine during acceleration. However to implement the dynamic torque control a larger margin is needed for the diesel engine to account for dynamic load. The induction machine is therefore loaded with a larger part of the static propeller load. During steady state the induction machine maintains the desired shaft speed. In the static power distribution a small margin is left to ensure there is power available for the induction machine to control the shaft speed.

Figure 4.70: Combinator curves

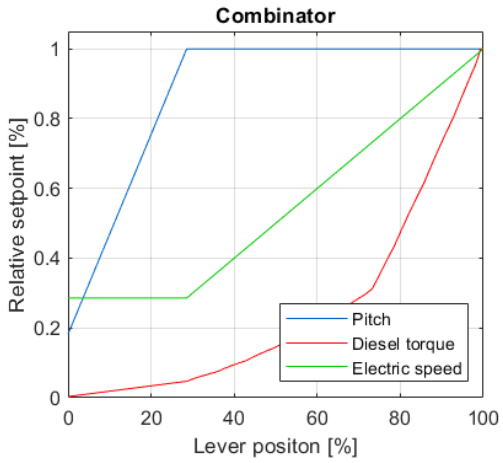

Tuning & trade offs

During tests it became clear that the need for a lever setpoint rate limiter was reintroduced by the additional speed loop for the torque setpoint of the diesel engine. Without the lever setting rate limiter the diesel engine will start producing a large part of the increased dynamic load propeller load, exceeding the diesel engine envelope.

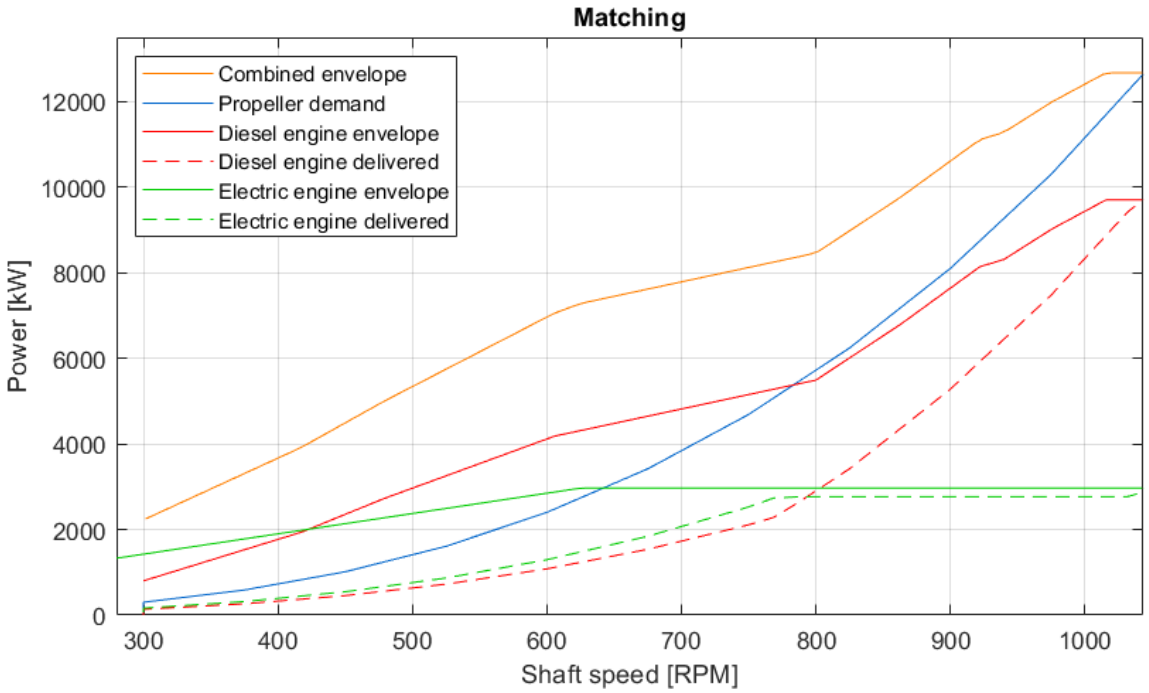

Figure 4.71: Static matching of the propeller power to the diesel engine and induction machine

4.9.2. Slam start: simulation results

During the slam start the induction machine produces the maximum torque after 36 seconds and continues to do so for the rest of the acceleration as shown in Figure 4.74. The diesel engine is loaded very close to its maximum after the STC switching region of 800 rpm as can be seen in Figure 4.72. The combined produced power of the diesel engine and induction machine is close to the combined envelope, meaning that the total installed power is used. Figure 4.73 shows the acceleration of the vessel. It takes 114.8 seconds to reach 90 % of the speed setpoint using dynamic torque control for the diesel engine. The maximum acceleration is 0.17 m/s^2 which occurs at 52 seconds. In simulation number 4 which uses electrical speed control the peak acceleration is 0.01 m/s^2 larger and occurs faster after the start of the acceleration. However, the total acceleration that is achieved with dynamic torque control as used in this scenario is 5 seconds faster. The higher and earlier peak in acceleration found in simulation 4 is the result the rate limiter needed in this simulation. The additional torque the diesel engine delivers later in the acceleration is the reason for the overall slightly faster acceleration. Figure 4.75 shows the increased torque delivered compared to the static torque setpoint.

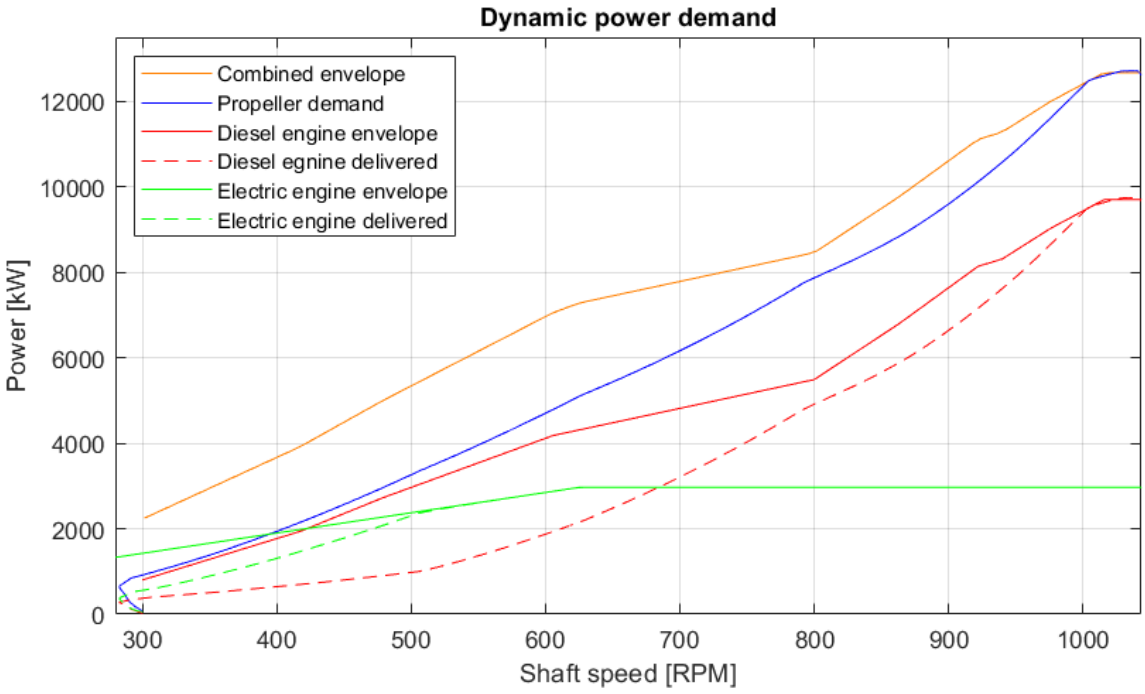

Figure 4.72: Dynamic load

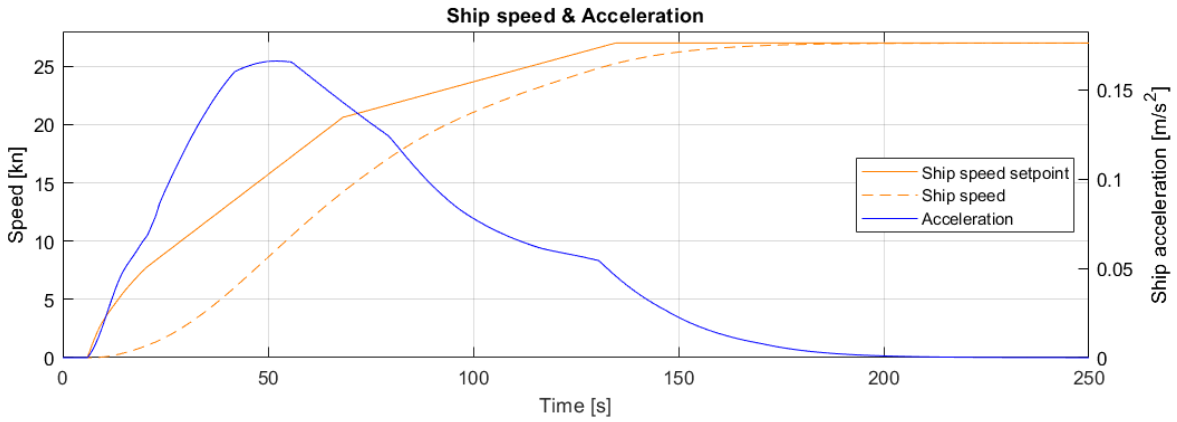

Figure 4.73: Ship speed and acceleration

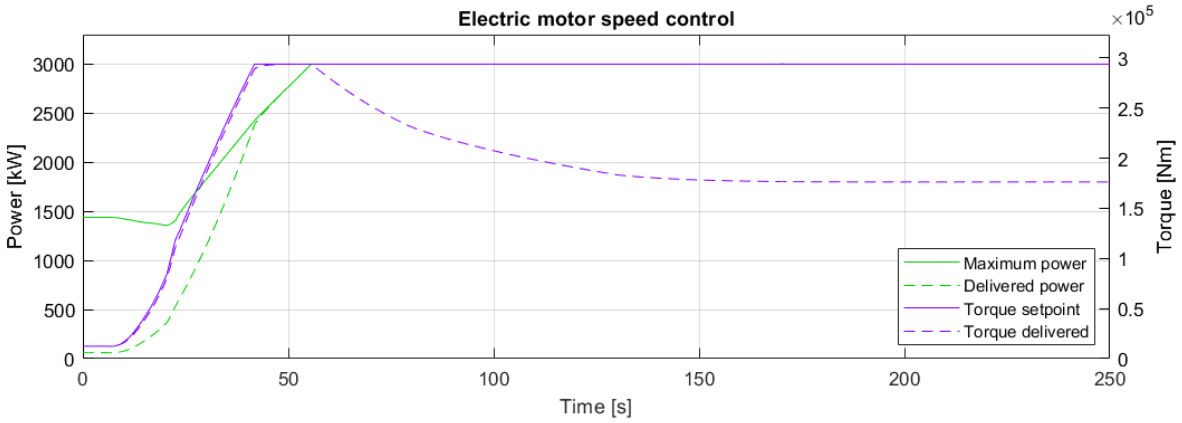

Figure 4.74: Induction machine torque and power

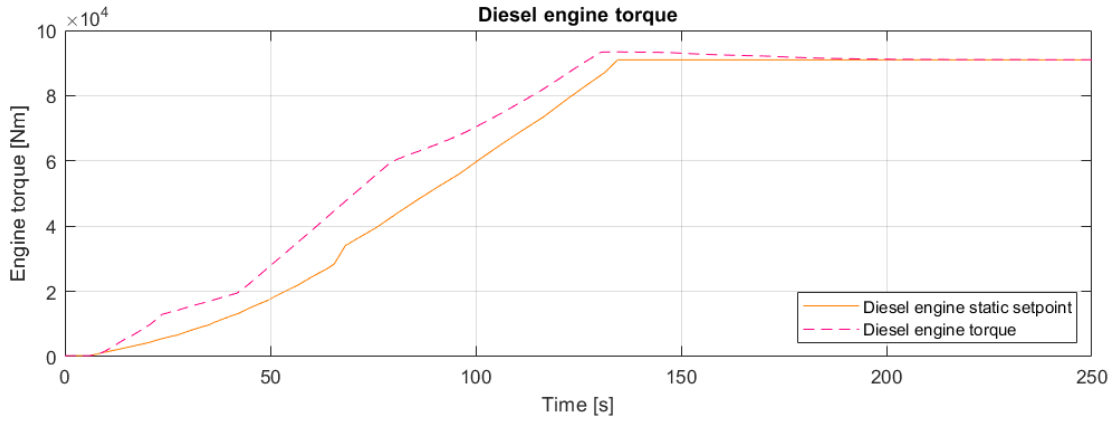

Figure 4.75: Diesel engine torque

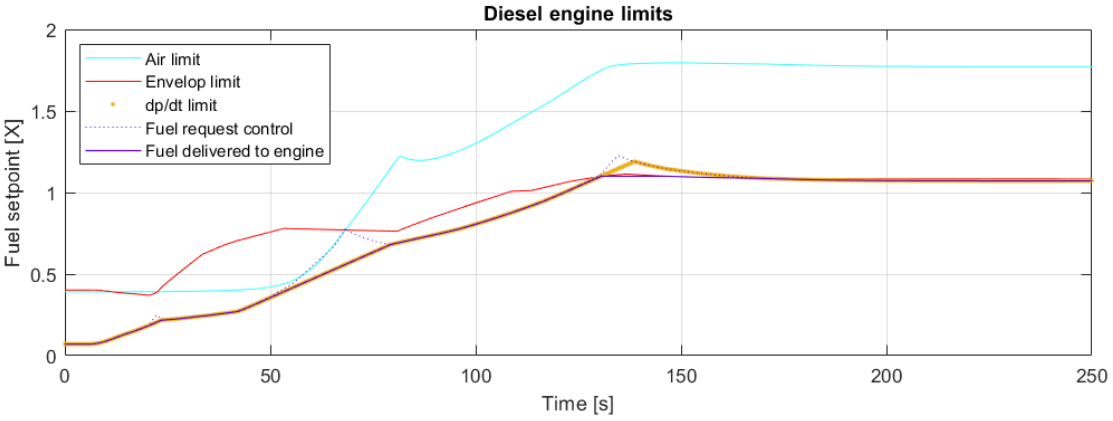

Figure 4.76: Diesel engine limits

4.9.3. Staircase sprint: simulation results

Figure 4.77 shows hubs in the delivered power of both the induction machine as the diesel engine, indicating that both produce a part of the dynamic power demand from the propeller. The acceleration peaks as seen in Figure 4.78 show that the peak acceleration develops early in the acceleration and are very similar in shape but lower in height when compared to the static torque control of simulation number 4. The control method is however slower than the simpler electrical speed control using static torque support for the diesel engine. For example the intermittent sprint from 15 to 20 kn takes 37.8 seconds and has a peak acceleration of 0.078 m/s^2 for this dynamic torque support. The static power split of simulation number 4 only uses 26.9 seconds and had a acceleration peak of 0.095 m/s^2. The cause for the better performance from the static power split is found in both the lever setpoint rate limiter as well as the preferred static distribution that is possible with pure torque control for the diesel engine. The larger static torque contribution of the diesel engine in simulation number 4 is possible because no dynamic load is added, making it possible to have a larger power reserve for the induction motor. This power reserve is used during the acceleration.

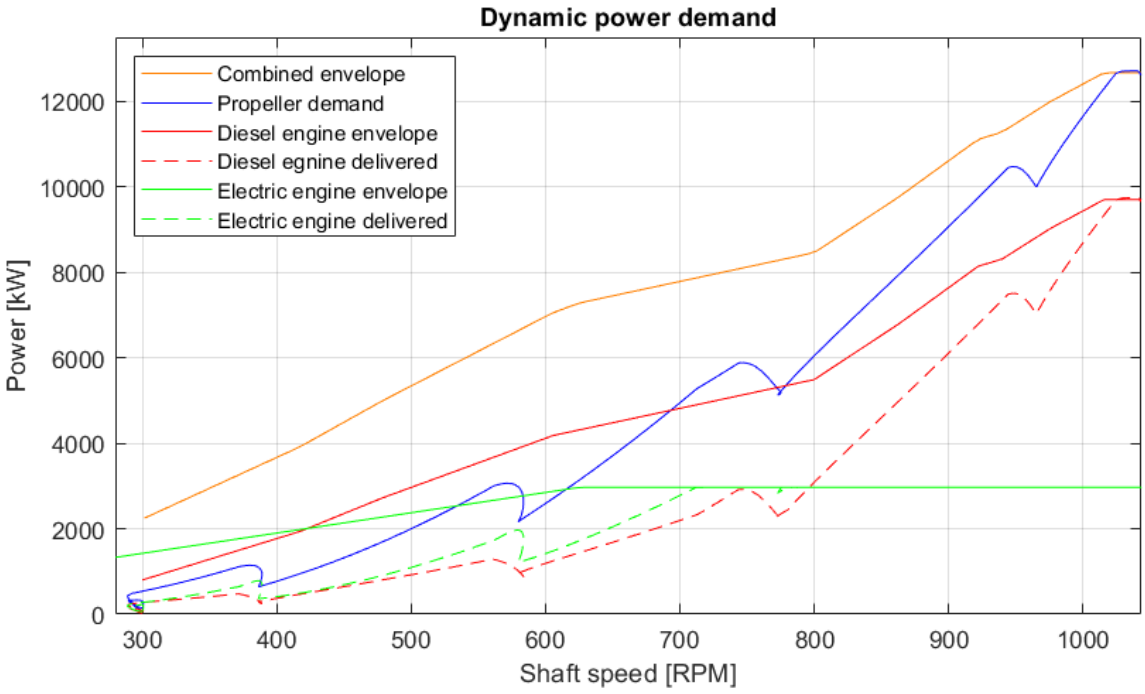

Figure 4.77: Dynamic power demand

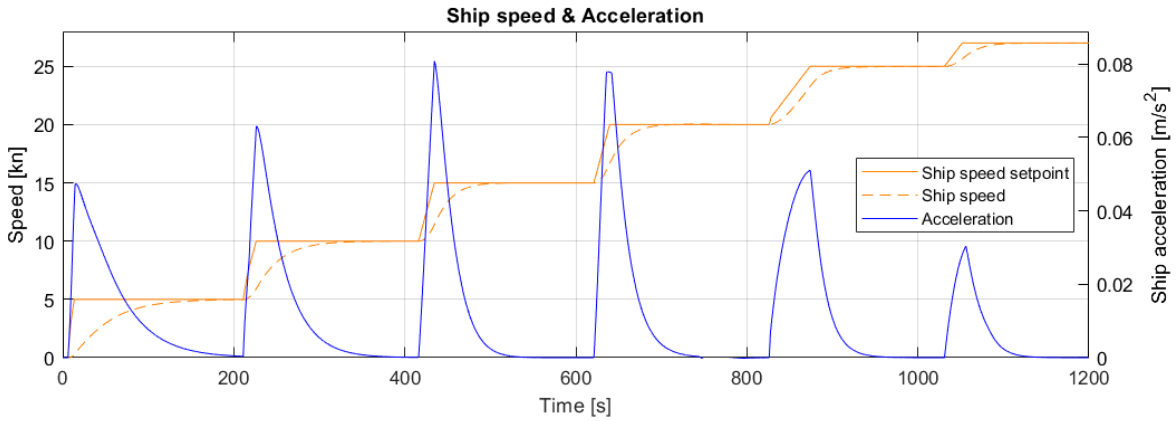

Figure 4.78: Ship speed and acceleration

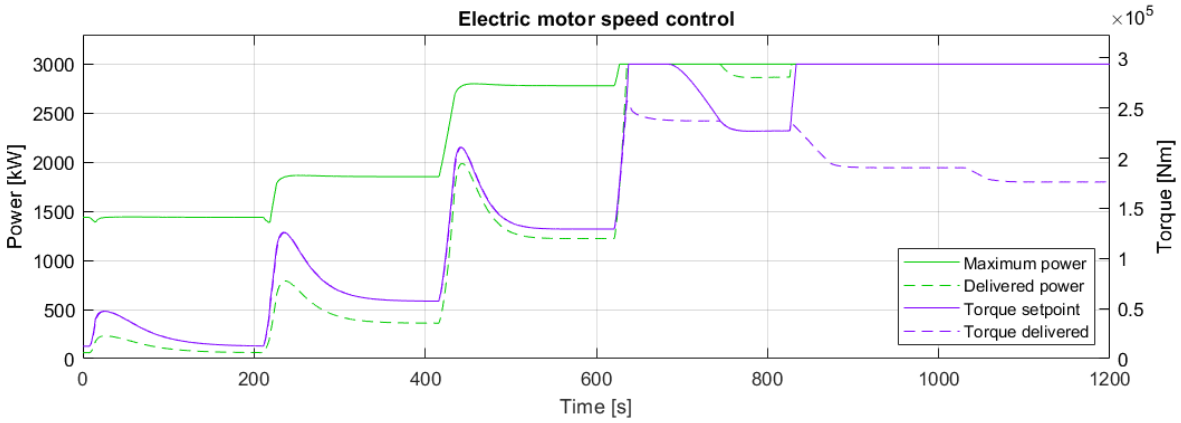

Figure 4.79: Induction machine power and torque

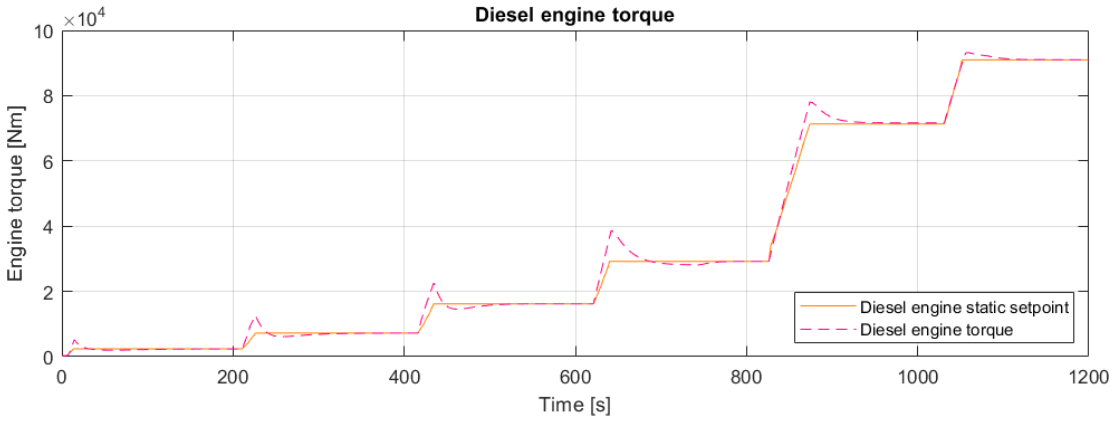

Figure 4.80: Diesel engine torque

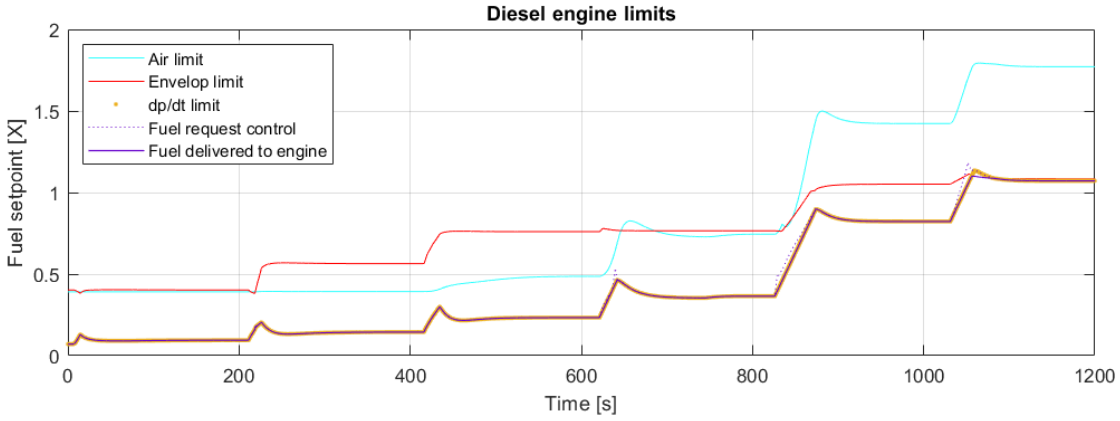

Figure 4.81: diesel engine limits

4.9.4. Control evaluation

Table 4.7 shows the quantitative representation of Figure 4.78. For accelerations above 20 kn the power delivered by the induction machine is very close to its maximum, leaving only a very small power reserve for the increased load during acceleration. This means that the much slower diesel engine needs to produce this power, explaining the larger acceleration time and different acceleration profile of these accelerations. It is concluded that although the acceleration is an improvement when compared to the benchmark scenario 1 the simpler electrical speed control of simulation number 4 utilising a static power split gives better results. From the sweep performed in simulation number 5 it became clear that a small contribution from the electrical machine in the static balance was beneficial for the acceleration. Contrary to this earlier conclusion to create a sufficient power reserve for the diesel engine to take on additional dynamic load the induction machine was set to produce a larger power contribution to the steady state propeller power demand. Explaining the reduction in acceleration performance.

Speed [kn]	**0-5**	**5-10**	**10-15**	**15-20**	**20-25**	**0-27**
Time [s]	120.6	70.9	38.6	37.8	53.2	114.8
Maximum acceleration $[m/s^2]$	0.047	0.063	0.08	0.078	0.050	0.17
Time at maximum acceleration$[s]$	9	15	18	18	48.3	52

Table 4.7: Simulation number 8: acceleration times

From the simulation results it is concluded that a dynamic power split with the diesel engine operating in torque mode gives slower accelerations than the static power split. During the staircase sprint it becomes clear that the need for a lever setting rate limiter has negative effects on the acceleration. In accelerations from 15-20, 20-25, 25-27 the dynamic torque control for the diesel engine underperformed compared to using torque control only for the diesel engine, meaning that dynamic torque control for the diesel engine is slower and reintroduces the possibility of overloading the diesel engine. It is therefore stated that if/when torque control becomes available from manufacturers a static power split with a large power reserve for the induction machine is preferred over a dynamic torque control for the diesel engine.

4.10. Scenario 9: Dynamic power split diesel engine speed control

Control mode	
Diesel engine	Speed control
Induction machine	Dynamic torque control
CP propeller	Standard combinator

Figure 4.82: Combinator curves

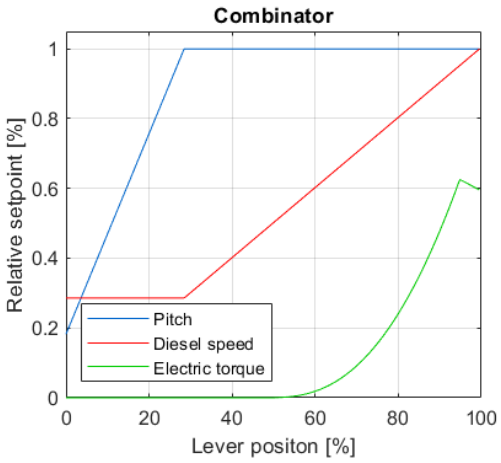

4.10.1. Description

This scenario uses speed control for the diesel engine, torque control for the induction machine and a pitch setpoint for the propeller. For the induction motor an additional torque component dependent on the error in shipspeed is added to the static setpoint during accelerations, resulting in a dynamic power split as described in section 3.2.6. In scenario 3 it was concluded that a fixed power split between the diesel engine and the induction machine would always remain a compromise between the slam start, accelerations at low speed or accelerations at high speed. It was further concluded during scenario 5 that it was preferred to match a heavy static loading on the diesel engine, leaving a large power reserve available at the induction machine. It was also concluded in scenario 5 and 8 that the induction machine needs to produce a large torque during accelerations. With a fixed power split once the electric machine delivers full power it cannot deliver additional power during the next acceleration, given that part of the power has now been reserved by static propeller load. The dynamic power split as implemented in this scenario will deliver a large amount of additional torque from the induction machine during the acceleration. When the shaft speed setpoint is reached the torque produced by the induction motor will reduce to the static distribution according to the combinator.

Tuning and limits

The dynamic power split is implemented according to the distribution in section 3.2.6. This control method does need a lever setting rate limiter as the diesel engine operates under speed control. The rate limiter prevents the diesel engine from exceeding its envelope during the slam start. A more detailed description of this rate limiter is provided in section 4.1.1 at the start of this chapter.

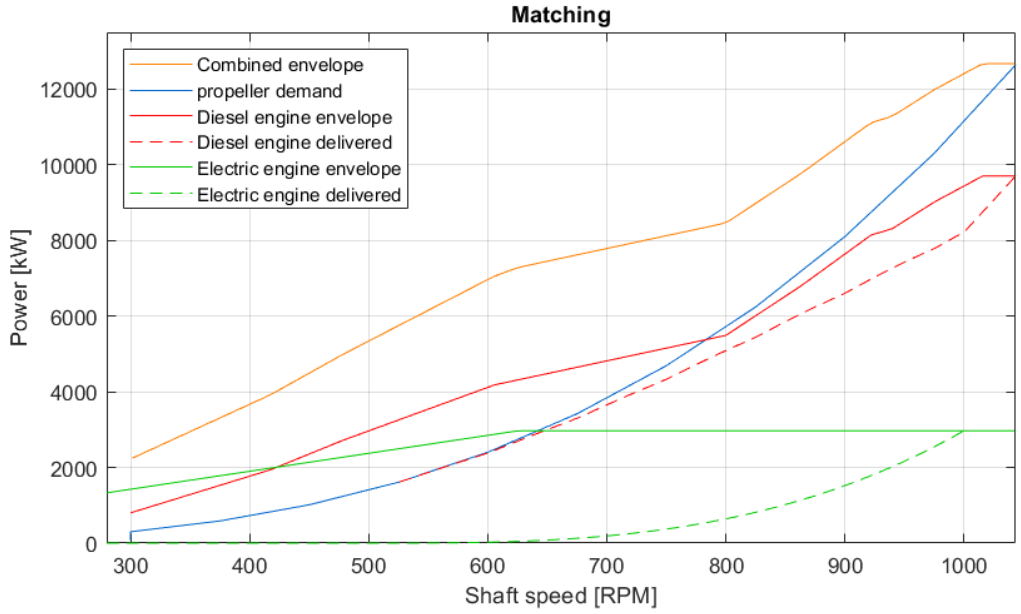

Figure 4.83: matching of the propeller power to the diesel engine and the induction machine

4.10.2. Slam start: simulation results

Figure 4.84 shows that during the entire acceleration the electrical machine delivers full power, which was according to scenario 5 the optimum for the slam start. It can be observed in Figure 4.88 that after 20 seconds the increase in power output by the diesel engine is limited by the maximum fuel increase rate. In addition Figure 4.84 shows that the diesel engine especially after the STC switching region at 800 rpm operates close to its maximum power, implying that the power output of the diesel engine during the slam start in this simulation is at its maximum. Figure 4.85 shows a high acceleration peak of 0.17 m/s^2 which develops fast being at its maximum at 40 seconds. This acceleration peak which holds for an extended amount of time, resulting in an overall fast acceleration from 0 to 27 kn that takes 124.6 seconds, making it only 4% slower than the electrical speed control of simulation number 4 which provides the fastest slam start of all control strategies.

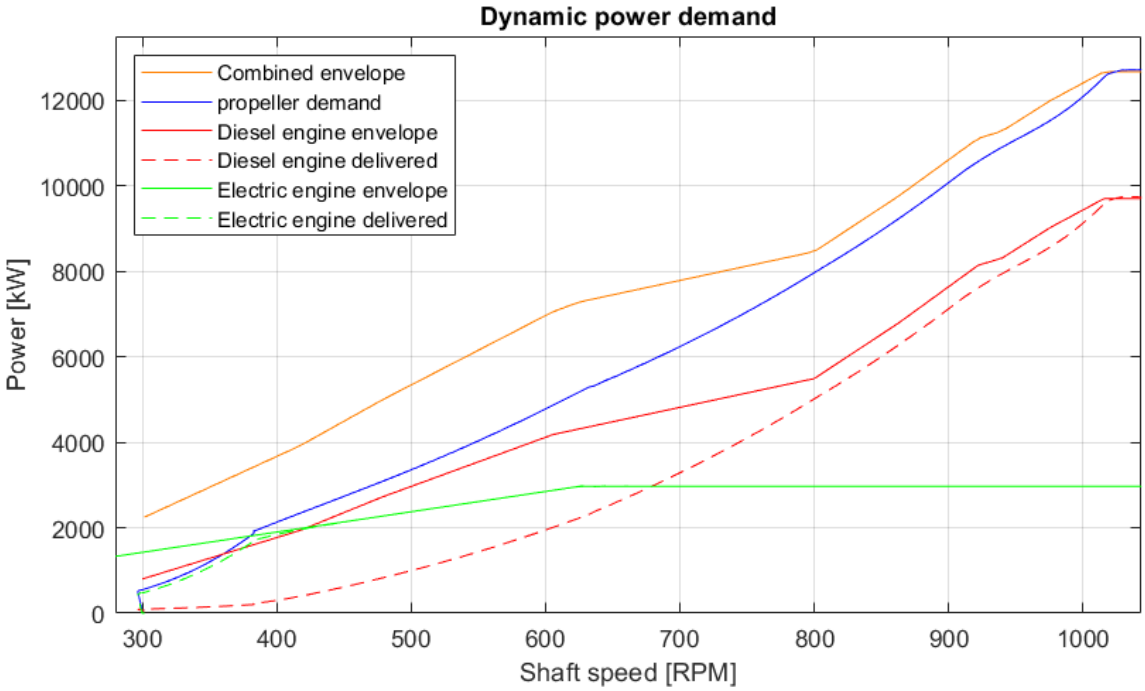

Figure 4.84: Dynamic power demand

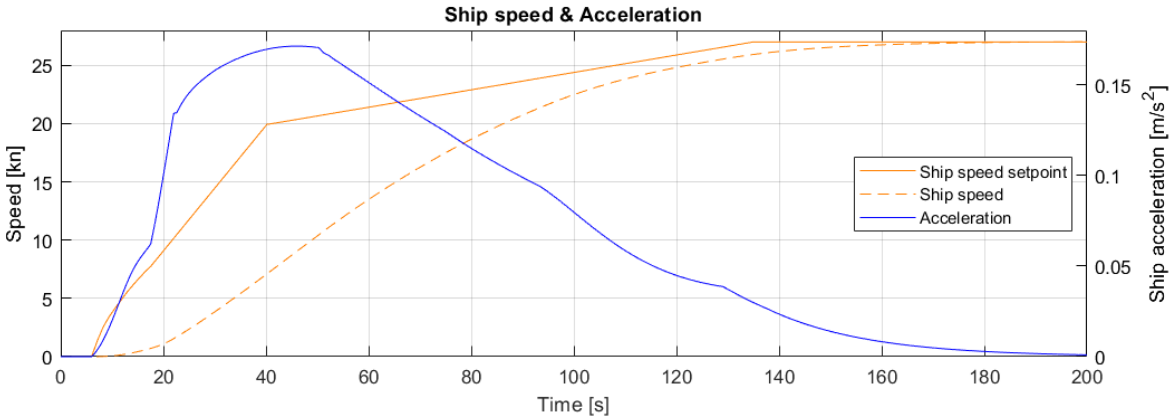

Figure 4.85: Ship speed and acceleration

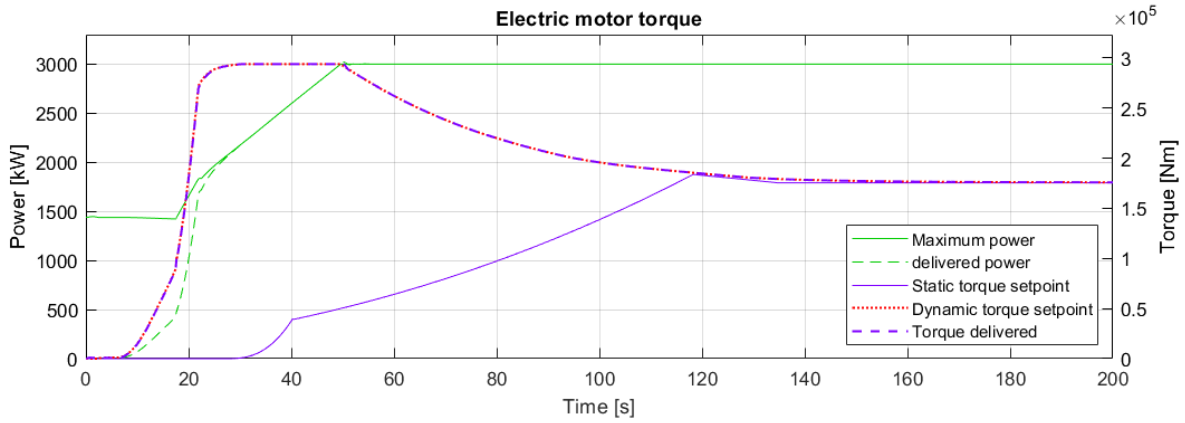

Figure 4.86: Induction machine torque

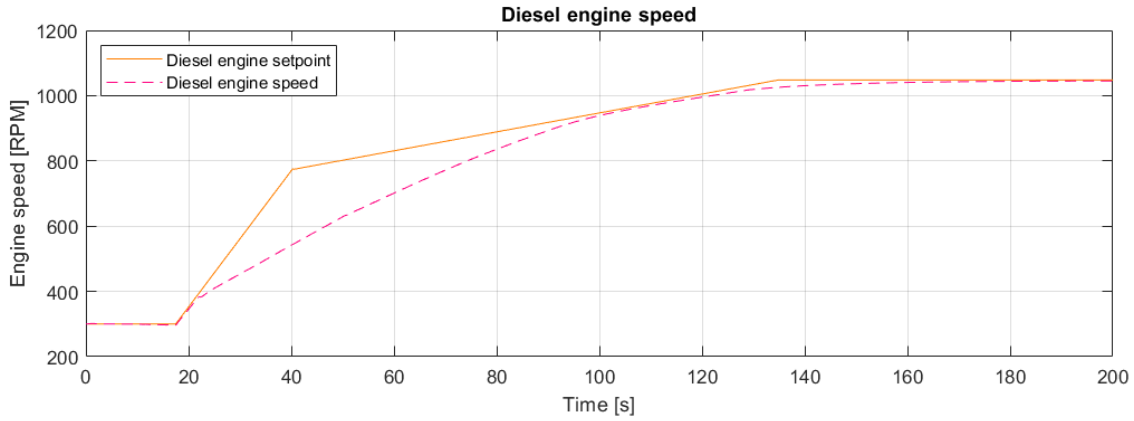

Figure 4.87: Diesel engine speed

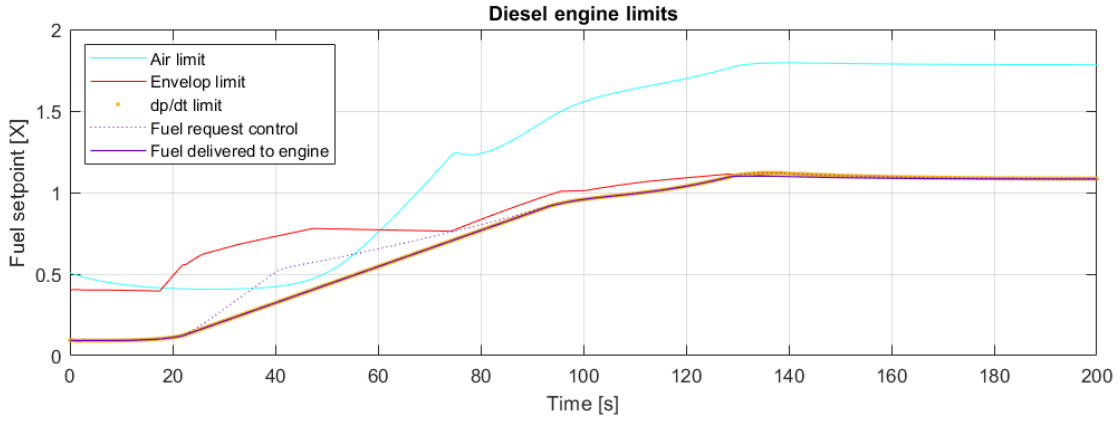

Figure 4.88: Diesel engine limits

4.10.3. Staircase sprint: simulation results

Figure 4.89 shows that during an acceleration the induction machine delivers a large part of the power to the propeller, while the diesel engine does deliver power, the torque peak associated with the acceleration is delivered by the induction machine. During the acceleration the diesel engine slowly starts delivering additional power, eventually taking over from the induction machine. At the end of an acceleration the induction machine only delivers the static power following the combinator cure. Figure 4.90 shows sharp and high acceleration peaks which develop almost immediately after an acceleration is started. This acceleration characteristic is the result of the power provided by the induction machine. This dynamic power split is slightly slower than electrical speed control. As an example the intermittent acceleration from 15 to 20 kn takes 29.9 seconds and has a peak acceleration of 0.097 m/s^2 which takes only 7 seconds to develop. meaning the inetmitand acceleration is 3 seconds slower then the electrical speed control tested in simulation number 4. The intermittent acceleration from 15 to 20 kn show the display a flatter peak, which is caused by the induction machine reaching it power limit as shown in Figure 4.91. The accelerations after 20 kn show a significantly lower peaks, this is due to the induction machine already delivering a large part of it power to produce the propeller power demanded at the steady state ship speed.

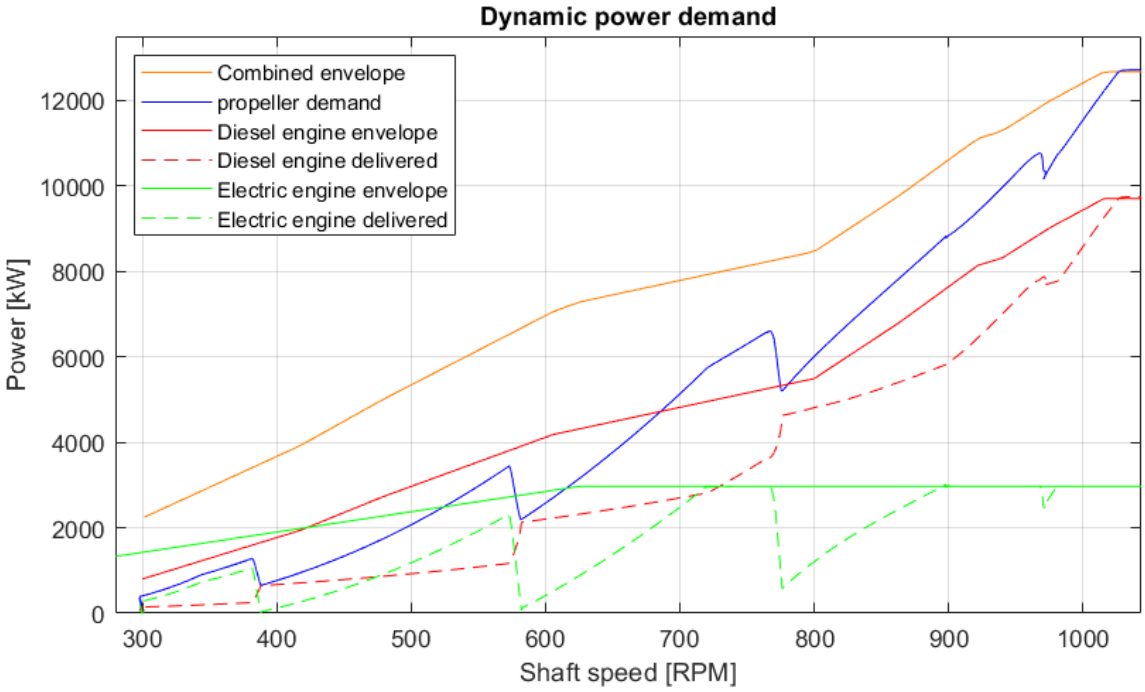

Figure 4.89: Dynamic power demand

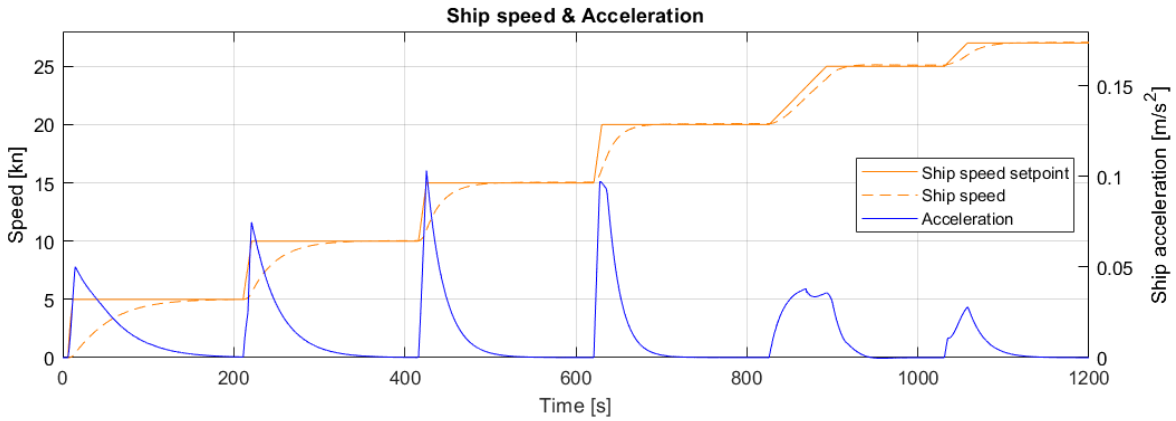

Figure 4.90: Ship speed and acceleration

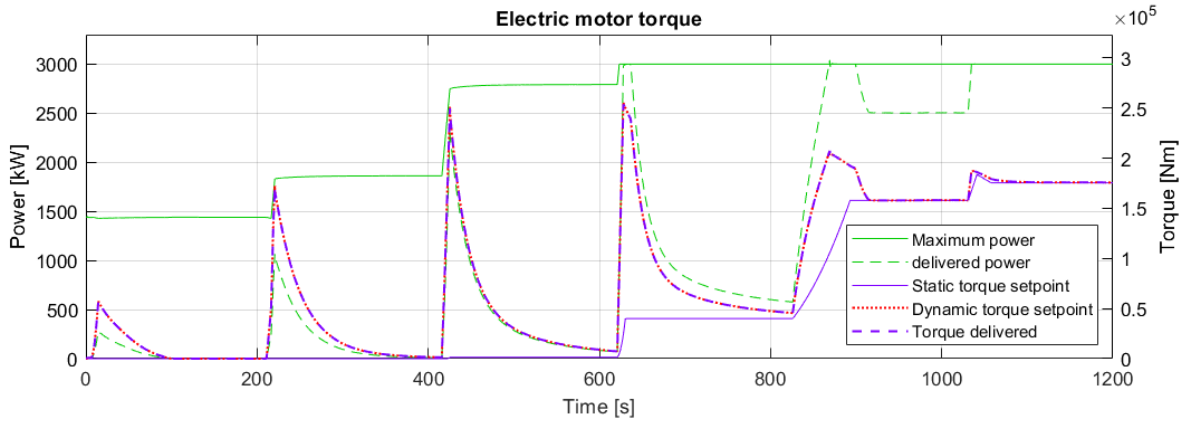

Figure 4.91: Induction machine torque

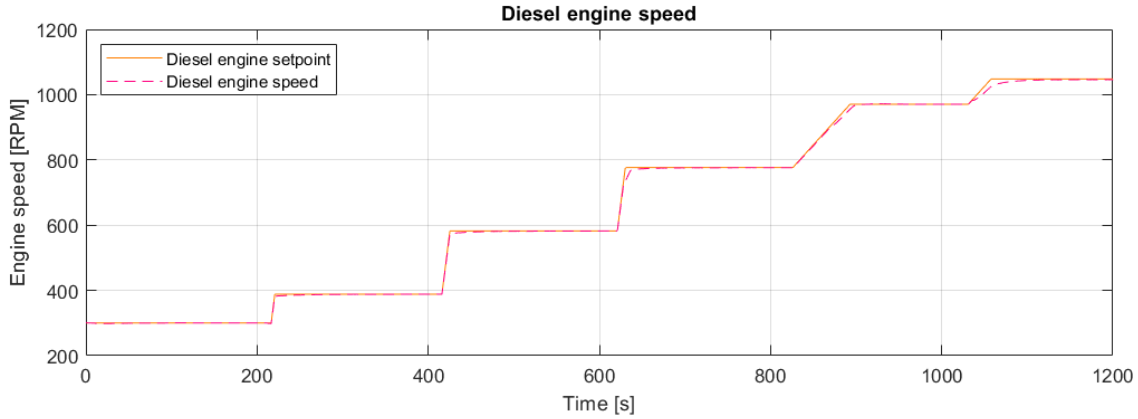

Figure 4.92: Diesel engine speed

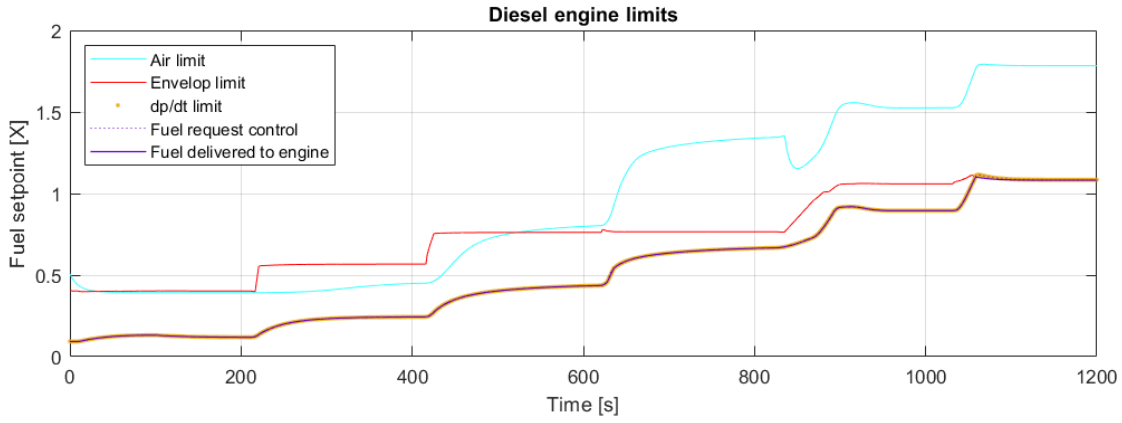

Figure 4.93: Diesel engine limitations

A very fast torque production of the induction machine can be seen in figure 4.91 and causes the fast acceleration of the propeller shaft. The increase in shaft speed increases the power availability for the diesel engine as can be seen in Figure 4.93. When the increased power availability has established the slower integrating control of the diesel engine starts delivering more fuel to the engine, replacing power delivered by the induction machine until the propeller power is produced in accordance to the static matching. Figure 4.93 During accelerations there is ample margin between the diesel engine and its envelope, reducing the risk of overloading the diesel engine.

4.10.4. Control evaluation

Table 4.8 shows a quantitative representation of the acceleration displayed in Figure 4.90. It is noted that the acceleration peaks develop fast for the intermittent accelerations from 0 till 20 kn the acceleration peak occurs between 7 and 8 seconds after the acceleration is started. Apart from the intermittent acceleration from 0 to 5 kn each acceleration of this dynamic power split is slightly slower than the electrical speed control tested in simulation number 4. Apart from the intermittent acceleration from 20 to 25 kn the difference in speed is minimal, ranging between 2 an 5 seconds. The intermittent acceleration form 20 to 25 kn is slower due to the power of the induction machine now been reserved by static propeller load. Using Torque control for the diesel engine, as is done in simulation number 4 the static power distribution can be matched much closer to the power envelope of the diesel engine, creating a larger power availability for the faster induction machine.

Speed [kn]	**0-5**	**5-10**	**10-15**	**15-20**	**20-25**	**0-27**
Total time [s]	120.4	72.3	42.3	29.9	64.1	124.6
Maximum acceleration [m/s^2]	0.05	0.074	0.10	0.097	0.038	0.17
Time at maximum acceleration[s]	8	9	9	7	43	40

Table 4.8: Simulation number 9: acceleration times

From the simulations it can be concluded that during the slam start the induction machine produced the maximum amount of power for the entire acceleration. Which is according to the optimum found in scenario 3. During the staircase sprint the induction machine produced large amounts of power for each acceleration up to 20 kn. The benefits of this control mode decrease after the 20 kn due to the power of the electric motor already being used in static propeller power demand. This power limitation is a limiting factor originating in the specific diesel engine and induction machine power. It is therefore a result common with all scenarios and can not be changed with control. At low ship speed the power demand from the propeller is produced by the diesel engine at low shaft speed. At high ship speed the propeller power demand is delivered by the diesel engine with minimal contribution from the induction machine. This means that at steady state over the entire ship speed range the diesel engine is loaded close to its envelope, ensuring operation in efficient operating points.

At the start of an acceleration manoeuvre the induction machine delivers a fast increase in power output, implying the full usage of the inherently fast qualities of the induction machine. It can be concluded that this method with a dynamic power split between the diesel engine and the induction machine gives excellent results. The usage of a rate limiter on the lever setpoint does raise the question if a lowered propeller load would result in a better acceleration, which will be tested in simulation number 10.

During testing it became apparent that using the dynamic torque control as described in section 3.2.6 creates a sharply rising power demand on the generator set. Accelerations from 10 to 15 kn and 15 to 20 kn are especially demanding. Figure 4.91 shows that during the acceleration from 10 to 15 kn which starts at 416 seconds the induction machine goes from 15 kW to 2466 kW in 9 seconds. The load increase is therefore 2450 kW per induction machine, resulting in a 40.8 % load increase for the in total 12.000 kW power available from the generator sets. The largest load increase happens at the acceleration from 15 to 20 kn. At time = 621 seconds the acceleration from 15 to 20 kn starts. During this acceleration the induction machine increases in power demand from 76 kW to 3152 kW resulting in an overall load increase of 3076 kW. This power increase results in an 51.2 % load increase in 7 seconds for the generator set, which is an acceptable step load for high quality generator sets but a drop in supply frequency is expected.

4.11. Scenario 10: Dynamic power split diesel engine speed control with reduced pitch

Control mode	
Diesel engine	Speed control
Induction machine	Dynamic torque control
CP propeller	Lowered pitch combinator

4.11.1. Description

This control method is very similar to scenario 9. Scenario 9 did need a rate limiter for the lever setting for the slam start, implying that the load of the propeller is to large during causing the diesel engine to exceed its limits. This scenario is therefore simulated using an adjusted combinator with a lower pitch. In addition to the lowered pitch the minimum diesel engine speed is increased from 300 rpm to 400 rpm. Both these adaptations result in a larger engine margin. Like scenario 9 this control mode delivers the needed the torque peak associated with the acceleration with added torque from the electric drive. There is a torque component added to the static torque setpoint for the induction machine. This temporally increase of the electrical power production allows for a faster acceleration. The downside of lowering the pitch setpoint is that it does lead to a stationary operating point which is located in the engine diagram in a less efficient location. Because this simulation is very similar to simulation number 9 only the differences will be discussed, meaning that for a more in dept review previous scenarios need to be referenced.

Figure 4.94: Combinator curves

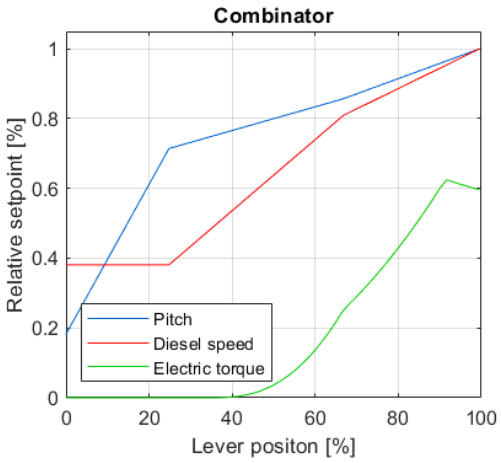

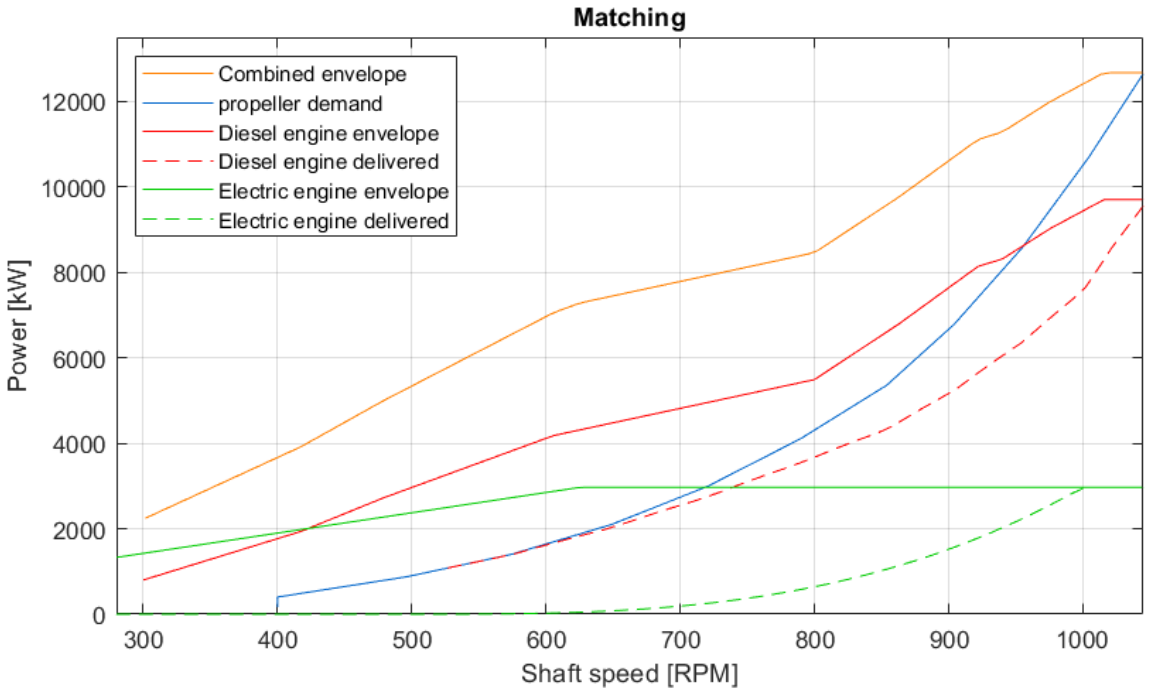

Figure 4.95: Matching of the propeller power to the diesel engine and induction machine

4.11.2. Slam start: simulation results

Figure 4.96 shows a slight hump in acceleration around the shaft speed of 500 rpm. This hump is caused by a change in the rate of change in pitch. It can be seen in Figure 4.97 that the acceleration has a large peak value of 19 m/s^2 which remains high for an extended amount of time, in addition this large acceleration develops early after 10.6 seconds. The slam start manoeuvre is therefore fast taking only 107 seconds. The slam start as performed using this dynamic power split with a reduced pitch setting is 10% faster than the electrical speed control from simulation 4, making it the fastest slam start.

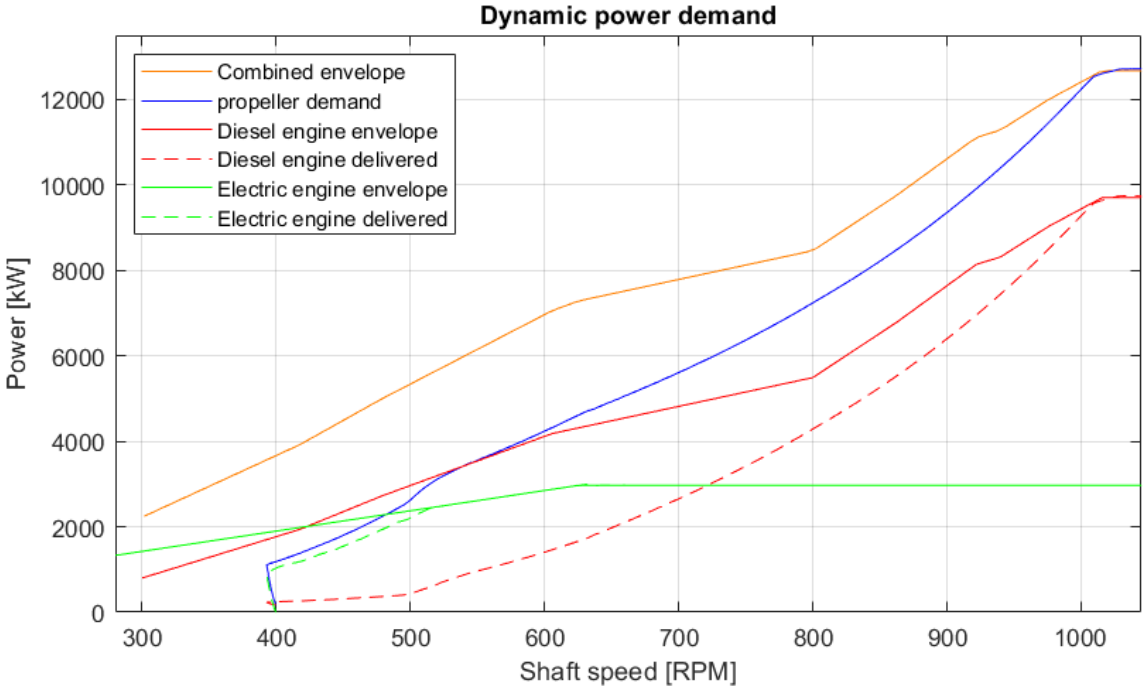

Figure 4.96: Dynamic power demand

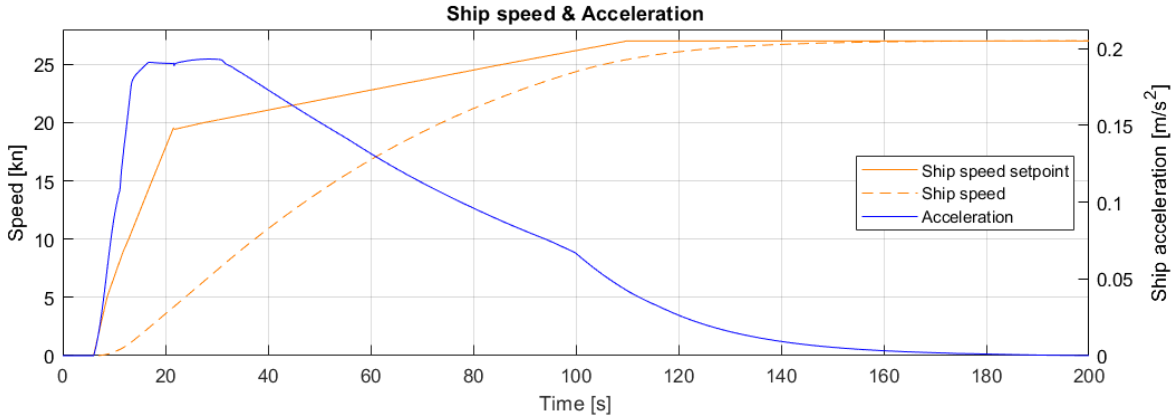

Figure 4.97: Ship speed and acceleration

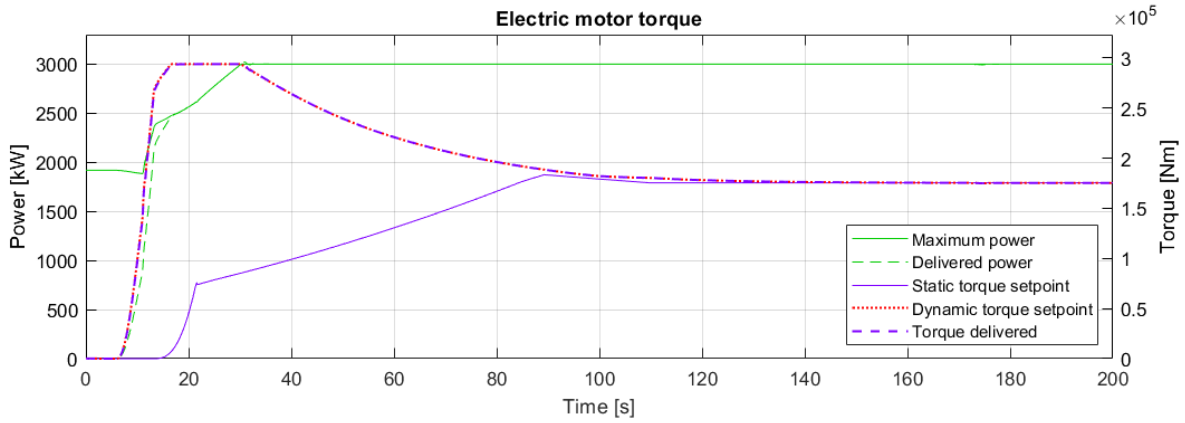

Figure 4.98: Induction machine torque

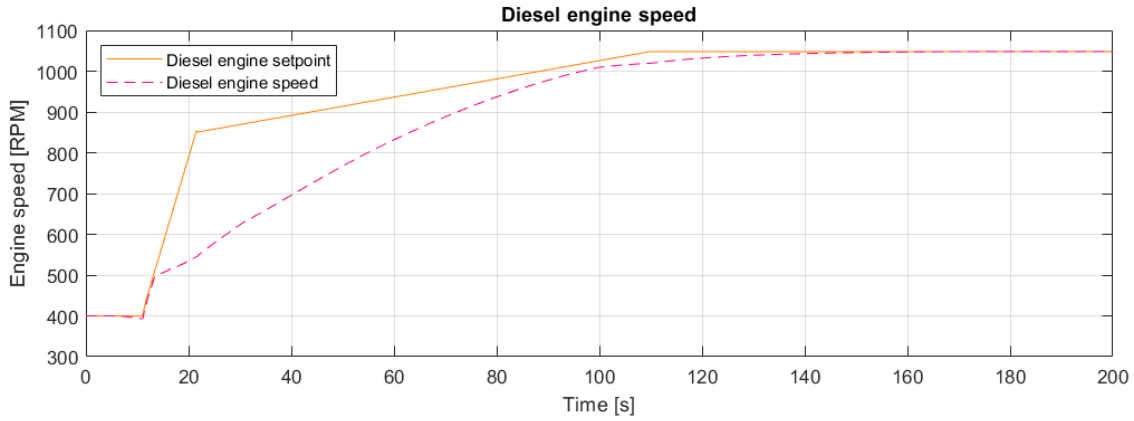

Figure 4.99: Diesel engine speed

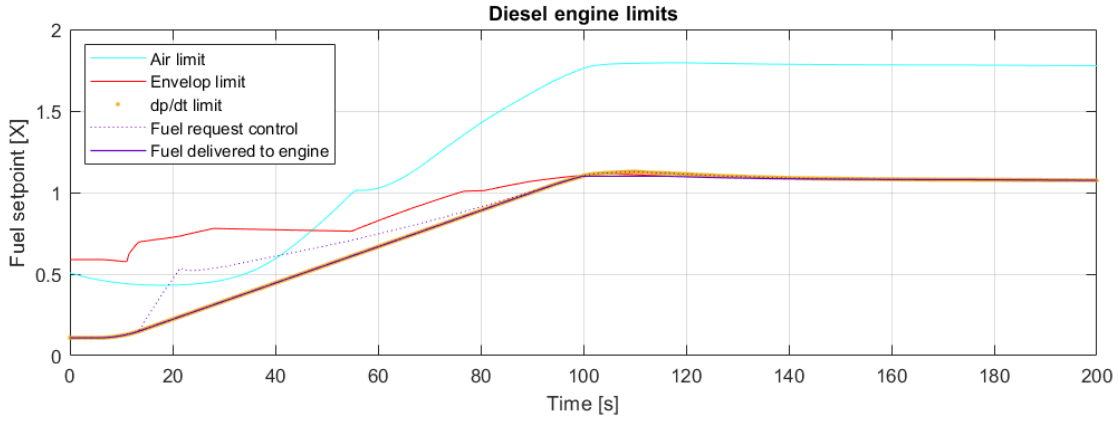

Figure 4.100: Diesel engine limitations

4.11.3. Staircase sprint: simulation results

Both the intermittent accelerations and behavior of the subsystems is very similar to simulation number 9. The reduced pitch and the increased minimum shaft speed produce a faster acceleration for all intermittent accelerations. This dynamic power split with a reduced pitch is 21% faster on the intermittent acceleration from 5 to 10 kn compared to the electrical speed control. This improvement compared to simulation 4 decreases for the intermittent acceleration at the mid range ship speeds, for example the acceleration from 10 to 15 kn is only 5% faster while. The accelerations above 20 kn are slower than with electrical speed control. This is due to the possibility of matching the diesel engine operating closer to its limiting power envelope when using torque control as is the case in simulation number 4. The heavier load on the diesel engine creates a larger power reserve for the induction machine, which can deliver this power more rapidly after the start of an acceleration.

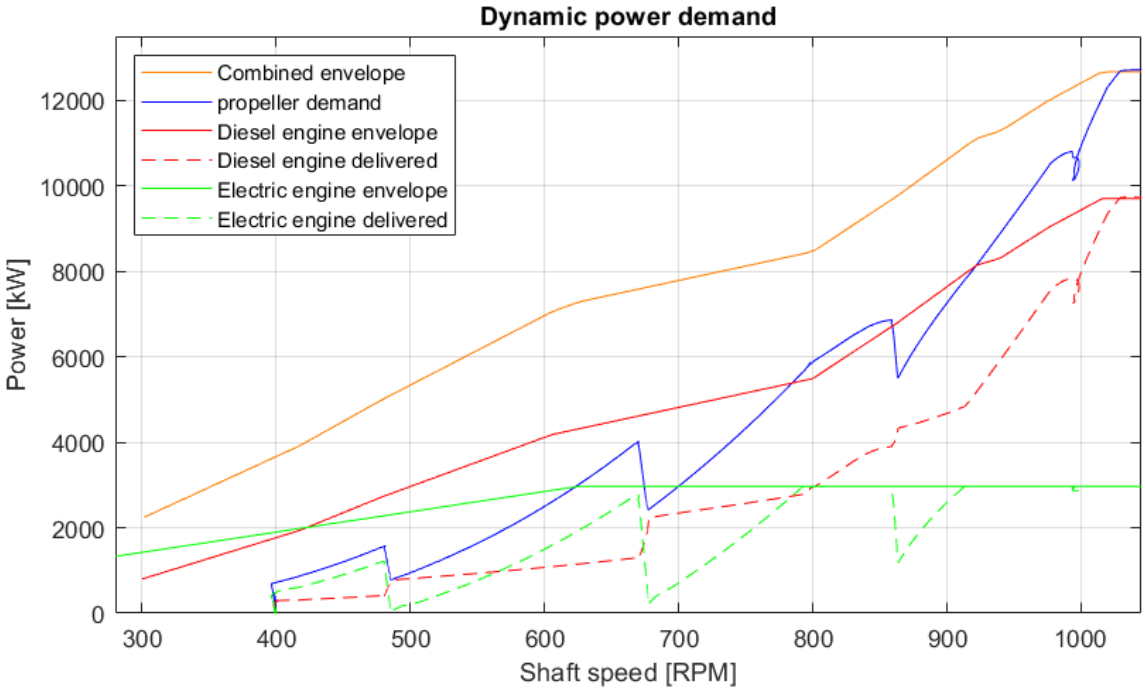

Figure 4.101: Dynamic power demand

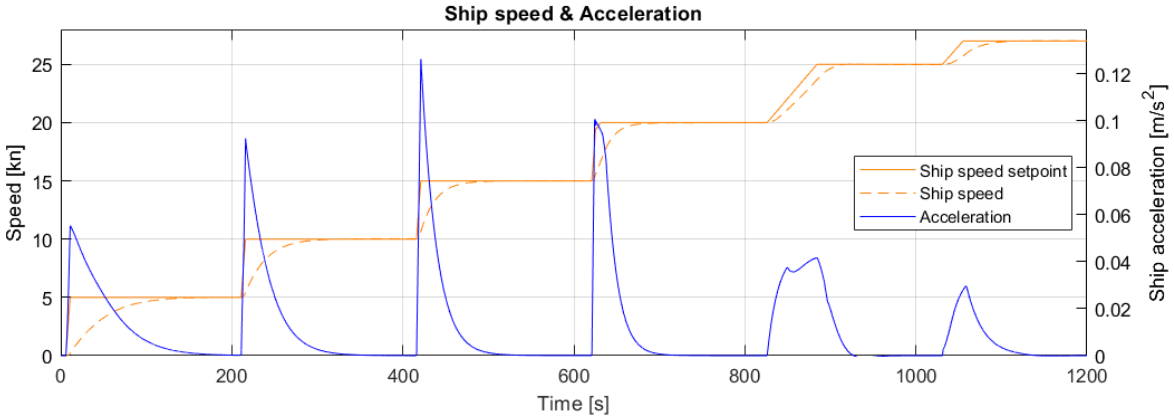

Figure 4.102: Ship speed and acceleration

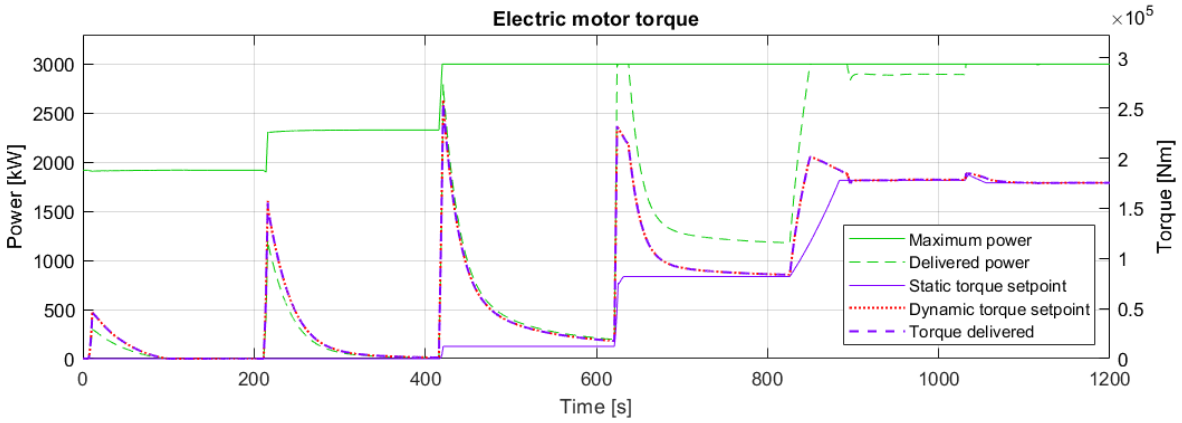

Figure 4.103: Induction machine torque and power

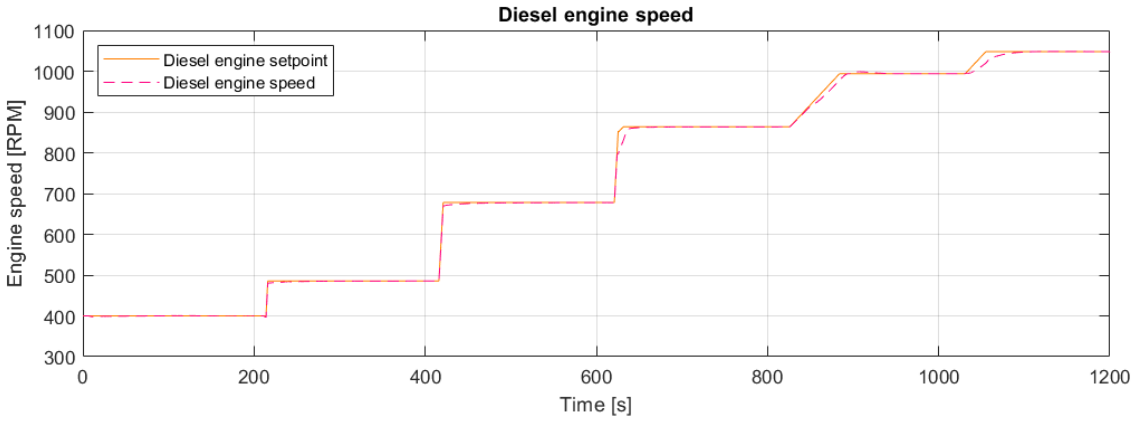

Figure 4.104: Diesel engine speed

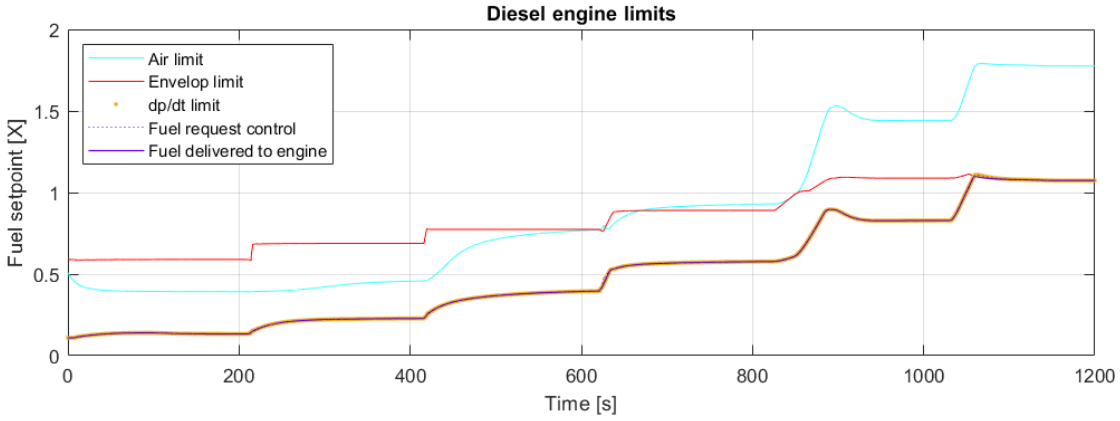

Figure 4.105: Diesel engine limitations

4.11.4. Control evaluation

Table 4.9 shows that all accelerations have improved compared to 9, meaning that the lowered pitch and increased minimum shaft speed effectively improve the acceleration characteristics. This dynamic power split performs better at low speed and the same until 20 kn as electrical speed control, which is tested in simulation number 4. Simulation 4 operates the diesel engine in torque control, almost eliminating the dynamic load, making it possible to use smaller margins to the diesel engine envelope. These smaller margins for the diesel engine create a larger power reserve for the induction machine. This power reserve is used effectively during an acceleration, explaining the better performance above 20 kn seen with simulation number 4.

Speed [kn]	**0-5**	**5-10**	**10-15**	**15-20**	**20-25**	**0-27**
Total time [s]	103.7	55.2	35.0	27.0	59.0	107.0
Maximum acceleration $[m/s^2]$	0.055	0.092	0.13	0.010	0.037	0.19
Time at maximum acceleration$[s]$	8	9	9	7	43	10.7

Table 4.9: Simulation number 10: acceleration times

Compared to Scenario 9 this simulation with a lowered pitch setpoint reduces the need for a lever setpoint rate limiter. Underspeed during the acceleration from 0 to 5 kn becomes almost non existing. Lowered pitch setpoints reduces the needed acceleration time for all accelerations apart from the acceleration from 25 to 27 kn. During the acceleration from 25 to 27 kn the pitch setpoint is increased to the design pitch setting, resulting in large load increase at a section of the engine envelope where the margin is small. This pitch increase makes the lever setpoint rate limiter more stringent during this final bit of acceleration, resulting in the larger acceleration time. During the simulation the diesel engine delivered a heavy load without overloading. During acceleration the inherent quality of the induction machine to almost instantly produce a fast and large torque was successfully used as can be seen in Figure 4.102. In general this implementation of a dynamic power split using dynamic torque control gives excellent results. These improved results come at the price of a reduced efficiency. The lowered pitch setpoints mean that the propeller is not operated at design pitch, reducing its efficiency. The steady state load on the diesel engine of sailing at constant speed has shifted towards higher shaft speeds, meaning the diesel is now operated in less efficient operating points within the diesel engine envelope.

Like with simulation number 9 it is apparent that using the dynamic torque control as described in section 3.2.6 creates a sharply rising power demand on the generator set. Accelerations from 10 to 15 kn and 15 to 20 kn are especially demanding. Figure 4.103 shows that during the acceleration from 10 to 15 kn which starts at 416 second the induction machine goes from 16 kW to 2770 KW in 5 seconds. The load increase is therefore 2754 kW per induction machine, resulting in a 45.9 % load increase for the combined power of 12.000 kW from the generator sets. The larger load increase happens at the acceleration from 15 to 20 kn. At time = 621 seconds the acceleration from 15 to 20 kn starts. During this acceleration the induction machine increases in power demand from 202 kW to 3134 kW resulting in an overall load increase of 2931 kW. This power increase results in a 48.86 % load increase in 3 seconds for the generator set. It is noted that this power increase develops faster but has a slightly lower amplitude than in simulation number 9, which is an acceptable step load for high quality generator sets but a drop in supply frequency is expected.

4.12. Scenario 11: Improved performance of a fixed pitch propeller with optimized electrical torque control

Control mode	
Diesel engine	Speed control
Induction machine	Torque control
CP propeller	Fixed pitch propeller

4.12.1. Description

This scenario uses speed control for the diesel engine, torque control for the induction machine and a fixed pitch propeller. The aim for this simulation is to improve the performance of a FP propeller using the findings in this report. From the sweep performed in scenario 3 it was concluded that when the aim is a large acceleration a very late start of the torque contribution from the electrical machine was not optimal. It was concluded that having the induction motor produce torque earlier in the acceleration manoeuvre led to better performance for all accelerations. However each intermittent acceleration preferred a different start for the induction machine to produce torque. To compromise between the slam start and the intermittent accelerations a matching is chosen that delivers full electrical power right after the STC switching region. Since this low point in the diesel envelope was the "bottleneck" in scenario 1 and 2. This matching uses the induction machine to create a sufficient engine margin for acceleration for the diesel engine.

Figure 4.106: Combinator curves

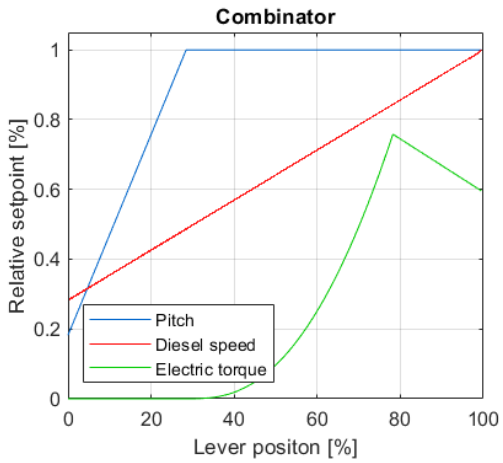

Tuning & trade offs

As described previously when speed control is used for the diesel engine a rate limiter for the lever setpoint is needed to prevent the diesel engine from overloading. Even with the increased clearance between the static loading of the diesel engine and the diesel engine envelope this rate limiter is still needed.

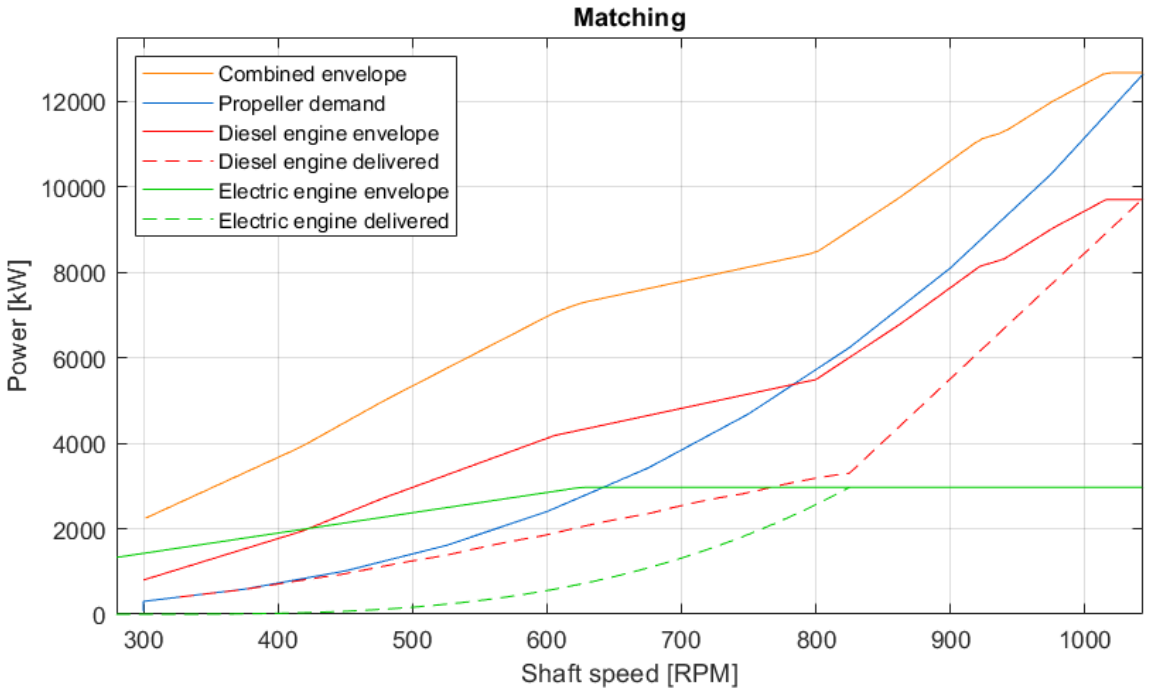

Figure 4.107: Matching of the propeller power to the diesel engine and induction machine

4.12.2. Slam start: simulation results

The acceleration starts from 7.7 kn as the fixed pitch and the minimum shaft speed dictate a minimum ship speed. From Figure 4.109 it can be seen that two large kinks in the acceleration curves are visible, both these kinks find their origin in the rate of change in the lever setpoint. By an earlier torque production by the induction machine the acceleration is improved when compared to the benchmark in scenario 1. The peak acceleration is higher and the total time needed to reach 90% of the top speed is 140 seconds. The benchmark takes twice as long to reach the maximum ship speed. It should be noted that the benchmark start at a ship speed of 0 kn while this scenario starts at 7.7 kn, nevertheless it is concluded that the acceleration has improved. The bottleneck in the diesel engine envelope found in simulation 1 that occurs after the STC switching region still exists, even with the induction machine delivering its additional torque in this region.

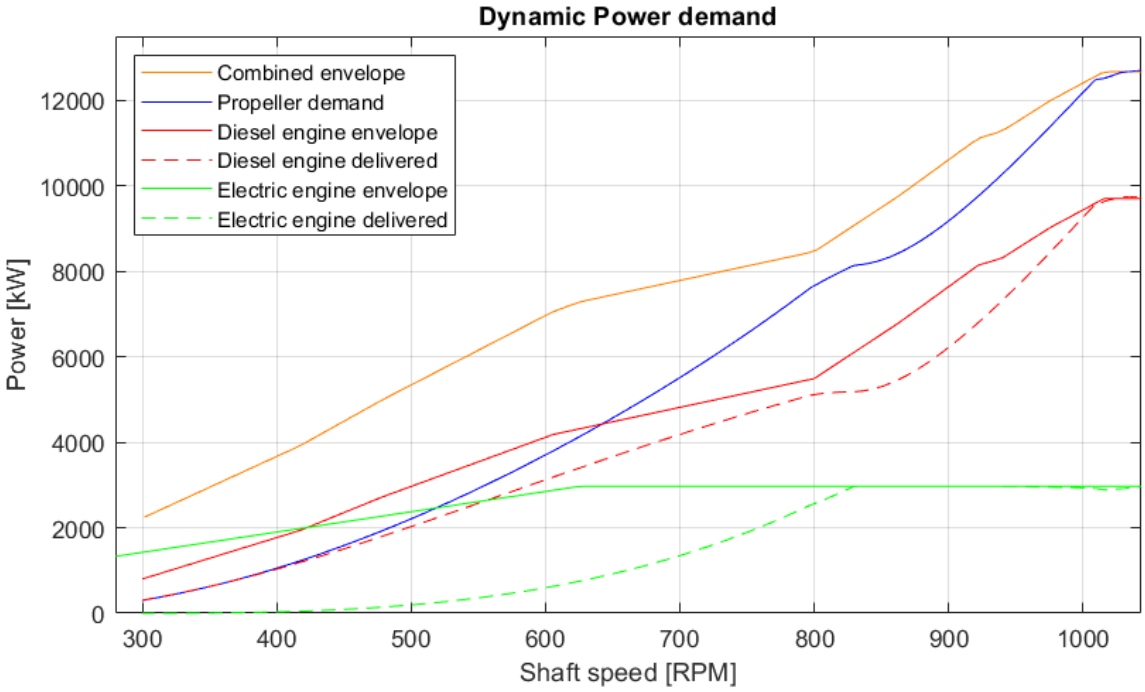

Figure 4.108: Dynamic power demand

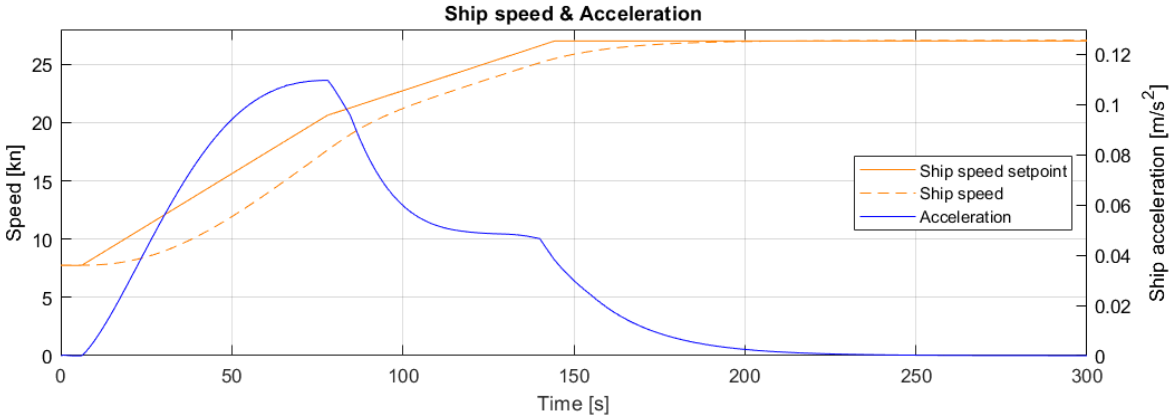

Figure 4.109: Ship speed and acceleration

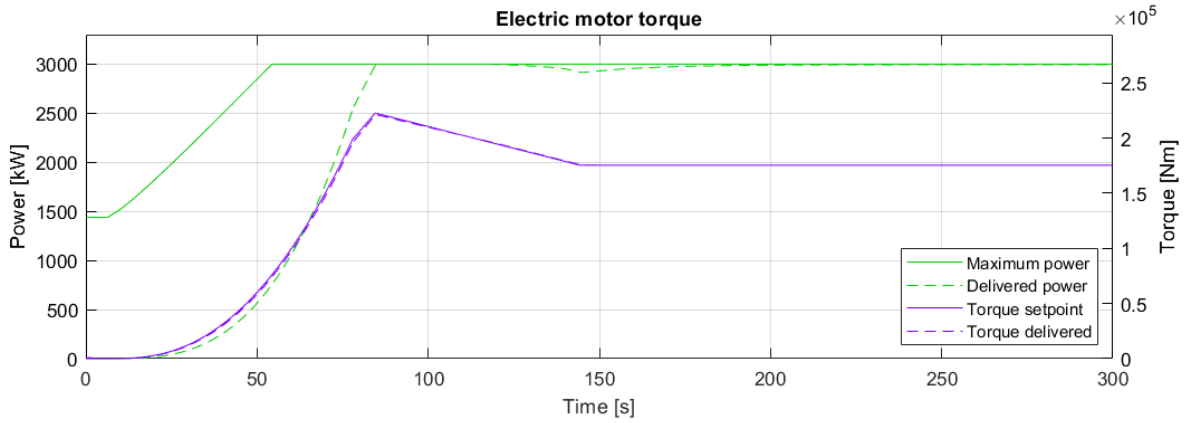

Figure 4.110: Induction machine torque and power

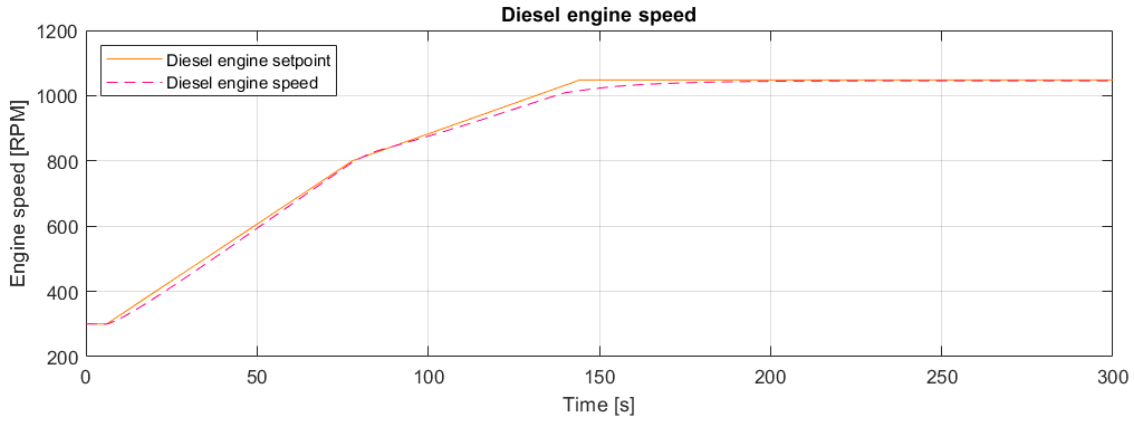

Figure 4.111: Diesel engine speed control

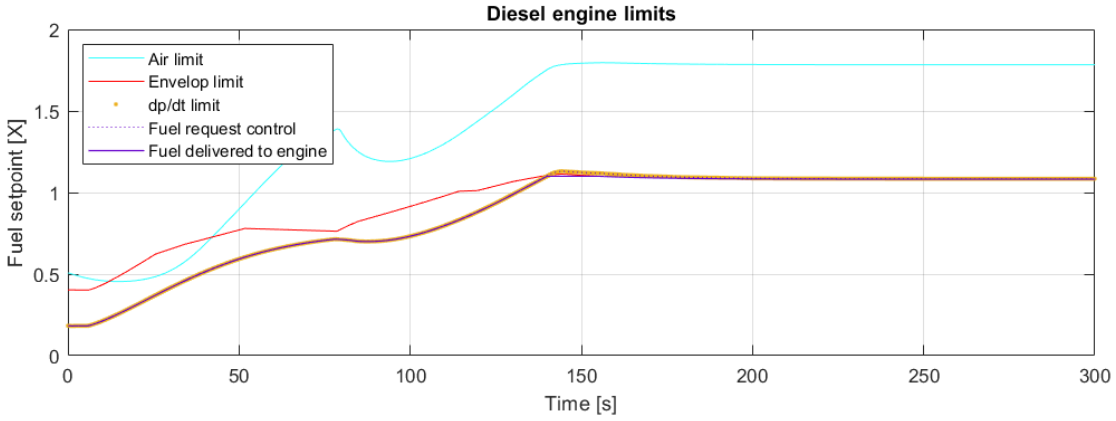

Figure 4.112: Diesel engine limitations

4.12.3. Staircase sprint: simulation results

The for acceleration improved matching of the induction machine effectively increases the power reserve for the diesel engine. Figure 4.117 shows that the diesel engine has sufficient clearance with its envelope. At 450 seconds in Figure 4.117 the diesel engine uses 88% of the total available power while the benchmark scenario 1 uses 94% of the available diesel engine power during the same intermittent acceleration from 15 to 20 kn. The acceleration from 15 to 20 kn is also faster, taking 39.9 seconds while the benchmark of simulation 1 needed 61.4 seconds.

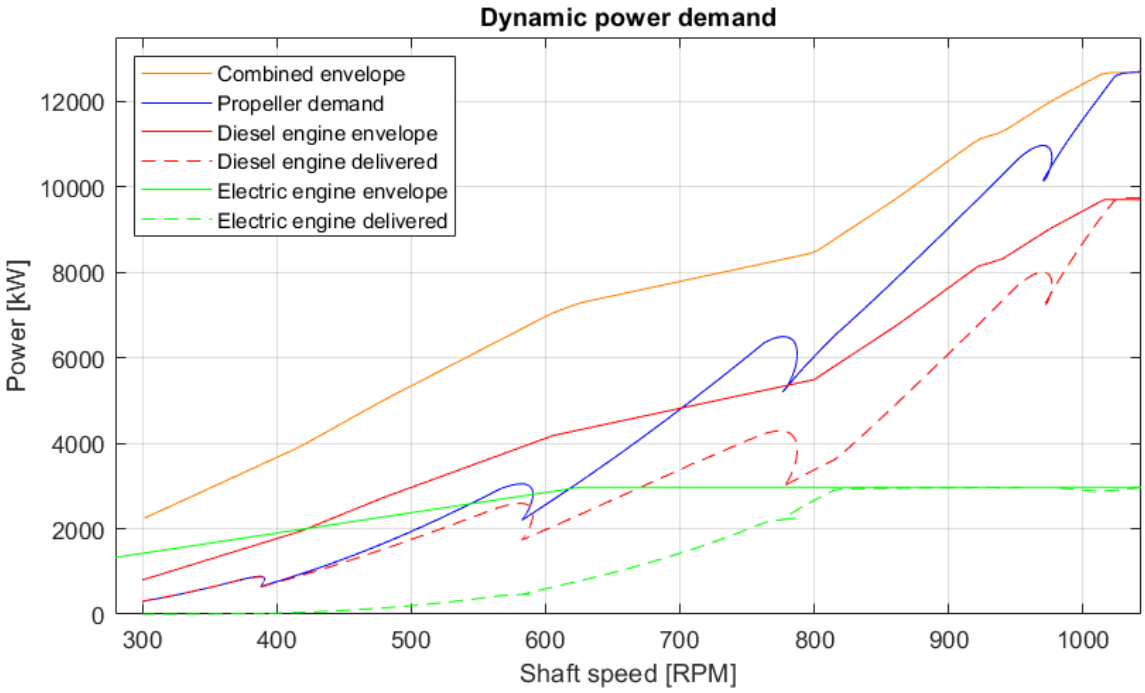

Figure 4.113: Dynamic load demand

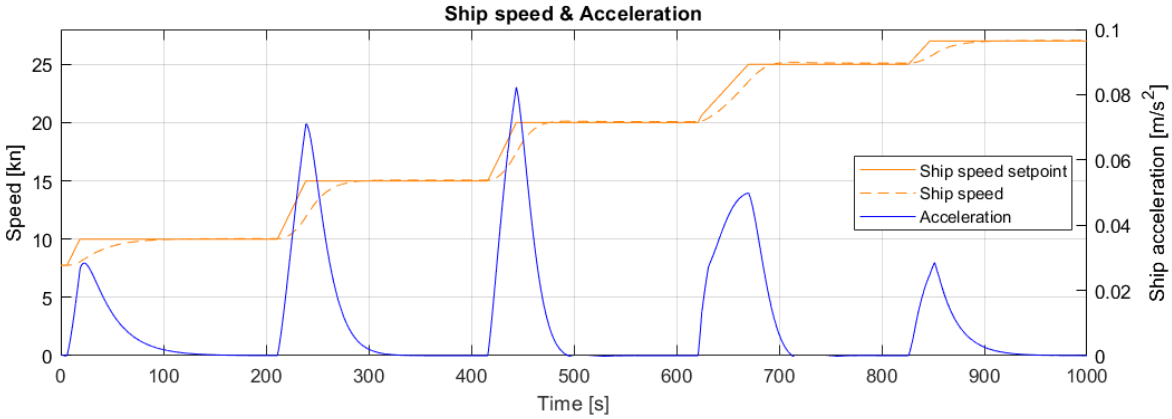

Figure 4.114: Ship speed and acceleration

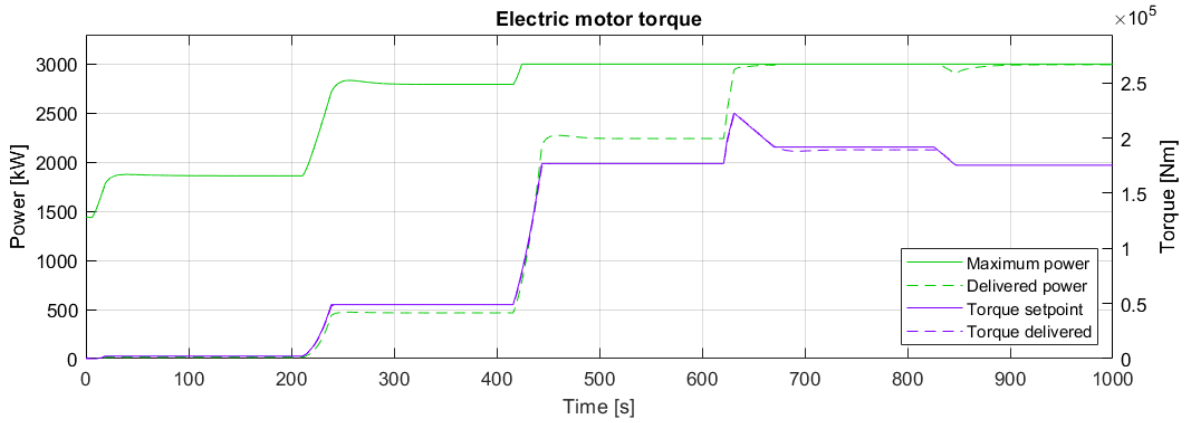

Figure 4.115: Indution amchine torque and power

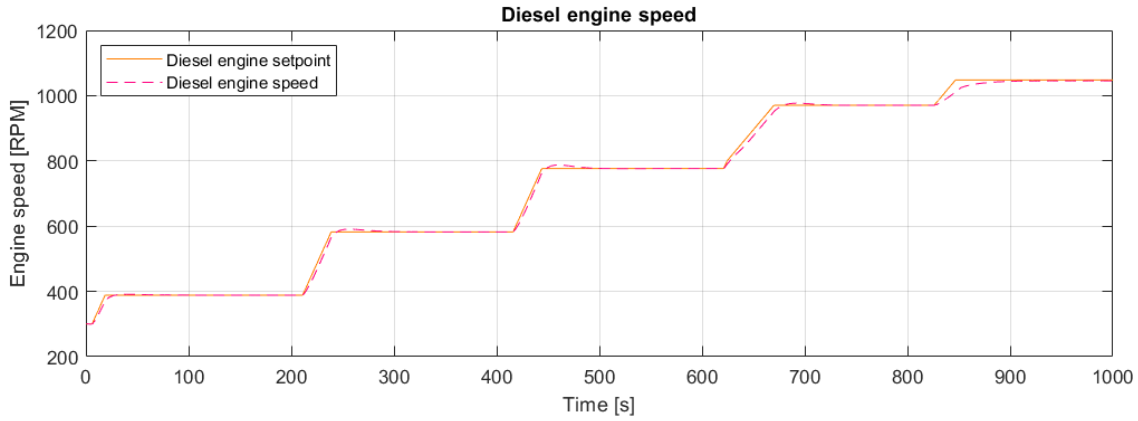

Figure 4.116: Diesel engine speed

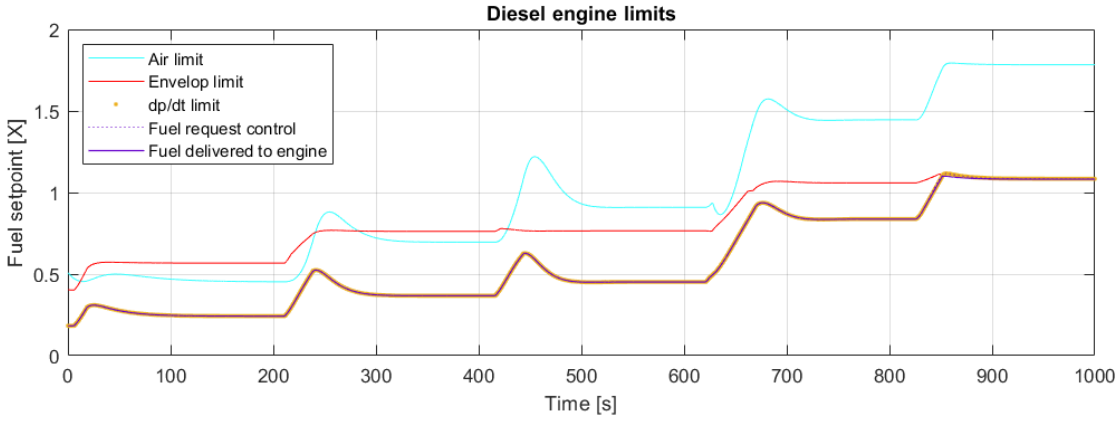

Figure 4.117: Diesel engine limitations

4.12.4. Control evaluation

Compared to the benchmark which uses conventional control and design pitch the acceleration is improved. Table 4.10 shows that all intermittent acceleration times as well as the slam start have improved. This is achieved by using the induction machine to create a larger power availability from the diesel engine, allowing for a larger acceleration without overloading the diesel engine.

Speed [kn]	**7.7-10**	**10-15**	**15-20**	**20-25**	**0-27**
Total time [s]	44.8	51.1	39.9	51.5	140.5
Maximum acceleration $[m/s^2]$	0.028	0.071	0.081	0.049	0.11
Time at maximum acceleration$[s]$	17	28	27	48	72

Table 4.10: Simulation number 11: acceleration time's

Using the settings found in scenario 3 for the induction motor does improve the acceleration characteristics significantly in comparison with the benchmark. The fixed pitch propeller results are very similar to the CP propeller results. For the manoeuvre as performed here, forward speed and forward acceleration, the drawback of a FP propeller are minimal. Due to scenario 3 operating at design pitch the only difference can be found at the minim shaft speed. The combination of design pitch and the minimum shaft speed results in a minimum ship speed of 7,7 kn. The induction machine would be able to propel the ship from 0 kn to above 15 kn if the diesel engine could be disconnected from the shaft line. This simulation proves that with simply shifting the shaft speed range in which the induction machine produces its torque the performance of a vessel equipped with a FP propeller can be improved by up to 30% till 35% for the intermittent accelerations. This simulation does not capture the more complex advantages the CP propeller provides during maneuvering which include but are not limited by the following two examples: reversing the thrust without reversing the shaft speed and the possibility of reducing the pitch in off-design conditions such as heavy weather or the loss of one propulsion shaft.

4.13. Scenario 12: Improved performance of a fixed pitch propeller with dynamic electrical torque control

Control mode	
Diesel engine	Speed control
Induction machine	Torque control
CP propeller	Fixed pitch propeller

4.13.1. Description

This scenario uses a fixed pitch propeller combined with the dynamic power split as discussed in simulation number 9 that can be found in section 3.2.6. The control strategies are directly implemented from simulation number 9. To allow the electric drive to be used effectively during accelerations the static power distribution has the minimum amount of torque matched to the electric drive. This gives the induction machine a larger power reserve. This larger power reserve allows for a larger contribution from the induction machine to the dynamic propeller load during acceleration. In simulation number 11 it was preferred to use a light matching for the induction machine. This was done because it would create margin for the diesel engine as it takes the dynamic load. When the induction machine is operated with dynamic torque control practically all dynamic load is provided by the induction machine. Since the dynamic load is delivered by the induction machine the need for a large margin between the diesel engine static power demand and the envelope is reduced. Since the control is identical to simulation 9, with the only difference being that the pitch is at the design pitch of P/D = 1.4, the discussion bellow will only contain the differences in performance. A more extensive evaluation can be found at simulation 9.

Figure 4.118: Combinator curves

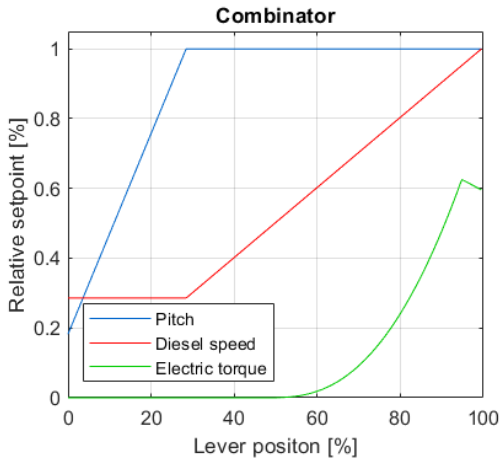

Tuning & trade offs

As described previously when speed control is used for the diesel engine a rate limiter for the lever setpoint is needed to prevent the diesel engine from overloading.

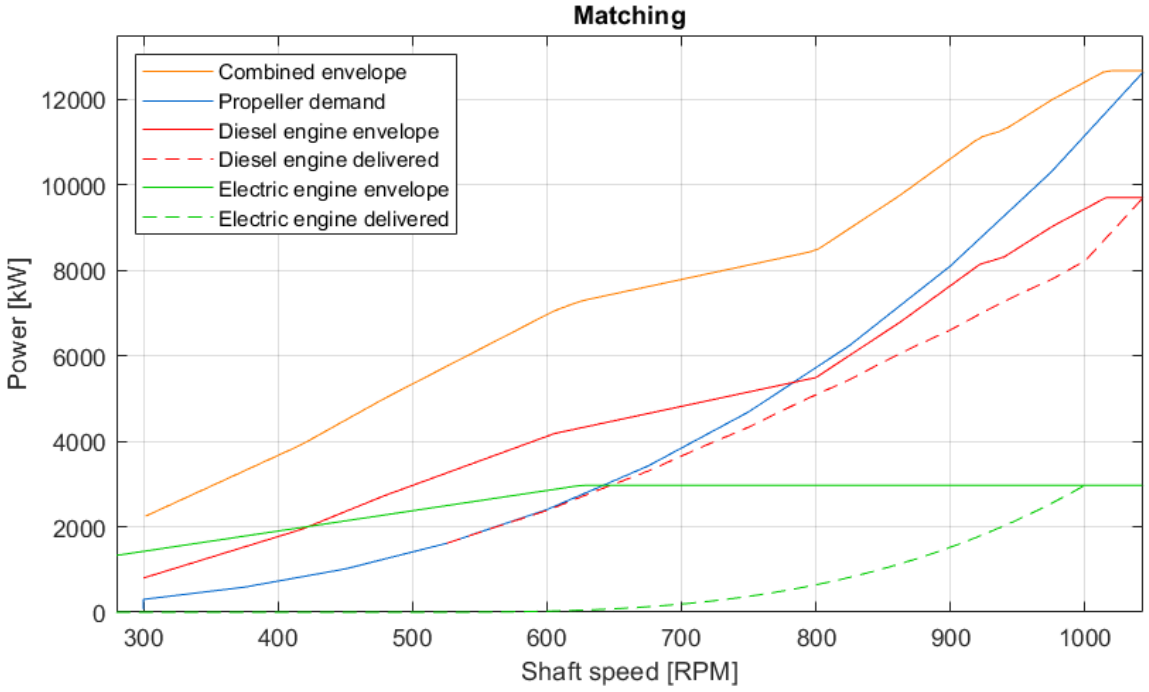

Figure 4.119: Matching of the propeller power to the diesel engine and induction machine

4.13.2. Slam start: simulation results

The shape of acceleration curve is given in Figure 4.121 and very similar to the acceleration of simulation 9 as can be seen in Figure 4.85. The deliverance can be found in the non existent hump in acceleration at the start of the manoeuvre between 6 and 10 seconds, which in simulation 9 originated from the increase in pitch setpoint. The larger more dominant peak in acceleration retains the same shape and character. The rate of acceleration increases fast to a value of 0.13 m/s^2, this peak is then hold for an extended amount of time ensuring a fast overall acceleration. it takes 104.6 seconds to reach 90% of the maximum speed starting at the minimum speed of 7.7 kn. The fast power development from the induction machine, which is taken slowly taken over by the diesel engine retains the characteristics which are described at simulation number 9.

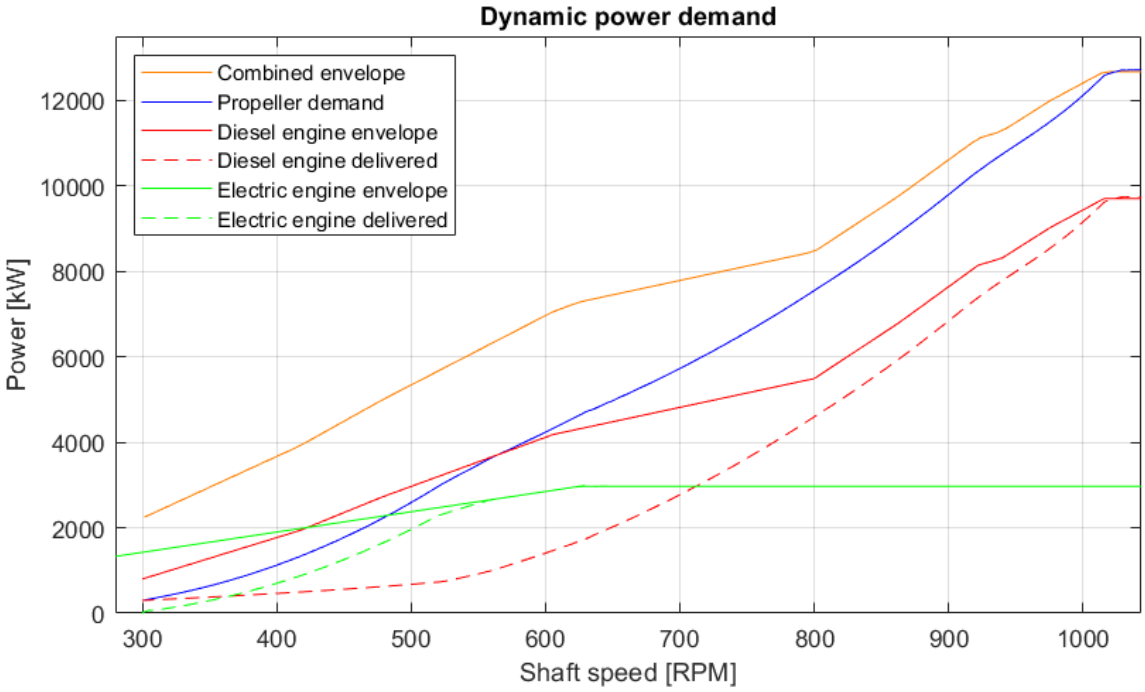

Figure 4.120: Dynamic power demand

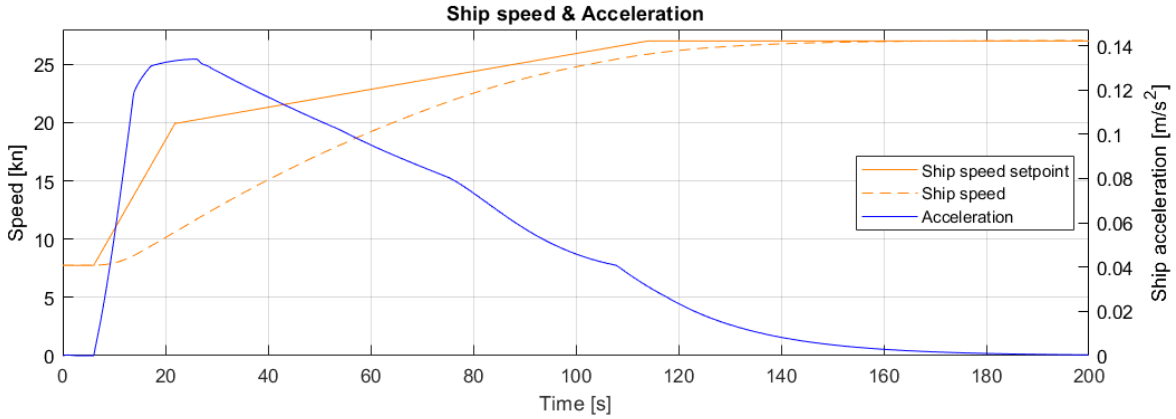

Figure 4.121: Ship speed and acceleration

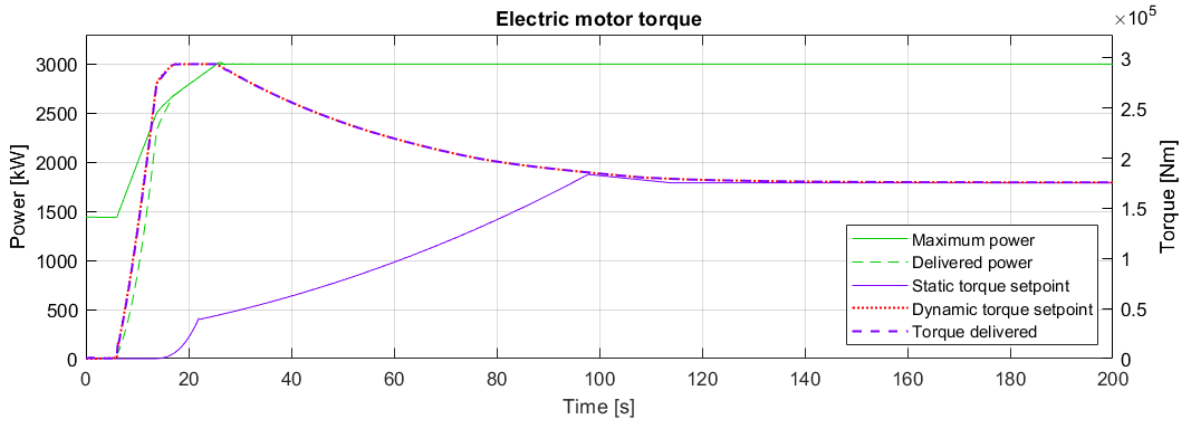

Figure 4.122: Induction machine torque and power

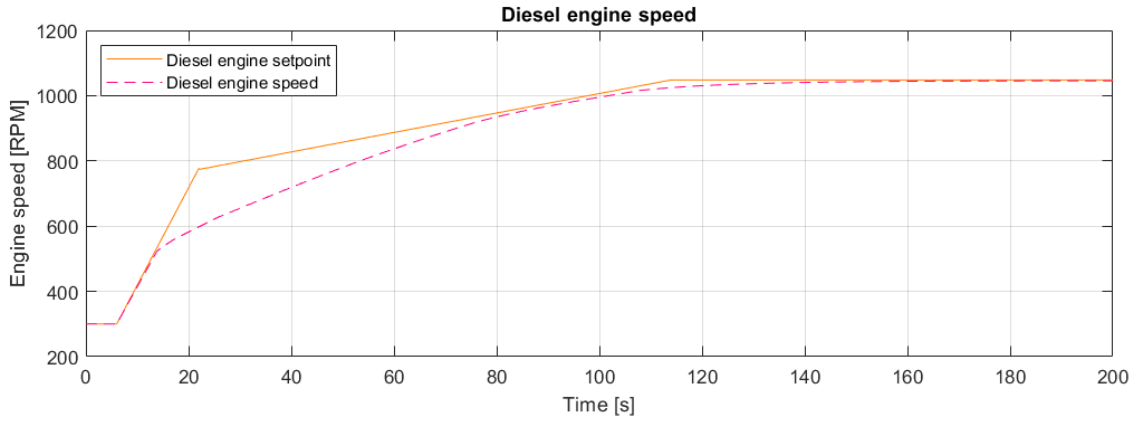

Figure 4.123: Diesel engine speed

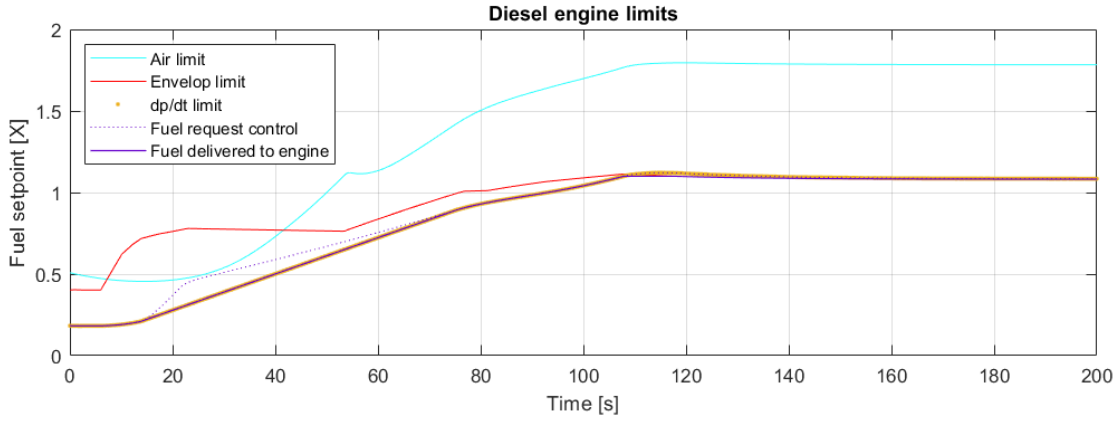

Figure 4.124: Diesel engine limitations

4.13.3. Staircase sprint: simulation results

The behavior of the subsystems retains the characteristics of simualation number 9. The induction machine delivers a fast increase in output power which is slowly taken over by the diesel engine. In the steady state after the acceleration the static power distribution follows the combinator. The acceleration graph of the intermittent accelerations is practically identical to simulation number 9. The shape, including the height of the acceleration peak, time for the peak to form as well as the time per acceleration is practically the same. The only difference is that the vessel is not able to sail at lower speeds than 7.7 kn.

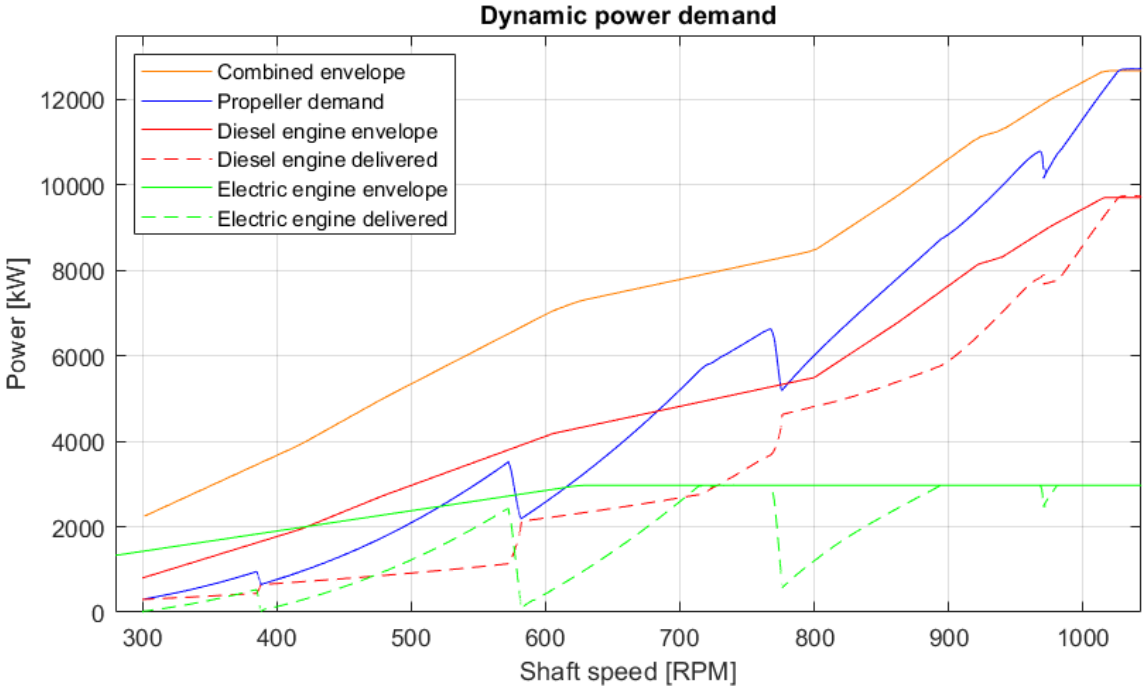

Figure 4.125: Dynamic power demand

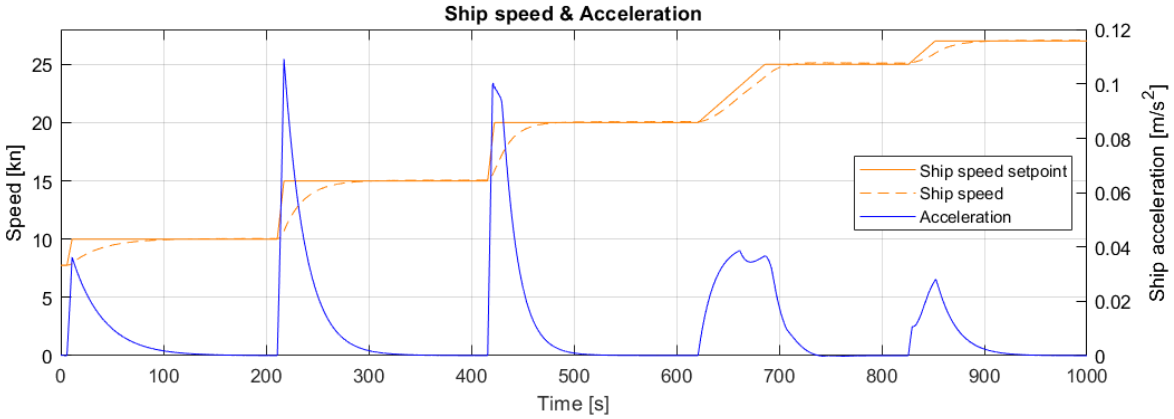

Figure 4.126: Ship speed and acceleration

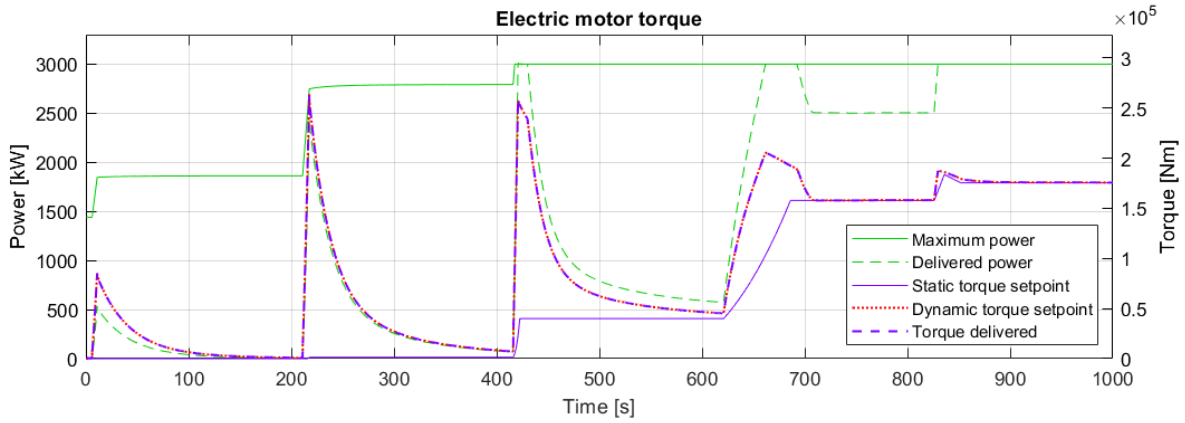

Figure 4.127: Induction machine torque

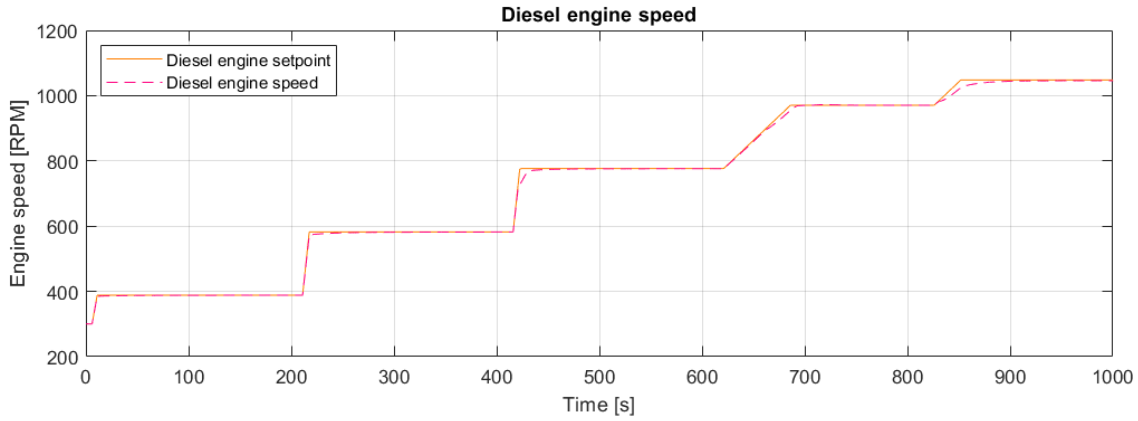

Figure 4.128: Diesel engine speed

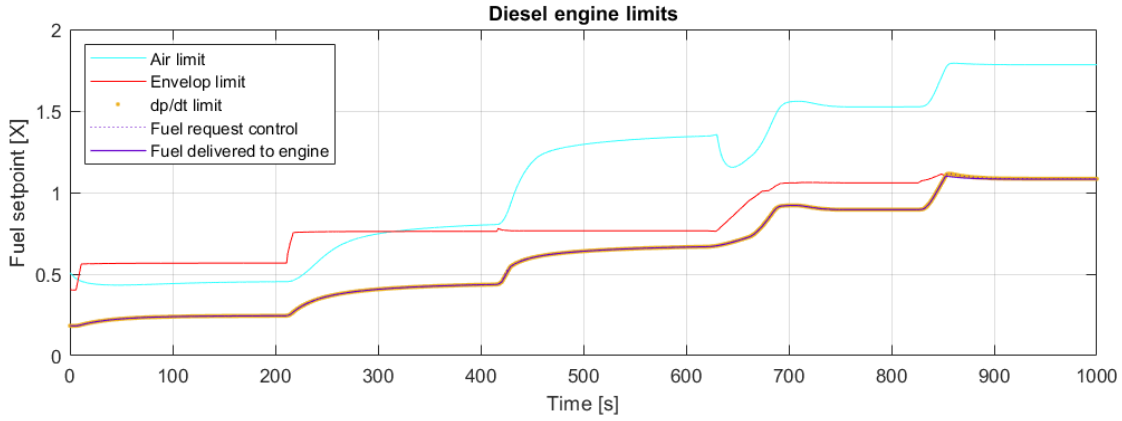

Figure 4.129: Diesel engine limitation

4.13.4. Control evaluation

Table 4.11 shows that the intermittent acceleration times as well as the slam start have improved. This is achieved by using the induction machines potential of delivering almost instant full torque at the start of an acceleration manoeuvre. The diesel engine slowly takes over the propeller load, allowing for a larger acceleration without overloading the diesel engine. The acceleration performance is almost identical to the simulation number 9, which also uses a dynamic power split with the design pitch. The difference being that there is now a minimum shaft speed with a fixed pitch, resulting in a minimum speed of 7.7 kn. Compared to the benchmark scenario 1 which uses conventional control and design pitch the dynamic power split as implemented in this scenario performs better. For example the time that is needed for the intermittent acceleration from 15 to 20 kn is reduced by 53 %. The dynamic power split also performs better than the improved FP propeller performance using a static power split as shown in simulation number 11. As an example again the time that is needed for the intermittent acceleration from 15 to 20 kn is taken, which is reduced by another 28 %. The lack of the possibility to reduce the pitch does mean that this simulation needs between 3% and 12% more acceleration time than simulation number 10, which uses a dynamic power split with a reduced pitch.

Speed [kn]	**7.7-10**	**10-15**	**15-20**	**20-25**	**0-27**
Total time [s]	45.0	40.7	28.6	62.7	104.6
Maximum acceleration [m/s^2]	0.036	0.11	0.099	0.038	0.13
Time at maximum acceleration[s]	5	6	5	10	21

Table 4.11: Simulation number 12: acceleration times

Using the diesel engine in speed control and the induction machine in torque control with a dynamic power split provided good acceleration to the vessel. With the diesel operating close to its envelope and the propeller at its fixed design pitch results in an efficient propulsion during steady state. The induction machine is also used to it full potential by using the possibility for delivering almost instant full torque for each acceleration. It is therefore concluded that this control strategy is a very promising option for improving the acceleration capabilities of a vessel equipped with a fixed pitch propeller.

This simulation does not capture the more complex advantages the CP propeller provides during maneuvering which include but are not limited by the following two examples: reversing the thrust without reversing the shaft speed and the possibility of reducing the pitch in off-design conditions such as heavy weather or the loss of one propulsion shaft. Therefore for manoeuvring as well as the possibility of lowering the propeller load a CP propeller is still preferred.

5

Conclusions

5.1. Simulation results

From the control modes discussed in Chapter 4 three scenarios are further highlighted here. The first scenario to be highlighted is adaptive pitch control as shown in simulation numnbers 6 and 7 in sections 4.7 and 4.8. The second control strategy is electrical speed control with torque control for the diesel as shown in simulation number 4 is section 4.5. Thirdly, the implementation of the dynamic power split using speed control for the diesel engine and a dynamic torque for the induction machine is discussed, which corresponds with simulation number 9 and 10 as shown in section 4.10 and 4.11. Figure 5.1 shows the change of ship speed over time from the highlighted control strategies as well as the benchmark. Table 5.1 shows the absolute measurement at which time 90% of the new speed setpoint is reached.

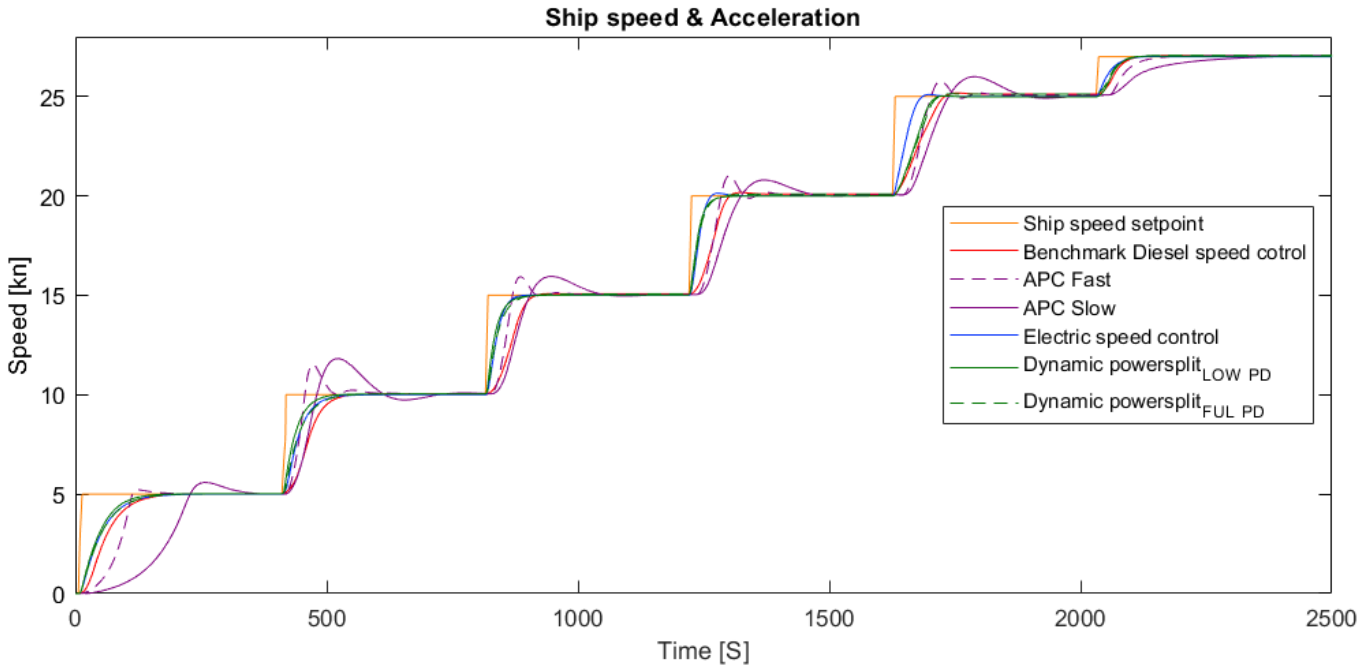

Figure 5.1: Comparison of the staircaise sprint for the highlighted scenarios

	0-5 [kn]	5-10 [kn]	10-15 [kn]	15-20 [kn]	20-25 [kn]	0-27 [kn]
Conventional control [s]	130.3	88.8	72.9	61.4	73.3	288.0
APC-slow [s]	213.3	59.6	67.0	69.1	68.4	369.5
APC-fast [s]	104.5	38.1	39.0	41.6	43.3	280.9
Electrical speed control [s]	121.5	70.2	37.0	26.9	35.4	119.4
Dynamic power split $_{LOWPD}$ [s]	103.7	55.2	35.0	27.0	59.0	107.0
Dynamic power split $_{FULLPD}$ [s]	120.4	72.3	42.3	29.9	64.1	124.6

Table 5.1: Quantitative overview of acceleration time highlighted scenarios

Adaptive pitch control
From simulation numbers 6 and 7 it can be concluded that APC effectively eliminates peaks in angle of attack (AoA) experienced during an acceleration. The elimination of the peak in AoA also eliminates the peak in propeller torque, therefore reducing the peak loading on the diesel engine. However this avoidance of the peak in AoA also results in the avoidance of the peak in thrust that is achieved with the larger AoA. Figure 4.59 illustrates that the acceleration gradually increases and gradually decreases. This gradual development of acceleration is the result of the constant angle of attack, which ensures a spread out thrust peak. As can be seen in Figure 5.1 the slow APC does not produce good acceleration behavior. When APC is tuned fairly aggressive the engine speed rises quickly due to the lower load of the reduced pitch and the relatively large virtual shaft speed setpoint. In scenario 7 where large engine speed fluctuations were accepted APC did produce a very good acceleration, especially in the smaller sprints. During partial accelerations the shaft speed needed to be increased excessively. This large shaft speed was needed to produce the thrust at a fixed angle of attack. These large engine speed fluctuations needed to generate a large acceleration with APC is a direct downside of this control strategy. Figure 4.68 illustrates this large change in engine speed for each acceleration. It should be stated the actuation system needed to provide the fast and continuously actuating pitch are not available yet [6]. Conventional pitch actuation systems can change the pitch of the propeller during manoeuvres, doing so excessively would however cause a large amount of wear and consequently maintenance [11]. Nevertheless for this research it was assumed that fast and accurate pitch adjustments is possible. It should be noted that this control strategy is the only one that avoids the high angle of attack and therefore the only control strategy that limits cavitation during an acceleration manoeuvre. Both "electric speed control parallel with diesel engine torque" and "diesel engine speed control with dynamic power split" outperform the APC in terms of acceleration. Both these control strategies deliver a large amount of torque to the propeller pushing through the large angle of attack and as a consequence delivering a very large thrust and acceleration.

Electric speed control parallel with diesel engine torque control
Scenario 4 simulates torque control for the diesel combined with electric speed control. This control mode performs very well on both the staircase sprint and the slam start. By the manufacturer a given amount of load increase per unit of time is defined. During this simulation the static load could be matched very close to the engine envelope. This very close matching could be done because it is given a fixed torque contribution, making the diesel engine almost unaffected by the disturbances from the steady state working point that originate in the dynamics of the acceleration. A lever setpoint rate limiter was not necessary because the diesel engine is unaffected by the increased propeller load during an acceleration. The absence of a lever setpoint rate limiter made it possible to increase the power of the diesel engine by the maximum increase allowed by the manufacturer. This maximum amount of power that can be increased per unit of time for the diesel engine is the limiting factor for the overall acceleration. From simulation number 5 it is concluded that a high static load on the diesel engine in steady state combined with a large power input from the induction machine during an acceleration leads to a very fast acceleration. There are two things that imply that this control strategies is close to the maximum acceleration possible. The first is the fact that the diesel engine increases its power output with the maximum allowed power increase per unit of time. Secondly the induction machine produces almost full torque during each acceleration. Figure 5.1 shows that electrical speed control combined with diesel engine torque control is very fast compared to the other well highlighted control strategies.

Diesel engine speed control with dynamic power split

During simulation number 5 it was concluded that a large acceleration can be achieved with a heavy loading on the diesel engine in steady state supported by a large torque production during acceleration by the induction machine. While torque control is capable of achieving these goals, torque control itself is not available from manufacturers. Using the diesel engine with speed control parallel with the electric drive in torque control has its limitations. No optimal for all intermittent acceleration and the slam start was found by varying the point at which the electric machine starts contributing with a fixed power distribution. The shaft speed range at which the induction machine started contributing power to the propeller the accelerations was greatest, meaning that for optimal acceleration a power contribution from the induction machine at each intermittent acceleration is needed. The above described findings were combined resulting in a novel implementation of a dynamic power split described in scenario 9 and 10. This control strategy uses PI control for the diesel engine which is dominated by the integrating gain. The induction machine is operated in torque control that operates on a PI controller. In addition to the torque control a proportional speed control loop is added. This results in a control for which the diesel engine delivers the load changes with a low frequency and the induction machine that delivers the load changes with a high frequency. The diesel engine is matched with a small margin to its envelope. This small margin results in a heavy loaded diesel engine that operates efficiently in steady state. This small margin is possible because the induction machine delivers the increased load during acceleration. The proposed dynamic power split utilizes the full potential of a nearly instant delivery of torque from the induction machine while primarily using torque control. The diesel engine is loaded in a way that is very similar to torque control while operating in speed control. Although the induction machine does not have a limit for the increase in power over time, this power does have to be generated by a generator set. During simulations it was found that the induction machine creates a sharply increasing load that needs the generator set to increase its power by 51% of its maximum power in 7 seconds. According to the WÄRTSILÄ 31 product guide [31] this is too large to be considered a ramped load. For a step load a 51% load increase seems acceptable according to Welland [32]. It is worthwhile stating that in a DC-system supported by batteries, these loads may be even easier to cope with. A DC-system is considered as design option as a way of mitigating the problem of power availability aboard of a fast naval combatant.

5.2. Research questions

1. **What combination of control methods at machine level provides the best acceleration performance?**
   Speed control for the induction machine parallel with torque control for the diesel engine gives very good acceleration performance as shown in simulation number 4 is section 4.5. This makes it possible for the diesel engine to be loaded close to its operating limits without overloading. The electric machine is used to its full potential by delivering full torque during an acceleration. When using speed control for the induction machine the induction machine is made responsible for keeping the speed and coping with disturbances. For which it is inherently more suited than the diesel engine, due to its fast response as well as it being able to produce full torque or maximum power without any negative adverse effects.

   Since torque control for the diesel engine is not available from manufacturers, speed control for the diesel engine parallel with dynamic torque control for the electric dive is a good alternative. The dynamic torque control for the induction machine allow for optimal usage of the inherent characteristics of the electrical machine. Using dynamic torque control the induction machine is responsible for the high frequency load changes such as disturbances as well as the acceleration. The diesel engine governed by a slower integral dominated PI controller produces the low frequency load changes, including the higher load at a new steady sate.

2. **How should the load be distributed between the electric drive and diesel engine during acceleration?**
   When speed control is used for the diesel engine and torque control is used for the induction machine a dynamic power split has to be considered. The dynamic torque setpoint implemented in scenario 9 and 10 results in great acceleration in both the slam start as the staircase sprint scenario. The electrical torque is used for the heavy propeller load during an acceleration. The steady state load to maintain a constant speed is delivered by the diesel engine. The advantage of the dynamic power split is that it allows the induction machine to deliver large and fast torque during an acceleration. This results in a control strategy that behaves like torque control for the diesel engine during acceleration, while maintaining the advantages speed control provide. The timescale in which the induction machine produces full power varies between 3 and 7 seconds, underlining the advantage of fast power availability from the induction machine when compared to the diesel engine.

3. **What is the optimal propeller load distribution over time to achieve the maximum overall acceleration?**
   "Adaptive pitch control" and the proposed "diesel engine speed control with dynamic power split" operate at opposite sides of controlling the propeller load. APC avoids the angle of attack peak, meaning it needs a large shaft speed to be able in creating a large thrust. The main advantage is that APC limits the cavitation by maintaining the angle of attack. All other control strategies that maintain a large pitch need to power through the torque peak that occurs during acceleration. The proposed new strategy using diesel engine speed control with dynamic power split operates at very large angle of attack peaks. It is therefore very likely that cavitation will occur. Cavitation itself was not part of the scope of this research. The larger angle of attack on the propeller which occurs during an acceleration if the pitch is not lowered will result in a peak in propeller torque and thrust. This peak in thrust is beneficial for the acceleration. However this peak in thrust can only be delivered if the propulsion system is capable of delivering the peak torque without overloading the diesel engine.

How does hybrid diesel-electric propulsion equipped with a controllable pitch propeller needs to be controlled for maximum acceleration?
Maximum acceleration is achieved when both the diesel engine and the induction machine produce a large amount of power during the acceleration. Torque control for the diesel engine is close to ideal, making it possible for the diesel engine to be loaded close to its operating limits without overloading. This heavy loading on the diesel engine creates a large power availability from the induction machine, which needs to be used during an acceleration. Due to the fact that torque control for the diesel engine is at this moment not available from manufacturers the new dynamic power split as presented in simulation numbers 9 and 10 need to be consider. This uses dynamic torque control for the induction machine making the induction machine responsible for the high frequency load changes such as disturbances as well as the acceleration. The diesel engine governed by a slower integral dominated PI controller produces the low frequency load changes, including the higher load at a new steady sate.

5.3. Opportunities for future research

1. The proposed new strategy uses diesel engine speed control with dynamic power split but creates very large angle of attack peaks during an acceleration. It is therefore very likely that cavitation will occur, cavitation itself was not part of the scope of this research. It will need to be investigated separately to what extend cavitation occurs and how damaging it will be during the relatively short acceleration. Determining how severe the cavitation will be is important in determining the feasibility of this new control strategy.

2. The induction machine requests large power increases from the electrical grid. During some simulations the increase in power demand from the induction machines reached a maximum of 51% of the generators capacity in as little as 3 seconds. A more detailed simulation evaluating the response of the generator and electric grid is needed the need for additional generators, battery pack of even a DC power supply.

3. To be able to evaluate a large amount of control strategies the controllers for each strategy were rudimentary and kept as similar as possible. Due to the non linearity between the different intermittent accelerations as well as the slam start gain scheduling or other more complex controls should be made for the new dynamic power split control strategies. Besides properly tuning the new control system could further improve the results.

4. Improving the model of the CP propeller model will create results that more closely resemble the reality. The version used in this model is a very simple model of the CP propeller. This model directly sets a propeller angle following a first order differential equation. Although it is expected that the pitch actuation would have a different characteristic is is not expected that is would have a large effect on acceleration speeds. The low impact of the overall acceleration is expected because the time constant of the CP propeller is very small compared to the vessel dynamics.

5. The simulation of waves will assess the stability of the new diesel engine speed control with a dynamic power split. Waves cause an increased load on the propulsion system as well as a fluctuating advance velocity on the propeller. The fluctuating advance velocity will lead to a fluctuating load on the propulsion system. Since the induction machine responses to the high frequency load changes it is expected that the diesel engine will remain relatively uninfluenced. Furthermore it is expected that the possibility of a sharply increasing or decreasing torque production from the induction machine will minimize the shaft speed variations.

6. When the new control system is further developed more elaborate manoeuvres than simply accelerating forward will need to be tested and controlled.

Bibliography

[1] Francesco Baldi, Gerasimos Theotokatos, and Karin Andersson. Development of a combined mean value-zero dimensional model and application for a large marine four-stroke Diesel engine simulation. *Applied Energy*, 154:402–415, 2015. ISSN 03062619. doi: 10.1016/j.apenergy.2015.05.024. URL http://dx.doi.org/10.1016/j.apenergy.2015.05.024.

[2] DAMEN SCHELDE NAVAL SHIPBUILDING. 140 YEARS OF EXPERIENCE, 2020. URL https://www.damen.com/companies/damen-schelde-naval-shipbuilding.

[3] European Commission. Climate strategies & targets: 2020 climate and energy package, 2007. URL https://ec.europa.eu/clima/policies/strategies/2020{_}en.

[4] Turesson Gabriel. *Model-Based Optimization of Combustion-Engine Control Gabriel Turesson*. Lund University, 2018. ISBN 9789177537052. URL https://www.researchgate.net/figure/The-basic-geometry-of-an-engine-cylinder-Combustion-of-fuel-and-air-in-the-combustion{_}fig1{_}325

[5] R D Geertsma. *Autonomous control for adaptive ships with hybrid propulsion and power generation*. PhD thesis, TU delft, 2019. URL https://doi.org/10.4233/uuid:ad81b0ee-76be-4054-a7e8-bd2eeecdb156.

[6] R D Geertsma, R R Negenborn, K Visser, and J J Hopman. Torque control for diesel mechanical and hybrid propulsion on naval vessels. 2016.

[7] R. D. Geertsma, R. R. Negenborn, K. Visser, and J. J. Hopman. Parallel Control for Hybrid Propulsion of Multifunction Ships. *IFAC-PapersOnLine*, 50(1):2296–2303, 2017. ISSN 24058963. doi: 10.1016/j.ifacol.2017.08.229. URL https://doi.org/10.1016/j.ifacol.2017.08.229.

[8] R. D. Geertsma, R. R. Negenborn, K. Visser, M. A. Loonstijn, and J. J. Hopman. Pitch control for ships with diesel mechanical and hybrid propulsion: Modelling, validation and performance quantification. *Applied Energy*, 206(September):1609–1631, 2017. ISSN 03062619. doi: 10.1016/j.apenergy.2017.09.103.

[9] R. D. Geertsma, K. Visser, and R. R. Negenborn. Adaptive pitch control for ships with diesel mechanical and hybrid propulsion. *Applied Energy*, 228:2490–2509, oct 2018. ISSN 03062619. doi: 10.1016/j.apenergy.2018.07.080.

[10] Rinze Geertsma, Jasper Vollbrandt, Rudy Negenborn, Klaas Visser, and Hans Hopman. A quantitative comparison of hybrid diesel-electric and gas-Turbine-electric propulsion for future frigates. *2017 IEEE Electric Ship Technologies Symposium, ESTS 2017*, pages 451–458, 2017. doi: 10.1109/ESTS.2017.8069321.

[11] Milinko GODJEVAC. *Wear and Friction in a Controllable Pitch Propeller*. 2009. ISBN 978-90-8891-136-1. URL http://repository.tudelft.nl/assets/uuid:ebcaff3c-a203-49e4-aa41-0d9040f5d0c6/godjevac.pdf{%}5Cnpapers://d6f610b6-cff4-44d3-b5d2-ae22f81e9d7c/Paper/p6636.

[12] E. Hughes. A new chapter for MARPOL Annex VI – requirements for technical and operational measures to improve the energy efficiency of international shipping. Technical report, MAPOL, 2013.

[13] IMO MARPOL. International Convention for the Prevention of Pollution from Ships: Articel 3. URL http://www.marpoltraining.com/MMSKOREAN/MARPOL/intro/a3.htm.

[14] Mourik. L. Literature Review rarallel control for hybrid propulsion aboard a fast naval combatant, 2021.

[15] MAN. Man v28/33d stc, 2021. URL http://marengine.com/ufiles/MAN-V28{_}33D.pdf.

[16] Apollonia Miola, Biagio Ciuffo, Emiliano Giovine, and Marleen Marra. *Regulating Air Emissions from Ships: The State of the Art on Methodologies, Technologies and Policy Options*, volume 472. Publications Office of the European Union, Luxembourg, 2010. ISBN 9789279177330. doi: 10.2788/4171. URL https://publications.jrc.ec.europa.eu/repository/bitstream/JRC60732/jrcrrshipspubsynov29{_}red.pdf.

[17] P. Mizythras, E. Boulougouris, and G. Theotokatos. Numerical study of propulsion system performance during ship acceleration. *Ocean Engineering*, 149(July 2017):383–396, 2018. ISSN 00298018. doi: 10.1016/j.oceaneng.2017.12.010. URL https://doi.org/10.1016/j.oceaneng.2017.12.010.

[18] A. J. Murphy, A. J. Norman, K. Pazouki, and D. G. Trodden. Thermodynamic simulation for the investigation of marine Diesel engines. *Ocean Engineering*, 102:117–128, 2015. ISSN 00298018. doi: 10.1016/j.oceaneng.2015.04.004. URL http://dx.doi.org/10.1016/j.oceaneng.2015.04.004.

[19] Sangram Kishore Nanda, Boru Jia, Andrew Smallbone, and Anthony Paul Roskilly. Fundamental Analysis of Thermal Overload in Diesel Engines : Hypothesis and Validation. 2017. doi: 10.3390/en10030329.

[20] C. M. Ong. *Dynamic Simulations of Electric Machinary*. Prentice-Hall, Inc., 1998. ISBN 0-13-723785-5.

[21] David Dowling Pijush Kundu, Ira Cohen. *Fluid Mechanics*. 2016. ISBN 978-0-12-405935-1. doi: https://doi.org/10.1016/C2012-0-00611-4. URL https://www.sciencedirect.com/topics/engineering/lifting-line-theory.

[22] H Rajesh and U Arihant. Torque Control System for Diesel Engine. *IOSR Journal of Mechanical and Civil Engineering*, 2(5):32–32, 2012. doi: 10.9790/1684-0253032.

[23] Schottel. Controllable-Pitch Propeller, 2014. URL https://www.schottel.de.

[24] P.J.M. Schulten, R. D. Geertsma, and K. Visser. Energy as a weapon , part II. In *Conf. proc. EAAW VII*, Bristol UK, 2017.

[25] D Stapersma. Diesel Engines, Volume 2 Turbocharging. *Tu Delft*, 2(January):–, 2010.

[26] Congbiao Sui, Enzhe Song, Douwe Stapersma, and Yu Ding. Mean value modelling of diesel engine combustion based on parameterized finite stage cylinder process. *Ocean Engineering*, 136:218–232, 2017. ISSN 00298018. doi: 10.1016/j.oceaneng.2017.03.029.

[27] G. Theotokatos. On the cycle mean value modelling of a large two-stroke marine diesel engine. *Proceedings of the Institution of Mechanical Engineers Part M: Journal of Engineering for the Maritime Environment*, 224(3):193–205, 2010. ISSN 14750902. doi: 10.1243/14750902JEME188.

[28] A. M. Trzynadlowski. *Control of Induction Motors*, volume 6. Academic press series in engineering, 2001. ISBN 9788578110796.

[29] Taner Tuken, Jon H. Van Gerpen, and R. Rees Fullmer. Adaptive torque control of a diesel engine for transient test cycles. *SAE Technical Papers*, 1992. ISSN 26883627. doi: 10.4271/920238.

[30] A. Vrijdag, D. Stapersma, and T. van Terwisga. Control of propeller cavitation in operational conditions. *Journal of Marine Engineering and Technology*, 9(1):15–26, 2010. ISSN 20568487. doi: 10.1080/20464177.2010.11020228.

[31] Wartsila. Wärtsilä 34DF Copyright by WÄRTSILÄ FINLAND Oy. Technical report, 2020. URL https://www.wartsila.com/docs/default-source/product-files/engines/ms-engine/product-guide-o-e-w31.pdf?utm{_}source=engines{&}utm{_}medium=dieselengines{&}utm{_}term=w31{&}utm{_}content=productguide{&}utm{_}campaign=msleadscoring.

[32] Welland. load acceptance on a diesel generator, 2020. URL https://support.wellandpower.net/hc/en-us/articles/206911685-How-to-get-100-load-acceptance-on-a-diesel-generator-.

[33] Dave Wisconsin Wilson. Teaching Your PI Controller to Behave, 2015. URL https://e2e.ti.com/blogs{_}/b/industrial{_}strength/posts/teaching-your-pi-controller-to-behave-part-i.

[34] Hans Klein Woud and Douwe Stapersma. *Design of Propulsion and Electric Power generation systems*. IMarEST, 2012. ISBN 1-902536-47-9.